ibvt
Institut für Bioverfahrenstechnik

Technische Universität Braunschweig

Band 47
ibvt-Schriftenreihe

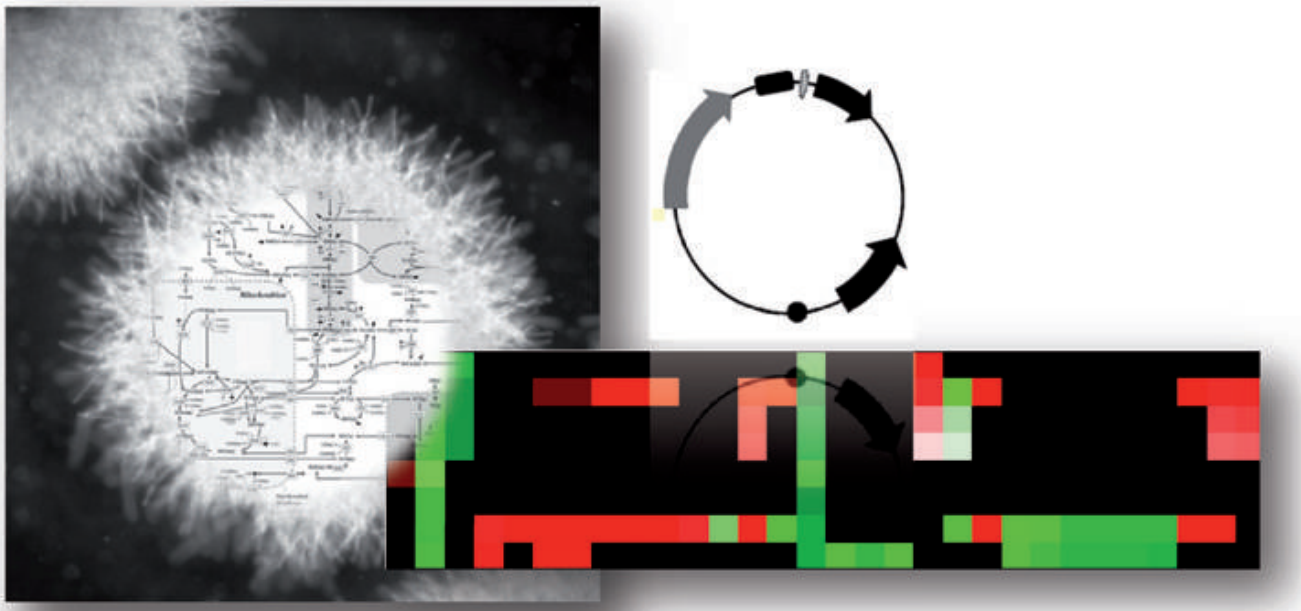

Metabolic Network Analysis of the Cell Factory *Aspergillus niger*

Guido Melzer

Cuvillier-Verlag

ibvt-Schriftenreihe

Schriftenreihe des Institutes für Bioverfahrenstechnik
der Technischen Universität Braunschweig

Herausgegeben von Prof. Dr. Christoph Wittmann

Band 47

Cuvillier-Verlag
Göttingen, Deutschland

Herausgeber
Prof. Dr. Christoph Wittmann
Institut für Bioverfahrenstechnik
TU Braunschweig
Gaußstraße 17, 38106 Braunschweig
www.ibvt.de

Bibliographische Informationen der Deutschen Nationalbibliothek
Die Deutsche Nationalbibliothek verzeichnet diese Publikation in der Deutschen Nationalbibliographie; detaillierte bibliographische Daten sind im Internet über *http://dnb.d-nb.de* abrufbar.
1. Aufl. – Göttingen: Cuvillier, 2010

Nonnenstieg 8, 37075 Göttingen
Telefon: 0551-54724-0
Telefax: 0551-54724-21
www.cuvillier.de

1. Auflage, 2010
Gedruckt auf säurefreiem Papier

ISBN 978-3-86955-456-3
ISSN 1431-7230

Metabolic Network Analysis of the Cell Factory *Aspergillus niger*

Von der Fakultät für Maschinenbau
der Technischen Universität Carolo-Wilhelmina zu Braunschweig

zur Erlangung der Würde
eines Doktor-Ingenieurs (Dr.-Ing.)
genehmigte Dissertation

von Dipl.-Ing. Guido Melzer
aus Cottbus

eingereicht am: 04.01.2010

mündliche Prüfung am: 01.02.2010

Erstreferent: Prof. Dr. Christoph Wittmann
Zweitreferent: Prof. Dr. Dieter Jahn
Prüfungsvorsitzender: Prof. Dr. Rainer Krull

2010

„There is no certainty where one of the mathematical sciences cannot be applied or where there is no bond with mathematics."

(Leonardo da Vinci)

Für meine Familie

Vorwort

„Leider lässt sich eine wahrhafte Dankbarkeit mit Worten nicht ausdrücken."
(Johann Wolfgang von Goethe)

Die vorliegende Arbeit entstand im Rahmen meiner Tätigkeit als wissenschaftlicher Mitarbeiter am Institut für Bioverfahrenstechnik der Technischen Universität Carolo-Wilhelmina zu Braunschweig im Teilprojekt B4 des Sonderforschungsbereiches SFB 578 „Integration gen- und verfahrenstechnischer Methoden zur Entwicklung biotechnologischer Prozesse – Vom Gen zum Produkt".

Für meine Doktorarbeit bin ich sehr vielen Menschen einen herzlichen Dank schuldig. Besonders möchte ich mich bei Prof. Dietmar Christian Hempel bedanken, der mir sehr viel Vertrauen entgegen brachte und mir die Arbeit am Institut ermöglichte.

Ein besonderes Wort des Dankes möchte ich an meinen Doktorvater und ersten Gutachter Prof. Christoph Wittmann richten, ohne den ich niemals ein Licht am Ende des Tunnels meiner Doktorarbeit gesehen hätte. Mit seiner Erfahrung, seinen fachspezifischen Fragen und Diskussionen und den vielen Ideen konnte diese Arbeit in die richtige Bahn gelenkt werden. Ebenso seine wertvollen und oft auch sehr persönlichen Ratschläge trugen sehr zum Gelingen der Arbeit bei.

Professor Dieter Jahn danke ich für die Übernahme des Co-Referates sowie für seine stete Diskussionsbereitschaft und die aufbauende und motivierende Art, die gerade in schweren Stunden sehr hilfreich war.

Dr. Bernd Nörtemann möchte ich für die Betreuung und vielen Diskussion danken. Seine lockere, ehrliche und sehr persönliche Art haben für eine sehr entspannte Arbeitsatmosphäre gesorgt, die sich nur positiv auf die Arbeit auswirken konnte.

Professor Ezequiel Franco-Lara möchte ich ganz besonders für die vielen konstruktiven Diskussionen und Anregungen danken, die durch seine Sicht aus anderer Perspektive zum Erfolg dieser Arbeit beigetragen haben.

Ein großer Dank geht auch an meine Kollegen, denn die Zusammenarbeit mit ihnen war ein essentieller Beitrag bei der Erstellung meiner Doktorarbeit, die mich nicht nur tatkräftig unterstützt haben, sondern mich stets begleiteten und für die erforderliche Abwechslung sorgten. Viele von meinen Kollegen sind meine Freunde geworden, und ich möchte Florian David, Christoph Bolten und Alex Dalpiaz nicht nur für die oben erwähnte Hilfe, sondern

auch für die netten gemeinsamen Abende, das gemeinsame Badminton-, Fußball-, Basketball- oder Squash-Spielen danken.
Auch möchte ich Verena Schoppe, Habib Driouch und Manely Eslahpazir danken, die durch ihre hervorragenden Studien- und Diplomarbeiten wesentliche Impulse gegeben haben. Marco Terzer von der ETH Zürich danke ich für die Bereitstellung des Algorithmus zur metabolischen Netzwerkanalyse. Ilona Biegler aus dem Institut für Mikrobiologie danke ich für die Ratschläge zur statistischen Analyse während der letzten Monate dieser Arbeit.
Des Weiteren gilt mein großer Dank Thomas Reichel und Matthias Gehder für die administrative Unterstützung.
Den studentischen Mitarbeitern Greta Gronau, Nadine Kallweit, Yvonne Gallenmüller und Sebastian Niedenführ danke ich herzlich für die tolle Unterstützung in Labor- und Computerarbeit.
Auch möchte ich mich bei meinen Freunden Ivonne und Sven Otto, meinen Schwiegereltern Martina und Rüdiger Schwerin, Familie Dounia, Familie Münch, Familie Malzahn, sowie bei Antje und Willm Heyken bedanken, die meiner Familie und mir stets zur Seite standen, tatkräftig unterstützt haben und für die schöne und zugleich erforderliche Abwechslung sorgten.
Last but not least, gilt mein großer und besonderer Dank meinen Eltern und meinen Geschwistern, ohne die das Studium und die Doktorarbeit niemals möglich geworden wären. Sie haben immer an mich geglaubt, mich fortwährend unterstützt und mit Ihrem Interesse an der Arbeit mich mit Motivation versorgt.
Ohne die grenzenlose und uneingeschränkte Unterstützung meiner Frau könnte ich nicht in der Position sein in der ich jetzt glücklicherweise bin. Sie war immer für mich da und hat gemeinsam mit meinem Sohn Leopold meine innere Ausgeglichenheit und Stärke aufgebaut und gefestigt, die ich während meiner Arbeit so dringend brauchte.

Scientific Publication

Partial results from this work have been published in advance in the following scientific contributions. This was authorized by the Department of Mechanical Engineering represented by Prof. Dr. Christoph Wittmann and Prof. Dr.-Ing. Dietmar Hempel:

Peer-reviewed Journals

Melzer G, Eslahpazir M, Franco-Lara E, Wittmann C (2009) Flux Design: *In silico* design of cell factories based on correlation of pathway fluxes to desired properties. *BMC Systems Biology*, 3: 120.

Melzer G, Dalpiaz A, Grote A, Kucklick M, Göcke Y, Jonas R, Dersch P, Franco-Lara E, Nörtemann B, Hempel DC (2007) Metabolic flux analysis using stoichiometric models for *Aspergillus niger* – Comparison under glucoamylase-producing and non-producing conditions. J Biotechnol. 132: 405-417.

Peer-reviewed Monographs

Melzer G, Dalpiaz A, Göcke Y, Grote A, Kucklick M, Franco-Lara E, Dersch P, Nörtemann B, Hempel DC (2007) Metabolic flux analysis of glucoamylase-producing fungus *Aspergillus niger* AB1.13 cultivations. IFAC-CAB Monographien. Michel Perrier und Jaime Moreno (Hrsg.) Vol. II: 339-344.

Conference Proceedings

Melzer G, Eslahpazir M, Franco-Lara E, Nörtemann B, Hempel DC, Wittmann C (2009) Advanced *in silico* analysis of *Aspergillus niger* for optimization of fructofuranosidase production. New Biotechnology. Abstracts of the 14th European Congress on Biotechnology Barcelona, Spain 13-16 September, 2009 25: S357.

Melzer, G, Eslahpazir, M, Franco-Lara, E, Nörtemann, B, Hempel, DC, Wittmann, C (2009) Elementary mode analysis of the *Aspergillus niger* metabolic network for optimization of recombinant sucrase production. Chem. Eng. Tech. 81: 1253.

Lectures

Melzer G, Eslahpazir M, Franco-Lara E, Nörtemann B, Hempel DC, Wittmann C (2009) Elementary mode analysis of the *Aspergillus niger* metabolic network for optimization of recombinant sucrase production. 27. DECHEMA Jahrestagung der Biotechnologen, 08. – 10. September, Mannheim, Deutschland

Melzer G, Eslahpazir M, Dalpiaz A, Kucklick M, Nörtemann B, Jahn D, Hempel DC, Franco-Lara E (2008) Elementarmodi bei *Aspergillus niger*: Wege zur Proteinproduktion. GVC/Dechema Vortrags- und Diskussionstagung: Modellierung - Von der Zelle zum Prozess, 28. – 30. April, Bremen, Deutschland

Melzer G, Dalpiaz A, Göcke Y, Grote A, Kucklick M, Franco-Lara E, Dersch P, Nörtemann B, Hempel DC (2007) Metabolic flux analysis of glucoamylase-producing fungus *Aspergillus niger* AB1.13 cultivations. European Bioperspectives, 30th May – 1st June, Cologne, Germany

Melzer G, Dalpiaz A, Göcke Y, Grote A, Kucklick M, Franco-Lara E, Dersch P, Nörtemann B, Hempel DC (2007) Metabolic flux analysis of glucoamylase-producing fungus *Aspergillus niger* AB1.13 cultivations. 10th International IFAC-Symposium on Computer Applications in Biotechnology, Cancun, Mexiko

Posters

Melzer G, Eslahpazir M, Franco-Lara E, Nörtemann B, Hempel DC, Wittmann C (2009) Advanced *in silico* analysis of *Aspergillus niger* metabolic network for optimization of the fructofuranosidase production. 14th European congress on biotechnology, September 13 – 16, Barcelona, Spain

Melzer G, Eslahpazir M, Nörtemann B, Hempel DC, Wittmann C, Franco-Lara E (2008) Quantification and analysis of *Aspergillus niger* metabolic network via nullspace approach. 9th International Conference on Systems Biology, August 22 – 26, Gothenburg, Sweden.

Table of Contents

1 Abstract

In the present work, a systems biology approach is presented, which enables the prediction of potential genetic targets and optimal pathways for protein production within a metabolic network, and thus, makes an important contribution to the rational strain optimization of micro-organisms. For this, elementary flux modes analysis was carried out using a metabolic model of *Aspergillus niger*, which was condensed from the genome based metabolic model. Hereby, a new approach was developed for the design of cell factories by the analysis of metabolic flux correlations between metabolic enzymes. This allowed the *in silico* prediction of deletion and amplification targets and thus provides an important prerequisite for rational strain optimization.

The network analysis was carried out using various target products under varying nutrient conditions. The approach revealed that the success of identification of genetic targets depends on the differentiation of biological states, the growth-associated or non-growth associated production of the target proteins. Only a few targets, such as the pathways of protein glycosylation and protein biosynthesis can be identified as independent of the biological state. The growth-associated targets include inter alia the pentose-phosphate pathway (amplification target) and the reactions of the tricarboxylic acid cycle (attenuation target). The results of this systems biology approach could be validated by enzyme kinetic studies and analyses of intracellular metabolic fluxes using metabolite balancing and continuous cultivations. In addition, metabolic networks of several industrially relevant hosts were investigated using this *in silico* approach and essential differences were elaborated. Comparisons with experimental studies for rational strain optimization of *Corynebacterium glutamicum* for lysine production support the applicability of this novel *in silico* approach.

2 Zusammenfassung

In der vorliegenden Arbeit wird ein systembiologischer Ansatz vorgestellt, der mit Hilfe von Computersimulationen potentielle genetische Targets und optimale metabolische Wege zur Proteinproduktion in metabolischen Netzwerken vorhersagt, und somit einen wichtigen Beitrag zur rationalen Stammoptimierung von Mikroorganismen liefert. Hierfür wurde für *Aspergillus niger* ein auf dem annotierten Genom basierendes metabolisches Modell des zentralen Kohlenstoffmetabolismus konstruiert, mit dem Elementarmoden-Analysen durchgeführt wurden. Durch Analyse von Korrelationen von Stoffflüssen zwischen Stoffwechselenzymen konnte hierbei ein neuer Ansatz zum Design von Zellfabriken entwickelt werden, der erstmals die *in silico* Vorhersage von Deletions- und Amplifikationstargets ermöglicht und damit eine wichtige Voraussetzung zur rationalen Stammoptimierung liefert. Die simulierte Produktion verschiedener Zielprodukte unter variierenden Medienbedingungen ergab, dass für die Identifizierung von Targets die Unterscheidung biologischer Zustände - die wachstumsassoziierte und wachstumsunabhängige Produktion - wichtig ist. Zu den vom metabolischen Zustand unabhängigen Targets zählen ausschließlich die biochemischen Wege der Protein-Glykosylierung und der Produktbiosynthese. Zu den wachstumsassoziierten Targets gehören unter anderen der Pentose-Phosphat Weg (Amplifikationstargets) und die Reaktionen des Citratzyklus (Attenuationstargets). Die Ergebnisse dieses systembiologischen Ansatzes konnten durch enzymkinetische Studien und Analysen der intrazellulären metabolischen Stoffflüsse mittels Metaboliten-Bilanzierung und kontinuierlicher Kultivierungen validiert werden. Des Weiteren wurden die *in silico* Analysen auf verschiedene industriell relevante Wirtssysteme angewendet und wesentliche Unterschiede im Hinblick auf die genetischen Targets herausgearbeitet. Vergleiche mit experimentellen Arbeiten aus der rationalen Stammentwicklung von *Corynebacterium glutamicum* zur Lysin-Produktion unterstützen die Anwendbarkeit dieser neuen *in silico* Analyse.

3 Introduction

3.1 General Introduction

Efficient protein production in *Aspergillus niger* requests for superior production strains, whereby metabolic engineering is a powerful strategy for targeted manipulation of the underlying biochemical pathways [1]. In particular, this requires the identification of genetic targets which should be either deleted or amplified to obtain the desired increase of protein production. However, the still limited knowledge on the underlying complex metabolic network and the resulting lack of appropriate strategies to identify genetic targets makes this optimization a difficult task. In this regard, recent studies on *A. niger* including experimental 'omics technologies display important contributions towards systems-oriented understanding of its complex metabolic processes [2-5]. Generally, modelling approaches applying flux balance analysis, metabolic flux analysis, metabolic control analysis or biochemical systems theory became also very popular in the past time and are still of high interest in relevant studies of the metabolic network of *A. niger* [6-10].

Since recent advances in sequencing and bioinformatical technologies [11] the reconstruction of cellular metabolism of many organisms based on information encoded in their genomes have expanded enormously [12-14]. Beyond that, the annotated genome of *A. niger* [15] has enabled the reconstruction of a genome scale metabolic network [2].

This provides the basis for a more systems-oriented investigation of the cellular metabolism of *A. niger* accounting for the high complexity of its metabolic network and selecting promising genes out of many possible candidates. In this regard, the bi-level optimization frameworks OptKnock [16] and OptStrain [17], or the design of deletion strains by prediction of optimum theoretical yield [18] display efficient gene deletion strategies that lead to overproduction of chemicals in microbial systems. They do, however, not provide the prediction of genes to be amplified for superior performance. This rather important information on potential amplification targets can be obtained from ^{13}C metabolic flux analysis [19] as demonstrated successfully for lysine producing *Corynebacterium glutamicum* [20, 21].

However, as in the latter case, such experimental approaches require the availability of appropriate mutants, which can be linked to increased experimental effort, and might not give access to all potentially interesting gene candidates. Additionally, efficient *in silico* methods for simultaneous genome-scale identification of targets to be amplified or deleted are still lacking.

3.2 Objectives of the Thesis

The objectives of the thesis included the development of a modeling framework to exploit the rich information on the genome of *A. niger*, one of the major industrial working horses. For this purpose, a metabolic network should be first constructed from available information extracted from genome scale information, literature data and *in vitro* enzyme studies.
Based on this, *in silico* analysis of the network by the elementary flux mode calculation should be carried out to provide new insights into the metabolic network behaviour. This should consider various nutrient conditions and different relevant products as a basis for new optimization strategies (Figure 1). Based on the simulation results, a new approach could utilize the correlation of pathway fluxes to desired properties of the organism to propose efficient *in silico* design strategies. This novel approach was developed and applied to the industrial cell factories *A. niger* and *C. glutamicum*. Continuous cultivations of *A. niger* were analyzed using stoichiometric flux analysis under varied environmental conditions, to contribute to the validation of the *in silico* approach.

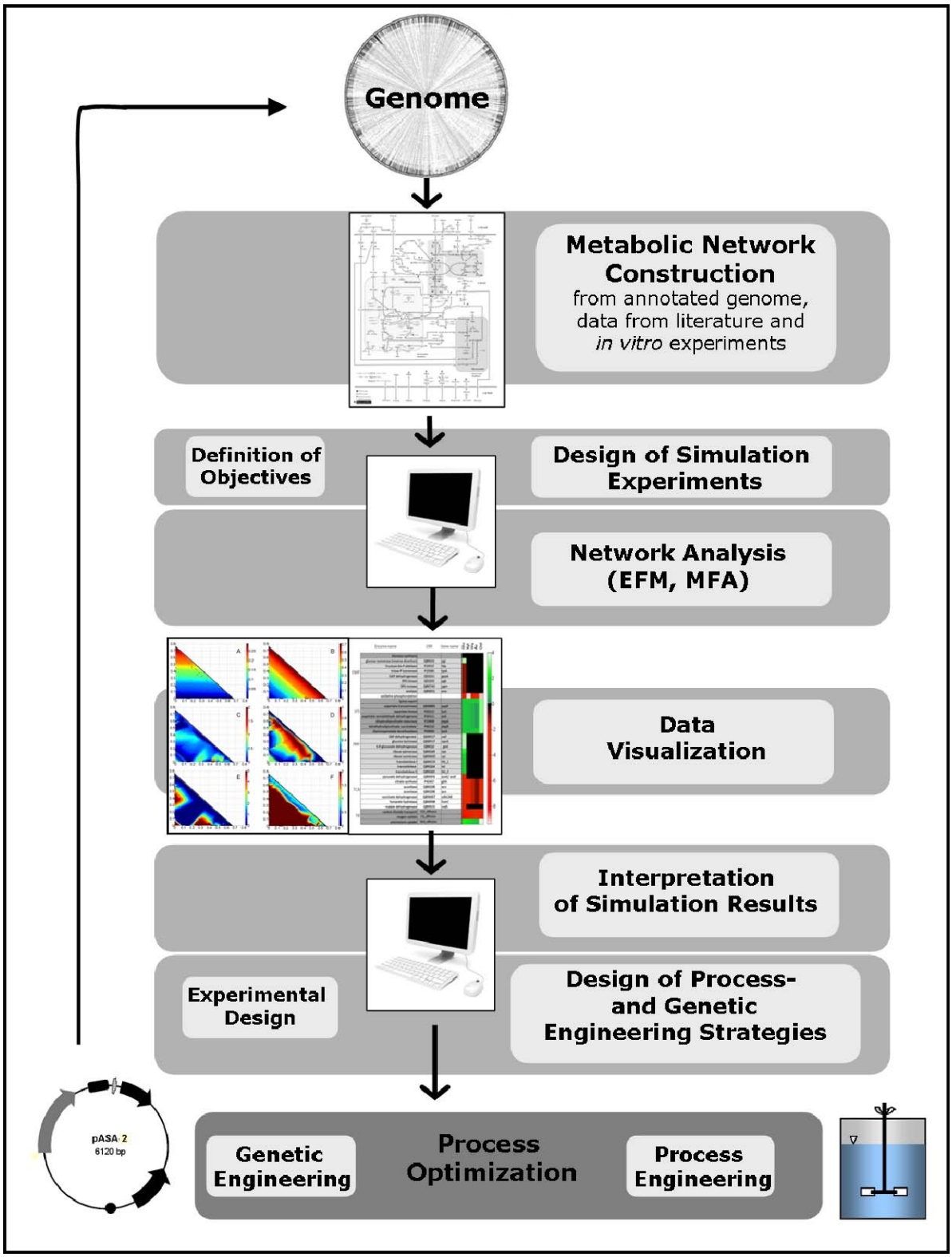

Figure 1: Flow chart visualizing the link between the structure of a metabolic network and the development of process optimization strategies. Abbreviations: MFA: Metabolic Flux Analysis, EFM: Elementary Flux Mode Analysis.

4 Theoretical Background

4.1 Systems Biology

A central goal of systems biology is the understanding of complex biological processes. Beyond exploring the molecular basis of individual reaction pathways, including their mathematical relationships, to comprehensive understanding of functional relationships between parts of the whole cell and more complex systems [22] can be modelled and simulated.

For this, the interactions at a molecular level in the cell, which are causally determined by the environment are investigated by attribution to their underlying processes [23, 24]. Computer simulations, here, provide a tool for understanding of functionality of cellular processes by linking the observed cellular components into functional network operation. This concept was already used in the seventies, where mathematical models were used to describe the complex reaction systems of ethanol production in yeast [25].

A crucial impetus of the enormous progress in recent years was the rapid technical development in modern 'omics technologies such as genomics [26, 27], high throughput metabolomics [28-30], proteomics including RNA-, DNA- and protein microarrays [31-33], high-resolution 2-D gel electrophoresis [34], GC- and LC-MS [35, 36] and fluxomics [19, 37]. Alongside the technical developments, considerable efforts have been made in the mathematical systems biology which includes large collaborative efforts [38].

4.2 *Aspergillus niger* – an Efficient Industrial Host

4.2.1 Biotechnological relevance and application

Aspergillus niger (black mold) is an ubiquitous soil fungus. It has gained high industrial importance for many decades and is one of the most important filamentous fungi used for

biotechnological purposes. *A. niger* has been utilized in industrial fermentations for more than 80 years because of its ability to accumulate and secrete large quantities of metabolites, such as organic acids [39-42], and large amounts of heterologous and homologous proteins [43, 44]. *A. niger* is most suited for producing industrially relevant food-enzymes, such as glucoamylase, chymosine [45-47] or highly glycosylated proteins, such as the β-fructofuranosidase [48]. The production of epoxide hydrolases by *A. niger* provide an important biocatalyst for the synthesis of chiral building blocks for the pharmaceutical, fine and specialty chemical industry [49, 50]. Since the organism is considered to be safe for human health [51], recent efforts to utilize *A. niger* for the production of pharmaceutically relevant heterologous proteins and antibodies have been increased [52, 53].

4.2.2 Genome

Currently, three strains of *Aspergillus niger* have been sequenced. Two of the strains, ATCC 9029 and ATCC 1015 are wild type strains, while *A. niger* ATCC 22343 (CBS 513.88) was isolated after mutagenesis and selection for improved glucoamylase secretion [54]. Most recently, in 2005, the genome of *A. niger* ATCC 1015, a wild type, historic strain was used in research that resulted in the first patented citric acid process that was accepted for sequencing through the US Department of Energy (DOE). Organisms accepted by this program are sequenced by the DOE's Joint Genome Institute (JGI). Another wild type *A. niger* strain, ATCC 9029, was sequenced by Integrated Genomics, an US based company. Finally, ATCC 22343 was sequenced by a Netherlands based company, DSM [15]. Size of the genome and corresponding data between different *A. niger* strains are listed in Table.

Table 1: Genome statistics for *A. niger* ATCC 1015 and ATCC 22343.

	ATCC 1015	ATCC 22343
Chromosomes	8	8
Genes predicted	11,200	14,165
Genome size [MB]	34.85	33.9
Gene length [bp]	1696.1	1572
Transcript length [bp]	1501.3	439.9
Protein length [aa]	484.3	439.9

4.2.3 Carbon core metabolism

A. niger belongs to the filamentous fungi. Its tubular cells, called hyphae, are divided into separate compartments by septa. These contain septal pores providing a connection that allows adjacent cellular compartments to cooperate and coordinate their activities.
Soluble carbohydrates enter the cell by active transport across the fungal membrane. For the saprophytic *A. niger* most carbon in the environment is present as a complex polymer like cellulose, chitin or lignin. Thus it has a wide set of extra-cellular enzymes including cellulases, chitinases, proteases and multi-component lignin degrading enzymes [55-57].
A. niger assimilates nitrogen sources like ammonia and nitrate or amino acids by direct uptake across the hyphal membrane. Moreover, *Aspergillus* is capable to secret many types of secondary metabolites [58] or organic acids [59, 60]. Since the subsequent catabolic pathways are described in detail in relevant literature [61], the chapter highlights the most relevant metabolic pathways implemented in the performed studies.

4.2.3.1 Substrate assimilation and catabolic break down

Mono-saccharides are actively transported into the cell by the MSTA proton symport system, while polyols and fatty acids can be easily transported via the hydrophobic membrane by diffusion [62]. After activation by hexokinases, the phosphorylated sugars are metabolized via the Embden-Meyerhof-Parnas (EMP) pathway, the Pentose-Phosphate pathway (PPP) as well as the 2-keto-3-deoxy-phosphogluconate (KDPG) pathway, whereby the latter pathways play an important role in bacteria, e.g. *Pseudomonas* sp. and *E. coli*, and are absent in *Aspergillus* (Figure 2).

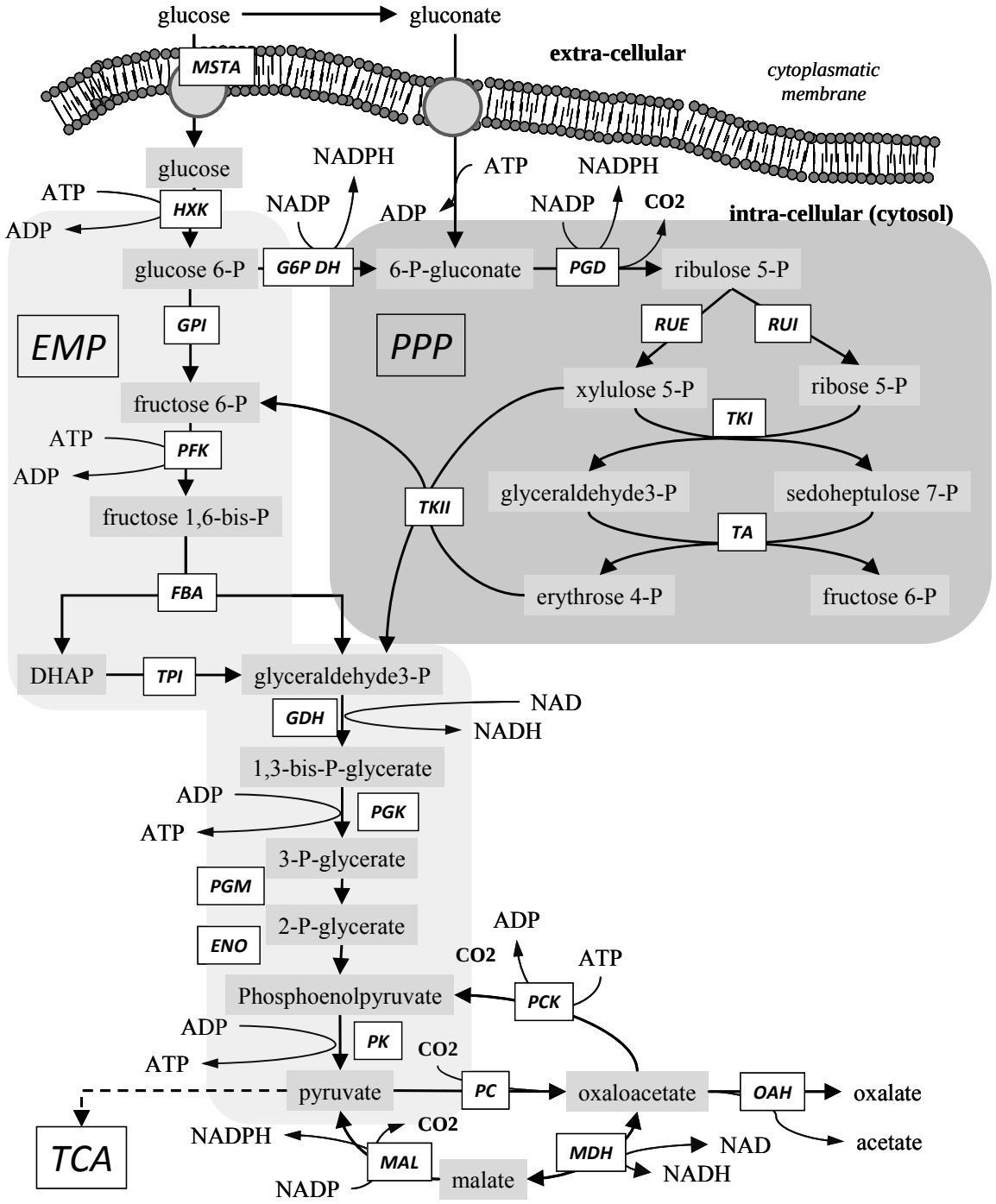

Figure 2: Central carbon metabolism in *A. niger* displaying reactions of glycolysis, pentose-phosphate pathway and anaplerosis involved in glucose degradation. EMP: Embden-Meyerhof-Parnas Pathway (glycolysis), ENO: enolase, FBA: fructose bis-phosphate aldolase, GDH: glyceraldehydes dehydrogenase, GPI: glucose 6-phosphate isomerase, HXK: hexokinase, MAL: malic enzyme, MDH: malate dehydrogenase, OAH: oxaloacetate hydrolase, PC: pyruvate carboxylase, PCK: PEP-carboxykinase, PFK: phosphofructokinase, PGD: phosphogluconate dehydrogenase, PGK: phospho-glycerate kinase, PGM: phospho-glycerate mutase, PK: pyruvate kinase, PPP: Pentose-Phosphate Pathway, RUE: ribulose 5-phosphate epimerase, RUI: ribulose 5-phosphate isomerase, TA: transaldolase, TKI: transketolase I, TKII: transketolase II, TPI: triose phosphate isomerase.

The entry of the pentose xylose occurs via the non-oxidative part of the PPP. In fungi, xylose is reduced by xylose reductase (XR), which accepts both, NADPH and NADH as cofactor. Xylitol is exported out of the cell via diffusion, if it is not further oxidized to xylulose by xylitol dehydrogenase (XDH). The product of the catabolic pathway of xylose is xylulose 5-phosphate formed at the expense of one ATP, which is catalyzed by xylulokinase (XK) (Figure 3).

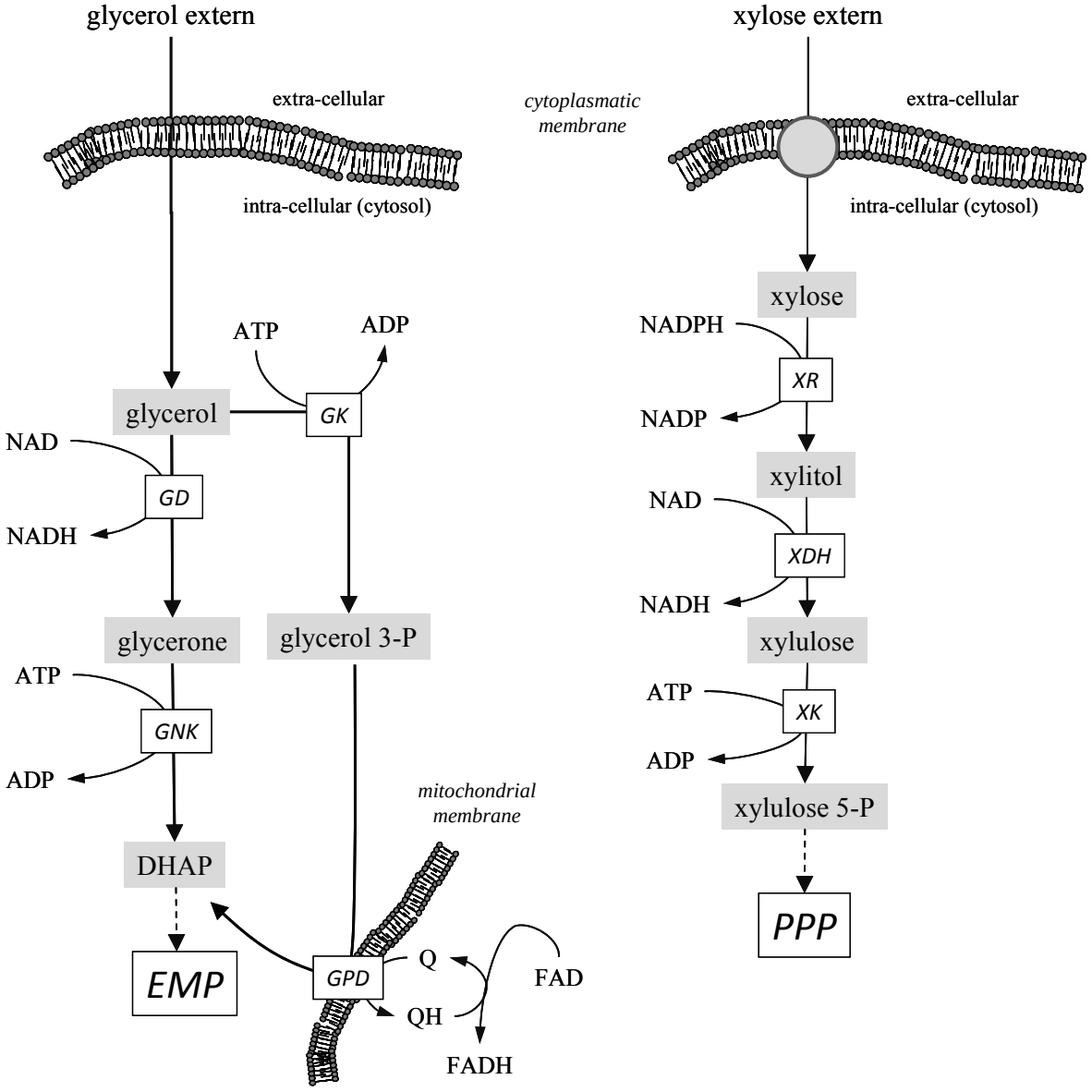

Figure 3: Schematical presentation of glycerol and xylose uptake in *A. niger*. DHAP: dihydroxyacetone phosphate, EMP: Embden-Meyerhof-Parnas Pathway (glycolysis), GD: glycerol dehydrogenase, GK: glycerol kinase, GPD: glycerol phosphate dehydrogenase, GNK: glycerone kinase, PPP: pentose-phosphate pathway, Q: Ubiquinone, XDH: xylulose dehydrogenase, XK: xylulose kinase, XR: xylose reductase.

Glycerol can pass the glycolysis via two different ways. First, it can be phosphorylated to glycerol 3-phosphate and then oxidized via a glycerol phosphate dehydrogenase which is localized in the mitochondrial membrane. Alternatively, it can also be oxidized by the glycerol dehydrogenase before phosphorylated by the glycerone kinase. In both cases, the uptake of glycerol leads to the formation of dihydroxyacetone phosphate, which is passed into the glycolysis (EMP) (Figure 3).

4.2.3.2 Supply of reducing power

NADPH is an essential cofactor for anabolic metabolism. In fungi, NADPH is generated in the oxidative part of the PPP involving glucose 6-phosphate and 6-phosphogluconate dehydrogenase (Figure 2). Additionally, oxidation of isocitrate by the NADP-dependent isocitrate dehydrogenase and of malate by decarboxylating malate dehydrogenase (malic enzyme) can also contribute to NADPH supply. Furthermore, a proposed cyclic pathway (Figure 4) in which the interconversion of fructose and mannitol is linked to the transfer of reducing equivalents from NADH to NADPH was discovered in fungi [63].

The mannitol metabolism occurs exclusively in the cytosol of *Aspergillus niger* and plays an important role in preventing oxidative stress and delivering internal carbon storage [64].

The presence of the enzymes of the mannitol cycle has been shown in earlier studies in Deuteromycetes [65], and their presence in *A. niger* could be proven recently [15]. Evidence suggesting its operation as a mechanism for NADPH generation has been obtained in earlier studies using *Alternaria alternata* [63]. In *Aspergillus niger* the enzymes of this mannitol cycle were shown to be localized exclusively in the cytosol. The exact role in terms of NADPH delivery is still not fully understood.

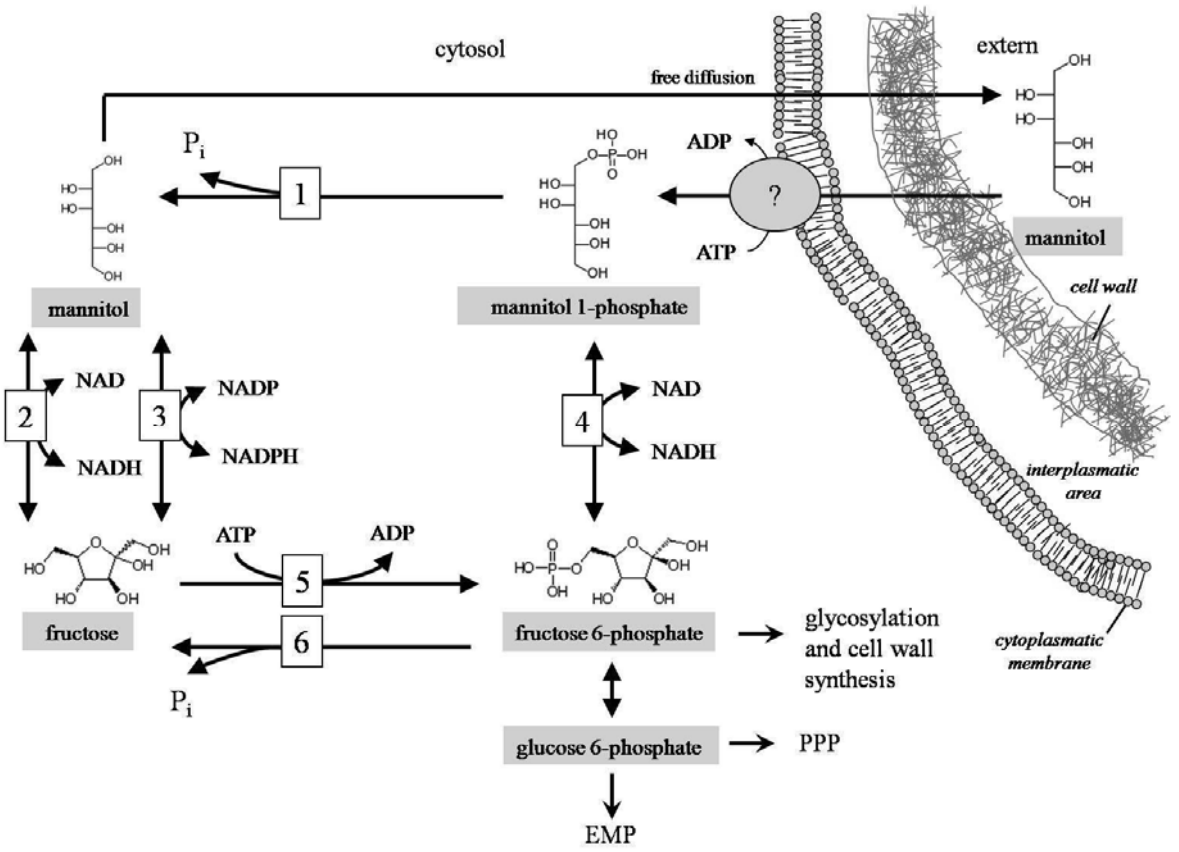

Figure 4: Proposed mannitol cycle in *A. niger*. 1: mannitol phosphatase, 2: NADH dependent mannitol 2-DH, 3: NADPH dependent mannitol 2-DH, 4: mannitol 1-phosphate DH, 5: hexokinase, 6: fructose 6-phosphatase.

4.2.3.3 Tricarboxylic acid cycle and glyoxylate bypass

The tricarboxylic acid cycle (TCA cycle) catalyses the oxidation of carbon to carbondioxide, whereby the electrons are transferred and lead to reduced NADH/ FADH. These are subsequently reoxidized via the electron transport chain leading to the formation of ATP. The TCA cycle intermediates originate from fatty acids (acetyl-CoA), sugars (acetyl-CoA) and amino acids (acetyl-CoA, alpha-ketoglutarate, succinate and ketosuccinate). In fungi, the enzymes of TCA cycle are localized in the lumen of mitochondria.

The glyoxylate bypass is required under conditions of consumption of C2 units, e.g. acetate [66] circumventing the decarboxylating steps of the tricarboxylic acid cycle (Figure 5). Additionally, changes in the activity of isocitrate lyase and malate synthase play also an important role during the initiation of conidiation of *A. niger* suggesting a specific function during germination [67].

In most fungi the enzymes of the glyoxylate cycle, isocitrate lyase and malate synthase, are localized in the matrix of cell organelles termed microbodies [68], or glyoxysomes [69].

They have been observed during the vegetative growth of several filamentous fungi, including *Neurospora crassa* [70], *A. nidulans* [71], *A. fumigates* [72] and are also assumed to be present in *A. niger* [10].

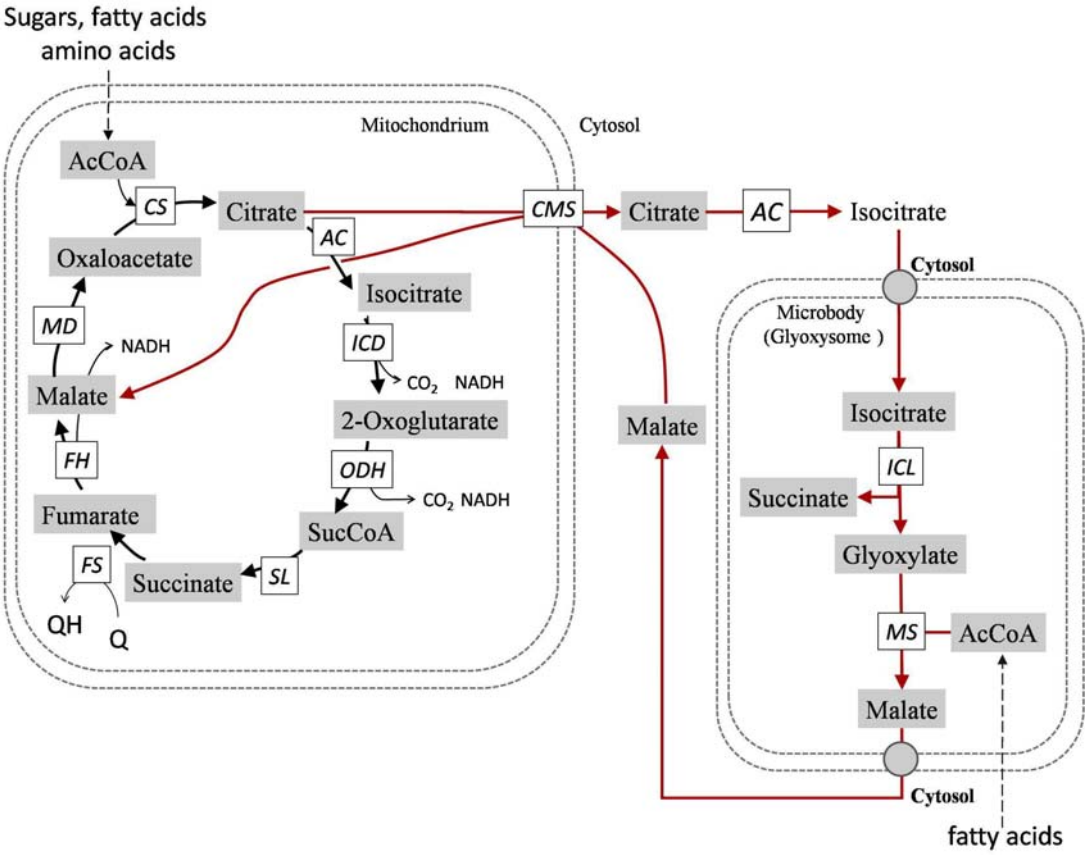

Figure 5: Proposed tricarboxylic acid cycle and glyoxylate cycle (red arrows) in *A. niger*. Enzymes involved are isocitrate lyase (ICL), malate synthase (MS), citrate-malate shuttle (CMS), citrate synthase (CS), cis-aconitase (AC), isocitrate dehydrogenase (ICD), oxo-glutarate dehydrogenase complex (ODH), succinate ligase (SL), fumarate synthase (FS), fumarate hydratase (FH) and malate dehydrogenase (MD).

4.2.4 Anabolism and cell compounds

The biomass composition plays a key role in the modelling approach, because the composition defines the drain of metabolites into the pool of macromolecules of the biomass.

The macromolecule composition of *Aspergillus niger* is shown in Table 2.

Amino acids are the building blocks for proteins which is the most abundant component in the cells. The biosynthetic pathways for all 20 proteinogenic amino acids are elucidated for eukaryotes and prokaryotes [61].

Table 2: Cellular composition considered for determination of the stoichiometric coefficients in biomass model taken from [2, 8].

Biomass components	Content [g/100 $g_{biomass}$]	Stoichiometric coefficients [mmol /$g_{biomass}$]
Protein	40.0	4.299
Carbohydrates	28.0	-------
Glycogen	0.1	0.002
Chitin	7.0	0.408
Glucan	20.8	1.515
DNA	0.8	0.030
RNA	5.3	0.194
Lipids	6.8	0.126
Mannitol	3.3	0.213
Glycerol	0.7	0.090
Ash	7.5	-------

There are only few deviations in the biosynthetic routes between eukaryotes and prokaryotes. The most important is the lysine synthesis. In bacteria and plants, lysine is synthesized via pyruvate and β-aspartic-semialdehyde, whereas in fungi, lysine is synthesized from α-ketoglutarate [61]. An overview of the biosynthetic pathways is schematically given in Table 3.

The major building blocks for the synthesis of storage carbohydrates, e.g. glucan and glycogen is UDP-glucose, which is formed from glucose 1-phosphate.

UDP-N-acetylglucosamine serves as a building block for chitin synthesis in fungi. It is synthesized from fructose 6-phosphate, acetyl-CoA and glutamine, whereby the latter is the amino donor. The overall energetic cost for the synthesis of 1 molecule UDP-N-acetylglucosamine and UDP-glucose is one molecule UTP.

Both molecules are also important precursors for the synthesis of fungal cell wall of fungi. The relative amount of cell wall regarding to the total cell mass of *A. niger* is 0.38 g/g [2], whereby data between 0.4 and 0.6 g/g were obtained for *A. niger* depending on the cultivation conditions, growth state and morphology [74].

Table 3: Overview of amino acid biosynthesis in eukaryotes modified from [73].

Amino acid family	Biosynthesis
Aspartate family	Oxaloacetate → Aspartate → Homoserine → Threonine → Isoleucine; Aspartate → Asparagine; Homoserine → Methionine
Aromatic family	PEP + Erythrose 4-P → Chorismate → Prephenate → Phenylalanine, Tyrosine; Chorismate → Tryptophane
Glutamate family	α-Ketoglutarate → Glutamate → Ornithine → Arginine; Glutamate → Proline; α-Ketoglutarate → Lysine; Glutamate → Glutamine
Histidine family	Ribose 5-P → Histidine
Pyruvate family	Pyruvate → α-Ketoisovalerate → Valine, Leucine
Serine family	3-Phosphoglycerate → Serine → Glycine, Cysteine

Nucleotides in the form of ribonucleotides and deoxyribonucleotides are the building blocks of RNA and DNA, respectively. They are also the constituents of a number of cofactors, e.g. NADH, NADPH, FAD and Coenzyme A, and some nucleotides such as ATP. The precursor molecules for nucleotide synthesis are 3-phosphoglycerate, oxaloacetate and ribose 5-phosphate.

The major building blocks for the lipids are fatty acids, whereas palmitic (C16:0), oleic (C18:1) and linoleic acids (C18:2) account for more than 75 % (w/w) of total in fungi [75]. Saturated fatty acids are synthesized by a successive addition of two carbon units to an activated form of acetyl-CoA. The carbon units are donated by malonyl-CoA, which is formed by carboxylation of acetyl-CoA. Mono-saturated fatty acids in fungi are synthesized by introduction of a double bond at the ninth carbon atom after the C_{16} or C_{18} fatty acids have been synthesized. This is performed by specific enzyme system associated in the endoplasmatic reticulum and the reactions requires oxygen and NADH [75].

4.2.5 Recombinant protein production

Among filamentous fungi, *Aspergillus niger* is important as the major world source of citric acid and higher-value enzyme products including pectinases, proteases, amyloglucosidases, cellulases, hemicellulases and lipases [55].

Bio-catalytic methodologies using enzymes are of high current interest, because of both economic and ecological advantages compared with chemical methodologies, which may lead to enormous amounts of waste if the processes are scaled up. Enzymes are very efficient catalysts because of the 10^8 to 10^{10} fold higher rates compared to non-enzymatic reactions [76]. Enzymes exhibit advantages compared to non-enzymatic reactions, for example, all enzymes are made from L-amino acids and thus are enantioselective (chiral) catalyst. Due to their three-dimensional structure the enzymes can distinguish between different functional groups (chemoselectivity), but also between groups which are situated on different sides of the same substrate molecule (regioselectivity). Furthermore, they can act under mild conditions (pH value 5-8, temperature around 20-40°C) and can catalyze a broad spectrum of reactions [77].

The products of interest in the present work, α–glucoamylase (EC 3.2.1.3), beta-fructofuranosidase (EC 3.2.1.26) and epoxide hydrolase (EC 3.3.2.3) are all provided by *A. niger*, belong to the enzyme class of hydrolases (EC 3.x.x.x). They are attractive due to their versatile biotechnological applications, which will be discussed in the following chapters.

4.2.5.1 Glucoamylase

Glucoamylase is produced by *A. niger* reaching concentrations up to 20 g/L [78]. It is an *exo*-enzyme and is capable of cleaving both α(1-4) and α(1-6) linked glucose units from the non-reducing ends of saccharides, such as starch (Figure 6).

Glucoamylase finds many applications in industry. It is used in dextrose production, in the baking industry, in the brewing of low calorie beer and in whole grain hydrolysis for the alcohol industry. The most important application of glucoamylase is the production of high-glucose syrups with an annual output of over 8 million tons [79].

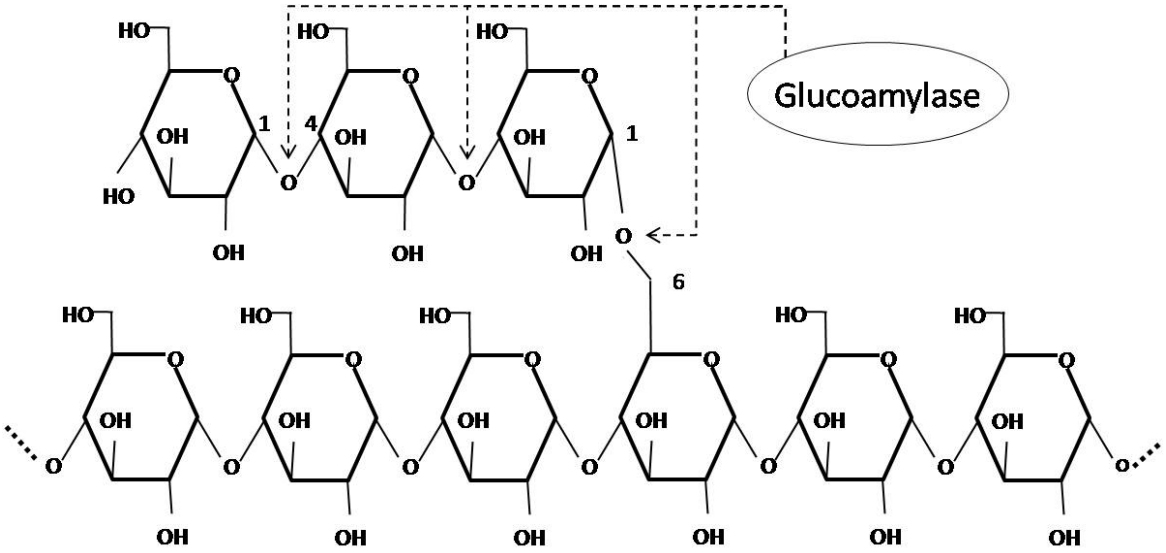

Figure 6: Cleavage sides of starch degrading glucoamylase.

The expression of the gene for glucoamylase is efficiently controlled by the *glaA* promotor, which is widely used for heterologous protein production [80, 81]. This promotor is active if starch, or the degradation products maltodextrine, maltose or glucose are present in the culture medium [82, 83].

4.2.5.2 β-Fructofuranosidase

Three extracellular β-fructofuranosidases Suc1 [84], Suc2 [85] and FopA [86] from different *A. niger* strains are known and have been characterized. The enzymes exhibit two different activities, the hydrolization of sucrose into the monomers glucose and fructose (sucrase activity), and the transfer of a fructose to a sugar molecule, e.g. sucrose, forming fructo-oligosaccharides.

The amino acid sequences of the three enzymes (Suc1, Suc2, FopA) are very similar, but the ratio of the fructosyltransfer/hydrolytic activity appears to be different for each enzyme [87]. On a structural and functional basis in their active sites, fructofuranosidases belong to the GH 32 family and are similar to fructansucrase enzymes such as levansucrase from *Bacillus subtilis* belonging to the glucosyl hydrolase family 68 [88, 89].

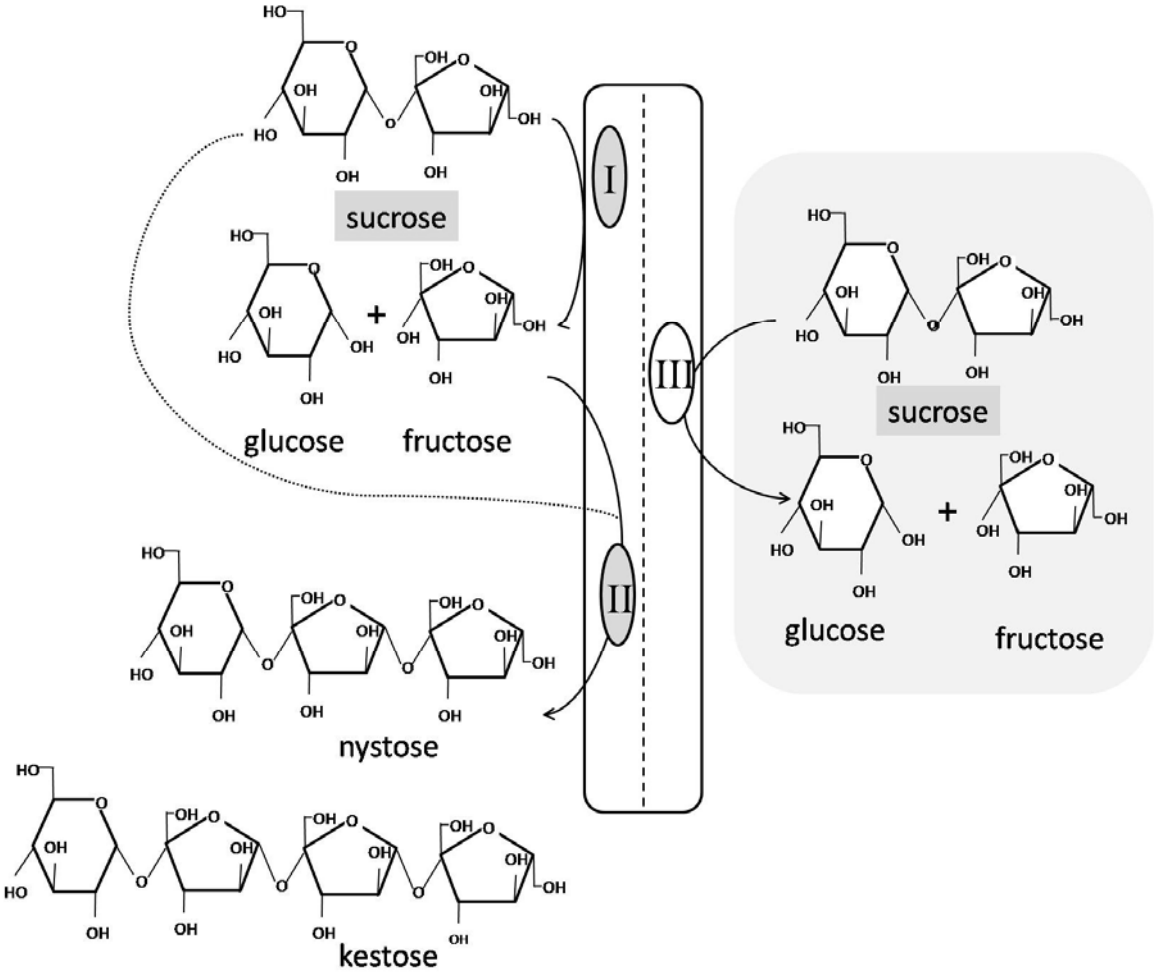

Figure 7: Schematic presentation of fructofuranosidase activity. On the left hand side (I + II), the enzyme with both, the hydrolase activity (I), which is followed by the transferase activity adding a fructose to a sucrose molecule (II) leading to nystose and, after 2 transfer steps, to kestose. On the right hand side, the enzyme is exclusively acting as a sucrase by hydrolyzing sucrose into glucose and fructose (III).

The production of indigestible oligosaccharides from sucrose analogues by the fructofuranosidase from *A. niger* seems promising for the synthesis of commercially attractive fructo-oligosaccharides. These are used since more than 20 years as artificial sweeteners in food [90] and have also a broad application range in the pharmaceutical industry [91]. For this reason, the increasing demand for the fructo-oligosaccharides is in a line with optimized fructofuranosidase production including bioprocess optimization [92] as well as genetic engineering [93].

4.2.5.3 Epoxide Hydrolase

Epoxide hydrolases have been found in all types of living organisms acting as important safeguards against the cytotoxic and genotoxic potential of oxirane derivatives, which are frequent intermediary metabolites during the biotransformation of foreign compounds.

The development of practical biocatalysts is attractive for asymmetric epoxide ring-opening reactions [94, 95]. Epoxide hydrolases are ubiquitous in nature and have been found in bacteria [96], yeasts [97], filamentous fungi [98, 99], plants [100], insects [101, 102], mammals [103, 104] and human tissues [105, 106]. Besides their medical and physiological relevance in human health [107, 108], the utilization of these enzymes for biocatalytic production of pharmaceutical compounds has gained special interest. The preparation of enantiopure epoxides and diols by enzymatic hydrolytic resolution of racemic epoxides is a promising synthesis strategy for chemicals and pharmaceuticals. Bacterial epoxide hydrolases from *Rhodococcus rhodochrous* as well as *Agrobacterium radiobacter* and fungal EHs from *A. niger* are already commercially available as versatile biocatalysts [109]. However, epoxide hydrolases from fungi, in particular *A. niger*, have attracted continued interest because of their high enantio-selectivity and wide range of substrate specificity [110, 111]. Among these fungal enzymes, the epoxide hydrolase from *A. niger* has been investigated in great detail. The soluble epoxide hydrolase (EC 3.3.2.3) from *A. niger* is a highly useful biocatalyst for hydrolytic kinetic resolution of racemic epoxides to give enantiopure building blocks [112] (Figure 8) and can be considered as a very efficient, mild and easy-to-use methodology for cost effective industrial scale processes, e.g. in the application to trifluoromethyl-substituted aromatic epoxides [113, 114]. The advantages in chemoselectivity by using this stable epoxide hydrolase is of much current interest for solving synthetic selectivity problems, e.g. for the epoxide ring-opening selectivity in aqueous environments [115]. For these reasons, considerable efforts in large-scale production of epoxide hydrolase in *A. niger* were developed [49] and will be still of high interest in the future.

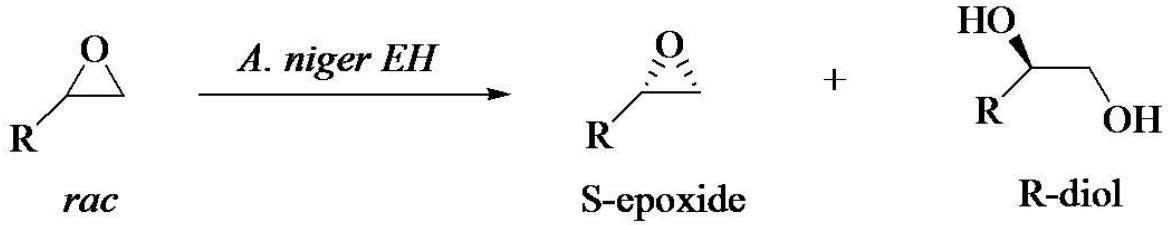

Figure 8: Enzymatic hydrolytic kinetic resolution of racemic (rac) epoxides catalyzed by *A. niger* epoxide hydrolase resulting in the formation of S-epoxide and the R-diol [49].

4.2.6 Metabolic modelling of *A. niger* and their applications

A number of stoichiometric models for *Aspergillus niger* of different complexity have been presented in the last two decades. Hereby the model size is adjusted to the specific modelling task (Table 4).

Table 4: Overview of modelling studies using stoichiometric approaches with *Aspergillus niger*. The corresponding network size is given by the number of metabolites (m) and reactions (q). Abbreviations: MFA: Metabolic Flux Analysis, MCA: Metabolic Control Analysis, BST: Biochemical Systems Theory, FBA: Flux Balance Analysis, EFM: Elementary Flux Analysis, MB: Metabolite Balancing.

Year	Reference	Method	Objective	Network size (m x q)
1994	[7]	Control theory	Kinetic modelling of citrate production	12 x 14
1999	[116]	MFA, (^{13}C)	Isotopomer labelling experiments	40 x 50
2000	[6]	BST, FBA	Optimization of citrate production	18 x 27
2000	[117]	FBA	Influence of knock out of *oah*A gene	n.d. x 40
2003	[8]	FBA	Optimization of succinate production	284 x 335
2003	[118]	MCA	Control analysis of xylose catabolism	10 x 8
2005	[119]	MCA	Control analysis of arabinose catabolism	13 x 8
2007	[9]	MFA (MB)	Optimization of specific growth rate	137 x 187
2007	[120]	MFA (MB)	Influence of external pH and medium on metabolic fluxes	100 x 130
2008	[2]	FBA	Assessing metabolic capabilities	1045 x 1119
2009	[10]	MFA, (^{13}C)	Studies of glyoxylate bypass	25 x 52
2009	[121]	EFM	Optimization of fructofuranosidase production	85 x 100

Small stoichiometric models were presented by Torres [7, 122] to specifically investigate major control steps of citric acid production using kinetic modelling approach [123] based on the Biochemical Systems Theory (BST) [124, 125]. Afterwards, the application of meta-

bolic flux analysis using ^{13}C-labelled glucose with *A. niger* was introduced by Schmidt et al. [116].

Extended stoichiometric models for the central metabolism of *A. niger* have previously been published. First, a metabolic model was introduced for optimization of succinate production by the application of flux balance analysis [8]. Another study of *A. niger* focussed on studying metabolic flux distributions as based on the late model and more literature information, which was used for studying metabolic flux distributions as function of the pH value of the cultivation medium [120].

The most comprehensive metabolic model today based on the genome data includes 1190 reactions and 1045 metabolites [2]. The reaction network of *A. niger* comprises catabolic pathways for 115 different carbon sources and 23 different nitrogen sources.

4.3 Mathematical Modelling of Metabolic Networks

Major tasks of mathematical models in systems biology comprise the integration of experimental data for the derivation of empirical rules and qualitative or quantitative prediction and design of the behaviour of biological systems. Currently there are three major fields of application for the mathematical modelling in systems biology.

The first field utilizes the rapid progress in genome sequencing [11] and performs bioinformatic analysis of genomes for reconstruction of metabolic networks [13, 14, 126]. For this purpose, in particular, statistical methods are applied [127, 128], which also help to uncover functional relationships in experimental high throughput data.

A second field is based on the application of optimization methods. The basic assumption is that molecular interactions are controlled by regulatory mechanisms, which serve the condition that the cell or organism can execute its current function in an optimal way, such as the maximization of growth [129]. This concept has been applied to rather complex systems, where the principle of flux minimization was proposed [130]. Although these optimization approaches are very hypothetical, they provide very useful heuristic statements as a basis for further experiments.

The last area, often called structural modelling [131-133], is used to investigate pathways in a systematic manner. In this way, it can investigate, if a network is functional under certain conditions and which pathways are affected by the failure of a process, e.g. a gene defect

[134]. In contrast to the above mentioned optimization techniques, structural analysis can identify all metabolic flux vectors that exist in a metabolic network without requiring knowledge of fixed flux rates or imposing any objective function for cellular metabolism [135].

In summary, the above mentioned mathematical modelling tools are diverse in their methodologies and have been successfully established in the past. All methods have their respective merits and they all have become an essential part in the field of systems biology.

4.4 Metabolic Network Analysis

4.4.1 Prerequisites

Metabolic network analysis is based on the principle of mass conservation of internal metabolites within a system [136]. Let a cell be a biological system, in which metabolites are transformed into each other by enzyme catalyzed reactions. The sum of these reactions then forms a functional network fulfilling a metabolic function in its entirety [137]. Let further be metabolic reactions transforming metabolites within the system internal reactions with the corresponding internal metabolites, while reactions involving the transport of metabolites in and out of the system are assumed as exchange reactions connecting the corresponding external with the internal metabolites [132]. The general equation to describe the mass conservation dynamics of metabolites in a system of defined volume can be written as

$$\frac{d\underline{c}}{dt} = \underline{\underline{S}}^{T} \cdot \underline{r} - \mu \cdot \underline{c} \qquad \textbf{(4-1)}$$

where $\underline{c}$ is the concentration vector of m internal metabolites, $\underline{r}$ is the reaction rate (flux) vector of k reactions, $\underline{\underline{S}}$ is the stoichiometric matrix with the dimension m×k whose element s_{ij} represents the stoichiometric coefficient of the element i involved in internal reaction j, and μ is the specific growth rate (Figure 9).

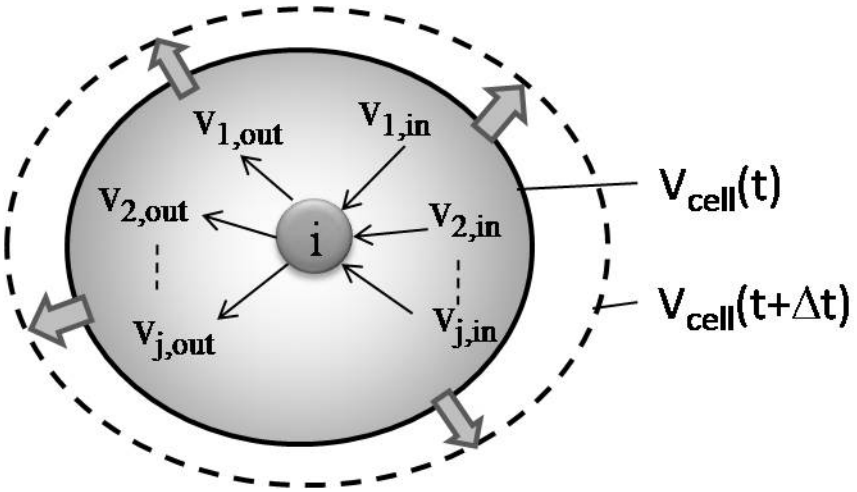

Figure 9: Effects influencing metabolite concentrations in a cell. Exchange fluxes and dilution effect are indicated by the bold grey arrows, which is caused by growth. $V_{cell}(t)$: cell volume at time t; $V_{cell}(t+\Delta t)$: cell volume at time t+Δt.

The product of $\mu \cdot \underline{c}$ is the dilution factor associated with the change in volume of the system. However, the term $\mu \cdot \underline{c}$ can be often be neglected due to low intracellular concentration of metabolites compared to the usually high conversion rates [73, 137]. Steady state conditions presume that the sum of all entering fluxes into a metabolite pool is equal the sum of fluxes leaving the metabolite pool, so that this neither accumulates nor decreases in the cell. Under the assumptions of constant flux and constant intracellular metabolite concentration, the set of linear relationships between the metabolic fluxes can be simplified to:

$$\frac{d\underline{c}}{dt} = \underline{\underline{S}}^{T} \cdot \underline{r} = \underline{0} \qquad \textbf{(4-2)}$$

Due to thermodynamic constraints, reactions have to proceed in the appropriate direction. Some reactions v_i in $\underline{r}$ are irreversible and require additional constraints on positive flux values, that is,

$$v_i \geq 0; \;\; (i \; \forall \; 1, 2, \ldots, q) \qquad \textbf{(4-3)}$$

where q is the total number of irreversible reactions.

4.4.2 Set-up of the stoichiometric matrix

Figure 10 demonstrates the formulation of the stoichiometric matrix for a simple metabolic network. The network consists of six reactions, which are all irreversible. The network includes three internal (A, B, C) and three external (S, P_1, P_2) metabolites. The entries of stoichiometric metabolites are listed in the rows and the fluxes in the columns, respectively. The number of metabolites defines the number of balance equations. External metabolites, e.g. S, P_1, P_2 in Figure 10, are found to exist in an excess in the cell (or out of the cell). For this, they are excluded from the matrix notation. The internal metabolite balances are represented in the rows, whereas the corresponding reactions are positioned in the columns.

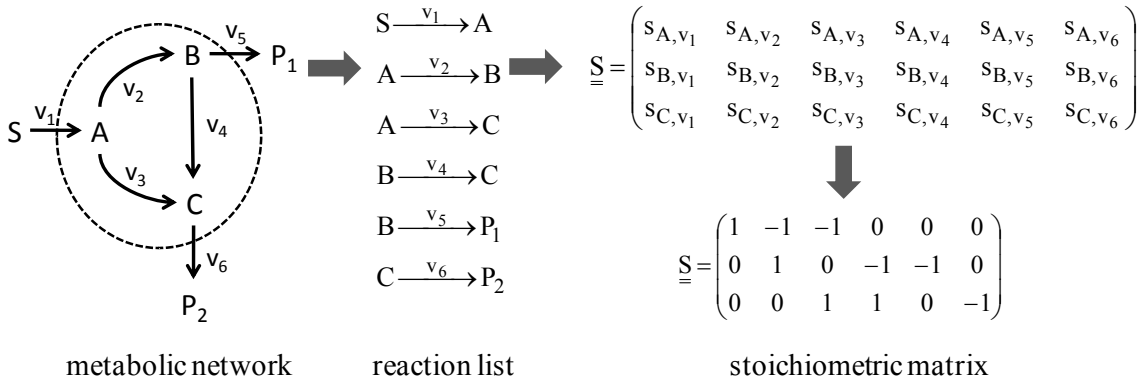

Figure 10: Illustration of stoichiometric matrix formulation from the corresponding simple metabolic network to the matrix notation. Conversion of substrates into metabolites and products leads to the formation of a reaction list, which can be converted to matrix notation including stoichiometric coefficients. The cell including internal metabolites is indicated by the dashed line.

Depending on the experimental objective and the available experimental data set, three main techniques have been proposed to solve the system of linear equation $\underline{\underline{S}}^T \cdot \underline{r} = \underline{0}$ together with the inequality constraints for metabolic flux vector $v_i \geq 0$. These techniques include elementary flux mode analysis, flux balance analysis, and metabolic flux analysis, which are discussed in the next chapters.

4.4.3 Elementary flux mode analysis

Computation algorithms of elementary flux modes are based on two fundamental equations. The metabolic network can be expressed via a matrix $\underline{\underline{S}}$ with dimension dim($\underline{\underline{S}}$) = m x q, namely the stoichiometric matrix, where m is the number of internal metabolites and q is the number of reactions. Under the assumption of the existence of a (quasi)-steady-state metabolism throughout the metabolic network, the first fundamental balancing equation can be written as

$$\underline{\underline{S}} \cdot \underline{r} = \underline{0} \tag{4-4}$$

where $\underline{r}$ represents a flux distribution and is consequently a vector with dimension q x 1. Any (bio)chemical reaction network should fulfill the thermodynamic feasibility constraint, i.e. the following inequality should be valid for all reversible and irreversible reaction rates r:

$$r_i \geq 0, \quad 1 \leq i \leq q \tag{4-5}$$

whereas q represents the number of metabolic reactions. In the case of a metabolic system consisting solely of irreversible reactions, combination of these two fundamental equations will lead to determination of the set of admissible reactions P:

$$P = \left\{ r \in R^q : \underline{\underline{S}} \cdot \underline{r} = 0; r_i \geq 0 \right\} \tag{4-6}$$

The set P is called a pointed polyhedral cone, which is the central core of the computation of elementary modes.

In contrast to linear programming, such as FBA, elementary mode analysis can identify all metabolic flux vectors that exist in a metabolic network without requiring knowledge of any fixed flux rates or imposing any objective function for cellular metabolism [135].
Computation of elementary flux modes allows the calculation of a solution space of all possible independent metabolic pathways in a steady state [132]. Elementary flux modes are thermodynamically and stoichiometrically possible pathways reducing the complex metabo-

lism into all unique, non-decomposable biochemical pathways [131], which simply connect the supplied substrates with the corresponding end products (see Figure 13). Each solution presents an elementary (flux) mode. The non-decomposability constraint ensures that each elementary mode is unique up to a positive scalar factor because removal of any reaction in an elementary mode will automatically disrupt the entire pathway. Therefore, each elementary mode can be defined as an unique minimal set of enzymes (participating reactions) to support steady state operation of a metabolic network with irreversible reactions to proceed in appropriate directions [132]. Such pathway definition provides a rigorous basis for systematic characterization of cellular phenotypes, metabolic network regulation, robustness, and fragility that facilitate understanding of cell physiology and implementation of metabolic engineering strategies [131, 135, 138-140]. It has been applied to different biological systems involving rational design of L-methionine production by *E. coli* and *C. glutamicum* [141] or to the identification of genetically independent pathways in recombinant yeast [142]. Furthermore, the construction of a minimal *E. coli* cell for high yield ethanol production was enabled through predictions of the potential genetic targets using elementary flux mode analysis [18]. However, little work has been dedicated so far towards the analysis of metabolic flux distributions during the expression of heterologous proteins [143].

In the following, a simple example is presented to describe the main principle of the null space method for the calculation of elementary flux modes.

A substrate S and the products P_1 and P_2 are regarded as external metabolites, which can be assumed to exist in excess. The metabolic network consists of six irreversible reactions (v_1, v_2, v_3, v_4, v_5, v_6).

A trivial solution of the equation $\underline{\underline{S}}^T \underline{r} = \underline{0}$ would be obtained if no fluxes, ($\underline{r} = \underline{0}$) occurred within the metabolic reaction network (trivial solution), which would be similar to a thermodynamical equilibrium. However, the non-trivial solution can be obtained by presuming a matrix $\underline{\underline{K}}$,

$$\underline{\underline{S}}\,\underline{\underline{K}} = \underline{\underline{0}} \qquad \textbf{(4-7)}$$

whereas $\underline{\underline{K}}$ (*kernel*) is the null-space of the matrix $\underline{\underline{S}}$ including entries of vectors $\underline{k}$, which represent the relative rates of the reactions exclusively in the corresponding independent pathway.

$$\underline{\underline{K}} = (\underline{k}_1, \underline{k}_2, \underline{k}_3 ..., \underline{k}_n) \qquad \textbf{(4-8)}$$

The kernel basis vectors form the basis space which any flux distribution can be described with via linear combinations of the basis vectors.

Concerning the stoichiometric network with the internal metabolites A, B and C and six irreversible reactions $v_1 - v_6$, the resulting elementary modes are displayed by the red paths.

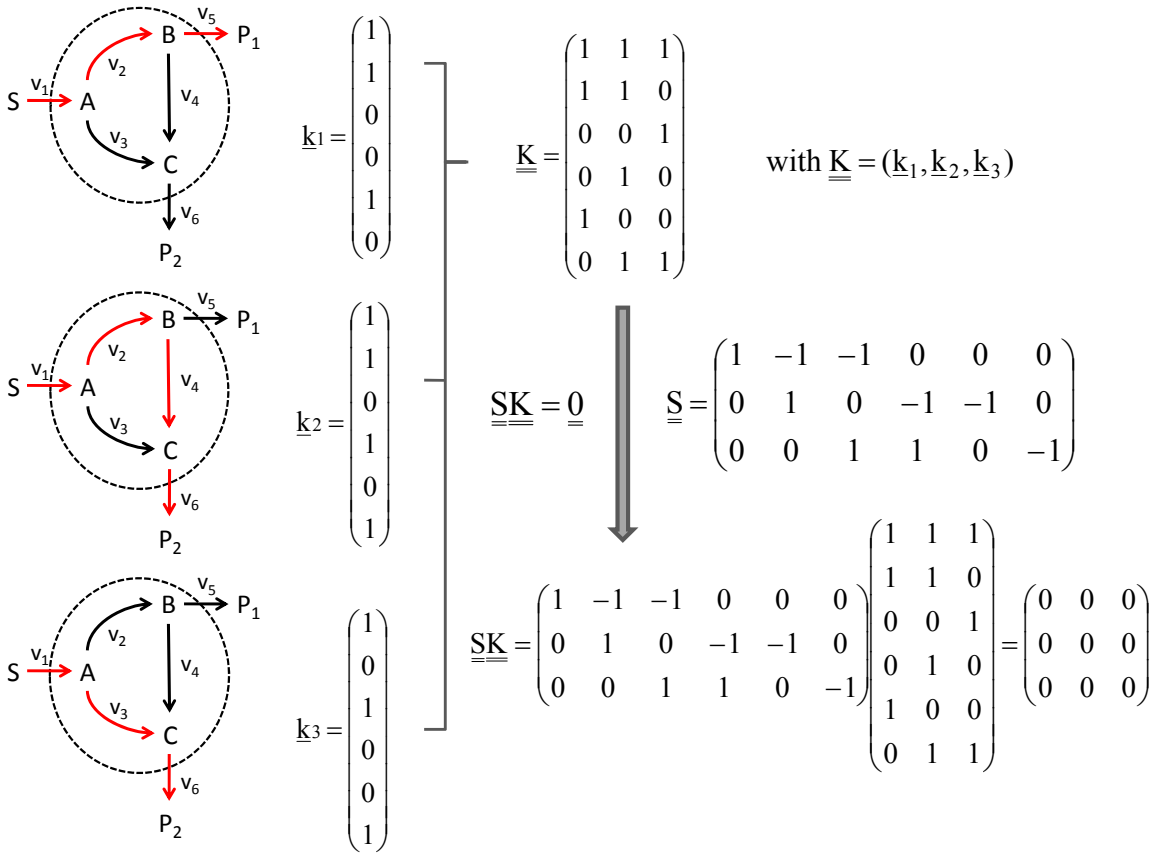

Figure 11: Calculation of elementary flux modes based on the stoichiometric matrix S using the null-space (K) approach. The example network consists of 3 internal metabolites (A, B, C) and the 3 external metabolites S (substrate), P_1 (product 1) and P_2 (product 2) in a biological system indicated by the dashed line. All reactions are irreversible (thermodynamical constraint). The resulting stoichiometric matrix S includes the internal metabolites (rows) and the reactions (columns). One elementary flux mode is indicated by the red arrows connecting the substrate with the corresponding product. The stoichiometric coefficients of the reactions are listed in a vector k. All vectors are comprised to a matrix K, which is the nullspace of S. The product of SK results in the zero-matrix. The vectors are indicated by the underline, the matrices are indicated by the double underline.

4.4.4 Metabolic flux analysis

The quantification of intracellular fluxes is an important aspect of the investigation of metabolic reaction networks. The two common methods analyzing stoichiometric networks are metabolite balancing [144, 145] and the state-of-the-art ^{13}C flux analysis [37, 146]. The basis for both methods is provided by a stoichiometric model that describes the underlying metabolic network. The principles of the labelling methodology are explicitly described [19] and for this not further considered in this section. In general, metabolic flux analysis via balancing relies on extensive extracellular experimental data to increase the number of measurable fluxes such that an un-measurable intra-cellular flux vector can be estimated. It should be noted that metabolic flux analysis computes only a metabolic flux vector $\underline{r}$ for a particular growth condition. A change in measured fluxes $\underline{r}_m$ in different growth conditions will result in a different metabolic flux vector. The method of metabolite balancing was used in this work, whose principle is addressed in the following.

4.4.4.1 Black box elementary balancing

In a first step of metabolic flux analysis, the cell can be regarded as a black box. For this, three assumptions are necessary. The cells are not segregated, which means that the properties of all cells can be regarded as identical. The cellular system is not structured, which means that the cell can be regarded as one component. Balanced cell growth exists, which means that the cell composition does not depend on the development of the cell population. Under these assumptions, the cells can be considered as a black box. Fluxes in and out of the cells are the only variables measured (Figure 12).

The mass and composition of elements that enter the system through the corresponding entering fluxes must be equal to the mass and composition of elements leaving the system by the corresponding leaving fluxes, e.g. product formation. It is necessary that for each element, e.g. C, H, N, O, the elemental mass balance has to be fulfilled.

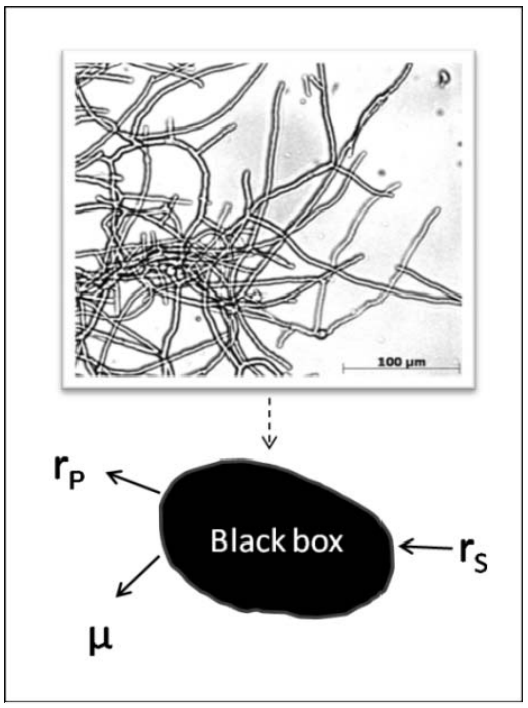

Figure 12: A black box presentation derived from morphological complex cells from *A. niger* (microscopical picture). The fluxes of the substrates are elements of the vector r_s and the fluxes of the products are elements of the vector r_p. The formation of new biomass is represented by the specific growth rate µ.

The balance equation for carbon is exemplified in Equation 4-9, whereas h corresponds to the C-mol content of each molecule i of products (P) and substrates (S) and f are the flux rates entering (S) and leaving the cells (P), whereby biomass itself is a product being its flux represented by µ:

$$\mu + \sum_{i=1}^{M} h_{P,i} \cdot f_{P,i} - \sum_{i=1}^{N} h_{S,i} \cdot f_{S,i} = 0 \qquad \textbf{(4-9)}$$

Elemental balancing can be used for the determination of estimation errors, which is described in detail in chapter 3. In the case that the extra-cellular fluxes have been adjusted in accordance to the results of elemental balancing, the unknown intra-cellular fluxes can now be calculated now by the use of the best estimated extra-cellular fluxes [73].

4.4.4.2 Metabolite balancing

A set of measured extracellular fluxes, typically uptake rates of substrates (carbon source) and production rates of metabolites, such as organic acids, polyols or carbon dioxide as well as the biomass formation is used as the input for the calculations. The intracellular fluxes are finally estimated by applying mass balances of each intra-cellular metabolite. This is based on the pseudo steady-state condition, so that the individual reaction rates correspond to the material flows.

For this, splitting the equation into known or measured rates and unknown rates leads to equation,

$$\underline{\underline{S}}_m^T \underline{r}_m + \underline{\underline{S}}_u^T \underline{r}_u = \underline{0} \qquad \textbf{(4-10)}$$

where the indices *m* and *u* refer to the measured known and unknown rates, respectively. The solution to the vector of unknown rates leads to the following equation:

$$\underline{r}_u = -(\underline{\underline{S}}_u^T)^{-1} \underline{\underline{S}}_m^T \underline{r}_m \qquad \textbf{(4-11)}$$

For an over-determined system, the matrix $\underline{\underline{S}}_u^T$ is not directly invertible and the Moore-Penrose pseudo-inverse is used for calculation (see chapter 3 for more details).

A simple example is illustrated in Figure 13. For this purpose, the metabolic network of the previous chapter (Figure 10) will be taken into account. The metabolite concentration of A, B and C is assumed to be constant, so that the resulting equation system for metabolite balances can be easily obtained as shown in Table 5.

Table 5: Equation system for the description of the metabolic network shown in Figure 13

pool	balance equations
A	$v_1 = v_2 + v_3$
B	$v_2 = v_4 + v_5$
C	$v_3 + v_4 = v_6$

Let the three fluxes, v_1, v_5 and v_6 be measured. Then the result of flux calculation is a metabolic flux map with an estimate of the steady state flux rates (Figure 13).

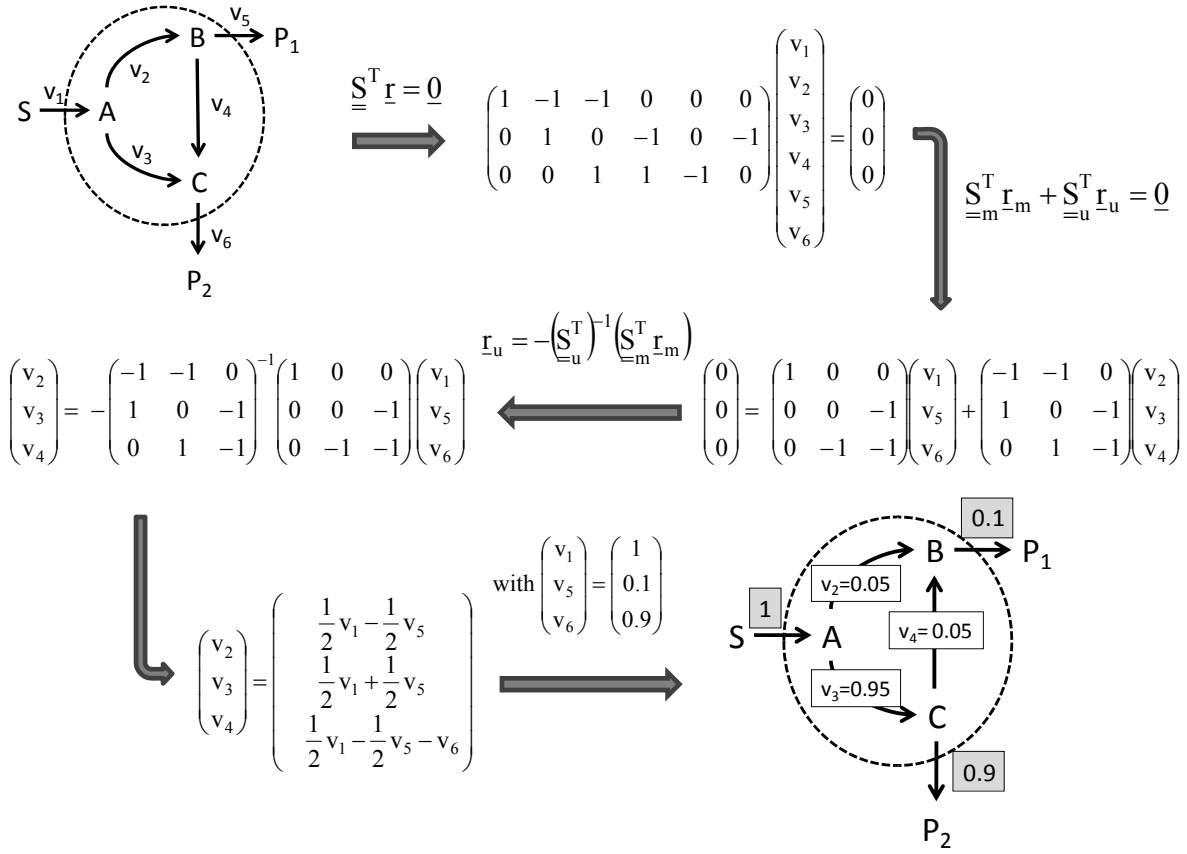

Figure 13: Illustration of the calculation principle of metabolite balancing using a simple metabolic network. S, P1 and P2 represent external metabolites, A, B and C internal/ intra-cellular metabolites. The reaction fluxes v_1=1, v_5=0.1 and v_6=0.9 are known, whereas v_2, v_3 and v_4 are unknown and can now be calculated with this method.

4.4.4.3 Degrees of freedom of the metabolic system

Equation 4-12 can be used to determine the fluxes of a metabolic system. However, it must be first determined whether the system is unique, over- or under-determined. In a unique determined system, the number of equations is exactly the same as the numbers of variables and the matrix has full rank. The rank f is defined as the maximal number of linear independent metabolic reactions within a metabolic system.

$$f = j - k \qquad \textbf{(4-12)}$$

If the degree of freedom f is as large as the number of known fluxes, all unknown fluxes can be estimated by the Equation 4-11.

Whereas under the condition that k equations are linearly independent and thus the rank of the matrix $\underline{\underline{S}}$ is equal to the number of the equations ($f = j = k = 0$). Otherwise, the matrix would be singular and the determinant det ($\underline{\underline{S}}_u$) = 0. In this case it would be an under-determined system.

In the over-determined system, there are more known rates than required. Here, additional measured rates are used to check the consistency of the system. For this, the method of least square deviations is applied and the best estimated rates can be obtained. Also here, the Moore-Penrose inverse is used to solve the Equation 4-11 (see chapter 5 for more details).

4.4.5 Flux balance analysis

Flux balance analysis (FBA) is a method to determine a metabolic flux vector $\underline{r}$ of a cellular physiological state when the knowledge of $\underline{r}_m$ is limited and $\underline{S}_u$ cannot be inverted to provide a unique solution.

It is based on convex analysis of the metabolic network structure by imposing an objective function to determine the metabolic flux vector [147] subject to several constraints such as substrate uptake rates and/or product secretion rates, thermodynamic constraints, metabolic regulation, and more.

The key of this approach is to figure out which objective functions are most likely represent the cellular metabolism for a given growth condition [148].

Linear programming, such as flux balance analysis, provides only a single solution to an optimization problem while alternative optima or also interesting suboptimal solutions cannot be obtained [134].

In general, flux balance analysis can estimate metabolic flux vectors based on limited experimental data. It requires specification of objective functions for cellular metabolism. The more fluxes can be measured, the more accurately the flux vector can be computationally determined.

This approach depends very much on the validity that the formulated objective function correctly represents the working system.

4.4.6 Rational strain optimization in practice

To date strain improvement of *A. niger*, e.g. phytase production, has depended largely on random mutagenesis and selection techniques [149]. However, development of a new generation of high production strains with this approach often takes 5 years or more [150]. In the past few years, techniques for molecular genetics have become increasingly sophisticated. Progress in genetics, transcriptional analysis, proteomics, metabolic reconstructions and metabolic flux analysis offer genetic engineering as an alternative approach for strain improvement in a targeted manner [151]. For example, insertion of specific genes thought to be involved as rate limiting steps can be achieved by inserting the desired gene(s) into a chromosome by homologous recombination or by site-specific integration [152]. Furthermore, disruption of negative regulatory genes or increased expression of positive regulatory genes [152] as well as the inactivation of pathways that compete for key precursors, intermediates, cofactors and energy supply [153] can result in elevated production of desired products. However, targeted genetic modification of the production strains is to a large extent still based on trial and error linked to high development times. A crucial impetus is the identification of the most relevant targets for improvement desired properties. All these become more and more accessible due to the rapid progress in 'omics technologies for global strain characterization, but still require high experimental effort.

In this regard, the use of *in silico* tools appears attractive to obtain key information about the underlying metabolism minimizing time and effort for rational strain development. Accordingly, computational tools which are based on analysis of metabolic network structures provide elegant approaches for analyzes and design of superior cell factories.

As example, optimization-based frameworks to predict genetic modifications to maximize the secretion of biochemicals have been recently introduced [154]. Additionally, the bi-level computational frameworks OptKnock [16] and OptStrain [17] display efficient *in silico* algorithms that allow the prediction of promising gene deletion targets towards overproduction of chemicals. This is accomplished by using maximization of biomass yield [144], minimization of metabolic adjustment (MOMA) [155] or other plausible cellular objective to estimate the redirected fluxes in the face of the imposed knock-outs.

However, these approaches do not provide a prediction of genes to be amplified for superior performance and thus, efficient *in silico* methods for simultaneous genome-scale identification of targets are still lacking.

5 Materials and Methods

5.1 Organisms

In this study, the filamentous fungi *Aspergillus niger* AB 1.13 and SKAn1015 were used for the experimental and considered for the modeling part. The strains were derived from the wild type strain NRRL 3. The genesis of the strains is illustrated in Table 6, at which several UV-mutagenesis's finally led to the strain construction of AB 1.13.
The strain *A. niger* AB 1.13 was used for continuous cultivation experiments. It is an uridine auxotrophic, protease deficient and α-glucoamylase producing strain [156] derived by UV-irradiation from *A. niger* AB 4.1 [157].

Table 6: Genesis of *Aspergillus niger* AB 1.13 and SKAn1015 from wild type strain NRRL 3.

***A. niger* strains**	**Method of modification**	**New properties (Reference)**
NRRL 3 (ATCC 9029)	wild type	high gluconic acid producer [158]
N 402	UV-mutagenesis	variant from NRRL 3 with short conidiophores [159]
AB 4.1	UV-mutagenesis	uridine auxothrophy [157]
AB 1.13	UV-mutagenesis	protease aspergillopepsin A and B deficient [156]
SKAn1015	AB 1.13 with integrated *suc1*-gene + plasmid with constitutive *pki*-promotor	sucrase over-production with restored uridine auxotrophy [87]

A. niger SKAn1015 homologously expresses *suc1* encoding fructofuranosidase. The gene was amplified by PCR from chromosomal DNA from AB 1.13 and sub-cloned into the pyrG+ expression vector ANIp8 under the control of the constitutive pyruvate kinase promoter *pki*A in order to overcome endogenous metabolic control systems. The resulting *suc1*+ plasmid pSKAn1015 was transformed into the *pyrG*-, protease-deficient *A. niger* strain AB 1.13. Finally, the resulting strain *A. niger* SKAn1015 harbours the pSKAn1015 plasmid integrated into the genome [87].

5.2 Preparation of Spore Suspension of *A. niger* AB 1.13

Spore stock suspension was stored in 30 % (v/v) glycerol at -80 °C. For the preparation of spore inoculums for the cultivation experiments, spores from stock suspension were streaked onto potato dextrose agar plates (PDA) including 30 g/L potato dextrose and 10 g/L agar (all from Sigma, Germany). After around 4 days of incubation at 30°C on PDA plates, 20 mL of 0.9 % (w/v) NaCl solution were added to each plate and spore suspensions were harvested with a spattle. The spore concentration was then determined at 600 nm with a spectrophotometer (BioRad smartspec 3000, Bio-Rad Laboratories GmbH, Munich, Germany). The suspension was maintained at 4°C for 24 h before used. The inoculum volume of spore suspension was 10 - 20 mL depending on the spore concentration.

5.3 Cultivation Medium

For submerged cultures, modified Vogel's medium [160] was supplemented with 2 mM (0.5 g/L) uridine. The initial concentration of the carbon source glucose was adjusted to 56 mM corresponding to 10 g/L (Table 7).

Table 7: Composition of modified Vogels's medium and corresponding trace element solution

Modified Vogel's medium		**Trace element solution of the Vogel's medium**	
Component	Concentration [g/L]	Component	Concentration [mg/L]
Carbon source	10	citric acid·H_2O	5.0
Uridine	0.5	$ZnSO_4$·7 H_2O	5.0
$(NH_4)_2SO_4$	6.6	$Fe(NH_4)_2(SO_4)_2$·$6H_2O$	1.0
KH_2PO_4	2.5	$CuSO_4$	0.16
$MgSO_4$·$7H_2O$	0.2	H_3BO_3	0.05
$CaCl_2$·H_2O	0.1	Na_2MoO_4·H_2O	0.05
trace element solution	0.1	$MnSO_4$·H_2O	0.037

5.4 Continuous Cultivation Experiments

Continuous cultivation was carried out in a volume of 2.2 litres (Applikon Biotechnology, Schiedam, Netherland) of working volume. This volume was maintained at constant level by removing the effluent from the reactor surface with a peristaltic pump. Concentration of glucose was 10 g/L in initial batch mode and 2 g/L in the feed solution in continuous mode, respectively. Cultivations was performed at a dilution rate of 0.1 h^{-1}. The aeration rate and temperature were maintained constant at 0.5 L/(L·min) and 30°C, respectively. Cultivations were carried out at four different pH values (3, 3.7, 4.7, and 5.5). At each pH, the set-point was controlled by 2 M NaOH or 2 M HCl. The agitation speed was kept constant at 550 min^{-1} using two six-bladed disc turbine impellers. All experiments were performed in biological duplicates.

5.5 Sampling and Sample Processing

10 mL of biomass suspension was collected from the bioreactor in 50 mL pre-cooled (4 °C) 10 mM sodium-acetate buffer (pH 4.5) and immediately filtered and washed twice. The biomass was collected from the filter for further use.

Cell disruption was carried out with lyophilized cells at -20°C. Samples were stored on ice. 100 mg of dried cells were re-suspended in 20 mL 10 mM Tris-HCl at pH 7.5 (4 °C). Cells were centrifuged at 12,000 x g for 5 min, at 4 °C. Each biomass pellet was re-suspended in 20 mL Tris-buffer and disrupted in a mortar mill (RM 100, Retsch GmbH, Haan, Germany) for 30 min in 10 mM Tris-buffer (4 °C, pH 4.5). After disruption, cell suspension and adherent cell residues were thoroughly rinsed with ice-cold 1 M NaCl from the mill pan and collected in a measuring glass. The suspension volume of the disrupted cells was determined and then centrifuged at 4°C, 12,000 x g for 15 min. After centrifugation, the supernatant was collected and immediately used for determination of enzyme activity and protein concentration.

5.6 Analytical Methods

5.6.1 Biomass dry weight

Samples were filtered through pre-weighted cellulose acetate filter, (pore size 0.7 µm), washed twice with 10 mM sodium acetate buffer (pH 4.5) and dried at 105 °C until constant weight.

5.6.2 Off-gas analysis

Carbon dioxide and oxygen concentrations in the gas phase were monitored online at the inlet and outlet of the bioreactor with an infrared CO_2 sensor (BCP-CO_2, BlueSens, Herten, Germany) and an electrochemical oxygen sensor (BCP-O_2, BlueSens, Herten, Germany), respectively. The error of the measurement for the gas composition measurement was ± 3 %.

5.6.3 Protein quantification

Bicinchoninic acid method (BCA)

The cell extracts were diluted to obtain 0.05 - 1 µg/µL protein in an assay tube containing a volume 100 µL. Protein standards containing a range of 0.05 - 1 µg/µL protein (bovine serum albumin) were prepared in tubes containing a volume 100 µL. After addition of 2 mL of working reagent (50:1 reagent A:B, see Pierce^{TM}, Rockford, Il, USA) and incubation at 37°C for 30 min the absorbance at 562 nm was measured (BioRad smartspec 3000, Bio-Rad Laboratories GmbH, Munich, Germany).

Coomassie brilliant blue method (Bradford)

Samples were diluted to obtain between 0.05 and 1 µg/µL protein in one assay tube containing a volume 100 µL. Protein standards contain a range of 5 to 100 µg protein (bovine serum albumin) in a volume of 100 µL. After addition of 5 mL Roti$^{(R)}$ -Quant Coomassie-dye reagent (Roth, Karlsruhe, Germany) the samples were incubated at RT for 5 min. The absorbance was measured at 595 nm (BioRad smartspec 3000, Bio-Rad Laboratories GmbH, Munich, Germany).

5.6.4 Quantification of sugars, organic acids and polyols

The quantification of extra cellular metabolites was carried out using an HPLC system (Elite Lachrome HITACHI Ltd., Japan) under isocratic conditions. A reversed phase column (Metacarb 67H, 250 x 4.6 mm, 5 µm) was used with a mobile phase containing 1 mM H_2SO_4 in bi-distilled water at 70°C and a flow rate of 0.8 mL/min. Detection of sugars (glucose, xylose) and polyols (mannitol, xylitol) using a refractive index detector L-2490. Organic anions (formate, oxalate, acetate, butyrate) were quantified using a UV detector at 210 nm.

5.6.5 Enzyme assays

The enzymic activity of glucoamylase [161], glucose 6-phosphate dehydrogenase [162], isocitrate lyase [163], pyruvate kinase [164], NADP depending and NAD depending mannitol 2-dehydrogenase [165] were determined in the supernatant of cultivation broth and in the crude cell extract.

5.6.5.1 Glucoamylase assay

10 mL of fermentation broth were filtered, and the wet biomass was washed twice with 10 mM sodium-acetate buffer (pH 4.5). The biomass was re-suspended in fresh buffer and disrupted by a mortar mill for 6 min. The activity of glucoamylase in the suspension of disrupted cells was measured by the method of using para-nitro phenyl-alpha-glucopyranoside (pNPG) as substrate. 500 µL of pNPG solution (0.1 % (w/v) in sodium-acetate buffer, pH 4.8) were added to 250 µl of disrupted cells. After incubation for 20 min at 60°C, the enzymic reaction was stopped by adding 750 µL of 0.1 M sodium borate, and after filtration (0.2 µm pore size) the absorption was measured at 400 nm (BioRad smartspec 3000, Bio-Rad Laboratories GmbH, Munich, Germany). One unit of enzyme activity is defined as the amount of enzyme required to release 1 µmol para-nitrophenol per minute at pH 4.8 and 60°C.

5.6.5.2 Glucose 6-phosphate dehydrogenase

The assay was performed by the method of [162]. The reagents used for the reaction mixture are given in (Table 8).

Table 8: Composition of reagents for the glucose 6-phosphate DH assay.

Reagent	Content
A	250 mM glycylglycine buffer, pH 7.4 at 25°C. Prepare 100 mL in deionized water using glycylglycine, free base, (Sigma). Adjust to pH 7.4 at 25°C with 1 M NaOH. It is important to maintain pH 7.4 to ensure reproducibility.
B	60 mM glucose 6-phosphate solution. Prepare 2 ml in deionized water using glucose 6-phosphate, sodium salt, (Sigma)
C	20 mM ß-Nicotinamide adenine dinucleotide phosphate solution (NADP). Prepare 2 mL in deionized water using ß-NADP, sodium salt (Sigma)
D	300 mM magnesium chloride solution ($MgCl_2$). Prepare 2 mL in deionized water using magnesium chloride hexahydrate (Sigma)
E	Glucose 6-phosphate dehydrogenase enzyme solution. Before use, prepare a solution containing 0.3 - 0.6 unit/mL of glucose 6-phosphate dehydrogenase in cold reagent A.

Reagents A, B, C and D were used for the preparation of the reaction mixture. The composition is shown in Table 9.

.

Table 9: Composition of the reaction mixture for the glucose 6-phosphate DH assay.

components	volume [mL]
deionized water	21
reagent A	5
reagent B	1
reagent C	1
reagent D	1

The reaction mixture was warmed up to 25°C. The pH value was adjusted to 7.4 with 1 M NaOH. For the enzyme test, the following mixture was prepared for the enzyme analysis in suitable cuvettes:

Table 10: Test mixture for the glucose 6-phosphate DH assay.

	test [mL]	blank [mL]
Reaction mixture	2.9	2.9
Reagent A (buffer)	---	0.1
Reagent E	0.1	---

The mixture was immediately mixed and the increase in absorption at 340 nm was recorded for approximately 5 minutes using a spectrophotometer (BioRad smartspec 3000, Bio-Rad Laboratories GmbH, Munich, Germany). The maximum linear rate for both the test and the blank value were used for the calculation of enzyme activity. The volumetric activity was calculated by the following equation:

$$\frac{\text{Unit}}{\text{mL}} = \frac{\left.\frac{\Delta A_{340\text{nm}}}{\text{min}}\right|_{\text{Test}} - \left.\frac{\Delta A_{340\text{nm}}}{\text{min}}\right|_{\text{Blank}}}{(E^{340\text{nm}}_{\text{NADPH}})(V_{\text{enzyme}})} V_{\text{total}}(\text{df}) \qquad \textbf{(5-1)}$$

whereas ΔA represents the change of absorption, V_{total} is the total volume of the reaction mixture (3 mL), V_{enzyme} is the volume of enzyme used (0.1 mL), E is the extinction coefficient for NADPH at 340 nm (6.22 mmol/mL·cm) and (df) the dilution factor. The conver-

sion of the volumetric into the specific activity (related to the biomass or protein concentration) was calculated by equation.

$$\frac{\text{Unit}}{\text{mg}} = \frac{\left.\text{U}/\text{mL}\right|_{\text{enzyme}}}{\left.\text{mg}/\text{mL}\right|_{\text{enzyme}}} \qquad \textbf{(5-2)}$$

One unit will oxidize 1.0 µM of glucose 6-phosphate to 6-phospho-gluconate per minute in the presence of NADP at pH 7.4 at 25°C.

5.6.5.3 Pyruvate Kinase

The activity of pyruvate kinase was determined by the method of [164]. Pyruvate kinase dephosphorylates phosphoenolpyruvate (PEP) into pyruvate using ADP. Pyruvate is measured by the formation of NAD in presence of lactate dehydrogenase. The required solutions are listed in Table 11.

Table 11: Composition of reagents for the pyruvate kinase assay.

Reagent	Content
A	50 mM HEPES (N-2-hydroxyethylpiperazine-N'-2-ethane sulfonic acid) pH 7.5
B	100 mM MgCl2
C	500 mM KCl
D	40 mM ADP
E	100 mM PEP
F	10 mM NADH
G	22 units of lactate dehydrogenase

For the enzyme test, the following mixture was prepared for the enzyme analysis in suitable cuvettes as listed in Table 12. The reaction mixture was warmed up to 25°C.

Table 12: Test mixture for the pyruvate kinase assay.

	test [µL]	control [µL]
bidest. H2O	328	428
Reagent A	200	200
Reagent B	100	100
Reagent C	100	100
Reagent D	50	50
Reagent E	100	0
Reagent F	50	50
Reagent G	22	22
Cell extract	50	50

The mixture was immediately mixed and the increase in absorption at 340 nm was recorded for approximately 2 minutes using a spectrophotometer (BioRad smartspec 3000, Bio-Rad Laboratories GmbH, Munich, Germany). The maximum linear rate for both the test and the blank value were used for the calculation of enzyme activity. The volumetric activity was calculated by the following equation:

$$\frac{\text{Unit}}{\text{mL}} = \frac{\left.\frac{\Delta A_{340nm}}{\text{min}}\right|_{\text{Test}} - \left.\frac{\Delta A_{340nm}}{\text{min}}\right|_{\text{Control}}}{(E_{NADH}^{340nm})(V_{enzyme})} V_{total}(df) \qquad \textbf{(5-3)}$$

whereas ΔA represents the change of absorption, V_{total} is the total volume of the reaction mixture, V_{enzyme} is the volume of enzyme used (0.05 mL), E is the extinction coefficient for NADH at 340 nm (6.22 mmol/mL·cm) and (df) the dilution factor. The conversion of the volumetric into the specific activity (related to the biomass or protein concentration) was calculated by equation.

$$\frac{\text{Unit}}{\text{mg}} = \frac{\left.\text{U}/\text{mL}\right|_{\text{enzyme}}}{\left.\text{mg}/\text{mL}\right|_{\text{enzyme}}} \qquad \textbf{(5-4)}$$

One unit will reduce 1.0 µM of pyruvate to lactate per minute in the presence of NADH at 25°C.

5.7 Metabolic network construction

5.7.1 Aspergillus niger

A large-scale network of *A. niger* was constructed based on the genome scaled metabolic network [2]. The metabolic network comprised 120 reactions and all relevant pathways of central carbon metabolism including glycolysis (Emden-Meyerhof-Parnas pathway), pentose phosphate pathway (PPP), tricarboxylic acid cycle (TCA), fructose-mannose metabolism (FMM), glyoxylate and dicarboxylate metabolism (GDM), cytosolic citrate metabolism (CM), anaplerotic reactions (ANAPL), the complete gluconate metabolism as well as the mannitol cycle. The validity of the compacted network in terms of metabolic significance was proven by comparing the maximal amino acid yields, calculated with both the genome scaled and the condensed metabolic models. A detailed description of the stoichiometric equations is given in the appendix. Data on biomass composition were required for metabolic network analysis and were derived from [8] and [2, 166].

5.7.2 Example network of TCA cycle and supporting pathways

The principle of the developed approach is elucidated using a simple metabolic network (see appendix Table 23) from *E. coli*, which was previously used for the introduction of the concept of elementary flux mode analysis [131]. It includes the TCA cycle, the glyoxylate shunt and connected reactions of amino acid biosynthesis. In this example, 2-phosphoglycerate, ammonium, carbon dioxide, and the cofactors, such as ATP and NAD, are considered as external metabolites. Succinyl-CoA is defined as desired product and its formation as an objective reaction.

5.7.3 Metabolic networks of alternative organisms

In addition to *A. niger*, a variety of micro-organisms are used for industrial purposes, whereby each type of organism has its own importance regarding to type of products, capacity and handling during the production process. While the yeast *Saccharomyces cerevisiae* is applied in the bakery and brewing industry for ethanol production, the gram-negative bacterium *Escherichia coli* is widely used for production of heterologous proteins, such as insulin and interferon [167]. The gram-positive *Bacillus subtilis* is used for riboflavin [168-170]

production and enzymes used in washing agents [171]. *Corynebacterium glutamicum* is a well known amino acid producer and used since more than 20 years for the biotechnological production of lysine and glutamate [172].

Because of the high industrial relevance of these organisms their metabolic networks were additionally considered for metabolic network analysis and compared with that of the filamentous fungus *Aspergillus niger*.

Saccharomyces cerevisiae

The metabolic reaction model of *S. cerevisiae* (see appendix Table 25) considered the actual knowledge from the genome scale model [173]. It included all relevant pathways of central carbon, nitrogen and sulphur metabolism as well as the entire subset of anabolism and the corresponding reactions linked to the formation and secretion of extracellular products acetate and ethanol. For elementary flux mode analysis, 9 external compounds were considered including the substrates glucose, ammonium, sulphate and oxygen and the products target protein, biomass, ethanol, acetate and carbon dioxide. Additionally, ATP, required for maintenance, was considered as an external metabolite. The stoichiometric equation for biomass synthesis included all relevant precursor metabolites. The relative amount and composition of the macromolecules DNA, carbohydrates, lipids, protein and RNA was taken from thorough analysis of cellular composition [174]. For ATP production from NADH and ubiquinone in the respiratory chain, a P/O ratio of 2 was assumed and a P/O of 1 for the cytosolic NADH [173].

Bacillus subtilis

The considered metabolic reaction model of *B. subtilis* (see appendix Table 27) was taken from the genome based model, which has been reconstructed recently [175]. It included all relevant pathways of central carbon, nitrogen and sulphur metabolism as well as the entire subset of anabolism and the corresponding reactions linked to formation and secretion of extracellular products. For elementary flux mode analysis, 8 external compounds were considered including the substrates carbon source, ammonium, sulphate and oxygen and the products target product, biomass, acetate and carbon dioxide. Additionally, ATP, required for maintenance, was considered as an external metabolite. The stoichiometric equation for biomass synthesis included all relevant precursor metabolites. The relative amount and

composition of the biomass was based on experimental data [176, 177]. For ATP production from NADH in the respiratory chain, a P/O ratio of 2 was assumed.

Escherichia coli

The model construction for the central metabolism of *E. coli* (see appendix Table 24) was based on literature [178] and databases (http://www.genome.jp/kegg/metabolism.html). The model comprised the phospho-transferase system (PTS) for glucose uptake, EMP, PPP, Entner-Doudoroff Pathway (EDP), TCA cycle, anaplerosis, respiratory chain and sulfate assimilation. For elementary flux mode analysis, 8 external compounds were considered including the substrates carbon source, ammonium, sulphate and oxygen and the products target product, biomass, acetate and carbon dioxide. Additionally, ATP, required for maintenance, was considered as an external metabolite. The stoichiometric equation for biomass synthesis included all relevant precursor metabolites [179]. For ATP production from NADH in the respiratory chain, a P/O ratio of 2 was assumed [178].

Corynebacterium glutamicum

The metabolic reaction model of *C. glutamicum* (see appendix Table 26) considered the actual knowledge from the genome scale model recently created [180]. It included all relevant pathways of central carbon, nitrogen and sulphur metabolism as well as the entire subset of anabolism and the corresponding reactions linked to formation and secretion of extracellular products. For elementary flux mode analysis, 7 external compounds were considered including the substrates glucose, ammonium, sulphate and oxygen and the products lysine, biomass and carbon dioxide. Additionally, ATP, required for maintenance, was considered as an external metabolite. The stoichiometric equation for biomass synthesis included all relevant precursor metabolites. The relative amount and composition of the macromolecules DNA, carbohydrates, lipids, protein and RNA was taken from thorough analysis of cellular composition [177]. For ATP production from NADH and menaquinol in the respiratory chain, a P/O ratio of 2 was assumed [180].

The metabolic network structures from other industrially relevant organism differ significantly from *A. niger* which is summarized in Table 13.

Table 13: Comparative illustration of most important differences of metabolic network properties of industrial hosts and its industrial applications.

Host	Metabolic network properties			
	compart-mented	mannitol cycle	glyoxylate bypass	KDPG
A. niger	+	+	+	-
S. cerevisiae	+	-	+	-
E. coli	-	-	+	+
B. subtilis	-	-	-	+/-
C. glutamicum	-	-	+	+/-

5.8 Computational Methods

5.8.1 Calculation of elementary flux modes

Calculation of elementary flux modes was performed using the double description method (nullspace approach) introduced by Wagner [181] and extended with the recursive enumeration strategy with bit pattern trees by Terzer and Stelling [182]. An implementation of the algorithm in Java, with integration into MatLab (Mathworks Inc., Natick, MA) is available at http://csb.inf.ethz.ch and was applied in this work.

All tests were performed on Windows Vista machine with AMD Phenom 9650 Quad-core processor (3.58 GB RAM), using a Java 32-bit runtime environment (version 1.6.0).

Computation times for the different scenarios varied between a few seconds and ca. 5 h depending on the applied substrate combinations and thus complexity of the underlying network.

5.8.2 Analysis of elementary modes

On basis of the determined elementary modes, a detailed investigation of metabolic network properties was carried out. This included the estimation of theoretical maximum yield, relative fluxes through intracellular metabolic pathways, and target potential based on flux correlation analysis. Calculations were partially automated and implemented into MatLab (Mathworks Inc., Natick, MA) and evaluated in Excel™ (Microsoft Office 2007, version 12.0).

5.8.2.1 Calculation of maximum theoretical yield

The theoretical target product and biomass production yield ($Y_{P/C,j}$) was calculated for each elementary mode *j* according to (Equation 5-5). The symbol ξ refers to the molar carbon content expressed in C-mol per mol (product or carbon source). The variable s refers to the stoichiometric coefficient of the product (*P*) and carbon source (*C*) The variable n refers to the numbers of elementary modes respectively.

$$Y_{P/C,j} = \frac{s_{P,j}}{s_{c,j}} \frac{\xi_{P,j}}{\xi_{C,j}}, 1 \le j \le n \qquad \textbf{(5-5)}$$

The unit of theoretical production yield is

$$Y_{P/C,j} = \frac{\text{molcarbon(product)}}{\text{molcarbon(substrate)}} \quad \textbf{(5-6)}$$

Since each real flux distribution in a biological system is a linear combination of elementary modes, the mode with the highest product or biomass yield, respectively, gives direct access to the maximum capacity of the underlying network, i.e. the maximum theoretical yields $Y_{P/C,max}$, and $Y_{X/C,max}$ [141].

5.8.2.2 Identification of target potential based on flux correlation

A new method was developed to investigate, weather a reaction *i* displays a potential target, a chosen set of elementary flux modes was searched for statistically relevant correlation between the relative flux through the objective reaction *obj* and that through the reaction *i*. For this purpose the slope of the linear regression between the objective flux ($\nu_{obj,j}$) and the corresponding flux ($\nu_{i,j}$) through each elementary mode *j* was determined. This was carried out for each reaction, so that the entire network could be screened for potential targets. Only statistically valid correlations were further considered. For this purpose a cut-off value of $r^2 = 0.7$ was set for the regression coefficient of each linear correlation. Such a cut-off has been proven valid in previous studies processing correlated data [183, 184]. Additionally, the statistical significance of these targets was further proven by the *t*-test (Equation 5-12). For this purpose, relative metabolic fluxes ($\nu_{i,j}$) of each metabolic reaction *i* were first determined (Equation 5-7) and then normalized to one unit of hexose (glucose) (Equation 5-8).

$$\nu_{i,j} = \frac{s_{i,j}}{s_{C,j}} \frac{\xi_{hexose}}{\xi_C}, \quad 1 \le i \le q,\ 1 \le j \le n \quad \textbf{(5-7)}$$

$$\left[\nu_{i,j}\right] = \frac{\text{mol (i)}}{\text{mol (hexose)}} \quad \textbf{(5-8)}$$

The variable q refers to the number of metabolic reactions in the metabolic network. Subsequently, the potential of a metabolic reaction as genetic target was expressed as target validity coefficient ($\alpha_{obj,j}$). The slope of the linear regression, equal to $\alpha_{obj,j}$ was derived from a

linear fit between, for example, the relative flux of fructofuranosidase synthesis $\nu_{obj,j}$ and the relative flux ν_i through metabolic reaction *i*. This can be represented as variables x and y in a linear equation $y = \alpha \cdot x \pm \beta$, respectively (Equation 5-9), whereas $\beta_{obj,j}$ is the intercept of the ordinate.

$$\alpha_{obj,j} = \frac{\nu_{i,j} \pm \beta_{obj,j}}{\nu_{obj,j}}, \quad \nu_{obj,j} > 0,\ 1 \le i \le q;\ 1 \le j \le n \qquad \textbf{(5-9)}$$

The calculation was carried out by determining the covariance (cov) of the variables of the relative fluxes $\nu_{obj,j}$ and $\nu_{i,j}$ divided by the square of the standard deviation δ of the corresponding relative fluxes of fructofuranosidase as shown in Equation 5-10.

$$\alpha_{obj,j} = \frac{\mathrm{cov}(\nu_{obj,j}, \nu_{i,j})}{\delta^2_{\nu_{obj}}}, \quad \nu_{obj,j} > 0,\ 1 \le i \le q;\ 1 \le j \le n \qquad \textbf{(5-10)}$$

Positive values of $\alpha_{obj,j}$ account for amplification targets, whereas negative values denote deletion or attenuation targets.

5.8.2.3 Statistical evaluation of genetic targets

Correlation Analysis

Correlation analysis examines relationships between random variables and a control sample. The correlation coefficient r reveals the measurement of the strength and direction of a linear relationship between two characteristics, x and y, whereas the values of r can be $-1 \le r \le 1$. If r = 0, the characteristic x and y are not correlated with each other, whereas if r converges to -1 or 1 the linear dependency between x and y is very likely. The larger the number of samples n, the better is the estimation for the true correlation coefficient. The calculation of the correlation coefficient is presented in Equation 5-11.

$$r = \frac{\sum_n xy - \frac{1}{n}(\sum_n x)(\sum_n y)}{\sqrt{[x^2 - \frac{1}{n}(\sum_n x)^2][y^2 - \frac{1}{n}(\sum_n y)^2]}} \qquad \textbf{(5-11)}$$

whereas n represents the number of characteristic pairs (x,y).

Regression Analysis

The regression coefficient (r^2) represents a measure of the goodness of a fit between two variables x and y. The values of the regression coefficients can be $0 \leq r^2 \leq 1$. If $r^2 = 0$, there is no linear connection between the two variables. For the statistical analysis in this work, a cut-off value of $r^2 = 0.7$ was considered for the regression coefficients.

***t*-test**

In addition to the determination of the regression coefficient, the statistical significance can now be proved by the *t*-test. The *t*-test allows a statistically reliable statement about the quality of the relationship, whereas TS (test statistic) follows a *t*-distribution with a degree of freedom of $f = n-2$, if x,y are normally distributed. If the absolute TS-value is higher than the *t*-value of the *t*-distribution (see table A, in appendix), then a statistically significant relationship with a given probability *P* can be assumed. The TS value can be calculated by Equation 5-12.

$$TS = \frac{r}{\sqrt{1-r^2}}\sqrt{n-2} = r\sqrt{\frac{n-2}{1-r^2}} \qquad \textbf{(5-12)}$$

If $TS > t(f, P)$, then a statistically significant relationship between the characteristics x and y exists.

The statistical analysis was carried out in a six-step algorithm. The initial matrix $\underline{\underline{K}}$ (null-matrix) was analyzed by the following steps:

1. Find all stoichiometric coefficients of fructofuranosidase production with $v_{obj,j} \neq 0$.
2. Calculate the regression r^2 coefficient of value pairs $r^2(v_{obj,j}, v_{i,j})$.
3. If $r^2(v_{obj,i}, v_{j,i}) \geq 0.7$, go to step 4. If $r^2(v_{obj,j}, v_{i,j}) < 0.7$, there is no statistical relevance.
4. Calculation of the target validity (Equation 5-10).
5. Calculation of the *t*-test (Equation 5-12), if $TS > t(f, P)$ → OK.

All calculations were made in Excel (Microsoft Office 2007, version 12.0) or MatLab™ (Mathworks, version R2008a, Natick, MA, USA).

5.8.3 Metabolic flux analysis with over-determined systems

Generalization of Equation 4-1 with matrix notation leads to equation:

$$\underline{\underline{S}} \cdot \underline{r} = \underline{0} \qquad \textbf{(5-13)}$$

The splitting of the equation into known and unknown rates leads to Equation 5-14, where the indices m and u refer to measured known and unknown rates, respectively.

$$\underline{\underline{S}}_m \cdot \underline{r}_m + \underline{\underline{S}}_u \cdot \underline{r}_u = \underline{0} \qquad \textbf{(5-14)}$$

For an over-determined system, the unknown rates r_u can be calculated after conversion of Equation 5-14 to:

$$\underline{r}_u = -\left(\underline{\underline{S}}_u^{\#}\right) \cdot \underline{\underline{S}}_m \cdot \underline{r}_m \qquad \textbf{(5-15)}$$

Whereby $S^{\#}$ is the so called Moore-Penrose inverse (pseudo inverse) of S_u and is given by:

$$\underline{\underline{S}}^{\#} = \left(\underline{\underline{S}}_u \cdot \underline{\underline{S}}_u^T\right)^{-1} \cdot \underline{\underline{S}}_u^T \qquad \textbf{(5-16)}$$

The unknown metabolic fluxes were estimated using the exchange fluxes of the extra-cellular metabolites quantified via HPLC. Precision in the measurements was taken into account using the diagnosis and gross error analysis proposed previously [185]. A more general method [186], which considers the simultaneous estimation of unknown fluxes and the correction of the original measured fluxes, did not deliver any noticeable differences. All calculations were implemented in MatLab (Mathworks Inc., Natick, MA, USA).
The detailed description of the method can be found in the appendix.

6 Results and Discussion

6.1 Large-scale Metabolic Network Model of *Aspergillus niger*

A large-scale metabolic reaction model of *A. niger* was constructed on basis of the genome scale model recently published [2]. The model included all relevant pathways of central carbon, nitrogen and sulphur metabolism as well as the entire subset of anabolism and the corresponding reactions linked to formation of extracellular products (Figure 14). Hereby, the cellular compartments mitochondrion, glyoxysome and cytosol were considered together with the respective transport reactions. The complete model in stoichiometric formulation and a detailed description of the model reactions are listed in the appendix (Table 22). This model displayed the basis of a detailed *in silico* investigation of the properties of the metabolic network of *A. niger* via elementary flux modes. This should provide a most comprehensive insight into possible functional states of the cell to unravel key pathways for superior performing as cell factories. For elementary flux mode analysis, the metabolites in the network are sorted into external and intracellular compounds. The external compounds considered were substrates (source of carbon, nitrogen, sulphur, oxygen) and products (enzyme, biomass, carbon dioxide, gluconate, oxalate, citrate). Additionally, ATP continuously withdrawn for maintenance purposes was included as an external metabolite. With regard to energy stoichiometry the P/O ratio for mitochondrial NADH was assumed as 2.64. That for succinate and cytosolic NADH was assumed as 1.64 [2]. The condition number of the stoichiometric matrices representing the stoichiometric model and model extensions varied between 11.8 and 12.6, which indicates well-conditioned matrices [73].

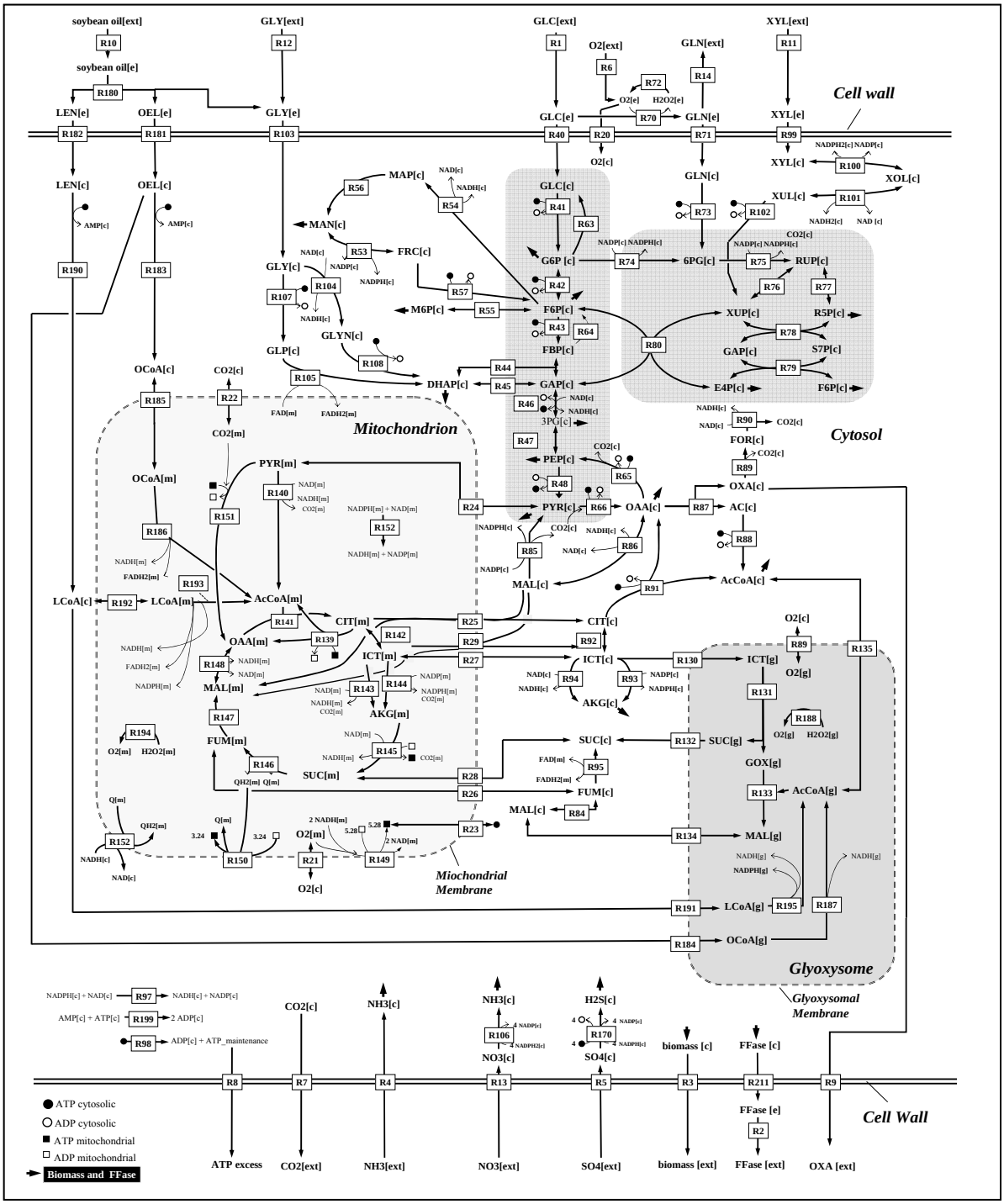

Figure 14: Schematical representation of the large-scale metabolic model for *A. niger* used in the present work. Reactions and metabolites are compartmentalized in extracellular [e], cytosolic [c], mitochondrial [m] and glyoxysomal [g] compartments. Reaction numbers refer to a detailed model description in the supplement (see appendix).

6.1.1 Anabolism and biomass formation

Relative amount and composition of the macromolecules protein, DNA, glucan, glycogen, lipid and RNA in *A. niger* was taken from previous detailed estimates [2, 8]. The amino acid composition of the cell protein was calculated from the average protein content of *A. niger* using the program IdentiCS [166]. In addition, the glycosylation of cellular protein was considered, taking $Galf_2Man_8(GlcNAc)$ as an average composition of the glycosylation residues in filamentous fungi [187] and an average number of 33 sugar residues [188] into account. This resulted in the stoichiometric fraction of $Galf_6Man_{24}(GlcNAc)_3$ per protein. The calculation of the exact demand was based on previous estimates that average 64 % of all proteins are glycosylated [189]. This detailed information on the cellular composition allowed a precise estimation of the demand of precursor compounds for anabolism (Table 14). Stoichiometric coefficients for energy metabolism in *A. niger* (Table 15) were taken from [2].

Table 14: Stoichiometric coefficients for biomass synthesis in *A. niger*.

Precursor	stoichiometric coefficients [$mmol/g_{biomass}$]
3-P glycerate	0.89
α-Ketoglutarate	1.14
AcCoA	3.86
ATP	61
Dihydroxyacetone phosphate	0.08
Erythrose 4-P	0.36
FADH	0.08
Fructose 6-P	0.44
Glucose 6-P	0.018
Mannitol	0.213
Mannose	0.42
NADPH	13.18
NH3	7.1
Oxaloacetate	1.03
Phosphoenolpyruvate	0.65
Pyruvate	1.91
Ribose 5-P	0.37

Table 15: Stoichiometric coefficients energy metabolism in *A. niger*.

Energy metabolism	
ATP maintenance	1.9 mmol/$g_{biomass}$·h
P/O coefficients	5.28 (mitochondrial NADH)
	3.28 (ubiquinone)
	3.28 (cytosolic NADH)

6.1.2 Target protein production

The cellular demand for the synthesis of the enzymes fructofuranosidase, glucoamylase and epoxide hydrolase investigated in this work was calculated as follows. Fructofuranosidase is highly glycosylated [87], whereby 50 % of the total enzyme mass consists of sugar chains (NetNGlyc, http://www.cbs.dtu.dk/). Hereby, the glycosylation pattern of $Galf_{18}Man_{308}(GlcNAc)_{8.5}$ is known [190]. The amino acid composition of fructofuranosidase was derived from the corresponding open reading frame-ID An08g11070 [15]. Similarly, the amino acid composition of glucoamylase (An03g06550) and epoxide hydrolase (An16g02170) from *A. niger* was derived [15]. The resulting precursor demand is shown in Table 16.

Table 16: Precursor demand for target protein.

Precursor	Stoichiometric coefficients mol/$mmol_{target\ protein}$		
	β-Fructofuranosidase	α-Glucoamylase	Epoxide Hydrolase
3-P glycerate	126	119	62
α-Ketoglutarate	104	103	91
AcCoA	12	13	16
ATP	5,482	5,180	4,935
Erythrose 4-P	65	72	48
Fructose 6-P	332	650	0
NADPH	1,156	1,034	897
Oxaloacetate	242	272	156
Phosphoenolpyruvate	115	130	62
Pyruvate	42	65	31
Ribose 5-P	25	23	19

6.1.3 Validation of the large-scale network of *A. niger*

The large-scale metabolic network was validated by calculating the theoretical maximum yield for all 20 proteinogenic amino acids synthesizing from various pathways of central carbon metabolism and display the central precursors of the target products, i.e. proteins, studied. These were compared to previous data obtained with the genome scaled metabolic model [2]. The highest deviations are lower than 1.5 % for the amino acids threonine, histidine, tyrosine and proline (Figure 15).

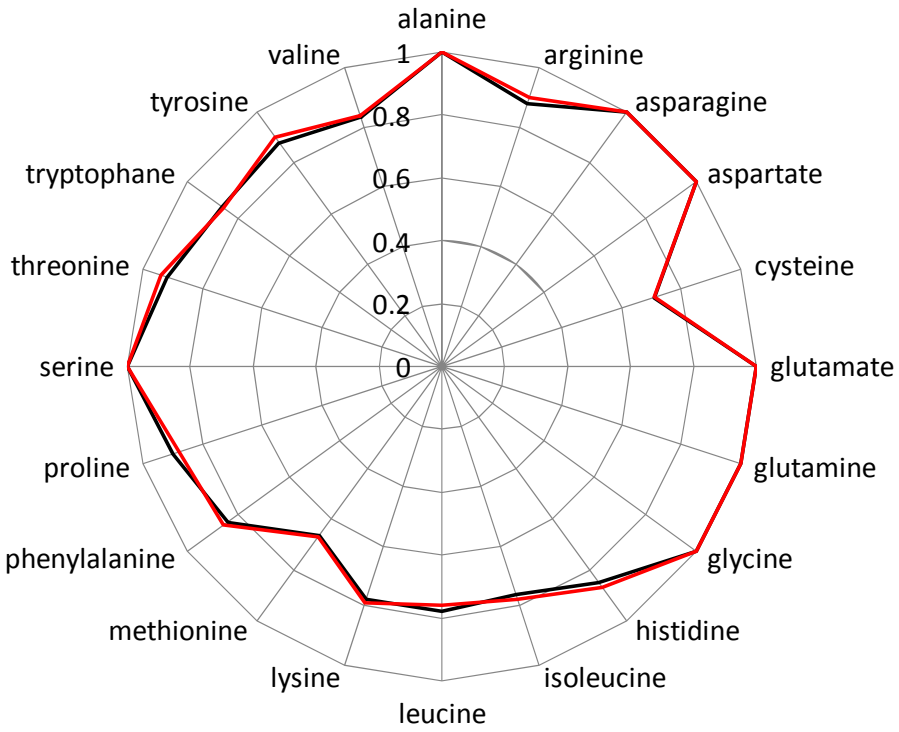

Figure 15: Radar plot of theoretical maximum yield for amino acid synthesis using the genome scale model (red line, [2]) and large-scale metabolic model (black line, this work) of *A. niger*.

The obtained theoretical maximum yield revealed excellent agreement for all compounds of the genome scale model. Thus the model constructed utilized here provided a good representation of the genome-scale model for the central pathways which were in the focus of this work.

6.2 Prediction of Enzyme Production and Optimal Pathways

Elementary flux mode calculations using the large-scale model were carried out for the prediction of theoretical maximum enzyme production yields and the corresponding optimal pathways. For this, different nutrient scenarios, e.g. carbon and nitrogen source, were compared with respect to the maximal enzyme yields and optimal pathway usage.

6.2.1 Fructofuranosidase production on glucose

6.2.1.1 Maximum theoretical yield

Figure 16(A) displays the elementary flux modes for the production of fructofuranosidase on glucose. Overall, about 21,100 modes were obtained on glucose and ammonium.

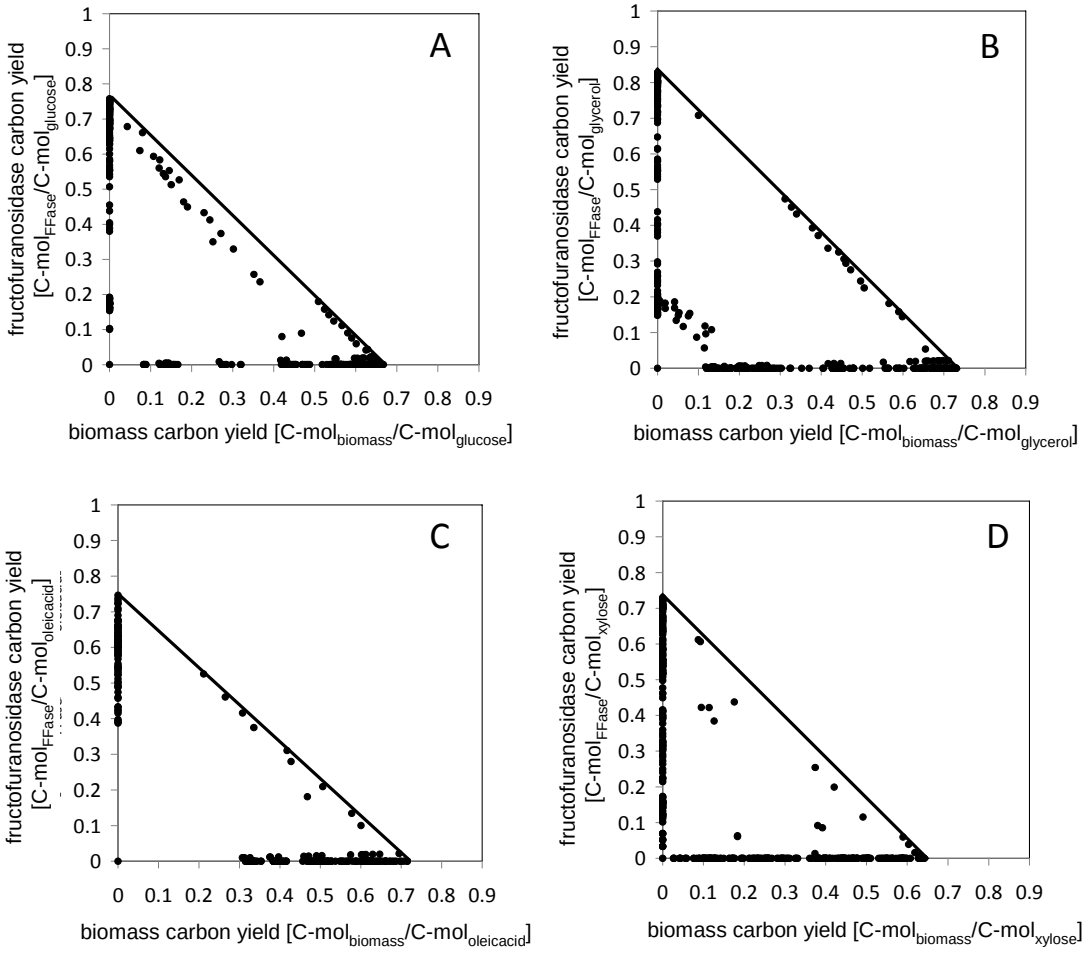

Figure 16: Comparison of elementary modes for biomass and fructofuranosidase production in *A. niger* on different carbon sources. A: glucose, B: glycerol, C: oleic acid, D: xylose. The solution space of the elementary modes, represented by the black dots, is marked through the interior as well as the sides of the rectangular triangle. The modes on the axes represent extreme modes exclusively linked to production of either biomass or fructofuranosidase (FFase).

The modes differed substantially in the corresponding yield for the target-enzyme or biomass. The dominating fraction of modes was linked to exclusive production of either fructofuranosidase or biomass, respectively. Since every real flux state in a cell can be described by a linear combination of flux modes, the best mode with respect to production allowed predicting the maximum theoretical potential, i.e. the maximum theoretical yield.
This was 0.76 C-mol / C-mol for fructofuranosidase and 0.67 C-mol / C-mol for biomass (Table 17). In comparison, 1,986 elementary modes (9 %), located within the interior of the triangular solution space, exhibited simultaneous formation of both compounds. Only 0.8 % of all modes allowed maximum enzyme yield, all at zero growth.

Table 17: Elementary flux mode analysis of fructofuranosidase production by *A. niger* on different carbon and nitrogen sources.

Maximum carbon yield [C-mol / C-mol]			**Number of elementary modes**		
Carbon / Nitrogen Source	FFase	Biomass	total	Modes linked to FFase production (% of total EFM)	Modes linked to Biomass and FFase production (% of total EFM)
Glucose / NH3	0.76	0.67	21,147	7,045 (33)	1,986 (9)
Glycerol / NH3	0.83	0.73	21,122	8,070 (38)	2,267 (11)
Oelic acid / NH3	0.75	0.72	20,895	9,071 (43)	1,702 (8)
Xylose / NH3	0.73	0.64	13,364	3,896 (29)	187 (1)
Mannitol / NH3	0.80	0.70	20,507	7,422 (36)	1,926 (9)
Sucrose / NH3	0.76	0.67	52,926	16,046 (30)	5,190 (10)
Fructose / NH3	0.76	0.67	17,680	5,033 (28)	1,810 (10)
Mannose / NH3	0.76	0.67	13,196	4,536 (34)	1,313 (10)
Glucose / NO3	0.61	0.54	29,435	13,160 (45)	1,425 (5)
Glycerol / NO3	0.67	0.59	33,462	14,090 (42)	2,984 (9)
Oelic acid / NO3	0.65	0.59	27,753	12,652 (46)	1,724 (6)
Xylose / NO3	0.59	0.52	24,098	8,443 (35)	249 (5)
Mannitol / NO3	0.64	0.57	40,751	17,816 (44)	2,755 (7)
Sucrose / NO3	0.61	0.54	82,812	31,684 (38)	5,268 (6)
Fructose / NO3	0.61	0.54	27,365	10,321 (38)	2,009 (7)
Mannose / NO3	0.61	0.54	22,207	9,804 (44)	1,489 (7)

6.2.1.2 Optimal pathways

As shown, 160 modes allowed maximum enzyme production. The average flux distribution extracted from the flux modes at maximum enzyme yield provides a detailed picture on the reactions involved under optimum performance (Figure 17).

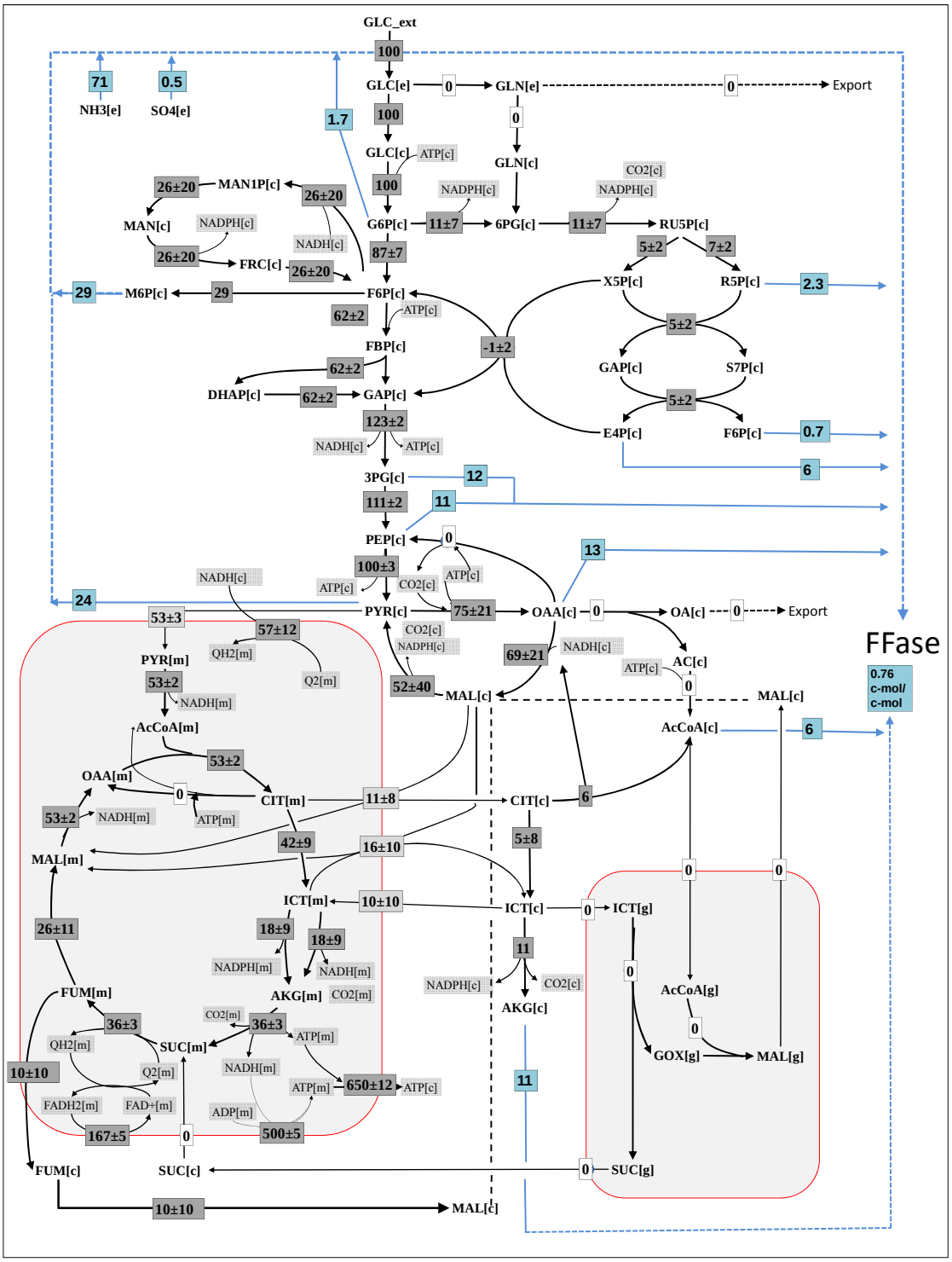

Figure 17: Flux distribution for theoretical maximum fructofuranosidase (FFase) production by *A. niger* using glucose and ammonium. The relative flux coefficients are averaged from 160 elementary flux modes for maximum production obtained. All fluxes are given as relative molar flux normalized to 1 mol of glucose unit [mol·(mol glucose)$^{-1}$·100].

The contribution of the non-oxidative PPP, the glycolysis, the fructofuranosidase synthesis as well as transport processes was rather constant as indicated by the low deviation of corresponding fluxes.
Other reactions showed a higher flexibility suggesting that key functions of the network under optimum production conditions can be realized by different flux states. Interestingly, this included a number of cytosolic enzymes which are all involved in the supply of NADPH, i.e. the oxidative PPP, malic enzyme and isocitrate dehydrogenase as well as mannitol 2-phosphate dehydrogenase. Furthermore, maximum production was linked to zero by-product formation. The entire ATP formed was completely recruited for fructofuranosidase production.

6.2.2 Impact of alternative carbon and nitrogen sources

Elementary flux mode analysis was further carried out for the industrially relevant carbon sources xylose, glycerol and oleic acid (Figure 16 B, C, D) (Table 17). For the reduced substrate glycerol a maximum enzyme production of 0.83 C-mol/C-mol was predicted. Among all substrates tested, it was thus the best carbon source (Figure 16 B). Oleic acid (0.75 C-mol/C-mol) and xylose (0.73 C-mol/C-mol) were slightly less efficient (Figure 16 C, D). Glycerol was metabolized by simultaneous usage of the NADH-dependent glycerol-dehydrogenase and the FAD-dependent glycerol 3-phosphate dehydrogenase (Figure 18 B). Due to this, reducing equivalents are formed in the cytosol and mitochondrion, respectively. This causes an increased flux through the NADH-ubiquinone oxidoreductase, counterbalancing the NADH supply in the cytosol (Figure 18). Probably linked to the different entry point of glycerol into metabolism, the supply of NADPH differed for this carbon source with respect to the reactions involved. Here, the oxidative PPP played only a minor role, whereas mainly the mannitol cycle and the malic enzyme were recruited. For oleic acid the flux distribution differed drastically (Figure 18 C).
At theoretical maximum production, degradation of oleic acid involved the two parallel routes in the mitochondrion and in the glyoxysome. This resulted in a large relative flux through the glyoxylate shunt and through reactions of the TCA cycle with the corresponding mitochondrial shuttle systems (Figure 18 C).

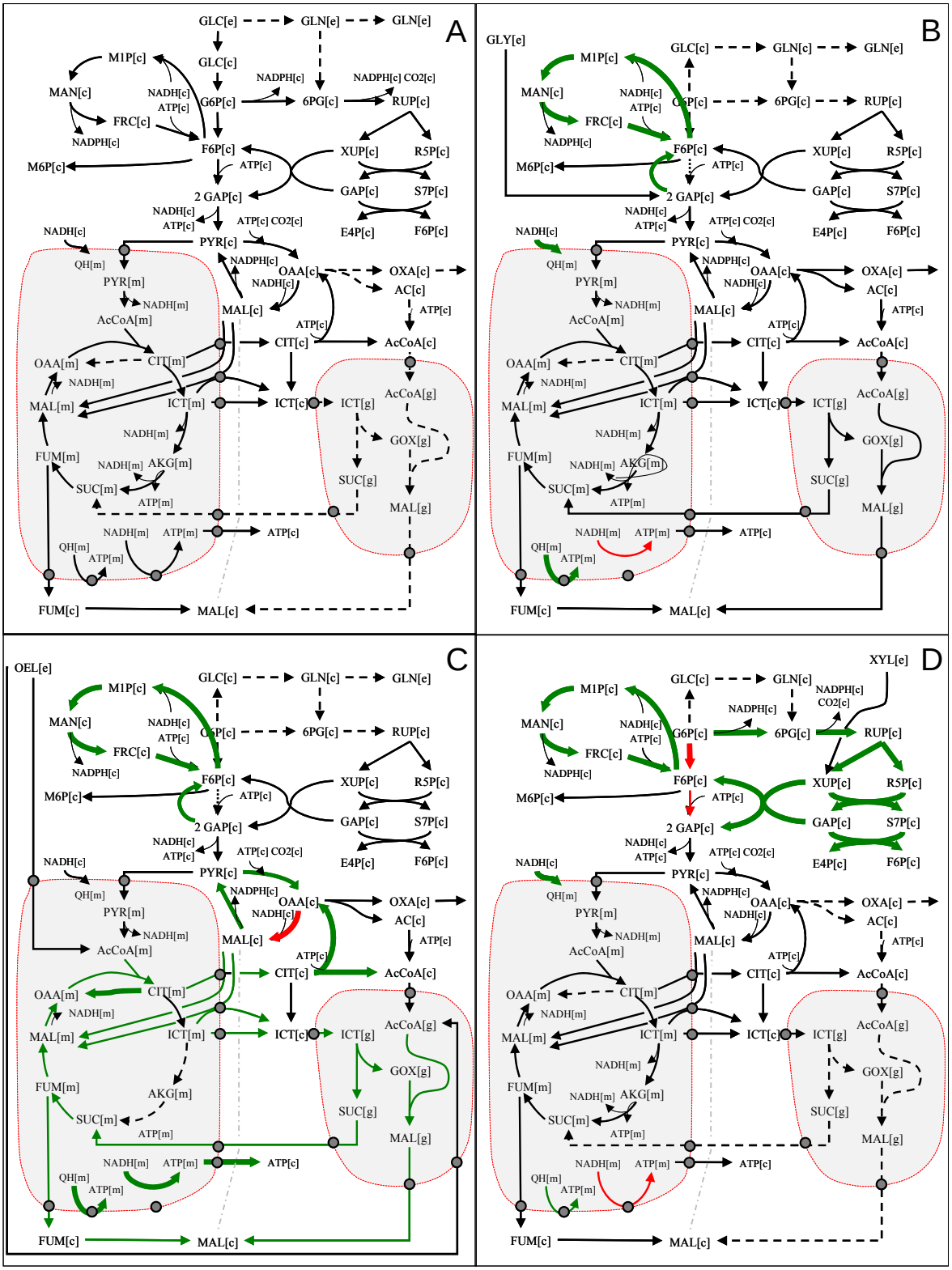

Figure 18: Flux distribution for theoretical maximum fructofuranosidase (FFase) production by *A. niger* on different substrates. A: glucose, B: glycerol, C: oleic acid, D: xylose. Increased and decreased metabolic fluxes are visualized by green and red arrows, respectively.

The high amount of NADH supplied during metabolization of the reduced fatty acids is utilized in the mannitol cycle to form NADPH. Accordingly, the oxidative PPP was not involved in NADPH supply. Thus the degree of reduction obviously influenced the flux state for optimum performance. Production on xylose demanded for increased NADPH supply, as indicated by average flux through the oxidative PPP (48 mol/mol hexose unit), the mannitol cycle (60 mol/mol hexose unit) and the malic enzyme (60 mol/mol hexose unit). This is partly attributed to the NADPH demand which is required for the xylose uptake system [118]. As for glucose, by-product formation was not observed for any of the alternative carbon sources under maximum production. The degree of reduction also played a role for the nitrogen source. The optimum yield decreased by about 18 % for all carbon sources when nitrate was used instead of ammonia.

Table 18: Fluxes in the reactions for maximum fructofuranosidase (FFase) production using different carbon sources and ammonium as nitrogen source. All fluxes are given as relative molar flux normalized to 1 mol of glucose unit [mol (mol glucose)$^{-1}$ 100]. The relative flux coefficients are averaged from 160 (glucose), 64 (glycerol), 523 (oleic acid) and 80 (xylose) elementary flux modes for maximum fructofuranosidase production obtained for each substrate. Metabolic reactions participate in the glycolysis (EMP), the Pentose-Phosphate Pathway (PPP), the anaplerosis (ANAPL), the fructose mannose metabolism (FMM), tricarboxylic acid cycle (TCA) and the energy metabolism (E).

	Metabolic Reactions	Carbon Source			
		Glucose	Glycerol	Oleic acid	Xylose
EMP	Glucose 6-P isomerase	87±7	-2±0	-2±0	-49±21
	Enolase	111±2	107	-84±0	101±7
	Pyruvate kinase	100±3	95±0	77±45	91±7
PPP	Glucose 6-P DH	11±7	0	0	48±21
	Transketolase/ Transaldolase	5±2	1.4±0	1.2±0	57±7
ANAPL	Malic enzyme	52±40	54±27	82±31	60±42
	Pyruvate carboxylase	75±21	79±27	135±53	82±42
FMM	Mannitol 2-DH	26±20	54±27	100±45	60±42
	Mannose 6-P isomerase	29±0	31±0	28±0	28±0
TCA	Citrate synthase	53±2	43±0	272±50	46±7
	Isocitrate dehydrogenase	36±18 (mit)	24±12 (mit)	0 (mit)	30±18 (mit)
		11±0 (cyt)	12±0 (cyt)	12±0 (cyt)	10±0 (cyt)
E	ATP synthase	500±5	780±0	898±68	678±35
	Ubiquinone reductase	57±12	124±50	69±27	124±32

The complete flux data for maximum fructofuranosidase production on glycerol (Figure 39) oleic acid (Figure 40) and xylose (Figure 41) are listed in the appendix.

6.3 Target Identification Based on Flux Correlation

A new *in silico* approach was developed for the design of cell factories by the analysis of metabolic flux correlations between metabolic enzymes to desired properties. This allowed the prediction of deletion and amplification targets and thus provides an important prerequisite for rational strain optimization.

6.3.1 Small example network of *Escherichia coli*

A small network comprising the TCA cycle, the glyoxylate shunt and the related amino acid metabolism from *E. coli* serves as an example to introduce the principle of the developed approach for target identification (Figure 19). The example network was derived from [131].

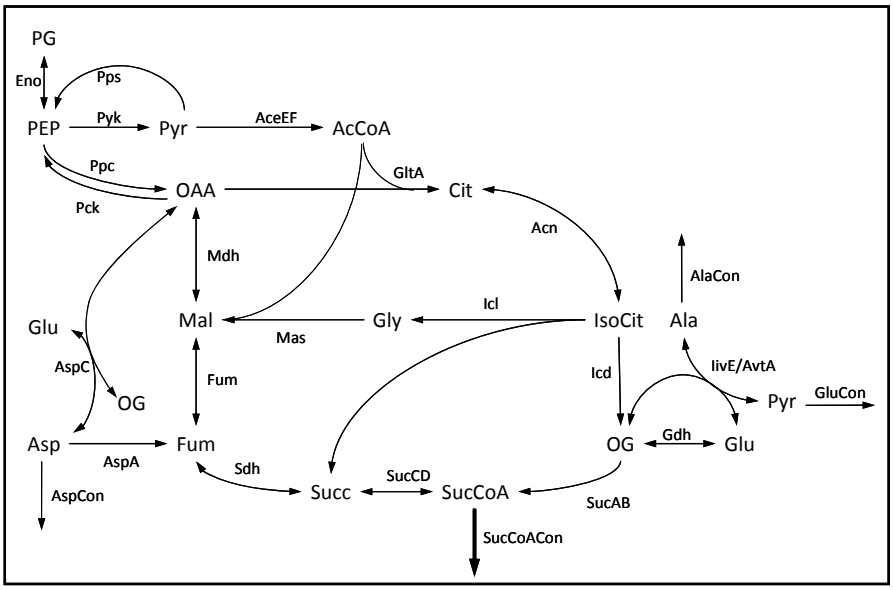

Figure 19: Reaction scheme consisting of the tricarboxylic acid cycle, glyoxylate shunt and some adjacent reactions of amino acid metabolism in *E. coli*. Abbreviations of metabolites: AcCoA, acetyl-CoA; Ala, alanine; Asp, aspartate; Cit, citrate; Fum, fumarate; Glu, glutamate; Gly, glyoxylate; IsoCit, isocitrate; Mal, malate; OAA, oxaloacetate; OG, 2-oxoglutarate; PEP, phosphoenolpyruvate; PG, 2-phosphoglycerate; Pyr, pyruvate; Succ, succinate; SucCoA, succinyl-CoA. Abbreviations of enzymes: AceEF, pyruvate dehydrogenase; Acn, aconitase; AspA, aspartase; AspC, aspartate aminotransferase; Eno, enolase; Fum, fumarase; Gdh, glutamate dehydrogenase; GltA, citrate synthase; Icd, isocitrate dehydrogenase (in *E. coli* with cofactors NADP/NADPH); Icl, isocitrate lyase; Mas, malate synthase; IlvE/AvtA, branched-chain amino acid aminotransferase/valine-pyruvate aminotransferase; Mdh, malate dehydrogenase; Pck, PEP carboxykinase (in *E. coli* with cofactors ADP/ATP); Ppc, PEP carboxylase; Pps, PEP synthetase; Pyk, pyruvate kinase; Sdh, succinate dehydrogenase; SucAB, 2-oxoglutarate dehydrogenase; SucCD, succinyl-CoA synthetase (in *E. coli* with cofactors ADP/ATP); AlaCon, AspCon, GluCon and SucCoACon, consumption of alanine, aspartate, glutamate and succinyl-CoA, respectively. Reversible reactions are indicated by double arrow-heads (Schuster et al., 1999).

All cofactors such as ATP and NAD as well as 2-phospho-glycerate (PG), succinyl-CoA, NH3 and CO_2 were considered as external metabolites. The calculation revealed 16 elementary modes, which are shown in the following matrix notation, whereby the coefficients of the matrix are the reaction coefficients s of each elementary mode (Figure 20). The reactions (enzymes) are listed in the columns, the elementary modes in the rows.

No. Emodes	Eno	AspCon	SucCoCon	AlaCon	GluCon	AspA	AspC	Pps	Pyk	AceEF	GltA	Pck	Ppc	Acn	Icl	Mas	Mdh	Fum	Sdh	SucCD	Gdh	IlvE/AvtA	SucAB	Icd
1	0	0	0	0	0	0	0	0	0	0	0	1	1	0	0	0	0	0	0	0	0	0	0	0
2	0	0	0	0	0	0	0	1	1	0	0	0	0	0	0	0	0	0	0	0	0	0	0	0
3	1	1	0	0	0	0	1	0	0	0	0	0	1	0	0	0	0	0	0	0	1	0	0	0
4	1	0	0	1	0	0	0	0	1	0	0	0	0	0	0	0	0	0	0	0	1	1	0	0
5	0	0	0	0	0	1	1	0	0	0	0	0	0	0	0	0	1	1	0	0	1	0	0	0
6	1	0	0	0	0	0	1	0	2	2	1	1	0	1	1	1	2	1	1	0	0	0	0	0
7	2	1	0	0	0	0	0	0	2	2	1	0	0	1	1	1	2	1	1	0	1	0	0	0
8	1	0	1	0	0	1	0	0	0	0	0	0	1	0	0	0	0	0	−1	−1	1	0	0	0
9	2	0	1	0	0	0	0	0	2	2	1	0	0	1	1	1	1	0	0	−1	0	0	0	0
10	1	0	1	0	0	0	0	0	0	0	0	0	1	0	0	0	−1	−1	−1	−1	0	0	0	0
11	3	0	2	0	0	0	0	0	2	2	1	0	1	1	1	1	0	−1	−1	−2	0	0	0	0
12	2	0	0	0	1	0	0	0	1	1	1	0	1	1	0	0	0	0	0	0	1	0	0	1
13	2	0	1	0	0	0	0	0	1	1	1	0	1	1	0	0	0	0	0	0	0	0	1	1
14	3	0	0	0	1	0	0	0	3	3	2	0	0	2	1	1	2	1	1	0	1	0	0	1
15	1	0	0	0	0	0	0	0	1	1	1	0	0	1	0	0	1	1	1	1	0	0	1	1
16	3	0	1	0	0	0	0	0	3	3	2	0	0	2	1	1	2	1	1	0	0	0	1	1

Figure 20: Matrix with the complete set of elementary modes for the example network (see Figure 19).

This displays the basic solution space for the prediction of amplification and deletion targets. In a first step, all flux modes with zero flux towards the target product (succinyl-CoA) are eliminated, resulting in a subset of 6 relevant modes. Subsequently, the remaining modes are normalized to the substrate entry reaction (here enolase) and arranged in matrix form (Figure 21).

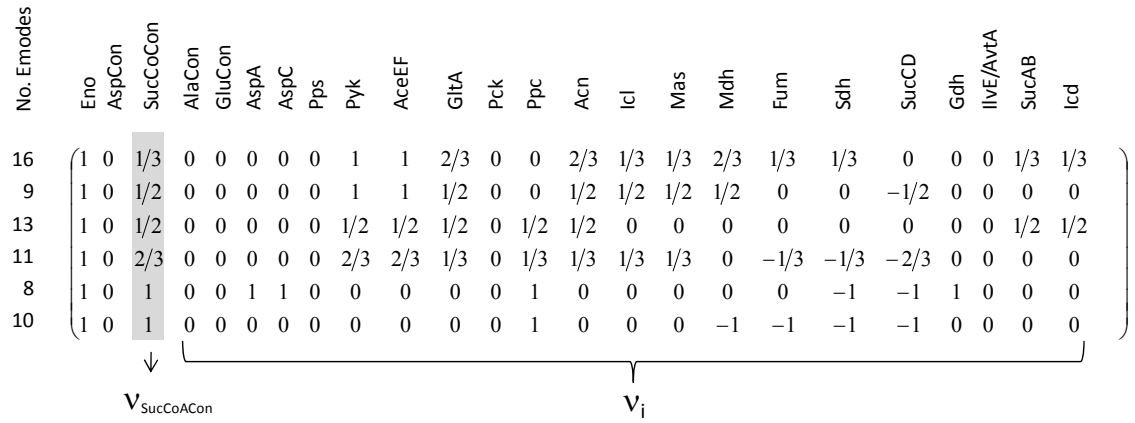

Figure 21: Remaining matrix including only yield coefficients of elementary modes for succinyl-CoA production. Coefficients are normalized to substrate entry reaction. The modes are sorted by increasing succinyl-CoA yield.

Obviously, the modes differ in the objective flux which is linked to substantial differences in the other network fluxes. This can now be exploited by scanning through the network reactions for their correlation to the objective flux as exemplified in Figure 22 B. reversible enzyme succinyl-CoA dehydrogenase (SucCD), only the forward direction from succinyl-CoA to succinate revealed negative correlation, whereas the reversal offered positive correlation. The visualization of the resulting target potential coefficient (α) as heat map or in network form provides direct access to promising targets with ranked priority (Figure 22A). Several reactions show insignificant or even no correlation. Phosphoenolpyruvate carboxylase (Ppc), however, is clearly identified as an amplification target. Moreover, a number of reactions, including pyruvate kinase (Pyk), pyruvate dehydrogenase (aceEF), citrate synthase (GltA), aconitase (Can) and succinyl-CoA dehydrogenase (SucCD) reveal negative correlation, i. e. are identified as deletion or attenuation targets. However, in the case of the This concept was now applied to the complex large-scale metabolic network of *A. niger* in order to predict targets to design a superior cell factory.

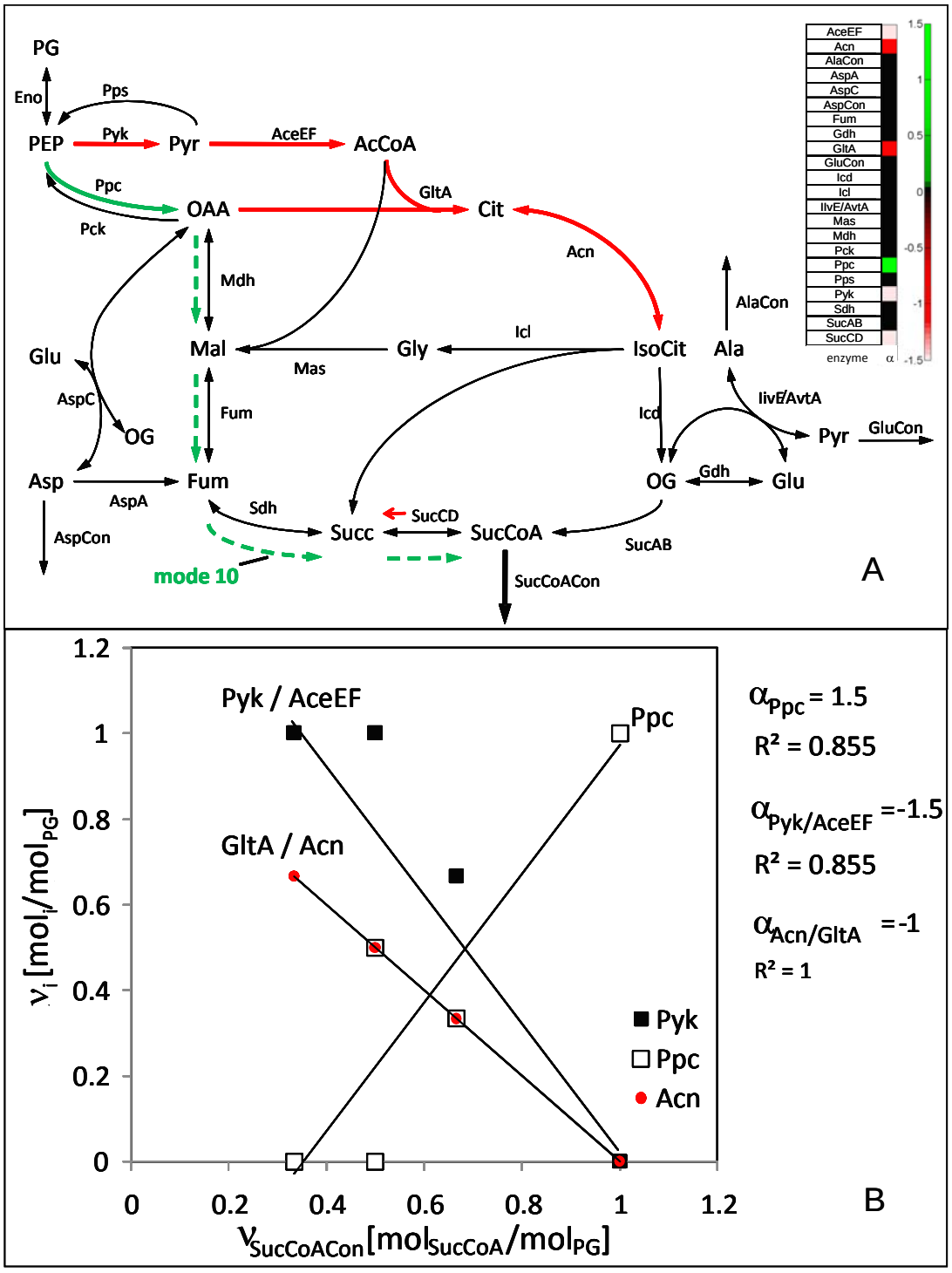

Figure 22: Principle of target identification by search for flux correlation to desired properties for succinyl-CoA production in a small example network taken from [131]. Calculation (B) of the target potential α by correlation analysis and data visualization (A) as heat map or in network form with colour coded representation of amplification targets (solid green arrow) and deletion targets (red arrows).

6.3.2 Structural analysis for the identification of genetic targets

The data provided by elementary mode analysis should now be utilized for the prediction of genetic targets for improved production of the target protein.

First investigations considering the whole set of elementary modes revealed a few significant reactions, correlated to the predicted flux. These involved fructofuranosidase synthesis, secretion and glycosylation (mannose 6-P isomerase) or ammonium transport as indicated in Figure 23A and B, respectively. The formation of the by-products oxalate (Figure 23C) and gluconate (Figure 23D) obviously does not correlate with the production of enzyme.

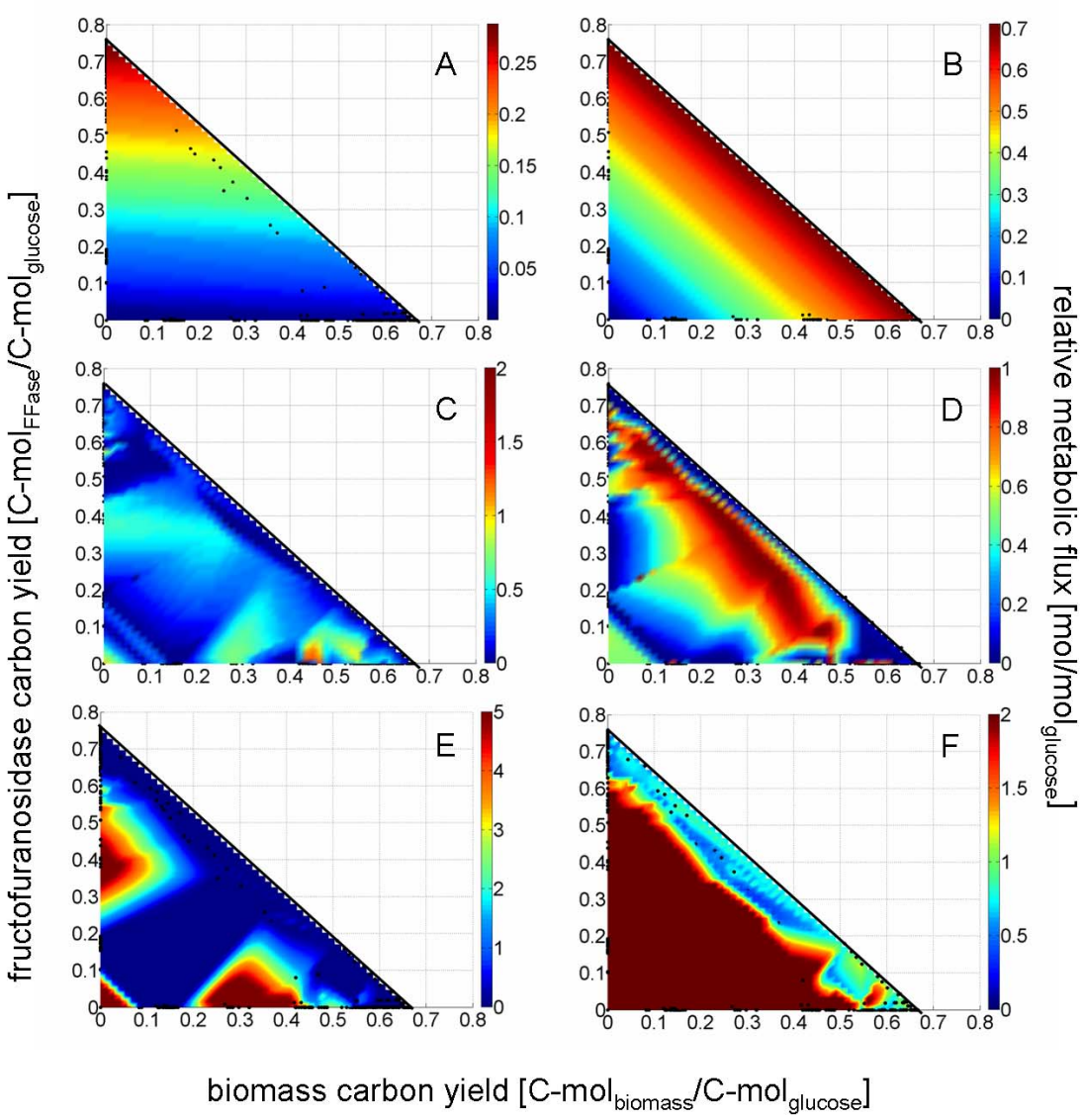

Figure 23: Relative metabolic fluxes of glycosylation (A), ammonium uptake (B), oxalate export (D), gluconate synthesis by glucose oxidase (D), ATP maintenance (E) and citrate synthase (F) as a function of total carbon yield for biomass and fructofuranosidase. The overlay plot was enabled by interpolation between values.

Also, ATP demand for maintenance wasn't found to correlate with production, but as qualitatively illustrated, a high requirement of ATP was linked to a lower product yield (Figure 23 E), so that this reaction obviously has disadvantages for efficient product formation.
Similarly, also the tricarboxylic acid cycle exhibits strong negative correlation to synthesis of the main products biomass and the target protein (Figure 23 F). These first findings provide the interesting result that fluxes obtained by elementary mode analyses are to some extent correlated. This appears as an important finding that seems attractive as a new concept for the identification of targets for superior network performance. Due to this, the obtained elementary modes were analyzed to look for statistically significant correlations between production flux and specific pathway fluxes in the network.
Since the representations in Figure 23 have a rather qualitative character, it was now important to introduce a quantitative concept as the basis for prediction of potential genetic targets. In this regard, the impact of a metabolic reaction as genetic target was then based on the target validity coefficient ($\alpha_{i,j}$), i.e. the slope of the linear correlation.
The results, comparing target validity for protein production on glucose (Glu), xylose (Xyl) and glycerol (Gly) under growth-associated (+) and non-growth-associated conditions (-) are visualized as heat map in Figure 24.
The reactions in the elementary modes were now screened for statistically significant correlation to the enzyme production. The potential of a metabolic reaction as genetic target was then expressed quantitatively whereby positive values denote amplification and negative values deletion targets, respectively. First investigations, considering the whole set of all 21,000 elementary modes, revealed only a few targets. A closer inspection showed that most targets are specifically attributed to the cellular state. To exploit this observation systematically, the elementary modes were grouped into subsets of growth-associated (simultaneous production of target protein and biomass) and non-growth-associated ones (production of target protein, no production of biomass) prior to analysis. Hereby, only modes with zero by-product formation were considered. This increased the hit rate of the approach substantially. The results for production on glucose, xylose, glycerol and oleic acid under growth-associated (+) and non-growth-associated conditions (-) are visualized as heat map (Figure 24). Fructofuranosidase synthesis and secretion and mannose 6-phosphate isomerase were identified as amplification targets independent of the biological state and also of the carbon source. These targets were also identified when all elementary modes were screened (data not shown). Other predicted targets strongly depended on the metabolic growth state. As an

example, the amplification of the PPP and deletion/attenuation of the glycolysis display promising targets only under growth associated conditions. Cytosolic NADPH-dependent isocitrate dehydrogenase, however, displayed a non-growth associated amplification target independent on the applied carbon source. Deletion or attenuation targets for non-growth conditions were found within the TCA cycle and also reactions linked to respiration and ATP metabolism. In comparison, no statistically valid correlations could be obtained for oleic acid as substrate in addition to the general findings.

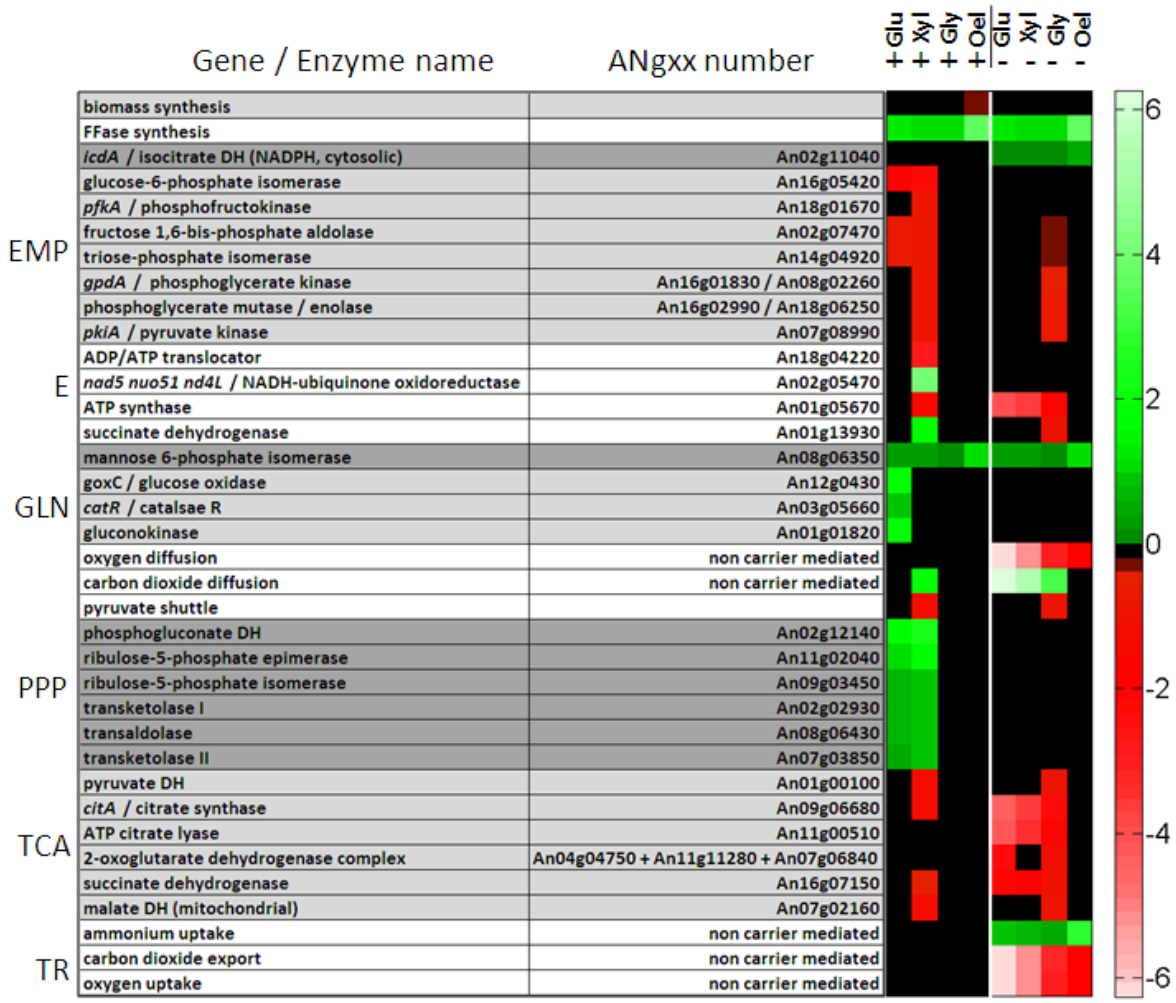

Figure 24: Prediction of genetic targets for improved fructofuranosidase production in *A. niger* based on the target validity coefficient. The target validity coefficient was obtained from correlation of flux through metabolic reactions and fluxes within the calculated elementary modes leading to fructofuranosidase production. A positive value (green colour) relates to a reaction, which positively correlates with the production, whereas negative correlation is indicated by a negative value (red colour). Black colour indicates statistically insignificant values (no correlation = nc). The investigated biological scenarios comprise growth- (+) and non-growth-associated production (-) on glucose (Glu), glycerol (Gly), xylose (Xyl) and oleate (Ole) as carbon source. The absolute values for the target validity coefficients together with statistical information are additionally available in the supplementary material (Table A2 – A7).

At this stage it appears that the underlying network for utilization of this complex substrate mixture is highly flexible and capable to achieve efficient production with significantly different underlying pathway usage.

6.3.3 Influence of nitrogen sources on fructofuranosidase production

The concept of flux correlation analysis was now further applied to *A. niger*.
In a further inspection the influence of the type of nitrogen source regarding to the optimal pathways of fructofuranosidase production was characterized (Figure 25).
For this, nitrate and ammonium were selected and, as it was already observed before, nitrate causes a substantial decrease in optimal fructofuranosidase yield of about 18 % independent of the applied carbon sources.
The analysis of the optimal fluxes revealed that the additional NADPH demand for the reduction of nitrate has been ensured by the increase in both the oxidative pentose phosphate pathway as well as the mannitol cycle regarding the mannitol 2-phosphate dehydrogenase (Figure 25).
In particular, the relative metabolic flux significantly increased from 11 % to 108 % using ammonium (see Figure 18A) or nitrate, respectively. Also, the relative flux through the mannitol cycle increased from 26 % to 46 % using ammonium or nitrate, respectively.
The impact of different nitrogen sources of the complete metabolic network compared with further carbon sources is visualized in Figure 26.
Here, the relative fluxes under nitrate supply were set in proportion with the resulting relative fluxes under ammonium supply. Additionally, only values with differences higher than 20 % between the relative fluxes of both nitrogen sources were considered.

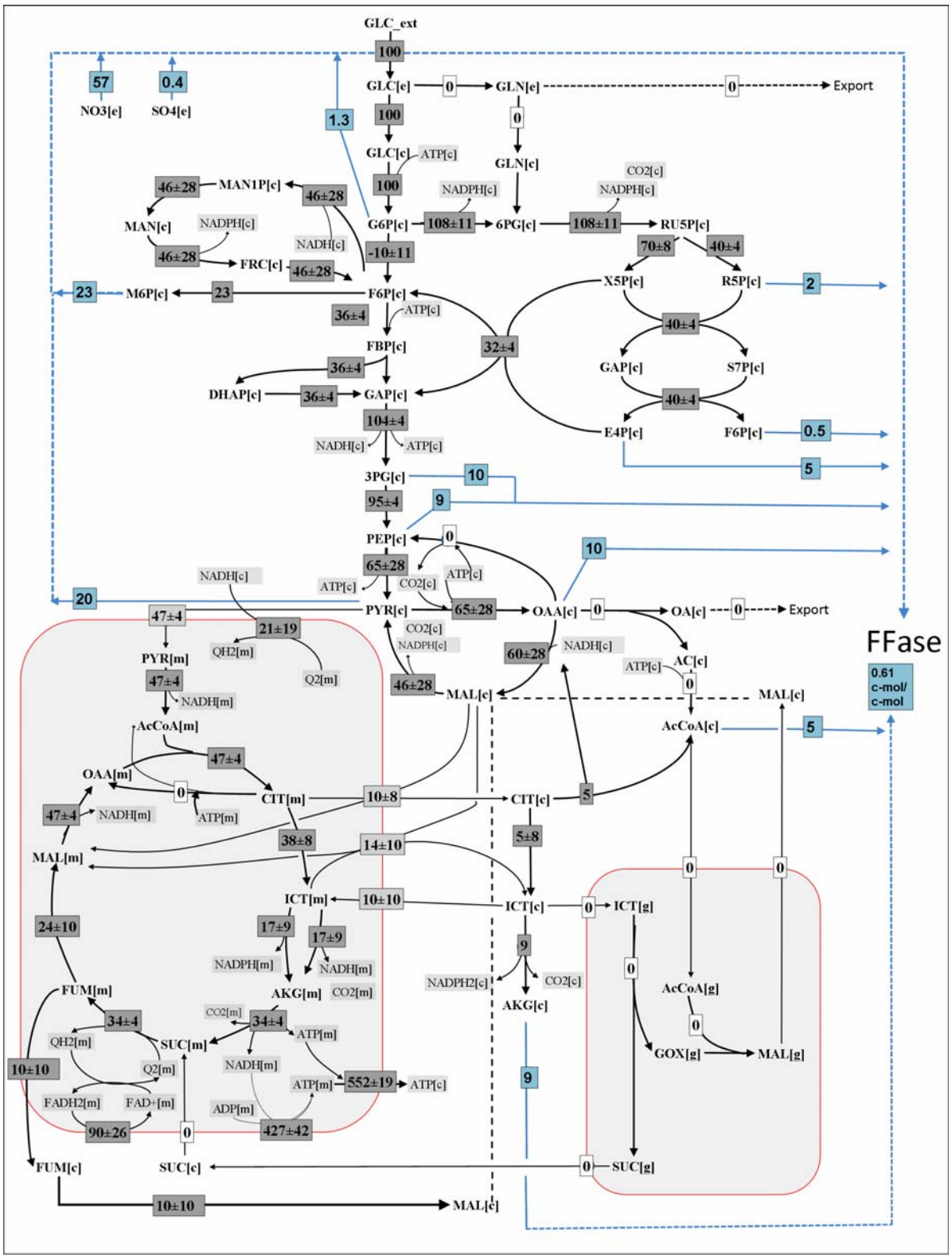

Figure 25: Optimal flux distribution for fructofuranosidase production in *A. niger* with glucose as carbon source and nitrate as nitrogen source. The relative flux coefficients are averaged from 80 elementary flux modes. All fluxes are given as relative percental molar flux [mol. (mol glucose)-1.100].

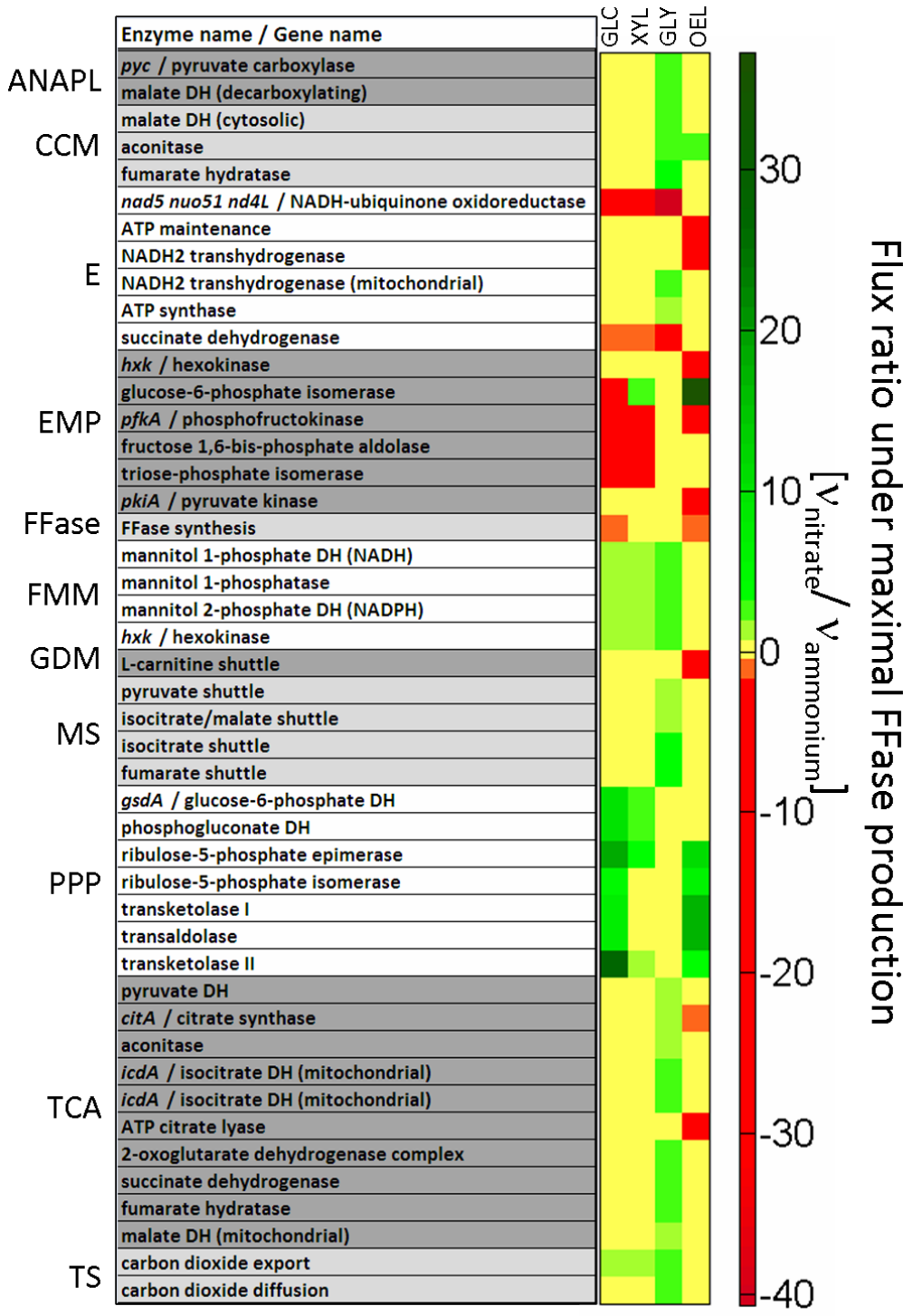

Figure 26: Metabolic flux ratios. Influence of nitrogen sources on optimal fructofuranosidase production in *A. niger* with glucose as carbon source. Ratios are calculated between relative metabolic fluxes under optimal fructofuranosidase production using nitrate ($v_{nitrate}$) and ammonium ($v_{ammonium}$) . Glucose was used as carbon source. The relative flux coefficients are averaged from 80 elementary flux modes. All fluxes are given as relative percental molar flux [mol· (mol glucose)$^{-1}$·100]. Anaplerotic reactions (ANAPL), cytosolic citrate metabolism (CCM), energy metabolism (E), glycolysis (EMP), fructose-mannose metabolism (FMM), glyoxylate and dicarboxylate metabolism (GDM), mitochondrial shuttle (MS), tricarboxy acid (TCA), pentose-phosphate pathway (PPP) and transport systems (TS).

As has been determined for glucose, the use of xylose revealed also an increase in the flux through the oxidative pentose phosphate pathway as well as the mannitol 2-phosphate dehydrogenase. However, when using glycerol, the NADPH formation was mainly ensured through the mannitol cycle and malic enzyme. As shown above, the type of nitrogen source led to significant changes in the pathway usage to achieve optimum production. Taking into account the complete set of elementary modes, however, no significant differences could be detected for the genetic targets under consideration the inspection of the case using ammonium, which is exemplarily depicted for glucose in Figure 27.

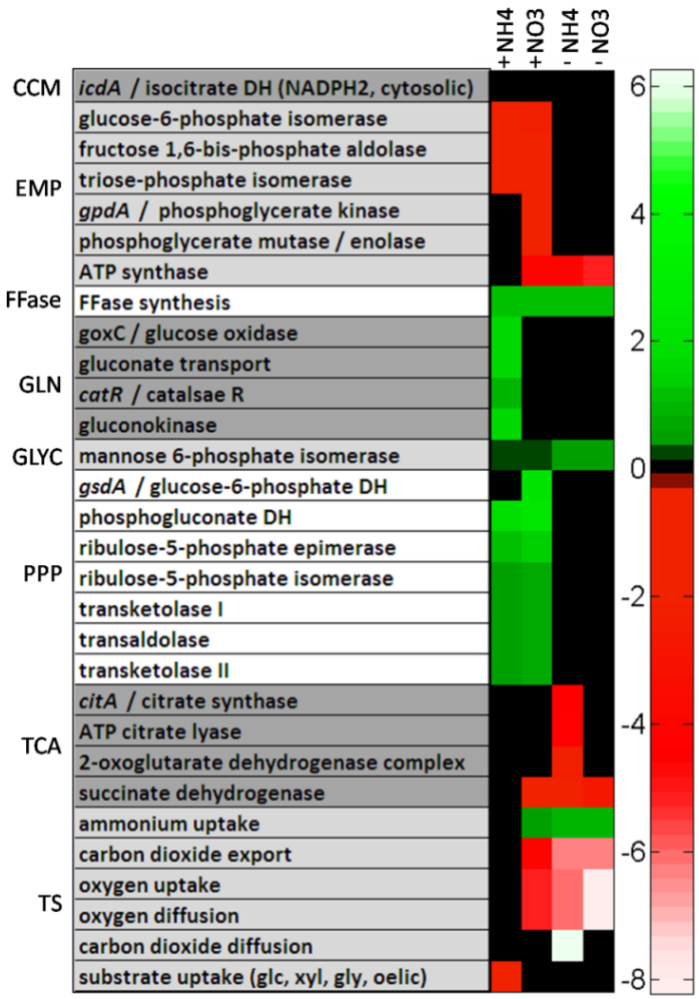

Figure 27: Prediction of genetic targets for improved fructofuranosidase production in *A. niger* based on the target validity coefficient. The target validity coefficient was obtained from correlation of flux through metabolic reactions with fructofuranosidase production flux within the calculated elementary modes. A positive value (green colour) relates to a reaction, which positively correlates with the production, whereas negative correlation is indicated by a negative value (red colour). Black colour indicates statistically insignificant values (no correlation = nc). The investigated biological scenarios comprise growth- (+) and non-growth-associated production (-) on glucose either with ammonium (NH_3) or with nitrate (NO_3).

6.4 Elementary Flux Mode Analysis for Production of Different Target Products

Elementary flux mode analysis was further carried out for the enzymes glucoamylase, epoxide hydrolase and the low molecular weight product citrate. The results were compared with those studied for fructofuranosidase production using glucose and ammonium as carbon and nitrogen sources, respectively (Figure 28).

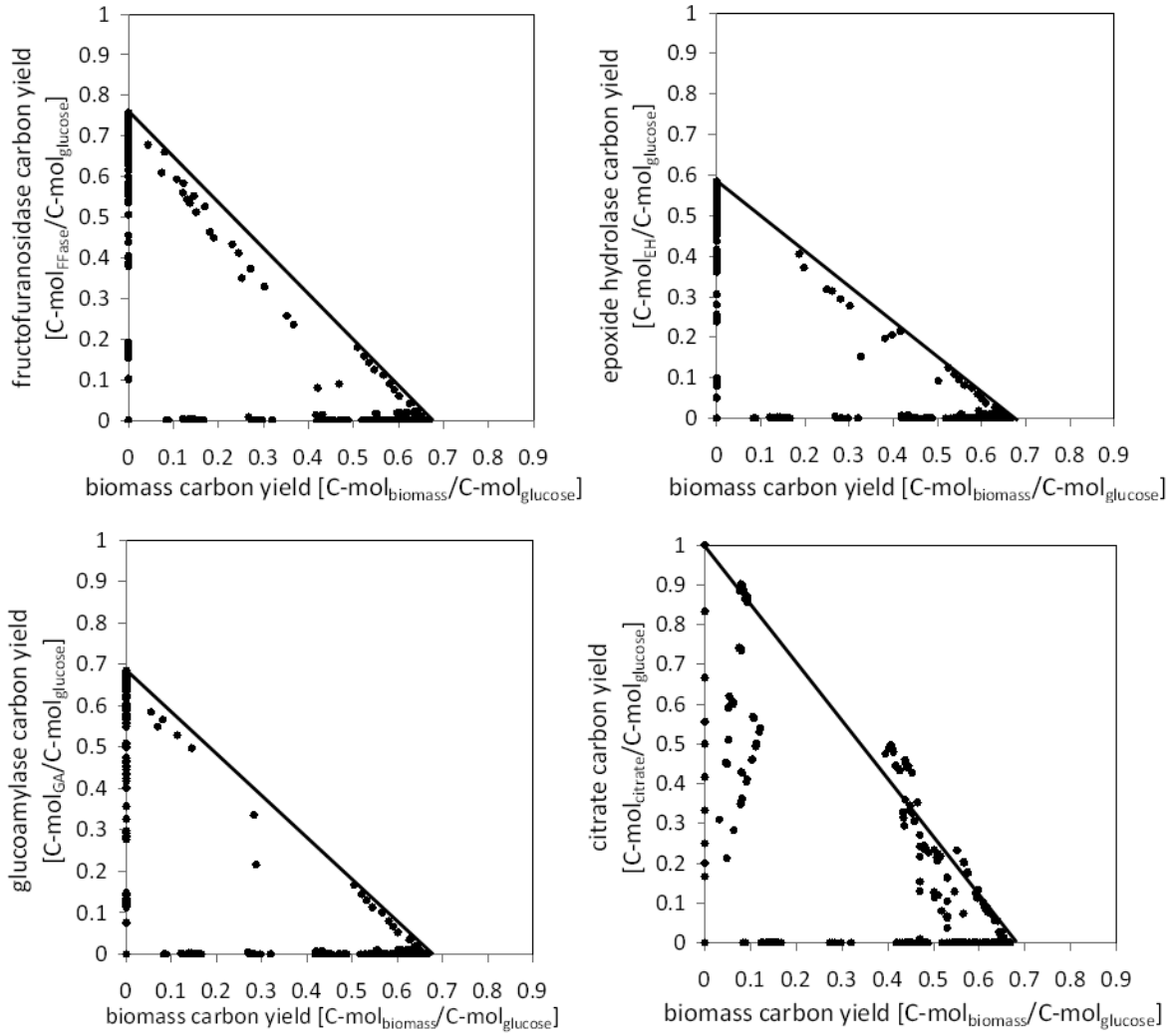

Figure 28: Elementary flux modes for production of biomass and different target products in *A. niger* on glucose. A: fructofuranosidase, B: epoxide hydrolase, C: glucoamylase, D: citrate.

The maximal carbon yield for glucoamylase (0.68 C-mol/C-mol) and epoxide hydrolase (0.58 C-mol/C-mol) was significantly lower than that for fructofuranosidase (0.76 C-mol/C-mol). The maximum yield for citrate was 1 C-mol/C-mol. This was also determined for other organic acids, such as oxalate and gluconate (not shown). *A. niger* is a well-known

organic acid producer and is capable to convert glucose to a number of organic acids with 100 % efficiency, as experimentally determined [2]. In contrast to the other products, several modes lie above the optimal line representing strategies that are more efficient in terms of total substrate carbon recovery than those using linear combination of the most efficient modes for each single product [191].

6.4.1 Optimal pathways

With exception of the upper part of the glycolysis leading to fructose bis-phosphate and the PPP, the relative metabolic fluxes at maximum protein production revealed significant differences (Figure 29). Unlike fructofuranosidase production, the relative flux through the TCA cycle (citrate synthase) increased by 20 % for glucoamylase and 40 % for epoxide hydrolase production. This is reflected by a higher flux through the glycolysis, e.g. the flux through the pyruvate kinase, which is increased by 25 % for glucoamylase and 34 % for the epoxide hydrolase production. Overall, this leads to an increased NADH supply in the cytosol allowing a higher flux through the ubiquinone dehydrogenase delivering mitochondrial NADH for the oxidative phosphorylation. A closer inspection revealed that the decreased flux through the glycolysis during fructofuranosidase production occurred at the expense of an increased flux through the glycosylation pathway delivering sufficient mannose 6-phosphate for glycosylation. In comparison to fructofuranosidase, glucoamylase is significantly less glycosylated, while the epoxide hydrolase does not contain any glycosyl residues.

It becomes obvious that branch point at fructose 6-phosphate plays a key role concerning the optimal pathway usage for maximum protein production. Neither by-product formation nor production of ATP excess for maintenance was observed under maximal glucoamylase and epoxide hydrolase production as it was also the case for fructofuranosidase production. Maximum production of citrate was enabled by a high flux through the glycolysis and the TCA cycle (citrate synthase, aconitase) without participation of the PPP. The release of citrate from the mitochondria into the cytosol was enabled by the citrate/malate shuttle, isocitrate shuttle and the isocitrate/malate shuttle.

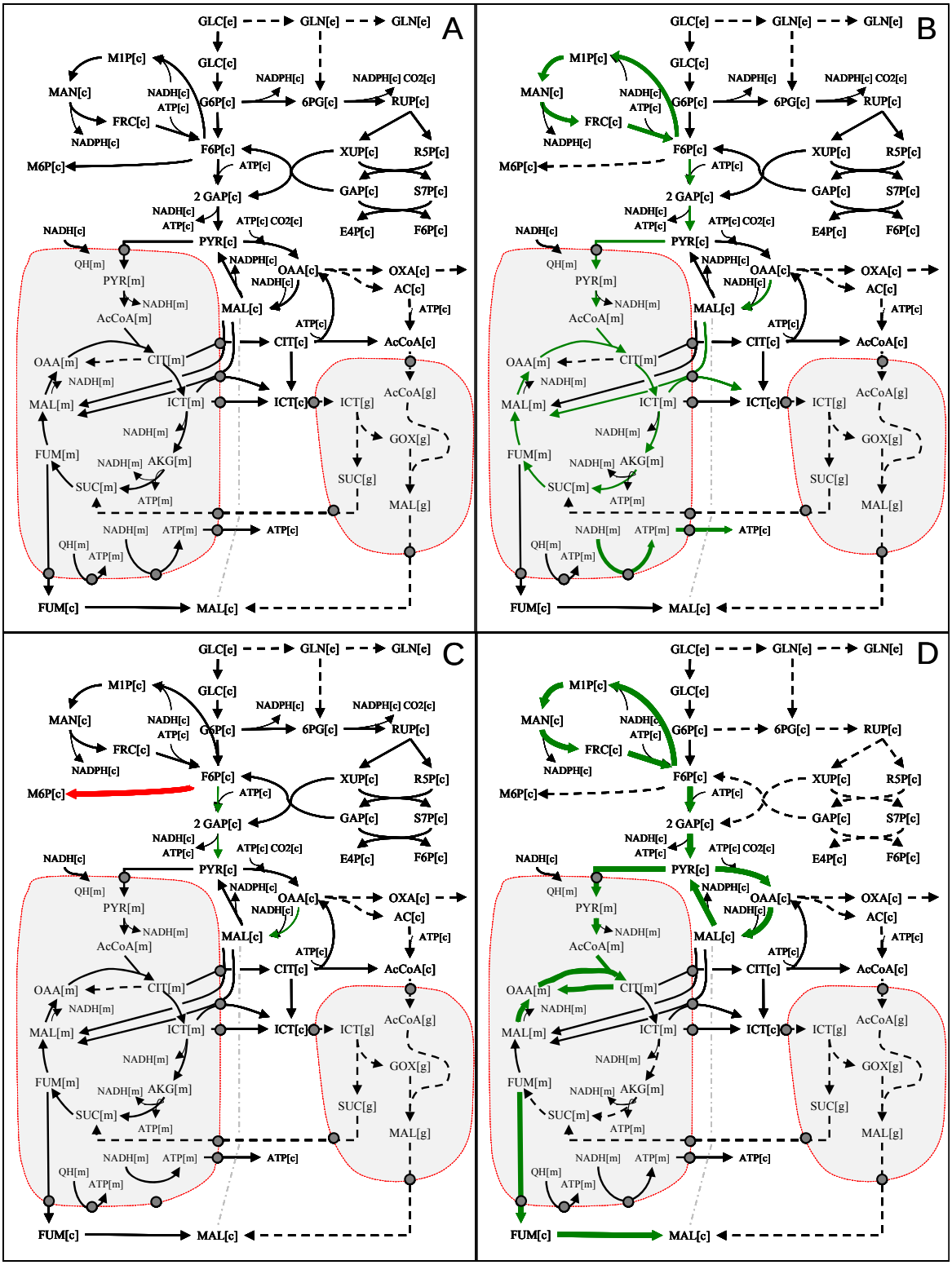

Figure 29: Flux distribution for main production of fructofuranosidase (A), epoxide hydrolase (B), glucoamylase (C) and citrate (D) production by *A. niger* on glucose and ammonium. The relative flux coefficients are averaged from 160 (FFase), 112 (EH), 112 (GA) and 36 (citrate) elementary flux modes for maximal production obtained for each target product. All fluxes are given as relative molar fluxes normalized to 1 mol of glucose unit [mol· (mol glucose)$^{-1}$·100].

Table 19: Optimal flux distribution for production of fructofuranosidase (FFase, epoxide hydrolase (EH), glucoamylase (GA) and citrate using glucose as carbon and ammonium as nitrogen source. All fluxes are given as relative molar fluxes normalized to 1 mol of glucose unit [mol (mol glucose)$^{-1}$ 100]. The relative flux coefficients are averaged from 160 (FFase), 112 (EH), 112 (GA) and 36 (citrate) elementary flux modes for maximal production obtained for each target product. Metabolic reactions participate in the glycolysis (EMP), Pentose-Phosphate Pathway (PPP), anaplerosis (ANAPL), fructose mannose metabolism (FMM) citrate cycle (TCA) and energy metabolism (E).

	Metabolic Reactions	Target Products			
		FFase	EH	GA	Citrate
EMP	Glucose 6-P isomerase	87 ± 7	82 ± 12	82 ± 12	100
	Enolase	111 ± 2	166 ± 4	148 ± 12	200
	Pyruvate kinase	100 ± 3	151 ± 4	133 ± 4	274 ± 55
PPP	Glucose 6-P DH	11 ± 7	18 ± 12	18 ± 12	0
	Transketolase/Transaldolase	5 ± 2	8 ± 4	8 ± 4	0
ANAPL	Malic enzyme	52 ± 40	55 ± 32	54 ± 32	148 ± 110
	Pyruvate carboxylase	75 ± 21	88 ± 32	88 ± 32	323 ± 83
FMM	Mannitol 2-DH	26 ± 20	55 ± 32	54 ± 32	74 ± 55
	Mannose 6-P isomerase	29 ± 0	0	7.5 ± 0	0
TCA	Citrate synthase	53 ± 2	88 ± 4	66 ± 4	446 ± 85
	Isocitrate dehydrogenase (mit)	36 ± 18	60 ± 30	44 ± 22	0
	Isocitrate dehydrogenase (cyt)	11 ± 0	18 ± 0	18 ± 0	0
E	ATP synthase	500 ± 5	781 ± 21	585 ± 42	528
	Ubiquinone reductase	57 ± 12	75 ± 20	67 ± 19	100

The complete flux data sets corresponding to optimal pathway usage for glucoamylase (Figure 43), epoxide hydrolase (Figure 42) and citrate (Figure 44) are given in the appendix.

6.4.2 Identification of genetic targets based on flux correlation

The established methodology should now be further applied to investigate specific differences in product formation concerning genetic targets related to the flux correlation.

As was investigated for fructofuranosidase considering the whole set of elementary modes, only a few significant targets such as protein synthesis and glycosylation for glucoamylase and fructofuranosidase were predicted as targets independent of the biological state. A closer inspection in terms of target validity coefficients under growth associated (+) and non-growth associated conditions (-) are visualized as heat map in Figure 30.

As is predicted for fructofuranosidase, the amplification of the PPP flux and down-regulation of glycolysis display promising targets under growth associated conditions for glucoamylase as target product.

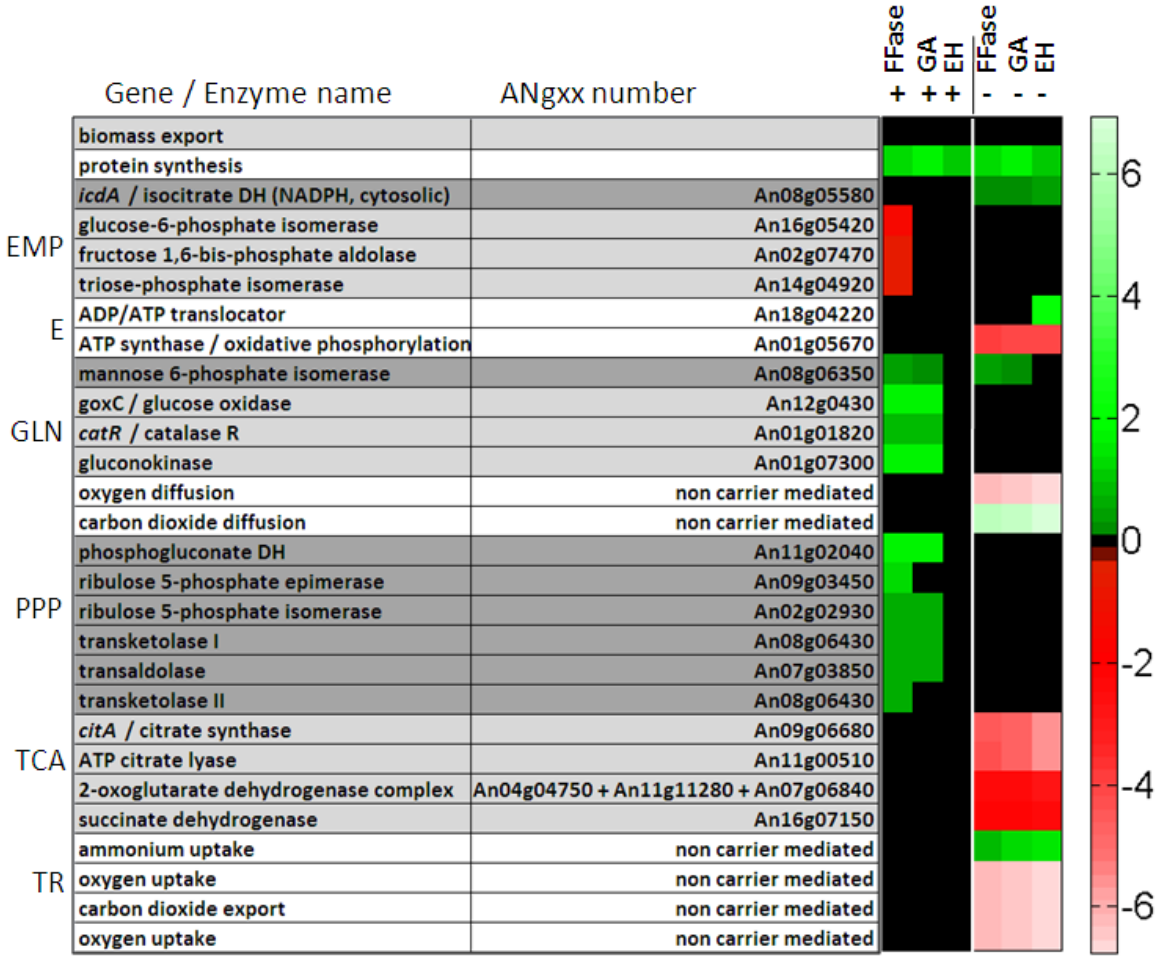

Figure 30: Prediction of genetic targets for improved fructofuranosidase (FFase), glucoamylase (GA) and epoxide hydrolase (EH) production by *A. niger* based on the target validity coefficient. The investigated biological scenarios comprise growth (+) and non-growth associated production (-) on glucose. The corresponding metabolic reactions refer to Embden-Meyerhof-Parnas pathways / glycolysis (EMP), energy metabolism (E), gluconate metabolism (GLN), pentose-phosphate pathway (PPP), tricarboxyca-cid cycle (TCA) and transport processes (TR).

For all proteins, negative correlation, i. e. genes to be attenuated, was found for the TCA cycle and reactions linked to respiration and ATP metabolism. Ammonium uptake as well as protein synthesis revealed a positive correlation independent of the target protein. Interestingly, while the PPP revealed positive correlation for the growth associated enzyme production, cytosolic NADPH isocitrate dehydrogenase seems to be significant for the non-growth associated production for all proteins.

In the case of citrate, the pathways of glycolysis showed a complete positive correlation and thus, genes to be amplified, while the oxidative and non-oxidative pentose phosphate pathway did negatively correlate (data not shown).

6.4.3 Effect of glycosylation degree on product formation

A closer examination of the effects of glycosylation on the metabolic network analyses was carried out. For this purpose, the stoichiometric model for fructofuranosidase synthesis was modified leading to several stages of glycosylation degree.

The supply of glycosylation precursors is accomplished via fructose 6-P and mannose 6-P. This result in a corresponding change of the flux through the EMP, TCA and oxidative phosphorylation, while, the PPP and the mannitol cycle are nearly unaffected (Figure 31).

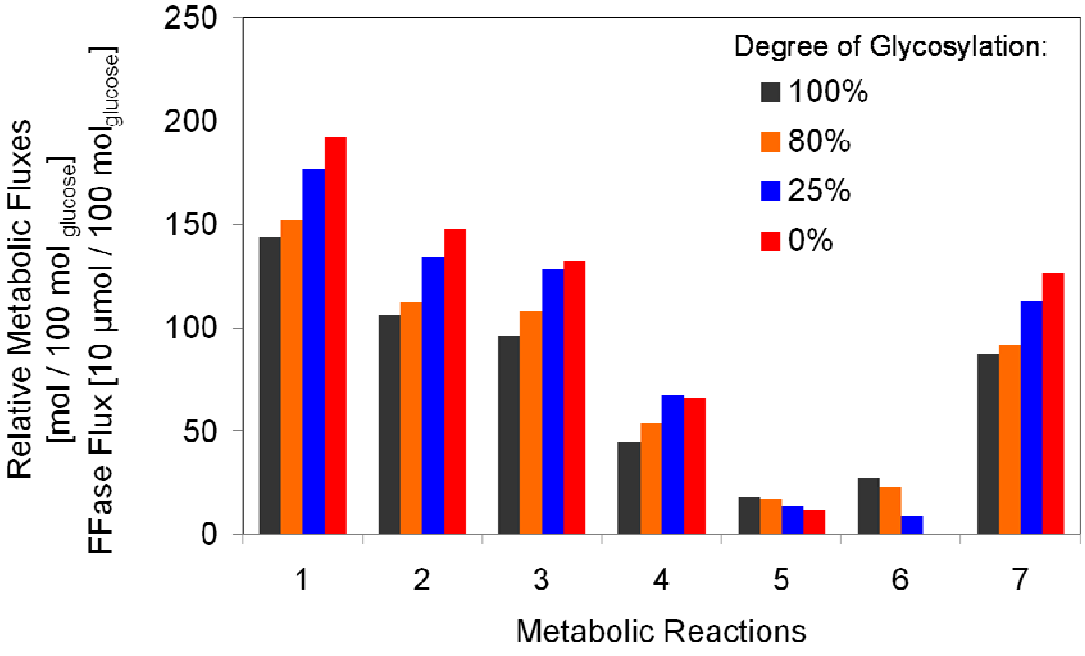

Figure 31: Flux distribution values for fructofuranosidase production using glucose by *A. niger* depending on the glycosylation degrees. The metabolic reactions are: 1: oxidative phosphorylation (energy metabolism), 2: pyruvate kinase (EMP), 3: citrate-malate shuttle (redox metabolism), 4: mannitol 2-dehydrogenase (mannitol-cycle), 5: 6-P-gluconate DH (PPP), 6: mannose 6-P isomerase (glycosylation), 7: molar yield of FFase production. The relative flux coefficients are averaged from 160 (100% glycosylation), 120 (80%), 147 (25%) and 54 (0%) elementary flux modes for maximal fructofuranosidase production (%: percentage of glycosyl content). All fluxes are given as relative molar flux normalized to 1 mol of glucose unit [mol · (mol glucose)$^{-1}$ · 100].

These changes of the flux pattern are very similar to the changes from the simulations using different proteins. Thus, the proportion of sugar residues significantly affected the pathway usage for optimal protein production. Because proteins are composed from a total of 20 amino acids, each of the amino acids is presented at a rather low proportion in the protein. Since, sugar residues in glycosylated proteins, such as the fructofuranosidase, represent the major proportion, the influences and flux changes induced by amino acids are therefore marginal in comparison to the influence of the sugar residues as is shown here. Each of the sugar molecules synthesized to oligosaccharide needs one molecule ATP for its activation to GMP-mannose. Therefore, the supply of ATP by the oxidative phosphorylation plays an imminent role to ensure sufficient energy equivalents for glycosylation, and, hence, the flux through the EMP must be increased providing high fluxes through the mitochondrion.

Interestingly, the flux distribution in the central carbon metabolism for the production of fructofuranosidase without glycosylation (not shown) was almost identical with the flux distribution for non-glycosylated epoxide hydrolase.

6.5 *In silico* Evaluation of other Industrial Production Hosts

In silico metabolic network analysis was used for comparative analysis of different industrial relavant production strains. For this purpose, two bacterial strains, gram-negative *E. coli* and gram-positive *B. subtilis*, were considered. Additionally, the yeast *S. cerevisiae* was considered for this study. In a first step, the metabolic networks were compared to each other in terms of epoxide hydrolase production. The model protein epoxide hydrolase from *A. niger* is an interesting protein for pharmaceutical applications, which is commercially produced by *A. niger* as well as *E. coli*. In a second step, comparative analysis of theoretical maximum amino acid production should give an insight into the metabolic capacities of different industrial strains and the advantages to use this EFM-based analysis method.

6.5.1 Maximal theoretical yield for epoxide hydrolase

The results from elementary flux mode analysis for epoxide hydrolase production using different industrial hosts are shown in Table 20.

Table 20: Elementary mode analysis of epoxide hydrolase production by different industrial hosts grown on glucose and ammonium.

Organism	Network Dimension (m x q)	Side Products	Number of Elementary Flux Modes		Maximal yield [C-mol/C-mol]	
			total	EH yielding modes (%)	EH	Biomass
A. niger	74 x 83	oxalate, gluconate	16,156	5,667 (35)	0.58	0.67
S. cerevisiae	67 x 79	acetate, ethanol	51,055	15,394 (36)	0.52	0.63
E.coli	48 x 54	acetate	2,328	912 (39)	0.56	0.84
B. subtillis	43 x 49	acetate	473	189 (40)	0.50	0.77

The number of elementary flux modes differs significantly between the organsim (Figure 32) (Table 20). The major reason for the different numbers was the different numbers of potential side products, which were considered on the basis of the referred metabolic mod-

els. In all cases, the dominating fraction of elementary flux modes was either linked to exclusive production of epoxide hydrolase or to growth. Concerning the theoretical yield for epoxide hydrolase and biomass, the highest maximal yield was obtained for *E. coli* with 0.56 C-mol/C-mol and 0.84 C-mol/C-mol, respectively.

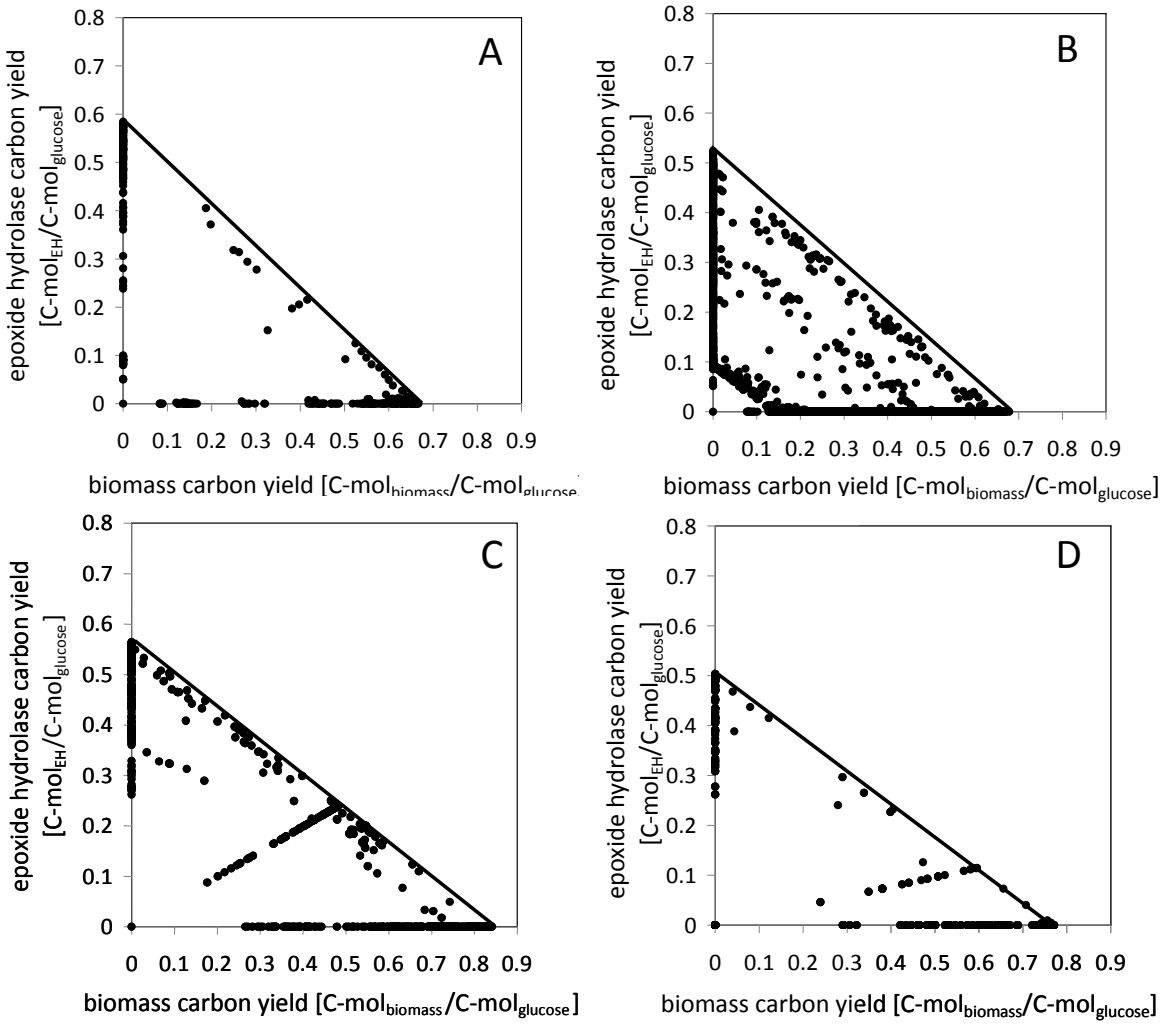

Figure 32: Comparison of elementary modes for biomass and epoxide hydrolase production on glucose in different industrial hosts. A: *A. niger*, B: *S. cerevisiae*, C: *E. coli* and D: *B. subtilis*.

6.5.2 Optimal pathways for Epoxide Hydrolase production

Significant differences in metabolic strategies for the NADPH generation were observed between the organisms explaining their differing production potential (Table 21). While NADPH generation in *A. niger* (for flux map see Figure 42 in appendix) occured mainly by mannitol 2-dehydrogenase (26 ± 20 %) as well as by decarboxylating malic enzyme

(52 ± 40 %), NADPH in *S. cerevisiae* (for flux map see Figure 45 in appendix) was mainly supplied by the cytosolic NADPH-dependent isocitrate dehydrogenase (55 ± 19 %), malic enzyme (33 ± 23 %) and ATP-depending transhydrogenase (33 ± 23 %).

Table 21: Flux distribution for epoxide hydrolase production using different production hosts. Glucose and nitrogen are used as carbon and nitrogen source, respectively. All fluxes are given as relative molar fluxes normalized to 1 mol of glucose unit [mol (mol glucose)$^{-1}$ 100]. The relative flux coefficients are averaged from 160 (*A. niger*), 28 (*S. cerevisiae*), 49 (*E. coli*) and 18 (*B. subtilis*) elementary flux modes for maximal epoxide hydrolase production obtained for each organism. Metabolic reactions participate in the glycolysis (EMP), Pentose-Phosphate Pathway (PPP), anaplerosis (ANAPL), fructose mannose metabolism (FMM) citrate cycle (TCA) and energy metabolism (E).

	Metabolic Reactions	**Production Hosts**			
		A. niger	***S. cerevisiae***	***E. coli***	***B. subtilis***
EMP	Glucose 6-P isomerase	82 ± 12	86 ± 9	56 ± 40	88 ± 5
	Enolase	166 ± 4	171 ± 3	157 ± 15	172 ± 2
	Pyruvate kinase	151 ± 4	157 ± 3	121 ± 21	138 ± 13
PPP	Glucose 6-P DH	18 ± 12	14 ± 9	40 ± 40	12 ± 5
	Transketolase/ Transaldolase	8 ± 4	6 ± 3	15 ± 14	5 ± 2
ANAPL	Malic enzyme	55 ± 32	33 ± 23	4 ± 4	7 ± 5
	Pyruvate carboxylase	88 ± 32	62 ± 22	6 ± 6	6 ± 6
FMM	Mannitol 2-DH	55 ± 32	---	---	---
	Mannose 6-P isomerase	0	0	0	0
TCA	Citrate synthase	88 ± 4	222 ± 20	76 ± 14	97 ± 2
	Isocitrate dehydrogenase (mit)	60 ± 30	37 ± 19	---	---
	Isocitrate dehydrogenase (cyt)	18 ± 0	55 ± 19	56 ± 30	97 ± 2
GOX	Isocitrate lyase	0	0	20 ± 20	---

In *A. niger* (15 ± 11 %) as well as *S. cerevisiae* (14 ± 9 %) the PPP showed only low activities. This was also the case for *B. subtilis*, which showed a minor participation (12 ± 5 %) (for flux map see Figure 46 in appendix). Here, NADPH was almost exclusively provided by the NADPH-dependent isocitrate-dehydrogenase (97 ± 2). In contrast, *E. coli* (for flux map see Figure 47 in appendix) exhibited a high flux through the oxidative PPP (40 ± 40) as well as through the isocitrate-dehydrogenase (56 ± 30).

Different metabolic strategies depending on the network structures were also identified for the supply of pyruvate. In the case of the eukaryotes *A. niger* and *S. cerevisiae*, the flux around the pyruvate pool was dominated by anaplerotic reactions. Here, the compartmentalization of the cells required high exchange flux of molecules between the cytosol and mitochondria. In both organisms, this was mainly realized by high flux through anaplerotic

reactions, such as pyruvate carboxylase, malate dehydrogenase, malic enzyme as well as citrate lyase. Bacterial systems are not compartmented. Here, the anaplerotic reactions are not required for this compartmented balancing purpose. Furthermore, a high participation of the tricarboxylic acid cycle could be detected for all organisms.

6.5.3 Amino acid production

Amino acids are the building blocks of life and have long played an important role in both human and animal nutrition and health maintenance [172]. In terms of market volume, development over the last 20 years has been tremendously bullish in the so-called feed amino acids lysine, methionine, threonine, and tryptophan, which constitute the largest share (56%) of the total amino acid market, estimated in 2004 at approximately 4.5 billion US Dollar [192]. For this, the establishment of new processes and high efficient production strains is still of high interest, whereas the type of organism plays a crucial role in terms of health risk for human, production capacities and handling regarding to genetic engineering.

Concerning the capacity, the industrial hosts *A. niger*, *S. cereviseae*, *E. coli* and *B. subtilis* were investigated related to their amino acid production ability in this chapter using network analysis. The organisms are already widely used in industrial processes due to their versatile production capabilities.

Using the metabolic networks of the previously described industrial hosts, the theoretical maximal yields for all amino acids from glucose, xylose, glycerol as well as oleic acid were examined. Hereby, the simulation experiments were carried out under the assumption that no by-product formation (biomass, organic acids) occurred in the cell.

Aspergillus niger is higly efficient for producing all 12 precursors for amino acid synthesis [2, 73]. However, as shown in Figure 33A the production capacities for all amino acids are not completely efficient when using glucose.

With the exception of lysine, the yields of amino acids showed no major difference between the organisms when using glucose. The significantly higher yields of lysine in bacteria can be explained by the different synthesis strategies for lysine. In fungi, lysine is synthezised via the glutamate pathway, whereas synthesis in bacteria occurrs via the aspartate pathway [61], which is obviously beneficial. The presence of glycerol enabled the highest theoretical yield of amino acids in all organisms. In particular, yields for arginine, cysteine, histidine and the aromatic amino acids tryptophane and tyrosine, were significantly increased. The beneficial property of glycerol has already been shown for protein synthesis in this study.

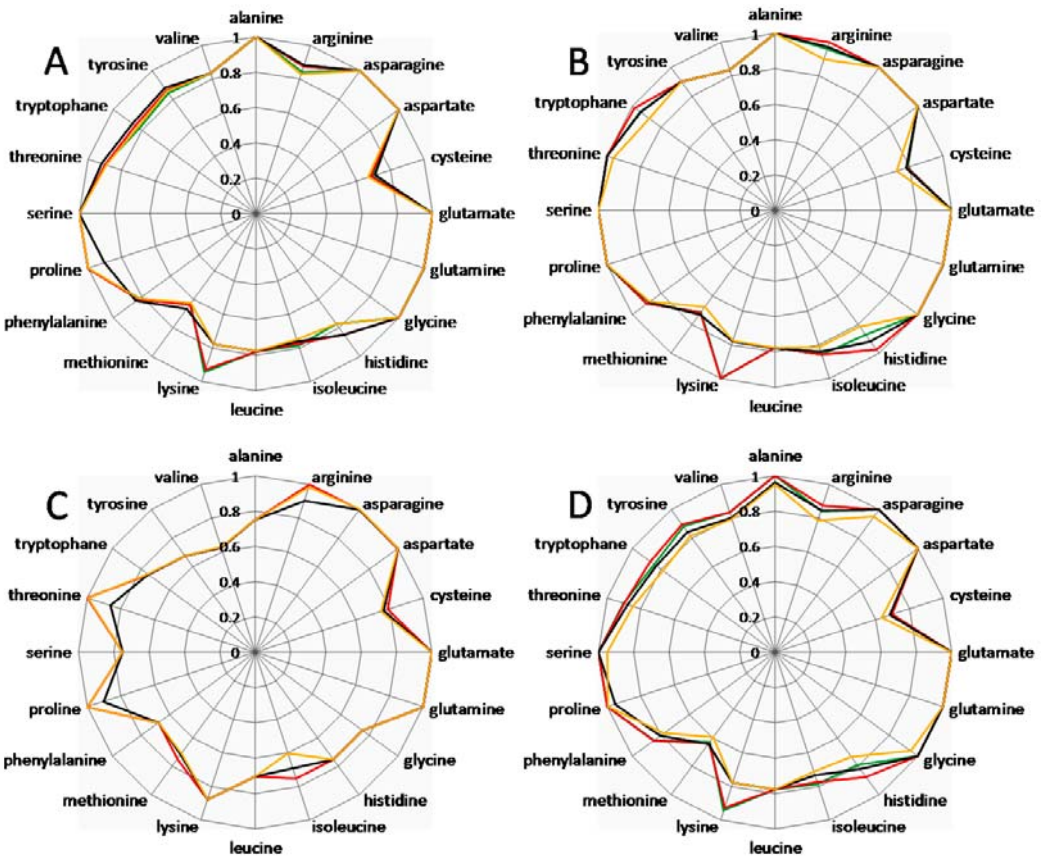

Figure 33: Radar plot of theoretical maximal yields (C-mol % amino acid per mol carbon source) for all 20 amino acids produced by industrial host *A. niger* (black), S. *cerevisiae* (yellow), *E. coli* (red) and *B. subtilis* (green) using different carbon sources glucose (A), glycerol (B), oleic acid (C) and xylose (D) and ammonium as nitrogen source.

When oleic acid was used, the maximal theoretical yields significantly decreased, in particular for the aromatic amino acids as well as serine and glycine. Here, the high release of reduction power in type of NADPH during the oxidation of fatty acids cannot be efficiently used. This may be related to the direct entry of acetate formed by the degradation in the glyoxylate metabolism.

Since *B. subtilis* is not able to grow on acetate, due to complete absence of the glyoxylate cycle, no elementary flux modes could be calculated when using oleic acid as the sole carbon source.

The pentose xylose seems to be more appropriate for bacteria than for fungi. In both organisms *A. niger* and *S. cerevisiae*, xylose is reduced by the xylitol dehydrogenase under the expense of NADPH leading to xylulose. In bacteria, xylose can be directly converted into xylulose by the xylose isomerase.

6.6 Experimental Evidence for Targets predicted by Flux Correlation

In the present work, the developed pathway analysis tool was applied and extended to predict systems-wide amplification and deletion targets as a useful approach to be used in metabolic engineering towards improved bio-production. Evidence that the reactions derived here open realistic chances for improvement can be obtained from recent studies.

6.6.1 Metabolic fluxes during glucoamylase production in *A. niger*

Continuous cultivation experiments were carried out under different pH values using glucose (for glucoamylase production) as sole carbon source. Steady state conditions could be verified by measurement of intracellular metabolite concentrations at a constant dilution rate of 0.1 h^{-1}. The variance of the concentration within a range of 5 to 9 volume changes was only 3.4, 7.8 and 5.8 % for glycerol, glucose-6-phosphate and glycine, respectively [120]. On the basis of these low variations, the assumption of a steady state condition could be verified.

In the presence of glucose, glucoamylase expression is induced by the *glaA*-promotor. The higher demand for NADPH leads to a higher flux through the PPP. The relative flux distribution through the oxidative PPP depends on the pH values, ranging from 24 to 42 % (Figure 34). The differences are apparently due to the increase of amino acid synthesis for glucoamylase production, which do depend on the pH value of the culture medium. Results suggest that the glucoamylase production is maximal at pH value of about 3.7. That might be the reason why the NADPH production through the oxidative part of the PPP presents a maximum at pH 3.7.

The mannitol cycle in *Alternaria* played a major role in NADPH generation compared to the transhydrogenase reaction [65]. In this work, the relative flux distribution of the mannitol cycle was rather constant under the different conditions studied. The values for the flux distributions of mannitol varied between 4 and 10 % at a pH of 3 and 5.5, respectively. These observations led to the conclusion that the increase of the NADPH demand in *A. niger* AB 1.13 is exclusively ensured by the oxidative PPP, as described for *Aspergillus oryzae* [193].

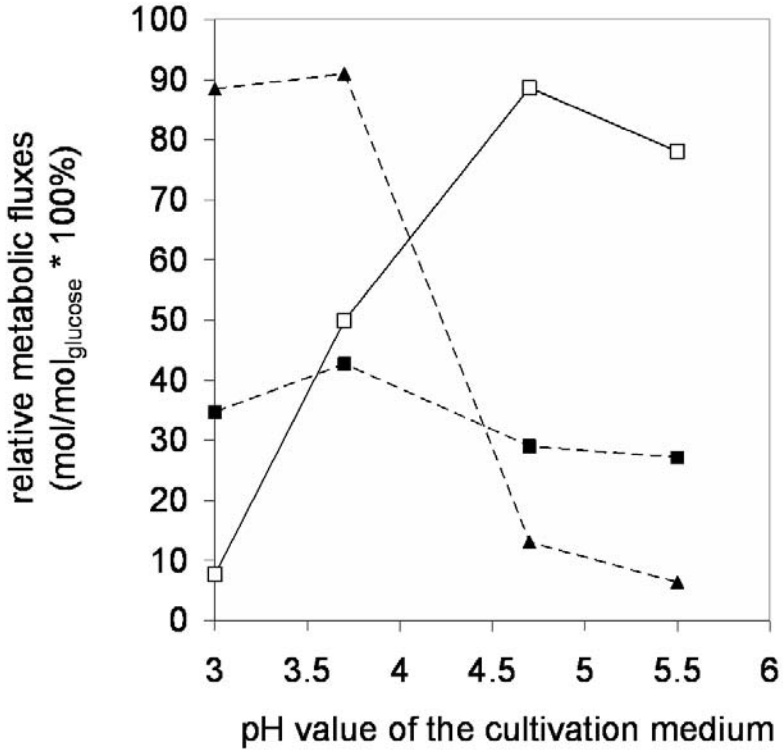

Figure 34: The relative flux distribution for the glucose-uptake under steady state conditions and glucoamylase production (black triangle, dashed line) as a function of pH value of the cultivation medium. The unit for glucoamylase production is µkat/g·h.

Additionally, the relative flux of the oxalate production rate catalysed by the oxaloacetate hydrolase shows an inversely proportional progress to the glucoamylase production indicating that a higher by-product formation of oxalate at the expense of glucoamylase synthesis.

6.6.2 Enzyme activities depending on biomass and glucoamylase production

Investigation of enzyme activities during continuous cultivation experiments under different growth rates revealed a correlation between oxidative PPP and the glucoamylase production, which both decreased with increasing growth rate. Simultaneously, pyruvate kinase, representing the EMP was significantly increased with increasing growth rate, and thus was negatively correlating to the glucoamylase production.

No significant differences could be identified for the isocitrate lyase, malate dehyrogenase, and mannitol 2-dehydrogenase representing the glyoxylate cycle, anaplerosis and mannitol metabolism, respectively (Figure 35).

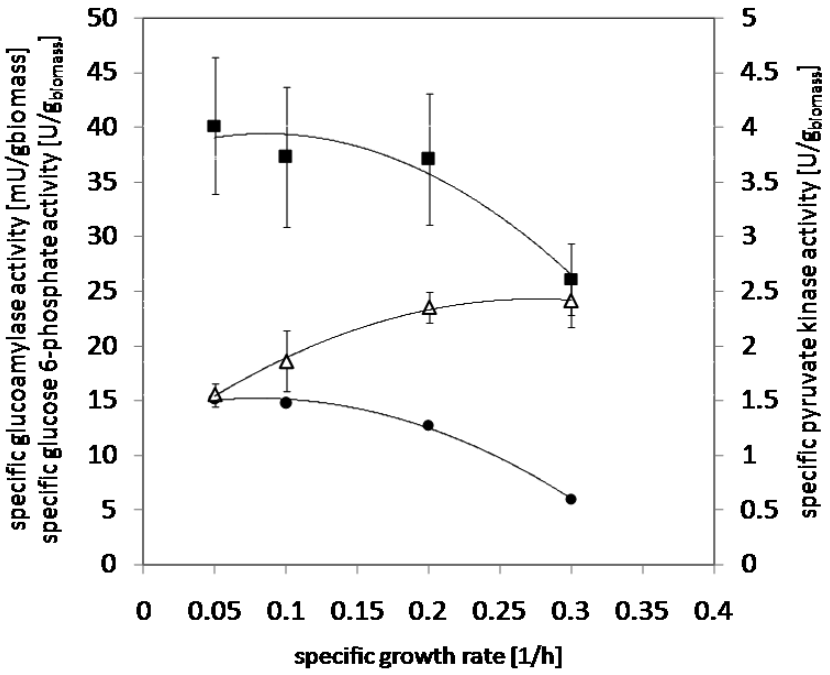

Figure 35: *In vitro* activities of glucose 6-phosphate dehydrogenase (filled square), glucoamylase (filled circle) and pyruvate kinase (open triangle) depending on the growth rate (biomass formation). Each point represents two continuous cultivation experiments (biological duplicate).

Although, *in vitro* enzyme kinetic studies may not represent the *in vivo* situation, but were at least consistent with the simulation studies because the glycolysis was identified as negative and the PPP as positive correlating targets, respectively.

6.6.3 Resume of experimental validations in *Aspergillus niger*

For protein production in *A. niger*, much less metabolic engineering progress of central carbon metabolism is reported. The few studies available, however, illustrate that targets predicted here have been valuably proven. As an example, the amplification of the synthesis of glycosylation residues increased protein over-production [4, 47]. Similarly, the amplification of the protein assembly route itself has been shown to result in an enhancement of production in *A. niger* [194]. Beyond, these experimental studies on more obvious targets, flux balance analysis and also stoichiometric flux analysis indicate the importance of sufficient NADPH supply for protein production in *A. niger* [117] and *A. oryzae* [193] whereby the PPP plays an important role which was also found in the present study as was shown before [120].

6.6.4 Lysine production with *Corynebacterium glutamicum*

6.6.4.1 Maximum production performance using glucose as carbon source.

Overall, 289 flux modes resulted for lysine production in *C. glutamicum*. Among the modes observed, the majority are extreme modes exclusively linked to the production of either biomass or lysine. In addition also flux modes with simultaneous production of biomass and lysine were observed. Among all modes, 6 modes enabled the optimum yield of 0.75 mol lysine/mol glucose which agrees with the value obtained by flux balance analysis [145, 180]. The average flux map from these optimum modes reveals the key pathways contributing to efficient lysine formation such as pentose phosphate pathway, ammonium metabolism, lysine biosynthesis and secretion (Figure 36).

The flux through most of these pathways is conserved. ATP linked reactions, however, reveal a substantial flexibility. The consumption of ATP under optimum production conditions either involves cellular maintenance requirement or “futile” cycling recruiting the carboxylation and decarboxylation reactions at the pyruvate node or the two enzymes phosphofructokinase and fructosebisphosphatase.

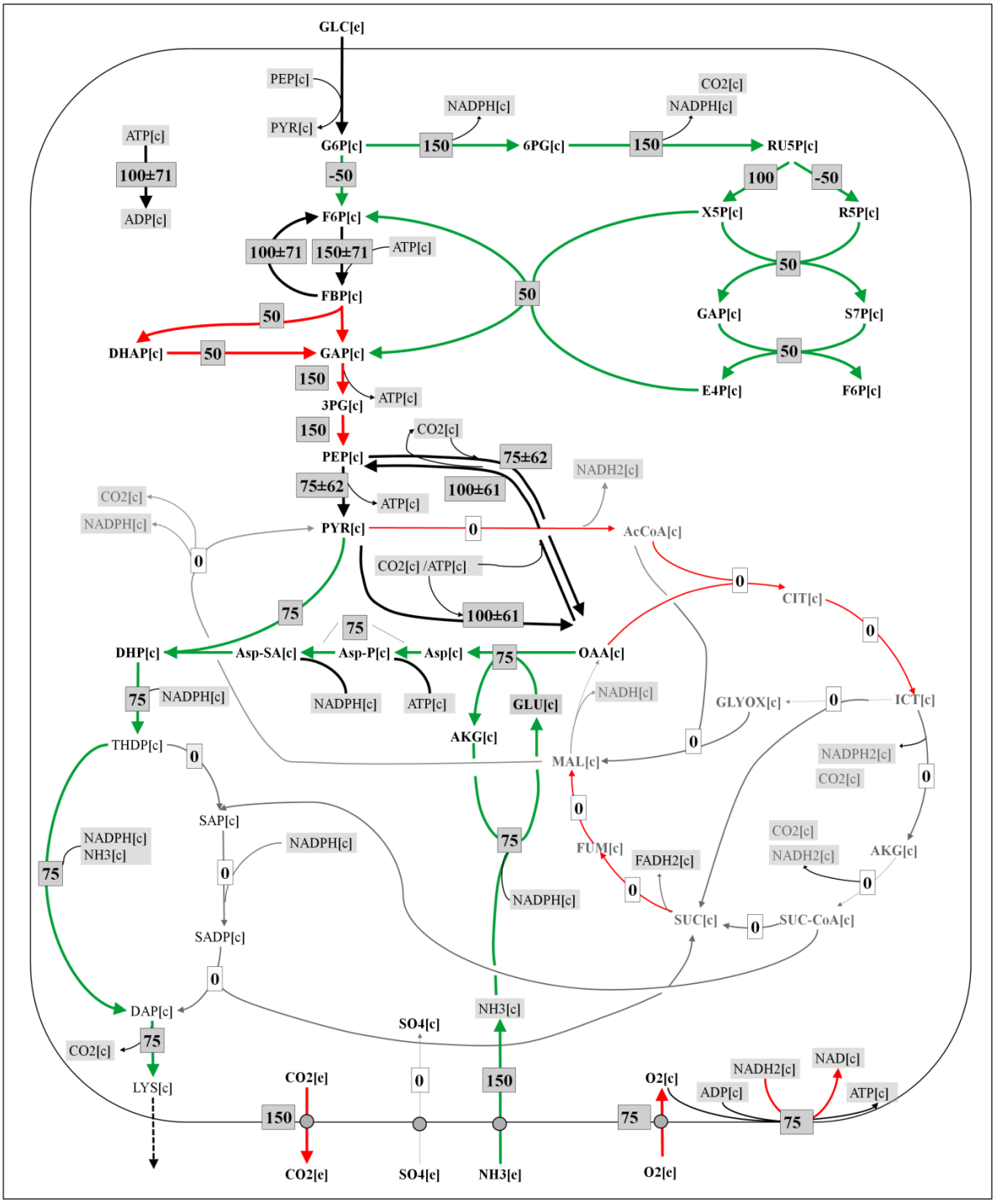

Figure 36: Optimal flux distribution for lysine production in *C. glutamicum* on glucose as obtained from elementary mode analysis and resulting target potential coefficients. In the flux map all fluxes are given as relative molar flux normalized to the uptake flux. The data shown display the average fluxes and deviations from the different elementary modes under optimum production conditions. The coloured arrows reflect identified amplification (green) and deletion/attenuation targets (red) for lysine production.

6.6.4.2 Prediction of amplification and deletion targets.

The obtained alternative optima and the various interesting suboptimal solutions provided a rich source for target search. The elementary modes were now screened for statistically significant correlation of fluxes as indicator of targets to be amplified or deleted. Most targets were identified for the subset of non-growth modes which do not exhibit biomass formation. Here, flux correlation analysis clearly identified a number of reactions as potential targets (Figure 37). Targets to be amplified are attributed to all reactions of the pentose phosphate pathway, as well as ammonium uptake and assimilation, different enzymes of the lysine biosynthesis and the lysine secretion. Interestingly, also the entry enzyme into the glycolysis, glucose 6-phosphate isomerase is classified as an amplification target. This can be understood from its role in re-cycling carbon back into the pentose phosphate cycle enabled by its reversible nature (Figure 36). Deletion or attenuation targets are located in the glycolysis, the TCA cycle and also the oxidative respiratory system. When ranked by priority, i.e. the value of the target potential coefficient α, the most striking targets predicted are located at the glucose 6-phosphate node, which reveals this node as key to successful engineering of *C. glutamicum* for improved lysine production. The simultaneous consideration of the potential targets reveals a systems-wide redirection of flux towards a superior producer as indicated by the desired flux distribution at optimal performance (Figure 36).

From the targets predicted here, various reactions have been successfully implemented towards superior production of lysine. This includes amplification of glucose 6-phosphate dehydrogenase [20], 6-phosphogluconate dehydrogenase [195], reactions within the lysine pathway [196] as well as product secretion [197], all show enhanced lysine production. Additionally, deletion of glucose 6-phosphate isomerase [198] or pyruvate dehydrogenase [199], have been successfully implemented into *C. glutamicum* for improved performance. Moreover, not yet validated targets such as the amplification of ammonium metabolism or reactions of the non-oxidative PPP or deletion/attenuation of TCA cycle reactions are predicted.

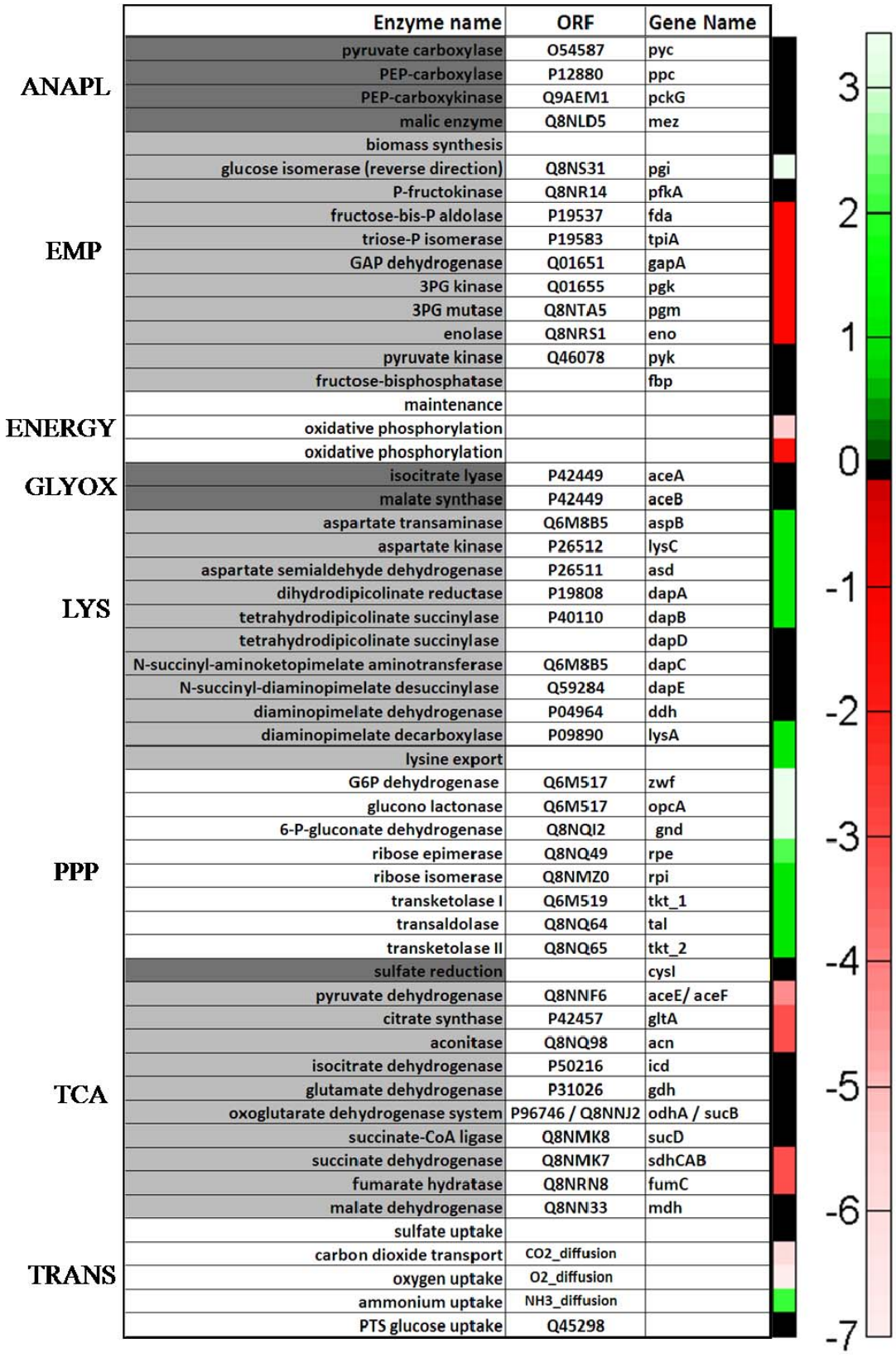

	Enzyme name	ORF	Gene Name
ANAPL	pyruvate carboxylase	O54587	pyc
	PEP-carboxylase	P12880	ppc
	PEP-carboxykinase	Q9AEM1	pckG
	malic enzyme	Q8NLD5	mez
	biomass synthesis		
EMP	glucose isomerase (reverse direction)	Q8NS31	pgi
	P-fructokinase	Q8NR14	pfkA
	fructose-bis-P aldolase	P19537	fda
	triose-P isomerase	P19583	tpiA
	GAP dehydrogenase	Q01651	gapA
	3PG kinase	Q01655	pgk
	3PG mutase	Q8NTA5	pgm
	enolase	Q8NRS1	eno
	pyruvate kinase	Q46078	pyk
	fructose-bisphosphatase		fbp
ENERGY	maintenance		
	oxidative phosphorylation		
	oxidative phosphorylation		
GLYOX	isocitrate lyase	P42449	aceA
	malate synthase	P42449	aceB
LYS	aspartate transaminase	Q6M8B5	aspB
	aspartate kinase	P26512	lysC
	aspartate semialdehyde dehydrogenase	P26511	asd
	dihydrodipicolinate reductase	P19808	dapA
	tetrahydrodipicolinate succinylase	P40110	dapB
	tetrahydrodipicolinate succinylase		dapD
	N-succinyl-aminoketopimelate aminotransferase	Q6M8B5	dapC
	N-succinyl-diaminopimelate desuccinylase	Q59284	dapE
	diaminopimelate dehydrogenase	P04964	ddh
	diaminopimelate decarboxylase	P09890	lysA
	lysine export		
PPP	G6P dehydrogenase	Q6M517	zwf
	glucono lactonase	Q6M517	opcA
	6-P-gluconate dehydrogenase	Q8NQI2	gnd
	ribose epimerase	Q8NQ49	rpe
	ribose isomerase	Q8NMZ0	rpi
	transketolase I	Q6M519	tkt_1
	transaldolase	Q8NQ64	tal
	transketolase II	Q8NQ65	tkt_2
	sulfate reduction		cysI
TCA	pyruvate dehydrogenase	Q8NNF6	aceE/ aceF
	citrate synthase	P42457	gltA
	aconitase	Q8NQ98	acn
	isocitrate dehydrogenase	P50216	icd
	glutamate dehydrogenase	P31026	gdh
	oxoglutarate dehydrogenase system	P96746 / Q8NNJ2	odhA / sucB
	succinate-CoA ligase	Q8NMK8	sucD
	succinate dehydrogenase	Q8NMK7	sdhCAB
	fumarate hydratase	Q8NRN8	fumC
	malate dehydrogenase	Q8NN33	mdh
TRANS	sulfate uptake		
	carbon dioxide transport	CO2_diffusion	
	oxygen uptake	O2_diffusion	
	ammonium uptake	NH3_diffusion	
	PTS glucose uptake	Q45298	

Figure 37: Heat map listing the predicted targets for lysine production in *C. glutamicum*. A positive value (green) relates to a reaction, which positively correlates with the production (amplification target), whereas negative correlation (red) displays a deletion/attenuation target. Black colour indicates statistically insignificant values.

7 Conclusions and Future Perspectives

The improvement of new processes for the production of biotechnological relevant products involves time consuming strain and process development. The major part of the process optimization accounts for steps of strain development, whereas only a minor part contributes to optimization of the cultivation process [200]. Therefore, it is crucial to increase the efforts in the field of strain development.

A novel strategy that is available today and seems also promising to be applied to recombinant protein production is targeting metabolic engineering of the central metabolic pathways which play a crucial role regarding supply of energy, cofactors and precursor molecules for the recombinant product [201]. In the field of protein production, however, only few successful metabolic engineering examples are reported for filamentous fungi such as *A. niger*. This is to a large extent due to the fact that metabolic engineering requires a detailed knowledge of the underlying metabolic network for the identification of promising targets.

Elementary flux mode analysis provides a rigorous basis to systematically characterize cellular phenotypes, metabolic flexibility and capacities that facilitate understanding of cell physiology and enables the implementation of metabolic engineering strategies [138-140]. In the present work, elementary flux mode analysis was applied and extended to predict systems-wide amplification and deletion targets as a useful approach to be used in metabolic engineering towards improved bio-production. First evidence that the reactions derived here open realistic chances for improvement can be obtained from recent studies. An excellent test case is the very well studied organism *C. glutamicum*. For enzyme production in *A. niger*, much less metabolic engineering progress of central carbon metabolism is reported. The few studies available, however, illustrate that several of the targets predicted here have been valuably proven.

Since the metabolic engineering strategies differ hardly between the substrates investigated here, the analysis can be extended for further nutrients as well as the impact of single metabolic clusters or reactions on protein formation, which can be studied in detail by *in silico* network modifications [141, 142].

One of the key findings is the high metabolic flexibility of *A. niger* to enable optimal production. The flexibility of *A. niger*, i.e. the possibility to recruit different pathway modes for high production, appears advantageous when approaching metabolic engineering strategies. Since it can be expected that certain genetic engineering strategies might not work for reasons of growth deficiency or undesired metabolic regulation, the possibility to choose among different promising directions seems useful. The relative large number of optimal modes is different to the behaviour of more simple prokaryotic networks and low molecular weight compounds, which often exhibit only one or very few optimal modes for production [141, 180]. A closer inspection of the underlying pathway fluxes here shows that the flexibility of *A. niger* originates from only a subset of reactions. These comprise alternative systems for NADPH supply, i.e. the PPP or the mannitol cycle, which acts as the cytosolic transhydrogenase in *A. niger* [65, 202] or the malic enzyme.

Due to the fact that elementary flux mode analysis enables the investigation of all possible physiological states in the cell, detailed insights into the underlying metabolism could be obtained. This includes the visualization of different flux states for optimum production which results from complementary pathways for the supply of NADPH (*A. niger*) or the regeneration of ATP (*C. glutamicum*). A closer inspection showed that this characteristic mainly originates from a small subset of reactions, adding flexibility and robustness to the networks. The possibility to recruit different pathway modes for high production appears advantageous when approaching metabolic engineering strategies. Since it can be expected that certain genetic engineering strategies might not work for reasons of growth deficiency or undesired regulatory behaviour, the possibility to choose among different promising directions seems useful.

The large-scale models used in the present work are condensed representations of the genome-wide metabolism relevant for the present study. Guided by the focus of the study, industrial relevant substrates and products were considered. However, it is easily possible to extend this approach to larger networks with additional substrates or even mixtures or also more detailed resolution of anabolic routes at the network periphery which were lumped here. The latter would require a more detailed experimental basis on cellular composition which is currently not available.

Combining elementary flux mode analysis with correlation of fluxes to desired network properties, potential amplification and deletion targets could be identified in industrial relevant production strains. Hereby, different scenarios considering the bioprocess environment

or the metabolic state of the cell provided a detailed insight into the underlying pathway network. These findings are very useful for improved strain engineering yielding high bioproduction. This also might include a comparison among different potentially interesting hosts [141]. Not every predicted target by this approach will necessary lead to improved production, since stoichiometric modelling as applied here can not consider e.g. cellular regulation or enzyme properties limiting or even blocking the desired network response towards targeted genetic perturbation. Still, the presented approach can be easily used to identify priority sorted amplification and deletion targets for metabolic engineering purposes under various conditions and thus displays a useful strategy to be incorporated into strain and bioprocess optimization.

The present approach did not reveal all relevant targets previously reported to redirect carbon flux. As example, the amplification of fructose bisphosphatase [21] or the deletion of phosphoenolpyruvate carboxykinase [203] both identified from ^{13}C flux analysis as major targets for improved lysine production in *C. glutamicum*, was not predicted here. Still, the presented approach can be generally used to identify priority sorted amplification and deletion targets for metabolic engineering purposes under various conditions and thus displays a useful strategy to be combined with other tools such as ^{13}C flux analysis for efficient strain and bioprocess optimization.

Interestingly, the prediction of genetic targets depended on the metabolic state of the cell. Thus it turned out as relevant to focus the target search to a specific relevant biological scenario. Growing and non-growing cells pose different burdens on the metabolism, competing with product formation, so different conclusions are derived. From practical perspective, both scenarios seem relevant since for production where non-growing as well as growing cells can be applied [204]. The metabolic state is therefore an important point which has to be considered, and for this, such general conditions and constraints should be integrated into a priori optimization.

8 List of Symbols

8.1 Abbreviations

6PG	6-phosphogluconate
AC	acetate
AcCoA	acetyl-CoA
ADP	adenosine diphosphate
AKG	α-ketoglutarate
Asn	asparagine
ATP	adenosine triphosphate
BST	Biochemical systems theory
CDW	cell dry weight
CIT	citrate
CM	cytoplasmatic membrane
CO2	carbon dioxide
CoA	coenzyme-A
CW	cell wall
DAP	dihydroxyacetone phosphate
det	determinant
DH	dehydrogenase
E4P	erythrose 4-phosphate
EC	enzyme commission
EFM	elementary flux mode
EH	epoxide hydrolase
EMP	Embden-Meyerhof-Parnas
F6P	fructose 6-phosphate
FAD	flavin adenine dinucleotide (oxidized)
FADH2	flavin adenine dinucleotide (reduced)
FBA	flux balance analysis
FBP	fructose 1,6-bisphosphate
FFase	fructofuranosidase
FMM	fructose mannose metabolism
FOR	formiate

FRC	fructose
FUM	fumarate
G6P	glucose 6-phosphate
GA	glucoamylase
Galf	galactofuranose
GAP	glyceraldehyde 3-phosphate
GC	gas chromatography
GH	gycoside hydrolase
GLC	glucose
GlcNAc	N-acetyl-glucosamine
GLN	gluconate
GLP	glycerol 3-phosphate
GLY	glycerol
GOX	glyoxylate
H2S	hydrogensulphide
ICT	isocitrate
IP	inter plasmatic area
KDPG	2-keto-3-deoxy-phosphogluconate
LC	liquid chromatography
LCoA	lenoate-CoA
LEN	lenoate
M6P	mannose 6-phosphate
MAL	malate
MAN	mannitol
MAP	mannitol 1-phosphate
MCA	metabolic control analysis
MFA	metabolic flux analysis
MS	mass spectrometry
MSTA	mono saccharide transporter with high affinity
NAD	nicotinamide adenine dinucleotide (oxidized)
NADP	nicotinamide adenine dinucleotide phosphate (oxidized)
NADH	nicotinamide adenine dinucleotide (reduced)
NADPH	nicotinamide adenine dinucleotide phosphate (reduced)
NH3	ammonium
NO3	nitrate
O2	oxygen
OAA	oxaloacetate
OCoA	oleate-CoA
OEL	oleate
OXA	oxalate

PCR	polymerase chain reaction
PEP	phosphoenolpyruvate
pNPG	para-nitro phenyl-alpha-glucopyranoside
PPP	pentose phosphate pathway
PYR	pyruvate
R5P	ribose 5-phosphate
RUP	ribulose 5-phosphate
S7P	sedoheptulose 7-phosphate
SO4	sulphate
SUC	succinate
TCA	tricarboxylic acid / citrate cycle
UV	ultra violet
XOL	xylitol
XUP	xylulose 5-phosphate
XYL	xylose

8.2 Latin Symbols

Symbol	Unit	Description
c	[g/L]	concentration
$\underline{\underline{E}}$		Evaluation value operator
D	[1/h]	dilution rate
f		degree of freedom
$\underline{\underline{K}}$		nullspace matrix
$\underline{k}$		kernel basis vectors
M	[g/mol]	molar mass
$\underline{\underline{N}}$		Elemental matrix
m		number of rows
n		number of elementary modes
P		probability
P/V	[W/m³]	volumetric power input
q		number of metabolic reactions
r		reaction vector
R	[Nm/mol·K]	molar gas constant
$\underline{\underline{R}}$		redundancy matrix
$\underline{\underline{R}}_r$		reduced redundancy matrix
s		stoichiometric coefficients of null-matrix
$\underline{\underline{S}}$		stoichiometric network matrix

t	[h]	time
V	[mL]	volume
v	[mol/g·h]	metabolic flux
V_N	[L/mol]	ideal gas volume, V_N=22.48 L/mol
$\tilde{X}$	[mol/mol]	mole fraction
X	[g/L]	biomass concentration
Y	[mol/mol]	yield coefficient

8.3 Greek Symbols

Symbol	Unit	Description
α		target validity coefficient
μ	[1/h]	specific growth rate
ν	[C-mol/C-mol]	flux yield
ξ	[C-mol/mol]	molar carbon content
σ		standard deviation

8.4 List of Indices

Indices	Description
C	carbon source
CO2	carbon dioxide
EH	epoxide hydrolase
FFase	fructofuranosidase
GA	glucoamylase
i	number of metabolites
j	number of reactions
m	measured
max	maximal
O2	oxygen
obj	objective
P	product
S	substrate
u	unknown
X	biomass

9 List of References

1. Kern A, Tilley E, Hunter IS, Legisa M, Glieder A: **Engineering primary metabolic pathways of industrial micro-organisms**. *J Biotechnol* 2007, **129**(1):6-29.
2. Andersen MR, Nielsen ML, Nielsen J: **Metabolic model integration of the bibliome, genome, metabolome and reactome of *Aspergillus niger***. *Mol Syst Biol* 2008, **4**:178.
3. Jorgensen TR, Goosen T, Hondel CA, Ram AF, Iversen JJ: **Transcriptomic comparison of *Aspergillus niger* growing on two different sugars reveals coordinated regulation of the secretory pathway**. *BMC Genomics* 2009, **10**:44.
4. Jacobs DI, Olsthoorn MM, Maillet I, Akeroyd M, Breestraat S, Donkers S, van der Hoeven RA, van den Hondel CA, Kooistra R, Lapointe T *et al*: **Effective lead selection for improved protein production in *Aspergillus niger* based on integrated genomics**. *Fungal Genet Biol* 2008.
5. Andersen MR, Nielsen J: **Current status of systems biology in Aspergilli**. *Fungal Genet Biol* 2009, **46 Suppl 1**:S180-190.
6. Alvarez-Vasquez F, Gonzalez-Alcon C, Torres NV: **Metabolism of citric acid production by *Aspergillus niger*: model definition, steady-state analysis and constrained optimization of citric acid production rate**. *Biotechnol Bioeng* 2000, **70**(1):82-108.
7. Torres NV: **Modeling approach to control of carbohydrate metabolism during citric acid accumulation by *Aspergillus niger*: II. Sensitivity analysis**. *Biotechnol Bioeng* 1994, **44**(1):112-118.
8. David H, Åkesson M, Nielsen J: **Reconstruction of the central carbon metabolism of *Aspergillus niger***. *European Journal of Biochemistry* 2003, **270**(21):4243-4253.
9. Gheshlaghi R, Scharer JM, Moo-Young M, Douglas PL: **Metabolic flux analysis for optimizing the specific growth rate of recombinant *Aspergillus niger***. *Bioprocess Biosyst Eng* 2007, **30**(6):397-418.
10. Meijer S, Otero J, Olivares R, Andersen MR, Olsson L, Nielsen J: **Overexpression of isocitrate lyase-glyoxylate bypass influence on metabolism in *Aspergillus niger***. *Metab Eng* 2009, **11**(2):107-116.
11. Benson DA, Karsch-Mizrachi I, Lipman DJ, Ostell J, Wheeler DL: **GenBank**. *Nucleic Acids Res* 2008, **36**(Database issue):D25-30.
12. Caspi R, Foerster H, Fulcher CA, Hopkinson R, Ingraham J, Kaipa P, Krummenacker M, Paley S, Pick J, Rhee SY *et al*: **MetaCyc: a multiorganism database of metabolic pathways and enzymes**. *Nucleic Acids Res* 2006, **34**(Database issue):D511-516.
13. Duarte NC, Becker SA, Jamshidi N, Thiele I, Mo ML, Vo TD, Srivas R, Palsson BO: **Global reconstruction of the human metabolic network based on genomic and bibliomic data**. *Proc Natl Acad Sci U S A* 2007, **104**(6):1777-1782.
14. Kanehisa M, Araki M, Goto S, Hattori M, Hirakawa M, Itoh M, Katayama T, Kawashima S, Okuda S, Tokimatsu T *et al*: **KEGG for linking genomes to life and the environment**. *Nucleic Acids Res* 2008, **36**(Database issue):D480-484.

15. Pel HJ, de Winde JH, Archer DB, Dyer PS, Hofmann G, Schaap PJ, Turner G, de Vries RP, Albang R, Albermann K *et al*: **Genome sequencing and analysis of the versatile cell factory *Aspergillus niger* CBS 513.88**. *Nat Biotechnol* 2007, **25**(2):221-231.
16. Burgard AP, Pharkya P, Maranas CD: **Optknock: a bilevel programming framework for identifying gene knockout strategies for microbial strain optimization**. *Biotechnol Bioeng* 2003, **84**(6):647-657.
17. Pharkya P, Burgard AP, Maranas CD: **OptStrain: a computational framework for redesign of microbial production systems**. *Genome Res* 2004, **14**(11):2367-2376.
18. Trinh CT, Unrean P, Srienc F: **Minimal *Escherichia coli* cell for the most efficient production of ethanol from hexoses and pentoses**. *Appl Environ Microbiol* 2008, **74**(12):3634-3643.
19. Wittmann C: **Fluxome analysis using GC-MS**. *Microb Cell Fact* 2007, **6**:6.
20. Becker J, Klopprogge C, Herold A, Zelder O, Bolten CJ, Wittmann C: **Metabolic flux engineering of L-lysine production in *Corynebacterium glutamicum*--over expression and modification of G6P dehydrogenase**. *J Biotechnol* 2007, **132**(2):99-109.
21. Becker J, Klopprogge C, Zelder O, Heinzle E, Wittmann C: **Amplified expression of fructose 1,6-bisphosphatase in *Corynebacterium glutamicum* increases in vivo flux through the pentose phosphate pathway and lysine production on different carbon sources**. *Appl Environ Microbiol* 2005, **71**(12):8587-8596.
22. Joyce AR, Palsson BO: **Toward whole cell modeling and simulation: comprehensive functional genomics through the constraint-based approach**. *Prog Drug Res* 2007, **64**:265, 267-309.
23. Snoep JL, Bruggeman F, Olivier BG, Westerhoff HV: **Towards building the silicon cell: a modular approach**. *Biosystems* 2006, **83**(2-3):207-216.
24. Sauer U, Heinemann M, Zamboni N: **Genetics. Getting closer to the whole picture**. *Science* 2007, **316**(5824):550-551.
25. Heinrich R, Rapoport TA: **Mathematical analysis of multienzyme systems. II. Steady state and transient control**. *Biosystems* 1975, **7**(1):130-136.
26. Smith LM, Sanders JZ, Kaiser RJ, Hughes P, Dodd C, Connell CR, Heiner C, Kent SB, Hood LE: **Fluorescence detection in automated DNA sequence analysis**. *Nature* 1986, **321**(6071):674-679.
27. Ansorge WJ: **Next-generation DNA sequencing techniques**. *N Biotechnol* 2009, **25**(4):195-203.
28. Wishart DS: **Applications of metabolomics in drug discovery and development**. *Drugs R D* 2008, **9**(5):307-322.
29. Gomase VS, Changbhale SS, Patil SA, Kale KV: **Metabolomics**. *Curr Drug Metab* 2008, **9**(1):89-98.
30. Cascante M, Marin S: **Metabolomics and fluxomics approaches**. *Essays Biochem* 2008, **45**:67-81.
31. Hood L: **A personal view of molecular technology and how it has changed biology**. *J Proteome Res* 2002, **1**(5):399-409.
32. Pariset L, Chillemi G, Bongiorni S, Spica VR, Valentini A: **Microarrays and high-throughput transcriptomic analysis in species with incomplete availability of genomic sequences**. *N Biotechnol* 2009, **25**(5):272-279.
33. Becker JS, Jakubowski N: **The synergy of elemental and biomolecular mass spectrometry: new analytical strategies in life sciences**. *Chem Soc Rev* 2009, **38**(7):1969-1983.

34. Agrawal GK, Thelen JJ: **A high-resolution two dimensional Gel- and Pro-Q DPS-based proteomics workflow for phosphoprotein identification and quantitative profiling**. *Methods Mol Biol* 2009, **527**:3-19, ix.
35. Feng X, Liu X, Luo Q, Liu BF: **Mass spectrometry in systems biology: an overview**. *Mass Spectrom Rev* 2008, **27**(6):635-660.
36. Trapp O: **Gas chromatographic high-throughput screening techniques in catalysis**. *J Chromatogr A* 2008, **1184**(1-2):160-190.
37. Wiechert W, de Graaf AA: ***In vivo* stationary flux analysis by ^{13}C labeling experiments**. *Adv Biochem Eng Biotechnol* 1996, **54**:109-154.
38. Tomita M, Hashimoto K, Takahashi K, Matsuzaki Y, Matsushima R, Saito K, Yugi K, Miyoshi F, Nakano H, Tanida S *et al*: **The E-CELL project: towards integrative simulation of cellular processes**. *New Generation Computing* 2000, **18**(1):1-12.
39. Cleland WW, Johnson MJ: **Tracer experiments on the mechanism of citric acid formation by *Aspergillus niger***. *J Biol Chem* 1954, **208**(2):679-689.
40. Cleland WW, Johnson MJ: **Studies on the formation of oxalic acid by *Aspergillus niger***. *J Biol Chem* 1956, **220**(2):595-606.
41. Karaffa L, Sandor E, Fekete E, Szentirmai A: **The biochemistry of citric acid accumulation by *Aspergillus niger***. *Acta Microbiol Immunol Hung* 2001, **48**(3-4):429-440.
42. Strasser H, Burgstaller W, Schinner F: **High-yield production of oxalic acid for metal leaching processes by *Aspergillus niger***. *FEMS Microbiol Lett* 1994, **119**(3):365-370.
43. Jeenes DJ, Mackenzie DA, Roberts IN, Archer DB: **Heterologous protein production by filamentous fungi**. *Biotechnol Genet Eng Rev* 1991, **9**:327-367.
44. van den Hondel CA, Punt PJ, van Gorcom RF: **Production of extracellular proteins by the filamentous fungus *Aspergillus***. *Antonie Van Leeuwenhoek* 1992, **61**(2):153-160.
45. Maras M, van Die I, Contreras R, van den Hondel CA: **Filamentous fungi as production organisms for glycoproteins of bio-medical interest**. *Glycoconj J* 1999, **16**(2):99-107.
46. Silveira ST, Oliveira MS, Costa JA, Kalil SJ: **Optimization of glucoamylase production by *Aspergillus niger* in solid-state fermentation**. *Appl Biochem Biotechnol* 2006, **128**(2):131-140.
47. van den Brink HJ, Petersen SG, Rahbek-Nielsen H, Hellmuth K, Harboe M: **Increased production of chymosin by glycosylation**. *J Biotechnol* 2006, **125**(2):304-310.
48. Park YK, Almeida MM: **Production of fructooligosaccharides from sucrose by a transfructosylase from *Aspergillus niger***. *World Journal of Microbiology and Biotechnology* 1991, **7**(3):331 - 334.
49. Naundorf A, Melzer G, Archelas A, Furstoss R, Wohlgemuth R: **Influence of pH on the expression of a recombinant epoxide hydrolase in *Aspergillus niger***. *Biotechnol J* 2009, **4**(5):756-765.
50. Morisseau C, Archelas A, Guitton C, Faucher D, Furstoss R, Baratti JC: **Purification and characterization of a highly enantioselective epoxide hydrolase from *Aspergillus niger***. *Eur J Biochem* 1999, **263**(2):386-395.
51. Schuster E, Dunn-Coleman N, Frisvad JC, Van Dijck PW: **On the safety of *Aspergillus niger* - a review**. *Appl Microbiol Biotechnol* 2002, **59**(4-5):426-435.

52. van den Hombergh JP, van de Vondervoort PJ, Fraissinet-Tachet L, Visser J: ***Aspergillus* as a host for heterologous protein production: the problem of proteases**. *Trends Biotechnol* 1997, **15**(7):256-263.
53. Ward M, Lin C, Victoria DC, Fox BP, Fox JA, Wong DL, Meerman HJ, Pucci JP, Fong RB, Heng MH *et al*: **Characterization of humanized antibodies secreted by *Aspergillus niger***. *Appl Environ Microbiol* 2004, **70**(5):2567-2576.
54. Baker SE: ***Aspergillus niger* genomics: past, present and into the future**. *Med Mycol* 2006, **44 Suppl 1**:S17-21.
55. Jones MG: **The first filamentous fungal genome sequences: *Aspergillus* leads the way for essential everyday resources or dusty museum specimens?** *Microbiology* 2007, **153**(Pt 1):1-6.
56. Contesini FJ, da Silva VC, Maciel RF, de Lima RJ, Barros FF, de Oliveira Carvalho P: **Response surface analysis for the production of an enantioselective lipase from *Aspergillus niger* by solid-state fermentation**. *J Microbiol* 2009, **47**(5):563-571.
57. Dashtban M, Schraft H, Qin W: **Fungal bioconversion of lignocellulosic residues; opportunities & perspectives**. *Int J Biol Sci* 2009, **5**(6):578-595.
58. Nielsen KF, Mogensen JM, Johansen M, Larsen TO, Frisvad JC: **Review of secondary metabolites and mycotoxins from the *Aspergillus niger* group**. *Anal Bioanal Chem* 2009.
59. Bennett JW: **Mycotechnology: the role of fungi in biotechnology**. *J Biotechnol* 1998, **66**(2-3):101-107.
60. Karaffa L, Kubicek CP: ***Aspergillus niger* citric acid accumulation: do we understand this well working black box?** *Appl Microbiol Biotechnol* 2003, **61**(3):189-196.
61. Michal G: **Biochemical pathways**. Heidelberg / Berlin: Spektrum Akademischer Verlag; 1999.
62. van Kuyk PA, Diderich JA, MacCabe AP, Hererro O, Ruijter GJ, Visser J: ***Aspergillus niger mstA* encodes a high-affinity sugar/H^+ symporter which is regulated in response to extracellular pH**. *Biochem J* 2004, **379**(Pt 2):375-383.
63. Hult K, Gatenbeck S: **Production of NADPH in the mannitol cycle and its relation to polyketide formation in *Alternaria alternata***. *Eur J Biochem* 1978, **88**(2):607-612.
64. Diano A, Bekker-Jensen S, Dynesen J, Nielsen J: **Polyol synthesis in *Aspergillus niger*: Influence of oxygen availability, carbon and nitrogen sources on the metabolism**. *Biotechnology and Bioengineering* 2006, **94**(5):899-908.
65. Hult K, Veide A, Gatenbeck S: **The distribution of the NADPH regenerating mannitol cycle among fungal species**. *Arch Microbiol* 1980, **128**(2):253-255.
66. Gosling JP, Duggan PF: **Activities of tricarboxylic acid cycle enzymes, glyoxylate cycle enzymes, and fructose diphosphatase in bakers' yeast during adaptation to acetate oxidation**. *J Bacteriol* 1971, **106**(3):908-914.
67. Galbraith JC, Smith JE: **Changes in activity of certain enzymes of the tricarboxylic acid cycle and the glyoxylate cycle during the initiation of conidiation of *Aspergillus niger***. *Can J Microbiol* 1969, **15**(10):1207-1212.
68. Cioni M, Pinzauti G, Vanni P: **Comparative biochemistry of the glyoxylate cycle**. *Comp Biochem Physiol B* 1981, **70B**(1):1-26.
69. Lammers PJ, Jun J, Abubaker J, Arreola R, Gopalan A, Bago B, Hernandez-Sebastia C, Allen JW, Douds DD, Pfeffer PE *et al*: **The glyoxylate cycle in an arbuscular mycorrhizal fungus. Carbon flux and gene expression**. *Plant Physiol* 2001, **127**(3):1287-1298.

70. Desel H, Zimmermann R, Janes M, Miller F, Neupert W: **Biosynthesis of glyoxysomal enzymes in *Neurospora crassa***. *Ann N Y Acad Sci* 1982, **386**:377-393.
71. Valenciano S, Lucas JR, Pedregosa A, Monistrol IF, Laborda F: **Induction of β-oxidation enzymes and microbody proliferation in *Aspergillus nidulans***. *Arch Microbiol* 1996, **166**(5):336-341.
72. Ebel F, Schwienbacher M, Beyer J, Heesemann J, Brakhage AA, Brock M: **Analysis of the regulation, expression, and localisation of the isocitrate lyase from *Aspergillus fumigatus,* a potential target for antifungal drug development**. *Fungal Genet Biol* 2006, **43**(7):476-489.
73. Stephanopoulos GN, Aristidou AA, Nielsen J: **Metabolic engineering - principles and methodologies**, 1 edn. London: Academic Press; 1998.
74. Schoppe V: **Charakterisierung der biochemischen Beschaffenheit der Sporen von *Aspergillus niger***. *diploma thesis.* Braunschweig: Technische Universität Braunschweig; 2007.
75. Ratledge C, Evans CT: **Lipids and their metabolism**. In: *The Yeasts.* Edited by Rose AH, Harrison JS, vol. 3. London: Academic Press; 1989: 367 - 455.
76. Menger FM: **Enzyme reactivity from an organic perspective**. *Accounts of Chemical Research* 2002, **26**(4):206-212.
77. Faber K: **Biotransformations in Organic Chemistry**, 5th edn. Berlin: Springer; 2004.
78. Finkelstein DB: **Improvement of enzyme production in *Aspergillus***. *Antonie Van Leeuwenhoek* 1987, **53**(5):349-352.
79. Lee BH: **Bioconversion of Starch Wastes.** In: *Bioconversion of Waste Materials to Industrial Products.* Edited by Martin AM. New York: Elsevier Applied Science; 1991: 265 - 291.
80. Punt PJ, van Biezen N, Conesa A, Albers A, Mangnus J, van den Hondel C: **Filamentous fungi as cell factories for heterologous protein production**. *Trends Biotechnol* 2002, **20**(5):200-206.
81. Nevalainen KM, Te'o VS, Bergquist PL: **Heterologous protein expression in filamentous fungi**. *Trends Biotechnol* 2005, **23**(9):468-474.
82. Fowler T, Berka RM, Ward M: **Regulation of the *glaA* gene of *Aspergillus niger***. *Curr Genet* 1990, **18**(6):537-545.
83. Schrickx JM, Krave AS, Verdoes JC, van den Hondel CA, Stouthamer AH, van Verseveld HW: **Growth and product formation in chemostat and recycling cultures by *Aspergillus niger* N402 and a glucoamylase overproducing transformant, provided with multiple copies of the *glaA* gene**. *J Gen Microbiol* 1993, **139**(11):2801-2810.
84. Boddy LM, Berges T, Barreau C, Vainstein MH, Dobson MJ, Ballance DJ, Peberdy JF: **Purification and characterisation of an *Aspergillus niger* invertase and its DNA sequence**. *Curr Genet* 1993, **24**(1-2):60-66.
85. Yuan XL, Goosen C, Kools H, van der Maarel MJ, van den Hondel CA, Dijkhuizen L, Ram AF: **Database mining and transcriptional analysis of genes encoding inulin-modifying enzymes of *Aspergillus niger***. *Microbiology* 2006, **152**(Pt 10):3061-3073.
86. Yanai K, Nakane A, Kawate A, Hirayama M: **Molecular cloning and characterization of the fructooligosaccharide-producing beta-fructofuranosidase gene from *Aspergillus niger* ATCC 20611**. *Biosci Biotechnol Biochem* 2001, **65**(4):766-773.
87. Zuccaro A, Gotze S, Kneip S, Dersch P, Seibel J: **Tailor-made fructooligosaccharides by a combination of substrate and genetic engineering**. *Chembiochem* 2008, **9**(1):143-149.

88. Homann A, Biedendieck R, Gotze S, Jahn D, Seibel J: **Insights into polymer versus oligosaccharide synthesis: mutagenesis and mechanistic studies of a novel levansucrase from *Bacillus megaterium***. *Biochem J* 2007, **407**(2):189-198.
89. van Hijum SA, Kralj S, Ozimek LK, Dijkhuizen L, van Geel-Schutten IG: **Structure-function relationships of glucansucrase and fructansucrase enzymes from lactic acid bacteria**. *Microbiol Mol Biol Rev* 2006, **70**(1):157-176.
90. Modi S, Borges V: **Artificial sweeteners: boon or bane?** *International Journal of Diabetes in Developing Countries* 2005, **25**(1):12-19.
91. Rafter J, Bennett M, Caderni G, Clune Y, Hughes R, Karlsson PC, Klinder A, O'Riordan M, O'Sullivan GC, Pool-Zobel B *et al*: **Dietary synbiotics reduce cancer risk factors in polypectomized and colon cancer patients**. *Am J Clin Nutr* 2007, **85**(2):488-496.
92. Driouch H, Sommer B, Wittmann C: **Morphology engineering of *Aspergillus niger* for improved enzyme production**. *Biotechnol Bioeng* 2009.
93. Maiorano AE, Piccoli RM, da Silva ES, de Andrade Rodrigues MF: **Microbial production of fructosyltransferases for synthesis of pre-biotics**. *Biotechnol Lett* 2008, **30**(11):1867-1877.
94. Steinreiber A, Faber K: **Microbial epoxide hydrolases for preparative biotransformations**. *Curr Opin Biotechnol* 2001, **12**(6):552-558.
95. de Vries EJ, Janssen DB: **Biocatalytic conversion of epoxides**. *Curr Opin Biotechnol* 2003, **14**(4):414-420.
96. Zou J, Hallberg BM, Bergfors T, Oesch F, Arand M, Mowbray SL, Jones TA: **Structure of *Aspergillus niger* epoxide hydrolase at 1.8 A resolution: implications for the structure and function of the mammalian microsomal class of epoxide hydrolases**. *Structure* 2000, **8**(2):111-122.
97. Visser H, Vreugdenhil S, de Bont JA, Verdoes JC: **Cloning and characterization of an epoxide hydrolase-encoding gene from *Rhodotorula glutinis***. *Appl Microbiol Biotechnol* 2000, **53**(4):415-419.
98. Melzer G, Junne S, Wohlgemuth R, Hempel DC, Gotz P: **Production of epoxide hydrolases in batch fermentations of *Botryosphaeria rhodina***. *J Ind Microbiol Biotechnol* 2008, **35**(6):485-493.
99. Liu Y, Wu S, Wang J, Yang L, Sun W: **Cloning, expression, purification, and characterization of a novel epoxide hydrolase from *Aspergillus niger* SQ-6**. *Protein Expr Purif* 2007, **53**(2):239-246.
100. Blee E, Summerer S, Flenet M, Rogniaux H, Van Dorsselaer A, Schuber F: **Soybean epoxide hydrolase: identification of the catalytic residues and probing of the reaction mechanism with secondary kinetic isotope effects**. *J Biol Chem* 2005, **280**(8):6479-6487.
101. Harris TR, Aronov PA, Jones PD, Tanaka H, Arand M, Hammock BD: **Identification of two epoxide hydrolases in *Caenorhabditis elegans* that metabolize mammalian lipid signaling molecules**. *Arch Biochem Biophys* 2008, **472**(2):139-149.
102. Khalil SM, Anspaugh DD, Michael Roe R: **Role of juvenile hormone esterase and epoxide hydrolase in reproduction of the cotton bollworm, *Helicoverpa zea***. *J Insect Physiol* 2006, **52**(7):669-678.
103. Marowsky A, Burgener J, Falck JR, Fritschy JM, Arand M: **Distribution of soluble and microsomal epoxide hydrolase in the mouse brain and its contribution to cerebral epoxyeicosatrienoic acid metabolism**. *Neuroscience* 2009.
104. Rawal S, Morisseau C, Hammock BD, Shivachar AC: **Differential subcellular distribution and colocalization of the microsomal and soluble epoxide hydrolases**

in cultured neonatal rat brain cortical astrocytes. *J Neurosci Res* 2009, **87**(1):218-227.
105. Decker M, Arand M, Cronin A: **Mammalian epoxide hydrolases in xenobiotic metabolism and signalling**. *Arch Toxicol* 2009, **83**(4):297-318.
106. Morisseau C, Hammock BD: **Gerry Brooks and epoxide hydrolases: four decades to a pharmaceutical**. *Pest Manag Sci* 2008, **64**(6):594-609.
107. Hengstler JG, Stewart JD, Bolt HM: **Epoxide hydrolases are not only a molecular sponge sucking up genotoxic epoxides: new roles in control of blood pressure, inflammation as well as nociception and cell proliferation**. *Arch Toxicol* 2009, **83**(4):289-291.
108. Gross GJ, Nithipatikom K: **Soluble epoxide hydrolase: a new target for cardioprotection**. *Curr Opin Investig Drugs* 2009, **10**(3):253-258.
109. Smit MS: **Fungal epoxide hydrolases: new landmarks in sequence-activity space**. *Trends Biotechnol* 2004, **22**(3):123-129.
110. Kotik M, Kyslik P: **Purification and characterisation of a novel enantioselective epoxide hydrolase from *Aspergillus niger* M200**. *Biochim Biophys Acta* 2006, **1760**(2):245-252.
111. Bisogno FR, Orden AA, Pranzoni CA, Cifuente DA, Giordano OS, Kurina Sanz M: **Atypical regioselective biohydrolysis on steroidal oxiranes by *Aspergillus niger* whole cells: some stereochemical features**. *Steroids* 2007, **72**(8):643-652.
112. Archelas A, Furstoss R: **Synthetic applications of epoxide hydrolases**. *Curr Opin Chem Biol* 2001, **5**(2):112-119.
113. Deregnaucourt J, Archelas A, Barbirato F, Paris J-M, Furstoss R: **Enzymatic Transformations 63. High-Concentration two liquid-liquid phase *Aspergillus niger* epoxide hydrolase-catalysed resolution: application to trifluoromethyl-substituted aromatic epoxides**. *Advanced Synthesis & Catalysis* 2007, **349**(8-9):1405-1417.
114. Vilotijevic I, Jamison TF: **Epoxide-opening cascades promoted by water**. *Science* 2007, **317**(5842):1189-1192.
115. Shichijo Y, Migita A, Oguri H, Watanabe M, Tokiwano T, Watanabe K, Oikawa H: **Epoxide hydrolase Lsd19 for polyether formation in the biosynthesis of lasalocid A: Direct experimental evidence on polyene-polyepoxide hypothesis in polyether biosynthesis**. *Journal of the American Chemical Society* 2008, **130**(37):12230-12231.
116. Schmidt K, Norregaard LC, Pedersen B, Meissner A, Duus JO, Nielsen JO, Villadsen J: **Quantification of intracellular metabolic fluxes from fractional enrichment and ^{13}C-^{13}C coupling constraints on the isotopomer distribution in labeled biomass components**. *Metab Eng* 1999, **1**(2):166-179.
117. Pedersen H, Christensen B, Hjort C, Nielsen J: **Construction and characterization of an oxalic acid nonproducing strain of *Aspergillus niger***. *Metab Eng* 2000, **2**(1):34-41.
118. Prathumpai W, Gabelgaard JB, Wanchanthuek P, van de Vondervoort PJ, de Groot MJ, McIntyre M, Nielsen J: **Metabolic control analysis of xylose catabolism in *Aspergillus***. *Biotechnol Prog* 2003, **19**(4):1136-1141.
119. de Groot MJ, Prathumpai W, Visser J, Ruijter GJ: **Metabolic control analysis of *Aspergillus niger* L-arabinose catabolism**. *Biotechnol Prog* 2005, **21**(6):1610-1616.
120. Melzer G, Dalpiaz A, Grote A, Kucklick M, Gocke Y, Jonas R, Dersch P, Franco-Lara E, Nortemann B, Hempel DC: **Metabolic flux analysis using stoichiometric**

models for *Aspergillus niger*: comparison under glucoamylase-producing and non-producing conditions. *J Biotechnol* 2007, **132**(4):405-417.
121. Melzer G, Eslahpazir M, Franco-Lara E, Wittmann C: **Flux Design: *In silico* design of cell factories based on correlation of pathway fluxes to desired properties**. *BMC Syst Biol* 2009, **3**(1):120.
122. Torres NV: **Modeling approach to control of carbohydrate metabolism during citric acid accumulation by *Aspergillus niger*: I. Model definition and stability of the steady state**. *Biotechnol Bioeng* 1994, **44**(1):104-111.
123. Guebel DV, Torres NV: **Optimization of the citric acid production by *Aspergillus niger* through a metabolic flux balance model**. *Electronic J Biotechnol* 1996, **4**(1):1-17.
124. Savageau MA: **Biochemical systems analysis. I. Some mathematical properties of the rate law for the component enzymatic reactions**. *J Theor Biol* 1969, **25**(3):365-369.
125. Savageau MA: **Biochemical systems analysis. II. The steady-state solutions for an n-pool system using a power-law approximation**. *J Theor Biol* 1969, **25**(3):370-379.
126. Feist AM, Henry CS, Reed JL, Krummenacker M, Joyce AR, Karp PD, Broadbelt LJ, Hatzimanikatis V, Palsson BO: **A genome-scale metabolic reconstruction for *Escherichia coli* K-12 MG1655 that accounts for 1260 ORFs and thermodynamic information**. *Mol Syst Biol* 2007, **3**:121.
127. Pinney JW, Shirley MW, McConkey GA, Westhead DR: **metaSHARK: software for automated metabolic network prediction from DNA sequence and its application to the genomes of *Plasmodium falciparum* and *Eimeria tenella***. *Nucleic Acids Res* 2005, **33**(4):1399-1409.
128. Bock C, Halachev K, Buch J, Lengauer T: **EpiGRAPH: user-friendly software for statistical analysis and prediction of (epi)genomic data**. *Genome Biol* 2009, **10**(2):R14.
129. Cornish-Bowden A, Cardenas ML: **Metabolic balance sheets**. *Nature* 2002, **420**(6912):129-130.
130. Holzhutter HG: **The principle of flux minimization and its application to estimate stationary fluxes in metabolic networks**. *Eur J Biochem* 2004, **271**(14):2905-2922.
131. Schuster S, Dandekar T, Fell DA: **Detection of elementary flux modes in biochemical networks: a promising tool for pathway analysis and metabolic engineering**. *Trends Biotechnol* 1999, **17**(2):53-60.
132. Schuster S, Hilgetag C: **On elementary flux modes in biochemical reaction systems at steady state**. *Journal of Biological Systems* 1994, **2**:165-182.
133. Papin JA, Price ND, Wiback SJ, Fell DA, Palsson BO: **Metabolic pathways in the post-genome era**. *Trends Biochem Sci* 2003, **28**(5):250-258.
134. Stelling J, Klamt S, Bettenbrock K, Schuster S, Gilles ED: **Metabolic network structure determines key aspects of functionality and regulation**. *Nature* 2002, **420**(6912):190-193.
135. Trinh CT, Wlaschin A, Srienc F: **Elementary mode analysis: a useful metabolic pathway analysis tool for characterizing cellular metabolism**. *Appl Microbiol Biotechnol* 2009, **81**(5):813-826.
136. Reder C: **Metabolic control theory: a structural approach**. *J Theor Biol* 1988, **135**(2):175-201.
137. Roels JA: **Energetics and kinetics in biotechnology.** Amsterdam: Elsevier Biomedical Press; 1983.

138. Papin JA, Stelling J, Price ND, Klamt S, Schuster S, Palsson BO: **Comparison of network-based pathway analysis methods**. *Trends Biotechnol* 2004, **22**(8):400-405.
139. Schuster S, Pfeiffer T, Moldenhauer F, Koch I, Dandekar T: **Exploring the pathway structure of metabolism: decomposition into subnetworks and application to *Mycoplasma pneumoniae***. *Bioinformatics* 2002, **18**(2):351-361.
140. Schuster S, Hilgetag C, Woods JH, Fell DA: **Reaction routes in biochemical reaction systems: algebraic properties, validated calculation procedure and example from nucleotide metabolism**. *J Math Biol* 2002, **45**(2):153-181.
141. Krömer JO, Wittmann C, Schröder H, Heinzle E: **Metabolic pathway analysis for rational design of L-methionine production by *Escherichia coli* and *Corynebacterium glutamicum***. *Metab Eng* 2006, **8**(4):353-369.
142. Carlson R, Fell D, Srienc F: **Metabolic pathway analysis of a recombinant yeast for rational strain development**. *Biotechnology and Bioengineering* 2002, **79**(2):121-134.
143. Vijayasankaran N, Carlson R, Srienc F: **Metabolic pathway structures for recombinant protein synthesis in *Escherichia coli***. *Appl Microbiol Biotechnol* 2005, **68**(6):737-746.
144. Varma A, Palsson BO: **Stoichiometric flux balance models quantitatively predict growth and metabolic by-product secretion in wild-type *Escherichia coli* W3110**. *Appl Environ Microbiol* 1994, **60**(10):3724-3731.
145. Vallino JJ, Stephanopoulos G: **Metabolic flux distributions in *Corynebacterium glutamicum* during growth and lysine overproduction. Reprinted from Biotechnology and Bioengineering, Vol. 41, Pp 633-646 (1993)**. *Biotechnol Bioeng* 2000, **67**(6):872-885.
146. Wiechert W: **^{13}C metabolic flux analysis**. *Metab Eng* 2001, **3**(3):195-206.
147. Kauffman KJ, Prakash P, Edwards JS: **Advances in flux balance analysis**. *Curr Opin Biotechnol* 2003, **14**(5):491-496.
148. Schuetz R, Kuepfer L, Sauer U: **Systematic evaluation of objective functions for predicting intracellular fluxes in *Escherichia coli***. *Mol Syst Biol* 2007, **3**:119.
149. Chelius MK, Wodzinski RJ: **Strain improvement of *Aspergillus niger* for phytase production**. *Applied Microbiology and Biotechnology* 1994, **41**(1):79-83.
150. Nielsen J: **Physiological engineering aspects of *Penicillium chrysogenum***. Singapore: World Scientific Pub Co Inc; 1997.
151. Baltz RH: **Genetic methods and strategies for secondary metabolite yield improvement in actinomycetes**. *Antonie Van Leeuwenhoek* 2001, **79**(3-4):251-259.
152. de Jongh WA, Nielsen J: **Enhanced citrate production through gene insertion in *Aspergillus niger***. *Metab Eng* 2008, **10**(2):87-96.
153. Paradkar AS, Mosher RH, Anders C, Griffin A, Griffin J, Hughes C, Greaves P, Barton B, Jensen SE: **Applications of gene replacement technology to *Streptomyces clavuligerus* strain development for clavulanic acid production**. *Appl Environ Microbiol* 2001, **67**(5):2292-2297.
154. Pharkya P, Maranas CD: **An optimization framework for identifying reaction activation/inhibition or elimination candidates for overproduction in microbial systems**. *Metab Eng* 2006, **8**(1):1-13.
155. Segre D, Vitkup D, Church GM: **Analysis of optimality in natural and perturbed metabolic networks**. *Proc Natl Acad Sci U S A* 2002, **99**(23):15112-15117.
156. Mattern IE, van Noort JM, van den Berg P, Archer DB, Roberts IN, van den Hondel CA: **Isolation and characterization of mutants of *Aspergillus niger* deficient in extracellular proteases**. *Mol Gen Genet* 1992, **234**(2):332-336.

157. van Hartingsveldt W, Mattern IE, van Zeijl CM, Pouwels PH, van den Hondel CA: **Development of a homologous transformation system for *Aspergillus niger* based on the *pyrG* gene**. *Mol Gen Genet* 1987, **206**(1):71-75.
158. Blom RH, Pfeifer VF, Moyer AJ, TraufRer DH, Conway HF, Crocker CK, Farison RE, Hannibal DV: **Sodium gluconate production. Fermentation with *Aspergillus niger***. *Industrial & Engineering Chemistry* 1952, **44**(2):435-440.
159. Debets F, Swart K, Hoekstra RF, Bos CJ: **Genetic maps of eight linkage groups of *Aspergillus niger* based on mitotic mapping**. *Curr Genet* 1993, **23**(1):47-53.
160. Vogel HJ: **A convenient growth medium for *Neurospora* (Medium N)**. *Microb Genet Bull* 1956, **243**:112–119.
161. Withers JM, Swift RJ, Wiebe MG, Robson GD, Punt PJ, van den Hondel CA, Trinci AP: **Optimization and stability of glucoamylase production by recombinant strains of *Aspergillus niger* in chemostat culture**. *Biotechnol Bioeng* 1998, **59**(4):407-418.
162. Noltmann EA, Gubler CJ, Kuby SA: **Glucose 6-phosphate dehydrogenase (Zwischenferment). I. Isolation of the crystalline enzyme from yeast**. *J Biol Chem* 1961, **236**:1225-1230.
163. Chell RM, Sundaram TK, Wilkinson AE: **Isolation and characterization of isocitrate lyase from a thermophilic *Bacillus sp.*** *Biochem J* 1978, **173**(1):165-177.
164. Malcovati M, Valentini G: **AMP- and fructose 1,6-bisphosphate-activated pyruvate kinases from *Escherichia coli***. *Methods Enzymol* 1982, **90 Pt E**:170-179.
165. Yamanaka K: **D-mannitol dehydrogenase from *Leuconostoc messenteroides***. *Methods Enzymol* 1975, **41**:138-142.
166. Sun J, Zeng AP: **IdentiCS - identification of coding sequence and *in silico* reconstruction of the metabolic network directly from unannotated low-coverage bacterial genome sequence**. *BMC Bioinformatics* 2004, **5**:112.
167. Konrad M: **Applications of genetic engineering to the pharmaceutical industry**. *Ann N Y Acad Sci* 1983, **413**:12-22.
168. Dauner M, Sonderegger M, Hochuli M, Szyperski T, Wuthrich K, Hohmann HP, Sauer U, Bailey JE: **Intracellular carbon fluxes in riboflavin-producing *Bacillus subtilis* during growth on two-carbon substrate mixtures**. *Appl Environ Microbiol* 2002, **68**(4):1760-1771.
169. Sauer U, Bailey JE: **Estimation of P-to-O ratio in *Bacillus subtilis* and its influence on maximum riboflavin yield**. *Biotechnol Bioeng* 1999, **64**(6):750-754.
170. Lehmann M, Degen S, Hohmann HP, Wyss M, Bacher A, Schramek N: **Biosynthesis of riboflavin. Screening for an improved GTP cyclohydrolase II mutant**. *Febs J* 2009, **276**(15):4119-4129.
171. Gupta R, Beg QK, Lorenz P: **Bacterial alkaline proteases: molecular approaches and industrial applications**. *Appl Microbiol Biotechnol* 2002, **59**(1):15-32.
172. Wittmann C, Becker J: **The L-lysine story: from metabolic pathways to industrial production**. In: *Amino Acid Biosynthesis ~ Pathways, Regulation and Metabolic Engineering.* 2007: 39-70.
173. Forster J, Famili I, Fu P, Palsson BO, Nielsen J: **Genome-scale reconstruction of the *Saccharomyces cerevisiae* metabolic network**. *Genome Res* 2003, **13**(2):244-253.
174. Frick O, Wittmann C: **Characterization of the metabolic shift between oxidative and fermentative growth in *Saccharomyces cerevisiae* by comparative ^{13}C flux analysis**. *Microb Cell Fact* 2005, **4**:30.

175. Oh YK, Palsson BO, Park SM, Schilling CH, Mahadevan R: **Genome-scale reconstruction of metabolic network in *Bacillus subtilis* based on high-throughput phenotyping and gene essentiality data**. *J Biol Chem* 2007, **282**(39):28791-28799.
176. Dauner M, Sauer U: **GC-MS analysis of amino acids rapidly provides rich information for isotopomer balancing**. *Biotechnol Prog* 2000, **16**(4):642-649.
177. Wittmann C, de Graaf AA: **Metabolic flux analysis in *Corynebacterium glutamicum***. In: *Handbook of Corynebacterium glutamicum.* Edited by Eggeling L, Bott M. Portland: Boca Raton: CRC Press; 2005: 277-304.
178. Carlson R, Srienc F: **Fundamental *Escherichia coli* biochemical pathways for biomass and energy production: identification of reactions**. *Biotechnol Bioeng* 2004, **85**(1):1-19.
179. Edwards JS, Palsson BO: **Metabolic flux balance analysis and the *in silico* analysis of *Escherichia coli* K-12 gene deletions**. *BMC Bioinformatics* 2000, **1**:1.
180. Kjeldsen KR, Nielsen J: ***In silico* genome-scale reconstruction and validation of the *Corynebacterium glutamicum* metabolic network**. *Biotechnol Bioeng* 2009, **102**(2):583-597.
181. Wagner C: **Nullspace approach to determine the elementary modes of chemical reaction systems**. *Journal of Physical Chemistry B* 2004, **108**(7):2425-2431.
182. Terzer M, Stelling J: **Large-scale computation of elementary flux modes with bit pattern trees**. *Bioinformatics* 2008, **24**(19):2229-2235.
183. Bernstein JA, Khodursky AB, Lin PH, Lin-Chao S, Cohen SN: **Global analysis of mRNA decay and abundance in *Escherichia coli* at single-gene resolution using two-color fluorescent DNA microarrays**. *Proc Natl Acad Sci U S A* 2002, **99**(15):9697-9702.
184. Butland G, Babu M, Diaz-Mejia JJ, Bohdana F, Phanse S, Gold B, Yang W, Li J, Gagarinova AG, Pogoutse O *et al*: **eSGA: *E. coli* synthetic genetic array analysis**. *Nat Methods* 2008, **5**(9):789-795.
185. van der Heijden RT, Romein B, Heijnen JJ, Hellinga C, Luyben KC: **Linear constraint relations in biochemical reaction systems: II. Diagnosis and estimation of gross errors**. *Biotechnol Bioeng* 1994, **43**(1):11-20.
186. Tsai SP, Lee YH: **Application of metabolic pathway stoichiometry to statistical analysis of bioreactor measurement data**. *Biotechnol Bioeng* 1988, **32**(5):713-715.
187. Deshpande N, Wilkins MR, Packer N, Nevalainen H: **Protein glycosylation pathways in filamentous fungi**. *Glycobiology* 2008, **18**(8):626-637.
188. Bier DM: **The energy costs of protein metabolism: lean and mean on Uncle Sam's team**. In: *The Role of Protein and Amino Acids in Sustaining and Enhancing Performance: 1999; Washington, DC*: National Academy Press; 1999: 109-119.
189. Apweiler R, Hermjakob H, Sharon N: **On the frequency of protein glycosylation, as deduced from analysis of the SWISS-PROT database**. *Biochim Biophys Acta* 1999, **1473**(1):4-8.
190. Trimble RB, Atkinson PH: **Structure of yeast external invertase Man8-14GlcNAc processing intermediates by 500-megahertz ^{1}H NMR spectroscopy**. *J Biol Chem* 1986, **261**(21):9815-9824.
191. Carlson R, Wlaschin A, Srienc F: **Kinetic studies and biochemical pathway analysis of anaerobic poly-(R)-3-hydroxybutyric acid synthesis in *Escherichia coli***. *Appl Environ Microbiol* 2005, **71**(2):713-720.
192. Leuchtenberger W, Huthmacher K, Drauz K: **Biotechnological production of amino acids and derivatives: current status and prospects**. *Appl Microbiol Biotechnol* 2005, **69**(1):1-8.

193. Pedersen H, Carlsen M, Nielsen J: **Identification of enzymes and quantification of metabolic fluxes in the wild type and in a recombinant *Aspergillus oryzae* strain**. *Appl Environ Microbiol* 1999, **65**(1):11-19.
194. Moralejo FJ, Cardoza RE, Gutierrez S, Martin JF: **Thaumatin production in *Aspergillus awamori* by use of expression cassettes with strong fungal promoters and high gene dosage**. *Appl Environ Microbiol* 1999, **65**(3):1168-1174.
195. Ohnishi J, Katahira R, Mitsuhashi S, Kakita S, Ikeda M: **A novel *gnd* mutation leading to increased L-lysine production in *Corynebacterium glutamicum***. *FEMS Microbiol Lett* 2005, **242**(2):265-274.
196. Eggeling L, Oberle S, Sahm H: **Improved L-lysine yield with *Corynebacterium glutamicum*: use of *dapA* resulting in increased flux combined with growth limitation**. *Appl Microbiol Biotechnol* 1998, **49**(1):24-30.
197. Broer S, Eggeling L, Kramer R: **Strains of *Corynebacterium glutamicum* with Different Lysine Productivities May Have Different Lysine Excretion Systems**. *Appl Environ Microbiol* 1993, **59**(1):316-321.
198. Marx A, Hans S, Mockel B, Bathe B, de Graaf AA, McCormack AC, Stapleton C, Burke K, O'Donohue M, Dunican LK: **Metabolic phenotype of phosphoglucose isomerase mutants of *Corynebacterium glutamicum***. *J Biotechnol* 2003, **104**(1-3):185-197.
199. Blombach B, Schreiner ME, Moch M, Oldiges M, Eikmanns BJ: **Effect of pyruvate dehydrogenase complex deficiency on L-lysine production with *Corynebacterium glutamicum***. *Appl Microbiol Biotechnol* 2007, **76**(3):615-623.
200. Han L, Parekh SR: **Development of Improved Strains and Optimization of Fermentation Processes**. In: *Microbial Processes and Products.* 2005: 1-23.
201. Balbas P: **Understanding the art of producing protein and nonprotein molecules in *Escherichia coli***. *Mol Biotechnol* 2001, **19**(3):251-267.
202. Ruijter GJ, Bax M, Patel H, Flitter SJ, van de Vondervoort PJ, de Vries RP, vanKuyk PA, Visser J: **Mannitol is required for stress tolerance in *Aspergillus niger* conidiospores**. *Eukaryot Cell* 2003, **2**(4):690-698.
203. Riedel C, Rittmann D, Dangel P, Mockel B, Petersen S, Sahm H, Eikmanns BJ: **Characterization of the phosphoenolpyruvate carboxykinase gene from *Corynebacterium glutamicum* and significance of the enzyme for growth and amino acid production**. *J Mol Microbiol Biotechnol* 2001, **3**(4):573-583.
204. Flickinger MC, Rouse MP: **Sustaining protein synthesis in the absence of rapid cell division: an investigation of plasmid-encoded protein expression in *Escherichia coli* during very slow growth**. *Biotechnol Prog* 1993, **9**(6):555-572.
205. Jernejc K, Legisa M: **Purification and properties of carnitine acetyltransferase from citric acid producing *Aspergillus niger***. *Appl Biochem Biotechnol* 1996, **60**(2):151-158.
206. Steinbock F, Choojun S, Held I, Roehr M, Kubicek CP: **Characterization and regulatory properties of a single hexokinase from the citric acid accumulating fungus *Aspergillus niger***. *Biochim Biophys Acta* 1994, **1200**(2):215-223.
207. Vasilev N, Vasileva M, Ganchev I: **Changes in the activity of Krebs cycle enzymes in an *Aspergillus niger* strain during the biosynthesis of citric acid**. *Acta Microbiol Bulg* 1985, **17**:46-51.
208. Osmani SA, Scrutton MC: **The sub-cellular localisation of pyruvate carboxylase and of some other enzymes in *Aspergillus nidulans***. *Eur J Biochem* 1983, **133**(3):551-560.

209. Bercovitz A, Peleg Y, Battat E, Rokem JS, Goldberg I: **Localization of pyruvate carboxylase in organic acid-producing *Aspergillus* strains**. *Appl Environ Microbiol* 1990, **56**(6):1594-1597.
210. Kubicek CP, Schreferl-Kunar G, Wohrer W, Rohr M: **Evidence for a cytoplasmic pathway of oxalate biosynthesis in *Aspergillus niger***. *Appl Environ Microbiol* 1988, **54**(3):633-637.
211. Falony G, Armas JC, Dustet Mendoza JC, Martinez Hernandez JL: **Production of extracellular lipase from *Aspergillus niger* by solid state fermentation**. *Food Technology and Biotechnology* 2006, **44**(2):235-240.
212. Maggio-Hall LA, Keller NP: **Mitochondrial β-oxidation in *Aspergillus nidulans***. *Mol Microbiol* 2004, **54**(5):1173-1185.
213. Eslahpazir Esfandabadi M: **Mathematische Analyse Biochemischer Netzwerke**. *student research project.* Braunschweig: Technische Universität Brausnchweig; 2007.

10 Appendix

10.1 Metabolic Networks

10.1.1 *Aspergillus niger* metabolic network

In the following, the metabolic reactions of the metabolism of *A. niger* were derived from the recently published genome scale metabolic model by Andersen et al. [2]. Also literature information of [8] Diano et al. [64] and Pel et al. [15] were considered if not other references were cited. The condition number of the stoichiometric matrices representing the stoichiometric model and model extensions varied between 11.8 and 12.6, which indicates well-conditioned matrices [73].

Transport processes. Monosaccharide (glucose, xylose) uptake by the cell (R40, R99) is carried out by a mono-saccharide transporter with high affinity [62].
Pyruvate is transported intracellularly between mitochondrial and cytosolic compartments via the pyruvate shuttle (R24). Additionally, the citrate/malate (R25), fumarate (R26), isocitrate/malate (R29) and succinate (R28) shuttle were considered [2, 8]. ATP can be transported via an ATP/ADP translocator (R23) localized in the mitochondrial membrane [2, 15]. Finally, succinate (R132), isocitrate (R130), malate (R134) and AcCoA (R135) are allowed to pass through the glyoxysomal membrane [8, 15, 205].

Embden-Meyerhoff-Parnas (EMP) and pentose-phosphate pathway. The enzymes for EMP and for the pentose-phosphate pathway (PPP) take place exclusively in the cytosol of the cell. Glucose is phosphorylated by ATP in a reaction catalysed by hexokinase (R41) [206]. The further degradation of D-glucose 6-phosphate to pyruvate takes place through the well known Embden-Meyerhoff pathway (EMP), which include 7 reactions (R42, R43, R44, R45, R46, R47, R48).

The channelling of the xylose carbon scaffold into the glycolytic pathway occurs through the non-oxidative part of the pentose phosphate pathway (PPP). Xylose is converted intracellular into the polyol xylitol by the NADPH-dependent polyol dehydrogenase (R100), which is then converted into xylulose by the NADH-dependent xylitol dehydrogenase (R101) [118].
The intracellular pool of xylulose is assumed to be phosphorylated by the ATP-depending xylulokinase (R102) producing xylulose-5-phosphate. Two molecules of xylulose-5-phosphate enter the non-oxidative part of PPP and are converted together with 1 molecule of ribose 5-phosphate (originating from the oxidative part of the PPP) by interlinked reactions catalysed by a transketolase (R78, R80) and a transaldolase (R79) into 2 molecules of fructose 6-phosphate and 1 of glyceraldehydes 3-phosphate.
The oxidative part of the PPP (R74, R75) generates reducing equivalents, in the form of NADPH, for reductive biosynthesis reactions within cells. Furthermore, it provides precursor in the form of ribose-5-phosphate, for the synthesis of the nucleotides and nucleic acids with the simultaneously release of carbon dioxide.

Fructose and mannose metabolism. Fructose can be phosphorylated by a hexokinase into fructose 6-phosphate (R57). Mannose 6-phosphate can be formed by isomerisation of fructose 6-phosphate (R55) and further used for the glycosylation of proteins. Fructose can be converted into mannitol by the reversible NADPH-depending mannitol 2-dehydrogenase (R53) in the cytosolic part of the cell. Mannitol as well as xylitol (see PPP) plays important roles in the prevention of oxidative stress, osmotic regulation and the provision of storage carbon sources. The production of these polyols has been described in recent work [64].

Anaplerotic reactions, citrate cycle, glyoxylate and dicarboxylate reactions. The citrate cycle has been described in detail [207] and was incorporated into the stoichiometric model (R141, R142, R143, R144, R145, R146, R147, R148). The pyruvate carboxylase reaction is assumed to be localized not only in the cytosol (R66) [208] but also in the mitochondrion (R151) [209]. The carbon dioxide used in this anaplerotic reaction, yielding mitochondrial oxaloacetate, comes from the decarboxylation of pyruvate by the pyruvate dehydrogenase complex (R140), which is localized in the mitochondrion. On the other hand, the oxaloacetate formed by the cytosolic pyruvate carboxylase is converted to malate by malate dehydrogenase (R86) and thereupon transported into the mitochondria (R25) [6]. Therefore,

malate serves an essential function of replenishing the metabolite pool of the citrate cycle and, in particular, oxaloacetate serves as precursor for biomass (R220) as well as for fructofuranosidase synthesis (R210).

The cytosolic oxaloacetate could be also transformed into phosphoenolpyruvate by the ATP-dependent phosphoenolpyruvate-carboxykinase (R65). Finally, it was assumed that the oxaloacetate-hydrolase (R87) is localized in the cytosol and is responsible for the production of oxalic acid, which accumulates in the culture medium [210]. Although, oxalic acid can be hydrolysed (R89) into formate and CO2 and subsequently oxidized by the formate dehydrogenase (R90) forming CO2 which is coupled with NADH generation. However, in the outmost cases, oxalic acid will be transported into the extra-cellular medium (R9).

As mentioned earlier, the generation of cytosolic NADPH deliver essential energy for the biosynthesis of numerous precursors for biomass and product synthesis, e.g. amino acids, nucleotides and fatty acids. Beside the oxidative part of the PPP, two further reactions have to be considered in the metabolic model, which are responsible for NADPH generation. The NADP-depending isocitrate dehydrogenase, which is localized not only in the mitochondrion (R144), but also in the cytosolic part (R93) forming 2-oxoglutarate, a precursor for biomass and product synthesis, was considered in the model.

The malic enzyme (R85), also known as decarboxylating malate dehydrogenase, utilizes NADP to catalyze the oxidative decarboxylation of malate to pyruvate and carbon dioxide. Finally, the reactions of the glyoxysomal cycle are considered in the model (R131, R133).

Energy metabolism. The oxidative metabolism of substrates takes place in the mitochondria. For ATP production in the respiratory chain a P/O ratio of 2.64 for NADH (R149) and 1.64 for succinate (R150) and cytosolic NADH was considered [2].

The inter-conversion of NADPH into NADH occurs via the transhydrogenase reaction (R97) in the cytosol [15]. However, the formation of NADPH from NADH is linked with an ATP consumption, which occurs only in the cytosol. This assumption was made under considering that the mannitol-cycle plays an important role in NADPH production, which was proposed for the fungus *Alternaria alternata* [65] and for *Aspergillus sp.* [202]. The net result of mannitol cycle (R53, R54, R56) is a transhydrogenase activity with a net consumption of ATP (NADH + NADP + ATP --> NAD + NADPH + ADP).

Cause of the compartmentalization, the ATP must be transported across the mitochondrial membrane, which is realized by an ATP/ADP-translocation (R23).

The assimilation of sulphate comprises uptake (R5) and subsequent reduction into hydrogen-sulphide (R170), whereas the latter include two subsequent reactions: reduction of sulphate to sulphite requiring 2 mol ATP and 1 mol NADPH and the reduction of sulphite to sulphide requiring 3 mol NADPH.

Lipid metabolism. Extracellular lipases hydrolyse triglycerides to fatty acids and glycerol. They can produced extracellularly by *A. niger* when different complex triglycerides are supplied [211]. The degradation of fatty acids in *Aspergillus sp.* occurred both in the mitochondria but also in the peroxisomes / glyoxysomes. The metabolic reactions (R180 – R198) in the metabolic model were applied according to literature data [212].

Format of reaction model. Listed in what follows (Table A) is the metabolic reaction model in Palsson-like formulation with compartments. Reactions with arrow '**-->**' are irreversible and reactions with double arrow '<==>' are reversible with respect to the thermodynamic constraints. External metabolites are indicated by the short-cut '[ext]'. The metabolic model included the compartmentalization with cytosol, extracellular area, golgi and mitochondrion indicated by [c], [e], [g] and [m], respectively. The stoichiometric coefficients are listed in parenthesis when the values are ≠ 1.

Table 22: Stoichiometric equations of the metabolic model. The reactions are either specific for a certain carbon source ("G": glucose, "g": glycerol, "S": soybean oil, "X": xylose), or relevant for all carbon sources ("for all"), which is indicated in the left column. The units of stoichiometric coefficients are in "mol" if not other mentioned in brackets beside the subheadings.

	Transport Systems	
Network		
G	R1:	glucose [ext] --> glucose[e]
for all	R2:	fructofuranosidase[e] --> fructofuransidase [ext]
for all	R3:	biomass[c] --> biomass [ext]
for all	R4:	NH3 [ext] --> NH3[c]
for all	R5:	SO4 [ext] --> SO4[c]
for all	R6:	O2 [ext] --> O2[e]
for all	R7:	CO2[c] --> CO2[ext]

for all	R8:	ATP_maintenance[c] --> ATP_maintenance[ext]
for all	R9:	oxalate[c] --> oxalate[ext]
S	R10:	soybean oil[ext]--> soybean oil[e]
X	R11:	xylose[ext] --> xylose[e]
g	R12:	glycerol[ext] --> glycerol[e]
for all	R13:	NO3[ext] --> NO3[c]
for all	R14:	gluconate[e] → gluconate[ext]

Shuttles (mitochondrial, extra-/intra-cellular)

for all	R20:	O2[e] <==> O2[c]
for all	R21:	O2[c] <==> O2[m]
for all	R22:	CO2[c] <==> CO2[m]
for all	R23:	ADP[c] + ATP[m] --> ADP[m] + ATP[c]
for all	R24:	pyruvate[c] <==> pyruvate[m]
for all	R25:	citrate[c] + malate[m] --> citrate[c] + malate[c]
for all	R26:	fumarate[c] <==> fumarate[m]
for all	R27:	isocitrate[c] <==> isocitrate[m]
for all	R28:	succinate[c] <==> succinate[m]
for all	R29:	isocitrate[m] + malate[c] --> isocitrate[c] + malate[m]

Embden-Meyerhof-Parnas Pathway

G	R40:	glucose[e] --> glucose[c]
for all	R41:	glucose[c] + ATP[c] --> glucose-6-P[c] + ADP[c]
for all	R42:	glucose-6-P[c] <==> fructose-6-P[c]
for all	R43:	fructose-6-P[c] + ATP[c] --> fructose-1,6-bis-P[c] + ADP[c]
for all	R44:	fructose-1,6-bis-P[c] <==> DHAP[c] + GA-3-P[c]
for all	R45:	DHAP[c] <==> GA-3-P[c]

for all	R46:	GA-3-P[c] + ADP[c] + NAD[c] <==> 3-P-glycerate[c] + ATP[c] + NADH[c]
for all	R47:	3-P-glycerate[c] <==> PEP[c]
for all	R48:	PEP[c] + ADP[c] --> pyruvate[c] + ATP[c]

Fructose and mannose metabolism

for all	R53:	fructose[c] + NADPH[c] <==> mannitol[c] + NADP[c]
for all	R54:	fructose-6-P[c] + NADH[c] <==> mannitol-1-P[c] + NAD[c]
for all	R55:	mannose-6-P[c] <==> fructose-6-P[c]
for all	R56:	mannitol-1-P[c] --> mannitol [c]
for all	R57:	fructose[c] + ATP[c] --> fructose-6-P[c] + ADP[c]

Gluconeogenesis

for all	R63:	glucose-6-P[c] --> glucose[c]
for all	R64:	fructose-1,6-bis-P[c] --> fructose-6-P[c]
for all	R65:	oxaloacetate[c] + ATP[c] --> PEP[c] + ADP[c] + CO2[c]
for all	R66:	pyruvate[c] + ATP[c] + CO2[c] --> oxaloacetate[c] + ADP[c]

Pentose phosphate pathway

G,X	R70:	glucose[e] + O2[e] --> gluconate[e] + H2O2[e]
G,X	R71:	gluconate[e] --> gluconate[c]
G,X	R72:	(2) H2O2[e] --> O2[e]
G,X	R73:	gluconate[c] + ATP[c] --> gluconate-6-P[c] + ADP[c]
for all	R74:	glucose 6-P[c] + NADP[c] --> gluconate-6-P[c] + NADPH[c]
for all	R75:	gluconate 6-P[c] + NADP[c] --> ribulose-5-P[c] + CO2[c] + NADPH[c]
for all	R76:	ribulose 5-P[c] <==> xylulose 5-P[c]
for all	R77:	ribulose 5-P[c] <==> ribose 5-P[c]
for all	R78:	ribose 5-P[c] + xylulose 5-P[c] <==> GA 3-P[c] + sedoheptulose 7-P[c]

for all	R79:	GA-3-P[c] + sedoheptulose 7-P[c] <==> erythrose 4-P[c] + fructose 6-P[c]
for all	R80:	erythrose 4-P[c] + xylulose 5-P[c] <==> fructose 6-P[c] + GA 3-P[c]

Cytosolic reactions

for all	R84:	malate[c] <==> fumarate[c]
for all	R85:	malate[c] + NADP[c] --> pyruvate[c] + NADPH[c] + CO2[c]
for all	R86:	NADH[c] + oxaloacetate[c] <==> malate[c] + NAD[c]
for all	R87:	oxaloacetate[c] --> acetate[c] + oxalate[c]
for all	R88:	acetate[c] + ATP[c] --> AcCoA[c] + ADP[c]
for all	R89:	oxalate[c] --> formate[c] + CO2[c]
for all	R90:	formate[c] + NAD[c] --> CO2[c] + NADH[c]
for all	R91:	citrate[c] + ATP[c] --> oxaloacetate[c] + AcCoA[c] + ADP[c]
for all	R92:	citrate[c] <==> isocitrate[c]
for all	R93:	isocitrate[c] + NADP[c] --> □-ketoglutarate[c] + CO2[c] + NADPH[c]
for all	R94:	isocitrate[c] + NAD[c] --> □ -ketoglutarate[c] + CO2[c] + NADH[c]
for all	R95:	fumarate[c] + FADH2[m] --> succinate[c] + FAD[m]
for all	R96:	NADH[c] + NADP[c] --> NAD[c] + NADPH[c]
for all	R97:	NADPH[c] + NAD[c] --> NADH[c] + NADP[c]
for all	R98:	ATP[c] --> ADP[c] + ATP_maintenance[c]
X	R99:	xylose[e] --> xylose[c]
X	R100:	xylose[c] + NADPH[c] <==> xylitol[c] + NADP[c]
X	R101:	xylitol[c] + NAD[c] <==> xylulose[c] + NADH[c]
X	R102:	xylulose[c] + ATP[c] --> xylulose-5-P[c] + ADP[c]
g, S	R103:	glycerol[e] --> glycerol[c]
g	R104:	glycerol[c] + NAD[c] --> glycerone + NADH[c]
g	R105:	glycerol 3-P[c] + FAD[m] --> DHAP[c] + FADH2[m]
for all	R106:	NO3[c] + (4) NADPH[c] --> NH3[c] + (4) NADP[c]

g	R107:	glycerol[c] + ATP[c] → glycerol 3-P[c] + ADP[c]
g	R108:	glycerone[c] + ATP[c] → DHAP[c] + ADP[c]

Glyoxysomal reactions

for all	R130:	isocitrate[c] <==> isocitrate[g]
for all	R131:	isocitrate[g] <==> glyoxalate[g] + succinate[g]
for all	R132:	succinate[g] <==> succinate[c]
for all	R133:	glyoxalate[g] + AcCoA[g] --> malate[g]
for all	R134:	malate[g] <==> malate[c]
for all	R135:	AcCoA[c] <==> AcCoA[g]

Mitochondrial reactions / Energy metabolism

for all	R139:	citrate[m] + ATP[m] --> oxaloacetate[m] + AcCoA[m] + ADP[m]
for all	R140:	pyruvate[m] + NAD[m] --> AcCoA[m] + NADH[m] + CO2[m]
for all	R141:	AcCoA[m] + oxaloacetate[m] --> citrate[m]
for all	R142:	citrate[m] <==> isocitrate[m]
for all	R143:	isocitrate[m] + NAD[m] --> α -ketoglutarate[m] + CO2[m] + NADH[m]
for all	R144:	isocitrate[m] + NADP[m] --> α -ketoglutarate[m] + CO2[m] + NADPH[m]
for all	R145:	α -ketoglutarate[m] + NAD[m] + ADP[m] --> succinate[m] + NADH[m] + ATP[m] + CO2[m]
for all	R146:	succinate[m] + Q[m] <==> fumarate[m] + QH2[m]
for all	R147:	fumarate[m] <==> malate[m]
for all	R148:	malate[m] + NAD[m] <==> oxaloacetate[m] + NADH[m]
for all	R149:	(2) NADH2[m] + O2[m] + (5.28) ADP[m] --> (2) NAD[m] + (5.28) ATP[m]
for all	R150:	(2) QH2[m] + O2[m] + (3.28) ADP[m] --> (2) Q[m] + (3.28) ATP[m]
for all	R151:	pyruvate[m] + CO2[m] + ATP[m] --> oxaloacetate[m] + ADP[m]
for all	R152:	NADH[c] + Q[m] --> NAD[c] + QH2[m]

	Sulphate assimilation	
for all	R170:	(4) ATP[c] + (4) NADPH[c] + SO4[c] --> (4) ADP[c] + H2S[c] + (4) NADP[c]
	Lipid metabolism / degradation of soybean oil in mitochondria and glyoxysomes	
S	R180:	soybeanoil[e] --> glycerol[e] + (2.1) linolicacid[e] + (0.9) oleicacid[e]
S	R181:	oleicacid[e] --> oleicacid[c]
S	R182:	linolicacid[e] --> linolicacid[c]
S	R184:	oleicacid[c] + ATP[c] --> oleicacid-CoA[c] + AMP[c]
S	R185:	oleicacid-CoA[c] --> oleicacid-CoA[g]
S	R185:	oleicacid-CoA[c] --> oleicacid-CoA[m]
S	R186:	oleicacid-CoA[m] + (7) FAD[m] + (8) NAD[m] --> (9) AcCoA[m] + (7) FADH2[m] + (8) NADH2[m]
S	R187:	oleicacid-CoA[g] + (7) O2[g] + (8) NAD[g] --> (9) AcCoA[g] + (7) H2O2[g] + (8) NADH[g]
S	R188:	H2O2[g] --> O2[g]
S	R189:	O2[g] <==> O2[c]
S	R190:	linolicacid[c] + ATP[c] --> linolicacid-CoA[c] + AMP[c]
S	R191:	linolicacid-CoA[c] --> linolicacid-CoA[g]
S	R192:	linolicacid-CoA[c] --> linolicacid-CoA[m]
S	R193:	linolicacid-CoA[m] + (6) FAD[m] + (8) NAD[m] + NADPH[m] + O2[m] --> (9) Ac-CoA[m] + (6) FADH[m] + (8) NADH2[m] + NADP[m] + H2O2[m]
S	R194:	H2O2[m] --> O2[m]
S	R195:	linolicacid-CoA[g] + (7) O2[g] + (8) NAD[g] + NADPH[g] --> (9) AcCoA[g] + (8) NADH[g]
S	R196:	NADH[c] + NAD[g] <==> NADH[g] + NAD[c]
S	R197:	NADPH[c] + NADP[g] <==> NADPH[g] + NADP[c]
S	R198:	AMP[c] + ATP[c] --> (2) ADP[c]
	Fructofuranosidase synthesis / transport [mol/mmol fructofuranosidase]	

for all R210: (0.067) AcCoA[c] + (0.258) pyruvate[c] + (0.126) 3-P-glycerate[c] + (5.482) ATP[c] + (1.156) NADPH[c] + (0.761) NH3[c] + (0.030) fructose-6-P[c] + (0.018) glucose-6-P[c] + (0.065) erythrose-4-P[c] + (0.115) PEP[c] + (0.005) H2S[c] + (0.134) oxaloacetate[c] + (0.116) -ketoglutarate[c] + (0.308) mannose-6-P[c] + (0.025) ribose-5-P[c] + (0.305) NAD[c] --> (1) fructofuranosidase[c] + (0.305) NADH[c] + (0.04) CO2[c] + (5.482) ADP[c] + (1.156) NADP[c]

for all R211: fructofuranosidase[c] + ATP[c] --> fructofuranosidase[e] + ADP[c]

Biomass synthesis [mol/1000 g biomass]

for all R220: (1.03) oxaloacetate[c] + (0.89) 3-P-glycerate[c] + (0.37) ribose-5-P[c] + (61) ATP[c] + (13.18) NADPH[c] + (7.1) NH3[c] + (2.51) NAD[c] + (3.86) AcCoA[c] + (0.08) FADH2[c] + (0.08) DHAP[c] + (1.6) glucose 6-P[c] + (0.33) O2[c] + (0.44) fructose-6-P[c] + (0.42) mannose-6-P[c] + (1.91) pyruvate[c] + (1.14) -ketoglutarate[c] + (0.36) erythrose-4-P[c] + (0.65) PEP[c] + (0.15) H2S[c] + (0.213) mannitol[c] --> biomass[c] + (0.08) FAD[c] + (13.18) NADP[c] + (2.51) NADH[c] + (61) ADP[c]

10.1.2 Small example network of TCA cycle and supporting pathways

In the following, the stoichiometric equations for the small example network of *Escherichia coli* [131]is given in Palsson-like formula. Abbreviations were taken from [131] and are partial notwithstanding from the list, which is indicated in the legend.

Table 23: Stoichiometric equations of the simplified *E. coli* model. Abbreviations: BPG: bis-phospho glycerate, FP2: fructose 1,2-bis-posphate, GO6P: 6-phospho gluconolactone.

metabolic reactions in Palsson-like formulation
'--> G6P[e]'
'Pyr[e] -->'
'R5P[e] -->'
'CO2[c] -->'
'--> ATP[e]'
'--> ADP[e]'
'ATP[c] -->'
'ADP[c] -->'
'NADPH[c] -->'
'--> NADP[c]'
'NADH[c] -->'
'--> NAD[c]'
'G6P[e] --> G6P[c]'
'G6P[c] <==> F6P[c]'
'F6P[c] + ATP[c] --> FP2[c] + ADP[c]'
'FP2[c] --> F6P[c]'
'FP2[c] <==> GAP[c] + DHAP[c]'
'GAP[c] <==> DHAP[c]'
'GAP[c] + NAD[c] --> BPG[c] + NADH[c]'
'BPG[c] + ADP[c] --> 3PG[c] + ATP[c]'
'3PG[c] <==> 2PG[c]'
'2PG[c] <==> PEP[c]'
'PEP[c] + ADP[c] --> Pyr[c] + ATP[c]'
'Pyr[c] --> Pyr[e]'
'G6P[c] + NADP[c] --> GO6P[c] + NADPH[c]'
'GO6P[c] --> 6PG[c]'

'6PG[c] + NADP[c] --> Ru5P[c] + NADPH[c] + CO2[c]'

'Ru5P[c] <==> Xyl5P[c]'

'Ru5P[c] <==> R5P[c]'

'R5P[c] + Xyl5P[c] <==> Sed7P[c] + GAP[c]'

'Sed7P[c] + GAP[c] <==> Ery4P[c] + F6P[c]'

'Ery4P[c] + Xyl5P[c] <==> F6P[c] + GAP[c]'

'R5P[c] --> R5P[e]'

'ATP[e] --> ATP[c]'

'ADP[e] --> ADP[c]'

10.1.3 *Escherichia coli* metabolic network

Stoichiometric equations for the metabolic network of *Escherichia coli* listed in Palsson-like formulation.

Table 24: Stoichiometric equations of the genome based *E. coli* model.

metabolic reactions in Palsson-like formulation
' --> glucose[e]'
'epoxidehydrolase[e] --> '
'biomass[c] -->'
' --> NH3[c]'
' --> SO4[e]'
' --> O2[c]'
'CO2[c] -->'
'acetate[c]-->'
'glucose[e] + PEP[c] --> glucose-6-P[c] + pyruvate[c]'
'glucose-6-P[c] <==> fructose-6-P[c]'
'glucose-6-P[c] + NADP[c] --> gluconate-6-P[c] + NADPH2[c]'
'gluconate-6-P[c] + NADP[c] --> ribulose-5-P[c] + CO2[c] + NADPH2[c]'
'ribulose-5-P[c] <==> xylulose-5-P[c]'
'ribulose-5-P[c] <==> ribose-5-P[c]'
'ribose-5-P[c] + xylulose-5-P[c] <==> GA-3-P[c] + sedoheptulose-7-P[c]'
'GA-3-P[c] + sedoheptulose-7-P[c] <==> erythrose-4-P[c] + fructose-6-P[c]'
'erythrose-4-P[c] + xylulose-5-P[c] <==> fructose-6-P[c] + GA-3-P[c]'
'fructose-6-P[c] + ATP[c] --> fructose-1,6-bis-P[c] + ADP[c]'
'fructose-1,6-bis-P[c] <==> DHAP[c] + GA-3-P[c]'
'fructose-1,6-bis-P[c] --> fructose-6-P[c]'
'DHAP[c] <==> GA-3-P[c]'
'GA-3-P[c] + ADP[c] + NAD[c] <==> 3-P-glycerate[c] + ATP[c] + NADH2[c]'

'3-P-glycerate[c] <==> 2-P-glycerate[c]'

'2-P-glycerate[c] <==> PEP[c]'

'PEP[c] + ADP[c] --> pyruvate[c] + ATP[c]'

'pyruvate[c] + NAD[c] --> AcCoA[c] + NADH2[c] + CO2[c]'

'AcCoA[c] + oxalacetate[c] --> citrate[c]'

'citrate[c] <==> isocitrate[c]'

'isocitrate[c] + NADP[c] --> 2-oxoglutarate[c] + CO2[c] + NADPH2[c]'

'2-oxoglutarate[c] + NAD[c] + ADP[c] --> succinate[c] + NADH2[c] + ATP[c] + CO2[c]'

'succinate[c] + FAD[c] <==> fumarate[c] + FADH2[c]'

'fumarate[c] <==> malate[c]'

'malate[c] + NAD[c] <==> oxalacetate[c] + NADH2[c]'

'isocitrate[c] <==> glyoxalate[c] + succinate[c]'

'glyoxalate[c] + AcCoA[c] --> malate[c]'

'pyruvate[c] + ATP[c] + CO2[c] --> oxalacetate[c] + ADP[c]'

'PEP[c] + CO2[c] --> oxalacetate[c]'

'oxalacetate[c] + ATP[c] --> PEP[c] + ADP[c] + CO2[c]'

'oxalacetate[c] + ADP[c] --> pyruvate[c] + ATP[c] + CO2[c]'

'malate[c] + NADP[c] --> pyruvate[c] + NADPH2[c] + CO2[c]'

'ATP[c] --> ADP[c] + ATP_maintenance[c]'

'ATP_maintenance[c] -->'

'(2) NADH2[c] + O2[c] + (4) ADP[c] --> (2) NAD[c] + (4) ATP[c]'

'(2) FADH2[c] + O2[c] + (2) ADP[c] --> (2) FAD[c] + (2) ATP[c]'

'SO4[e] + ATP[c] --> SO4[c] + ADP[c]'

'(4) ATP[c] + (4) NADPH2[c] + SO4[c] --> (4) ADP[c] + H2S[c] + (4) NADP[c]'

'NADPH2[c] + NAD[c] --> NADH2[c] + NADP[c]'

'ATP[c] + (3) NADH2[c] + (3) NADP[c] --> ADP[c] + (3) NADPH2[c] + (3) NAD[c]'

'glucose-6-P[c] + NADP[c] --> KDPG[c] + NADPH2[c]'

'KDPG[c] <==> pyruvate[c] + GA-3-P[c]'

'acetate[c] + ATP[c] <==> AcCoA[c] + ADP[c]'

epoxide hydrolase synthesis

'(0.058) AcCoA[c] + (0.171) pyruvate[c] + (0.062) 3-P-glycerate[c] + (4.935) ATP[c] + (0.897) NADPH2[c] + (0.513) NH3[c] + (0.048) erythrose-4-P[c] + (0.087) PEP[c] + (0.013) H2S[c] + (0.08) oxalacetate[c] + (0.107) 2-oxoglutarate[c] + (0.019) ribose-5-P[c] + (0.212) NAD[c] --> (1) epoxidehydrolase[c] + (0.212) NADH2[c] + (0.007) CO2[c] + (4.935) ADP[c] + (0.897) NADP[c]'

'epoxidehydrolase[c] + ATP[c] --> epoxidehydrolase[e] + ADP[c]'

biomass synthesis

'(1.481) oxalacetate[c] + (1.338) 3-P-glycerate[c] + (0.627) ribose-5-P[c] + (17.821) ATP[c] + (16.548) NADPH2[c] + (6.965) NH3[c] + (3.548) NAD[c] + (2.930) AcCoA[c] + (2.861) pyruvate[c] + (1.078) 2-oxoglutarate[c] + (0.361) erythrose-4-P[c] + (0.72) PEP[c] + (0.233) H2S[c] + (0.072) fructose-6-P[c] + (0.206) glucose-6-P[c] + (0.129) GA-3-P[c] --> biomass[c] + (16.548) NADP[c] + (3.548) NADH2[c] + (17.821) ADP[c] + (1.678) CO2[c]'

10.1.4 *Saccharomyces cerevisiae* metabolic network

In the following, the stoichiometric equations for the genome based network of *S. cerevisiae* is given in Palsson-like formula.

Table 25: Stoichiometric equations of the genome based *S. cerevisiae* model. Abbreviations: ACEADH: acetaldehyde.

metabolic reactions in Palsson-like formulation
' --> glucose[e]'
'biomass[c] -->'
' --> NH3[c]'
' --> SO4[c]'
' --> O2[e]'
'CO2[c] -->'
'ETOH[c] -->'
'acetate[c] -->'
'O2[e] --> O2[c]'
'O2[c] <==> O2[m]'
'CO2[c] <==> CO2[m]'
'ADP[c] + ATP[m] --> ADP[m] + ATP[c]'
'pyruvate[c] --> pyruvate[m]'
'malate[m] --> malate[c]'
'fumarate[m] + succinate[c] --> fumarate[c] + succinate[m]'
'citrate[m] + malate[c] --> citrate[c] + malate[m]'
'succinate[c] --> succinate[m]'
'2-oxoglutarate[c] + malate[m] --> 2-oxoglutarate[m] + malate[c]'
'oxalacetate[c] --> oxalacetate[m]'
'AcCoA[m] <==> AcCoA[c]'
'ETOH[c] <==> ETOH[m]'
'glucose[e] --> glucose[c]'
'glucose[c] + ATP[c] --> glucose-6-P[c] + ADP[c]'
'glucose-6-P[c] <==> fructose-6-P[c]'
'fructose-6-P[c] + ATP[c] --> fructose-1,6-bis-P[c] + ADP[c]'
'fructose-1,6-bis-P[c] <==> DHAP[c] + GA-3-P[c]'
'DHAP[c] <==> GA-3-P[c]'
'GA-3-P[c] + ADP[c] + NAD[c] <==> 3-P-glycerate[c] + ATP[c] + NADH2[c]'
'3-P-glycerate[c] <==> PEP[c]'
'PEP[c] + ADP[c] --> pyruvate[c] + ATP[c]'
'fructose-6-P[c] <==> mannose-6-P[c]'
'fructose-1,6-bis-P[c] --> fructose-6-P[c]'
'oxalacetate[c] + ATP[c] --> PEP[c] + ADP[c] + CO2[c]'
'pyruvate[c] + ATP[c] + CO2[c] --> oxalacetate[c] + ADP[c]'
'pyruvate[c] --> ACEADH[c] + CO2[c]'
'ACEADH[c] + NADH2[c] --> ETOH[c] + NAD[c]'

'ACEADH[c] + NADP[c] --> acetate[c] + NADPH2[c]'
'acetate[c] + ATP[c] --> AcCoA[c] + ADP[c]'
'glucose-6-P[c] + NADP[c] --> gluconate-6-P[c] + NADPH2[c]'
'gluconate-6-P[c] + NADP[c] --> ribulose-5-P[c] + CO2[c] + NADPH2[c]'
'ribulose-5-P[c] <==> xylulose-5-P[c]'
'ribulose-5-P[c] <==> ribose-5-P[c]'
'ribose-5-P[c] + xylulose-5-P[c] <==> GA-3-P[c] + sedoheptulose-7-P[c]'
'GA-3-P[c] + sedoheptulose-7-P[c] <==> erythrose-4-P[c] + fructose-6-P[c]'
'erythrose-4-P[c] + xylulose-5-P[c] <==> fructose-6-P[c] + GA-3-P[c]'
'AcCoA[c] + oxalacetate[c] --> citrate[c]'
'citrate[c] <==> isocitrate[c]'
'citrate[c] + ATP[c] --> oxalacetate[c] + AcCoA[c] + ADP[c]'
'malate[c] + NADP[c] --> pyruvate[c] + NADPH2[c] + CO2[c]'
'NADH2[c] + oxalacetate[c] <==> malate[c] + NAD[c]'
'citrate[c] <==> isocitrate[c]'
'isocitrate[c] + NADP[c] --> 2-oxoglutarate[c] + CO2[c] + NADPH2[c]'
'fumarate[c] + FADH2[c] <==> succinate[c] + FAD[c]'
'malate[c] <==> fumarate[c]'
'NADPH2[c] + NAD[c] --> NADH2[c] + NADP[c]'
'NADP[c] + NADH2[c] + ATP[c] --> NADPH2[c] + NAD[c] + ADP[c]'
'ATP[c] --> ADP[c] + ATP_maintenance[c]'
'ATP_maintenance[c] -->'
'isocitrate[c] <==> glyoxalate[c] + succinate[c]'
'glyoxalate[c] + AcCoA[c] --> malate[c]'
'pyruvate[m] + NAD[m] --> AcCoA[m] + NADH2[m] + CO2[m]'
'AcCoA[m] + oxalacetate[m] --> citrate[m]'
'citrate[m] <==> isocitrate[m]'
'isocitrate[m] + NAD[m] --> 2-oxoglutarate[m] + CO2[m] + NADH2[m]'
'2-oxoglutarate[m] + NAD[m] + ADP[m] --> succinate[m] + NADH2[m] + ATP[m] + CO2[m]'
'succinate[m] + Q[m] <==> fumarate[m] + QH2[m]'
'fumarate[m] <==> malate[m]'
'malate[m] + NAD[m] <==> oxalacetate[m] + NADH2[m]'
'malate[m] + NADP[m] --> pyruvate[m] + NADPH2[m] + CO2[m]'
'ETOH[m] + (2) ATP[m] + (2) NAD[m] --> AcCoA[m] + (2) ADP[m] + (2) NADH2[m]'
'(2) NADH2[m] + (0.5) O2[m] + (4) ADP[m] --> (2) NAD[m] + (4) ATP[m]'
'(2) QH2[m] + (0.5) O2[m] + (2) ADP[m] --> (2) Q[m] + (2) ATP[m]'
'NADH2[m] + Q[m] --> QH2[m] + NAD[m]'
'NADPH2[m] + NAD[m] --> NADP[m] + NADH2[m]'
'(4) ATP[c] + (4) NADPH2[c] + SO4[c] --> (4) ADP[c] + H2S[c] + (4) NADP[c]'

epoxide hydrolase synthesis

'(0.058) AcCoA[c] + (0.171) pyruvate[c] + (0.062) 3-P-glycerate[c] + (4.935) ATP[c] + (0.897) NADPH2[c] + (0.513) NH3[c] + (0.048) erythrose-4-P[c] + (0.087) PEP[c] + (0.013) H2S[c] + (0.08) oxalacetate[c] + (0.107) 2-oxoglutarate[c] + (0.019) ribose-5-P[c] + (0.212) NAD[c] --> (1) epoxidehydrolase[c] + (0.212) NADH2[c] + (0.007) CO2[c] + (4.935) ADP[c] + (0.897) NADP[c]'
'epoxidehydrolase[c] + ATP[c] --> epoxidehydrolase[e] + ADP[c]'

biomass synthesis
'(1.481) oxalacetate[c] + (1.338) 3-P-glycerate[c] + (0.627) ribose-5-P[c] + (17.821) ATP[c] + (16.548) NADPH2[c] + (6.965) NH3[c] + (3.548) NAD[c] + (2.930) AcCoA[c] + (2.861) pyruvate[c] + (1.078) 2-oxoglutarate[c] + (0.361) erythrose-4-P[c] + (0.72) PEP[c] + (0.233) H2S[c] + (0.072) fructose-6-P[c] + (0.206) glucose-6-P[c] + (0.129) GA-3-P[c] --> biomass[c] + (16.548) NADP[c] + (3.548) NADH2[c] + (17.821) ADP[c] + (1.678) CO2[c]'

10.1.5 *Corynebacterium glutamicum* metabolic network

In the following, the stoichiometric equations for the genome based metabolic network of *C. glutamicum* are given in Palsson-like formulation. Abbreviations are partial notwithstanding from the abbreviation list, which is indicated in the legend.

Table 26: Stoichiometric equations of the genome based *C. glutamicum* model. Abbreviations: RIBO-5P: ribose 5-phosphate, GLYOXY: glyoxylate, MK: , MKH2: reduced form of MK.

metabolic reactions in Palsson-like formulation
'--> GLC[e]'
'biomass[c] -->'
'LYS[c] -->'
'ATPmaintenance[c] -->'
'--> SO4[e]'
'CO2[c] -->'
'--> O2[c]'
'--> NH3[c]'
'PEP[c] + GLC[e] --> PYR[c] + G6P[c]'
'G6P[c] <==> F6P[c]'
'G6P[c] + NADP[c] --> GLC-LAC[c] + NADPH[c]'
'GLC-LAC[c] --> 6-P-Gluconate[c]'
'6-P-Gluconate[c] + NADP[c] --> RIB-5P[c] + CO2[c] + NADPH[c]'
'RIB-5P[c] <==> XYL-5P[c]'
'RIB-5P[c] <==> RIBO-5P[c]'
'S7P[c] + GA3P[c] <==> RIBO-5P[c] + XYL-5P[c]'
'S7P[c] + GA3P[c] <==> E-4P[c] + F6P[c]'
'F6P[c] + GA3P[c] <==> E-4P[c] + XYL-5P[c]'
'ATP[c] + F6P[c] --> ADP[c] + F-16-BP[c]'
'F-16-BP[c] <==> GA3P[c] + DAHP[c]'
'DAHP[c] <==> GA3P[c]'
'GA3P[c] + NAD[c] <==> 13-PG[c] + NADH[c]'
'ADP[c] + 13-PG[c] --> ATP[c] + 3-PG[c]'
'3-PG[c] <==> 2-PG[c]'
'2-PG[c] <==> PEP[c]'
'PEP[c] + ADP[c] --> PYR[c] + ATP[c]'

'PYR[c] + H-CoA[c] + NAD[c] --> AC-CoA[c] + NADH[c] + CO2[c]'
'AC-CoA[c] + OAA[c] --> CIT[c] + H-CoA[c]'
'CIT[c] <==> Cis-ACO[c]'
'Cis-ACO[c] <==> ICI[c]'
'ICI[c] + NADP[c] --> AKG[c] + CO2[c] + NADPH[c]'
'AKG[c] + NH3[c] + NADPH[c] --> GLU[c] + NADP[c]'
'AKG[c] + NAD[c] + H-CoA[c] --> SUCC-CoA[c] + NADH[c] + CO2[c]'
'SUCC-CoA[c] + ADP[c] --> SUCC[c] + H-CoA[c] + ATP[c]'
'SUCC[c] + MK[c] <==> FUM[c] + MKH2[c]'
'FUM[c] <==> MAL[c]'
'MAL[c] + NAD[c] --> OAA[c] + NADH[c]'
'ICI[c] --> GLYOXY[c] + SUCC[c]'
'GLYOXY[c] + AC-CoA[c] --> MAL[c] + H-CoA[c]'
'PYR[c] + ATP[c] + CO2[c] --> OAA[c] + ADP[c]'
'PEP[c] + CO2[c] --> OAA[c]'
'OAA[c] + ATP[c] --> PEP[c] + ADP[c] + CO2[c]'
'OAA[c] + GLU[c] <==> ASP[c] + AKG[c]'
'ASP[c] + ATP[c] --> ASP-P[c] + ADP[c]'
'ASP-P[c] + NADPH[c] --> ASP-SA[c] + NADP[c]'
'ASP-SA[c] + PYR[c] --> DHP[c]'
'DHP[c] + NADPH[c] --> THDP[c] + NADP[c]'
'THDP[c] + SUCC-CoA[c] --> SAP[c] + H-CoA[c]'
'SAP[c] + GLU[c] --> SADP[c] + AKG[c]'
'SADP[c] --> SUCC[c] + DAP[c]'
'THDP[c] + NADPH[c] + NH3[c] --> DAP[c] + NADP[c]'
'DAP[c] --> LYS[c] + CO2[c]'
'SO4[c] + (2) ATP[c] + NADPH[c] --> H2SO3[c] + ADP[c] + AMP[c] + NADP[c]'
'ATP[c] --> ADP[c] + ATPmaintenance[c]'
'MAL[c] + NADP[c] --> PYR[c] + CO2[c] + NADPH[c]'
'H2SO3[c] + (3) NADPH[c] --> H2S[c] + (3) NADP[c]'
'NADH[c] + (0.5) O2[c] + (2) ADP[c] --> NAD[c] + (2) ATP[c]'
'MKH2[c] + (0.5) O2[c] + (2) ADP[c] --> MK[c] + (2) ATP[c]'
'AMP[c] + ATP[c] --> (2) ADP[c]'
'SO4[e] + ATP[c] --> SO4[c] + ADP[c]'
'F-16-BP[c] --> F6P[c]'

'(6.231) NH3[c] + (0.233) H2S[c] + (0.205) G6P[c] + (0.071) F6P[c] + (0.879) RIBO-5P[c] + (0.268) E-4P[c] + (0.129) GA3P[c] + (1.295) 3-PG[c] + (0.534) PEP[c] + (1.807) PYR[c] + (2.5) AC-CoA[c] + (1.71) OAA[c] + (1.252) AKG[c] + (14.849) NADPH[c] + (29.2) ATP[c] + (3.111) NAD[c] --> biomass[c] + (14.849) NADP[c] + (2.5) H-CoA[c] + (2.537) CO2[c] + (29.2) ADP[c] + (3.111) NADH[c]'

10.1.6 *Bacillus subtilis* metabolic network

In the following, the stoichiometric equations for the metabolic network of *B. subtilis* are given in Palsson-like formulation.

Table 27: Stoichiometric equations of the *B. subtilis* metabolic network model.

metabolic reactions in Palsson-like formulation
' --> glucose[e]'
'epoxidehydrolase[e] --> '
'biomass[c] -->'
' --> NH3[c]'
' --> SO4[e]'
' --> O2[c]'
'CO2[c] -->'
'acetate[c]-->'
'glucose[e] + PEP[c] --> glucose-6-P[c] + pyruvate[c]'
'glucose-6-P[c] <==> fructose-6-P[c]'
'glucose-6-P[c] + NADP[c] --> gluconate-6-P[c] + NADPH2[c]'
'gluconate-6-P[c] + NADP[c] --> ribulose-5-P[c] + CO2[c] + NADPH2[c]'
'ribulose-5-P[c] <==> xylulose-5-P[c]'
'ribulose-5-P[c] <==> ribose-5-P[c]'
'ribose-5-P[c] + xylulose-5-P[c] <==> GA-3-P[c] + sedoheptulose-7-P[c]'
'GA-3-P[c] + sedoheptulose-7-P[c] <==> erythrose-4-P[c] + fructose-6-P[c]'
'erythrose-4-P[c] + xylulose-5-P[c] <==> fructose-6-P[c] + GA-3-P[c]'
'fructose-6-P[c] + ATP[c] --> fructose-1,6-bis-P[c] + ADP[c]'
'fructose-1,6-bis-P[c] <==> DHAP[c] + GA-3-P[c]'
'fructose-1,6-bis-P[c] --> fructose-6-P[c]'
'DHAP[c] <==> GA-3-P[c]'
'GA-3-P[c] + ADP[c] + NAD[c] <==> 3-P-glycerate[c] + ATP[c] + NADH2[c]'
'3-P-glycerate[c] <==> 2-P-glycerate[c]'
'2-P-glycerate[c] <==> PEP[c]'
'PEP[c] + ADP[c] --> pyruvate[c] + ATP[c]'
'pyruvate[c] + NAD[c] --> AcCoA[c] + NADH2[c] + CO2[c]'
'AcCoA[c] + oxalacetate[c] --> citrate[c]'
'citrate[c] <==> isocitrate[c]'
'isocitrate[c] + NADP[c] --> 2-oxoglutarate[c] + CO2[c] + NADPH2[c]'
'2-oxoglutarate[c] + NAD[c] + ADP[c] --> succinate[c] + NADH2[c] + ATP[c] + CO2[c]'
'succinate[c] + FAD[c] <==> fumarate[c] + FADH2[c]'
'fumarate[c] <==> malate[c]'
'malate[c] + NAD[c] <==> oxalacetate[c] + NADH2[c]'
'pyruvate[c] + ATP[c] + CO2[c] --> oxalacetate[c] + ADP[c]'
'PEP[c] + CO2[c] --> oxalacetate[c]'
'oxalacetate[c] + ATP[c] --> PEP[c] + ADP[c] + CO2[c]'
'oxalacetate[c] + ADP[c] --> pyruvate[c] + ATP[c] + CO2[c]'

'malate[c] + NADP[c] --> pyruvate[c] + NADPH2[c] + CO2[c]'

'ATP[c] --> ADP[c] + ATP_maintenance[c]'

'ATP_maintenance[c] -->'

'(2) NADH2[c] + O2[c] + (2.7) ADP[c] --> (2) NAD[c] + (2.7) ATP[c]'

'(2) FADH2[c] + O2[c] + (2) ADP[c] --> (2) FAD[c] + (2) ATP[c]'

'SO4[e] + ATP[c] --> SO4[c] + ADP[c]'

'(4) ATP[c] + (4) NADPH2[c] + SO4[c] --> (4) ADP[c] + H2S[c] + (4) NADP[c]'

'NADPH [c] + NAD[c] <==> NADH [c] + NADP[c]'

'acetate[c] + ATP[c] <==> AcCoA[c] + ADP[c]'

epoxide hydrolase

'(0.058) AcCoA[c] + (0.171) pyruvate[c] + (0.062) 3-P-glycerate[c] + (4.935) ATP[c] + (0.897) NADPH2[c] + (0.513) NH3[c] + (0.048) erythrose-4-P[c] + (0.087) PEP[c] + (0.013) H2S[c] + (0.08) oxalacetate[c] + (0.107) 2-oxoglutarate[c] + (0.019) ribose-5-P[c] + (0.212) NAD[c] --> (1) epoxidehydrolase[c] + (0.212) NADH2[c] + (0.007) CO2[c] + (4.935) ADP[c] + (0.897) NADP[c]'

'epoxidehydrolase[c] + ATP[c] --> epoxidehydrolase[e] + ADP[c]'

biomass synthesis

'(1.8915) oxalacetate[c] + (2.2415) 3-P-glycerate[c] + (0.5445) ribose-5-P[c] + (37.2775) ATP[c] + (15.327) NADPH2[c] + (9.539) NH3[c] + (4.402) NAD[c] + (1.8105) AcCoA[c] + (3.0685) pyruvate[c] + (1.2725) 2-oxoglutarate[c] + (0.4285) erythrose-4-P[c] + (0.6635) PEP[c] + (0.2105) H2S[c] + (0.578) glucose-6-P[c] + (0.3315) GA-3-P[c] --> biomass[c] + (15.327) NADP[c] + (4.402) NADH2[c] + (37.2775) ADP[c] + (2.9265) CO2[c]'

10.2 Composition of Target Proteins

Table 28: Amino acid demand for target protein.

Precursor	β-Fructofuranosidase	α-Glucoamylase	Epoxide Hydrolase
Alanin	42	65	31
Arginine	21	21	18
Asparagine	31	25	6
Aspartate	30	43	18
Cysteine	1	10	3
Glutamine	24	17	10
Glutamate	22	43	30
Glycin	54	22	27
Histidine	10	4	10
Isoleucine	24	24	20
Leucine	55	48	42
Lysine	12	13	16
Methionine	4	3	10
Phenylalanine	31	26	29
Proline	37	22	33
Serine	71	87	32
Threonine	45	74	26
Tryptophane	15	19	9
Tyrosine	19	27	10
Valine	41	42	18
Sugar			
fructose	6	0	0
glucose	18	3	0
mannose	308	62	0

10.3 Estimation of Measurement Errors

The estimation of measuring errors was carried out using the elemental balances. For an over-determined system, the checking of the consistency of measured and calculated reaction rates can be taken into account by the use of unused balances of the system. The elementary matrix $\underline{\underline{N}}$ consists of the elemental balances, which is multiplied by the flux vector $\underline{j}$. A separation of the reaction vector into known and unknown vectors and under the assumption of a non-singular over-determined system, the equation is obtained

$$\underline{j}_c = -\underline{\underline{N}}_c^{\#} \cdot \underline{\underline{N}}_m \cdot \underline{j}_m = \underline{0} \qquad \textbf{(10-1)}$$

with

$$\underline{\underline{N}}_c^{\#} = \left(\underline{\underline{N}}_c^T \cdot \underline{\underline{N}}_c\right)^{-1} \cdot \underline{\underline{N}}_c^T \qquad \textbf{(10-2)}$$

In an over-determined system, unused balances of measured reaction rates can be used to make an overall consistency check of measured and calculated reaction rates. For this, the redundancy matrix is introduced, which is defined as:

$$\underline{\underline{R}} = \underline{\underline{N}}_m - \underline{\underline{N}}_c \cdot \left(\underline{\underline{N}}_c^T \cdot \underline{\underline{N}}_c\right)^{-1} \cdot \underline{\underline{N}}_c^T \cdot \underline{\underline{N}}_m \qquad \textbf{(10-3)}$$

whereas it can be demonstrated that

$$\underline{\underline{R}} \cdot \underline{j}_m = \underline{0} \qquad \textbf{(10-4)}$$

The rank of the matrix $\underline{\underline{R}}$ specifies the number of independent equations. The dependent rows can be removed by matrix transformations and the reduced form of the redundancy matrix $\underline{\underline{R}}_r$ can be obtained. For this redundancy matrix, following equation also holds:

$$\underline{\underline{R}}_r \cdot \underline{j}_m = \underline{0} \tag{10-5}$$

Experimental data are usually prone by errors so the measured rate vector $\underline{j}_m$ can be described by the actual rate vector $\hat{\underline{j}}_m$ and its general measurement error σ as follows:

$$\hat{\underline{j}}_m = \underline{j}_m + \underline{\sigma} \tag{10-6}$$

The combination of equation and equation leads to:

$$\underline{\underline{R}}_r \cdot \left(\hat{\underline{j}}_m - \underline{\sigma}\right) = \underline{\underline{R}}_r \cdot \hat{\underline{j}}_m - \underline{\underline{R}}_r \cdot \underline{\sigma} = \underline{0} \tag{10-7}$$

And after further conversion,

$$\underline{\varepsilon} \equiv \underline{\underline{R}}_r \cdot \hat{\underline{j}}_m = \underline{\underline{R}}_r \cdot \underline{\sigma} \tag{10-8}$$

whereas $\underline{\varepsilon}$ is the vector of variances. If there are no systematic or random errors ($\underline{\sigma} = \underline{0}$) the equations are satisfied exactly and the residual value for ε is zero. However, in all data sets there is some noise present in the measurements that makes the residual vector different from zero. The best estimates are those that minimize the magnitude of the residual, and they are determined as follows.

Under the assumption that the error is normally distributed with a mean of zero and a variance-covariance matrix F (Equation 10-10) where E (Equation 10-11) is the expectation value operator, it can be shown that the residuals will be also normally distributed with a mean of zero (Equation 10-11).

$$E(\underline{\sigma}) = \underline{0} \tag{10-9}$$

$$F \equiv E\left[\left(\hat{\underline{j}}_m - \underline{j}_m\right) \cdot \left(\hat{\underline{j}}_m - \underline{j}_m\right)^T\right] = E(\underline{\sigma}\underline{\sigma}^T) \tag{10-10}$$

Than it can be demonstrated that the residual values are also normally distributed:

$$E(\underline{\varepsilon}) = \underline{\underline{R}}_r E(\underline{\sigma}) = \underline{0} \tag{10-11}$$

The variance-covariance matrix is given by

$$\underline{\underline{P}} \equiv E(\underline{\varepsilon}\underline{\varepsilon}^T) = \underline{\underline{R}}_r \cdot E(\underline{\sigma}\underline{\sigma}^T) \cdot \underline{\underline{R}}_r^T = \underline{\underline{R}}_r \cdot F \cdot \underline{\underline{R}}_r^T \tag{10-12}$$

The minimum variance estimate of the error vector $\underline{\sigma}$ is obtained by minimizing the sum of the squared errors, whereby the solution of the optimized rates $\underline{j}_m^{opt}$, using the identity matrix $\underline{\underline{I}}$ is given by:

$$\underline{j}_m^{opt} = \underline{\hat{j}}_m - \underline{\sigma} = \left(\underline{\underline{I}} - F \cdot \underline{\underline{R}}_r^T \cdot \underline{\underline{P}}^{-1} \cdot \underline{\underline{R}}_r\right) \cdot \underline{\hat{j}}_m \tag{10-13}$$

10.4 Optimal Flux Distribution for Fructofuranosidase Production

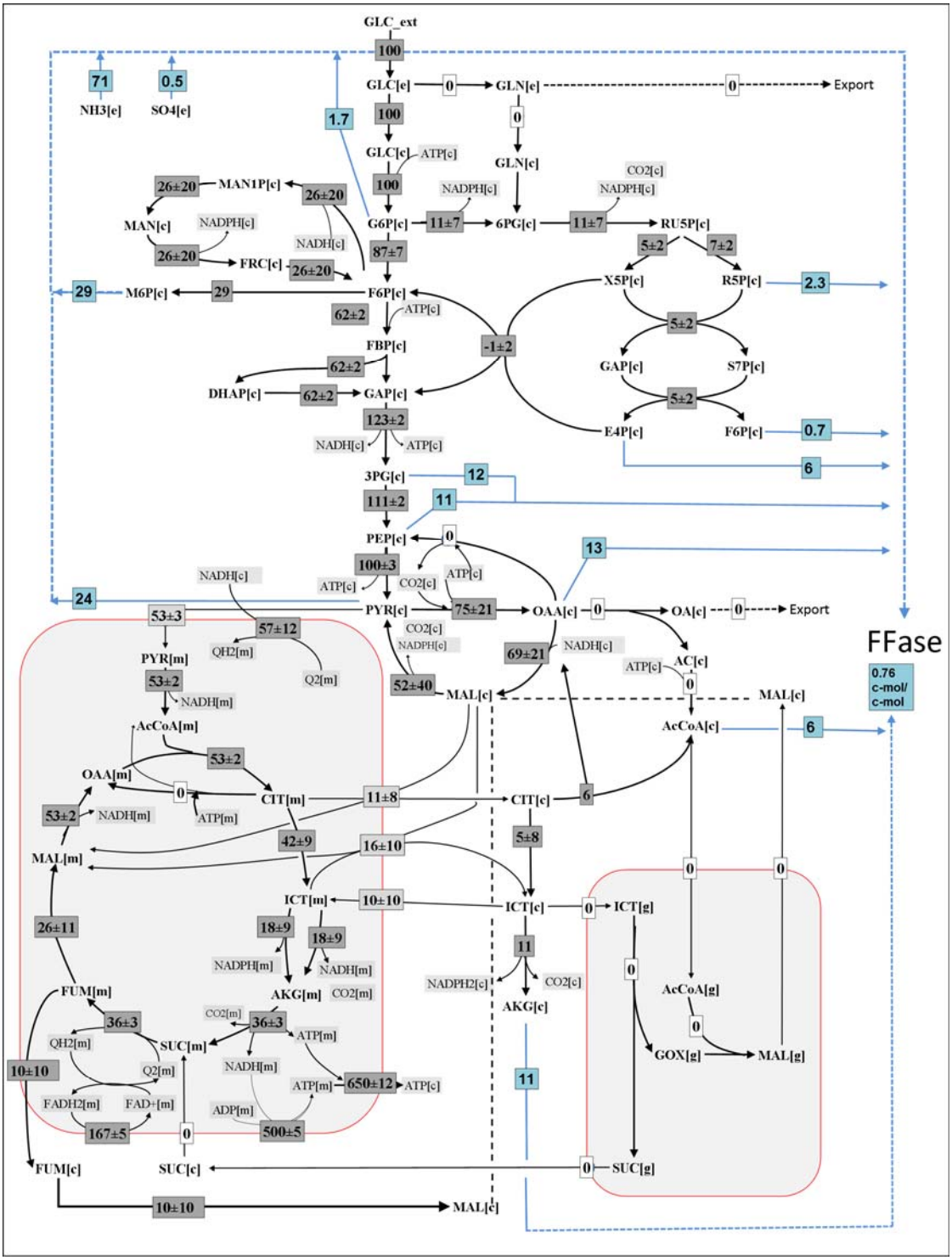

Figure 38: Optimal flux distribution for fructofuranosidase production by *A. niger* using glucose and ammonium. The relative flux coefficients are averaged from 160 elementary flux modes for maximal production obtained for each target product. All fluxes are given as relative molar fluxes normalized to 1 mol of glucose unit [mol.(mol glucose)-1.100].

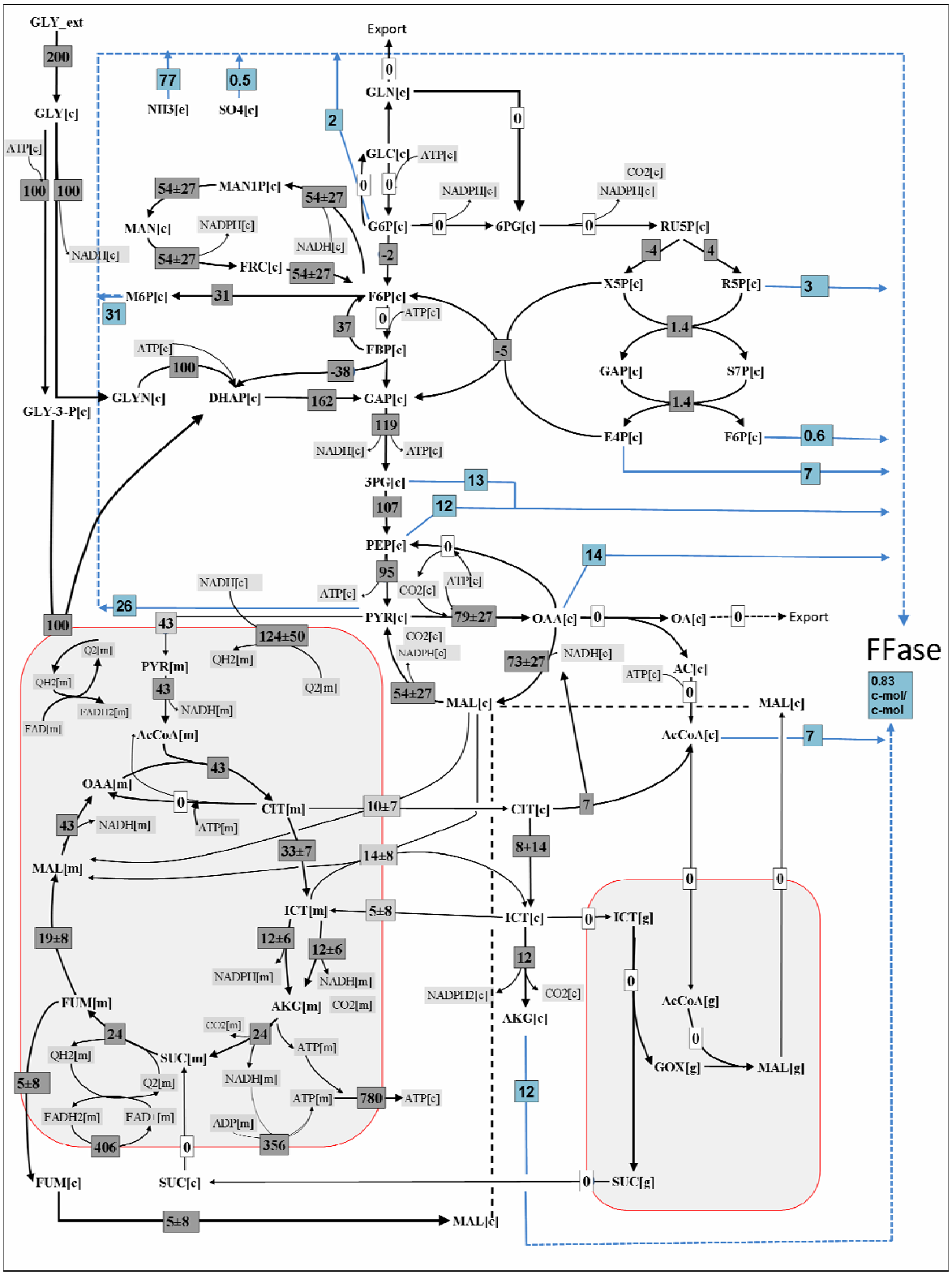

Figure 39: Optimal flux distribution for fructofuranosidase production by *A. niger* using glycerol. All fluxes are given as relative percental molar flux normalized to 1 mol of hexose unit [mol. (mol hexose)-1.100].

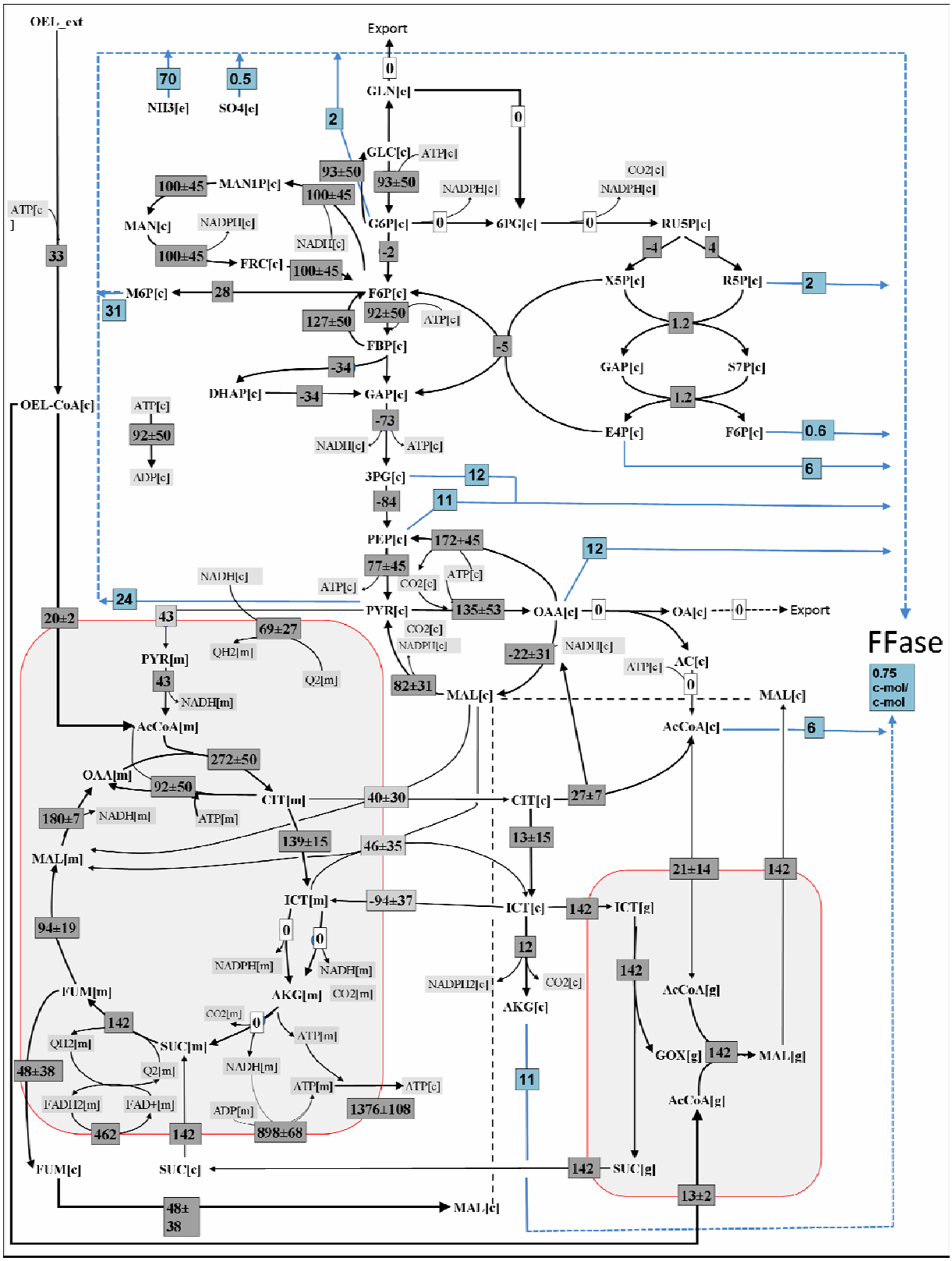

Figure 40: Optimal flux distribution for fructofuranosidase production by *A. niger* using oleic acid. All fluxes are given as relative percental molar flux normalized to 1 mol of hexose unit [mol. (mol hexose)-1.100].

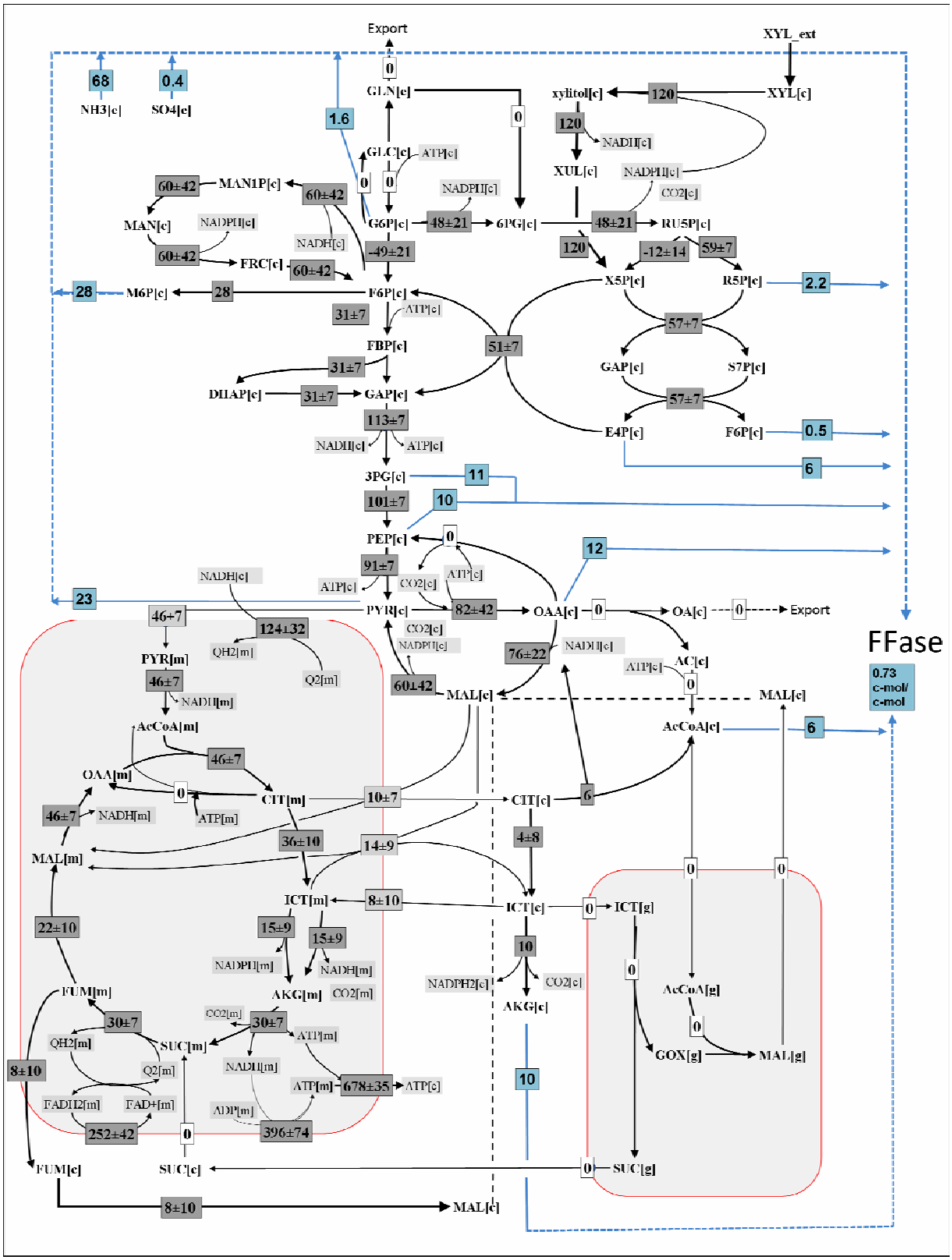

Figure 41: Optimal flux distribution for fructofuranosidase production by *A. niger* using xylose. All fluxes are given as relative percental molar flux normalized to 1 mol of hexose unit [mol. (mol hexose)-1.100].

10.5 Optimal Pathway Fluxes for Alternative Target Products

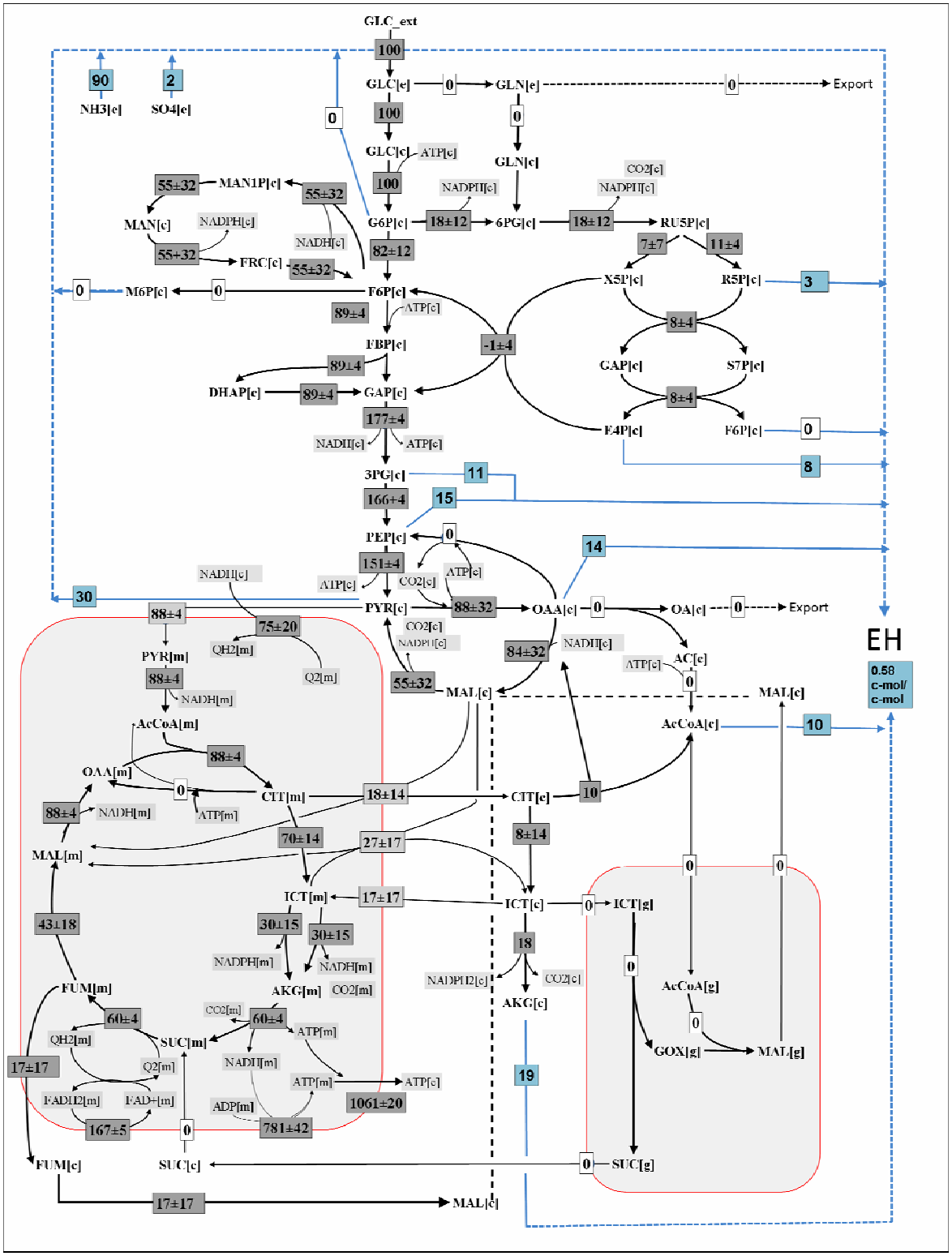

Figure 42: Optimal flux distribution for epoxide hydrolase production by *A. niger* using glucose and ammonium. The relative flux coefficients are averaged from 112 elementary flux modes for maximal production obtained for each target product. All fluxes are given as relative molar fluxes normalized to 1 mol of glucose unit [mol·(mol glucose)$^{-1}$·100].

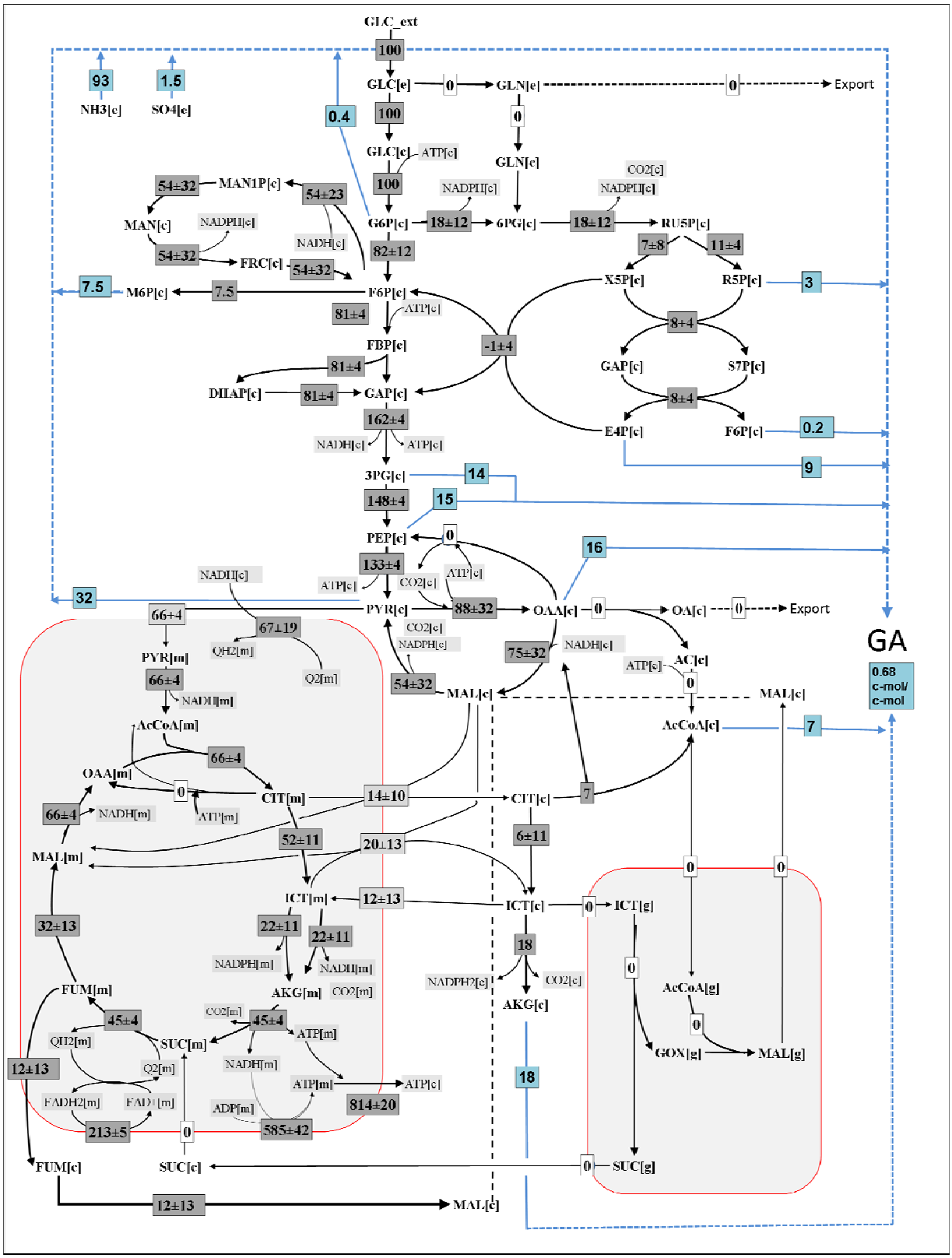

Figure 43: Optimal flux distribution for glucoamylase production by *A. niger* using glucose and ammonium. The relative flux coefficients are averaged from 112 elementary flux modes for maximal production obtained for each target product. All fluxes are given as relative molar fluxes normalized to 1 mol of glucose unit [mol·(mol glucose)$^{-1}$·100].

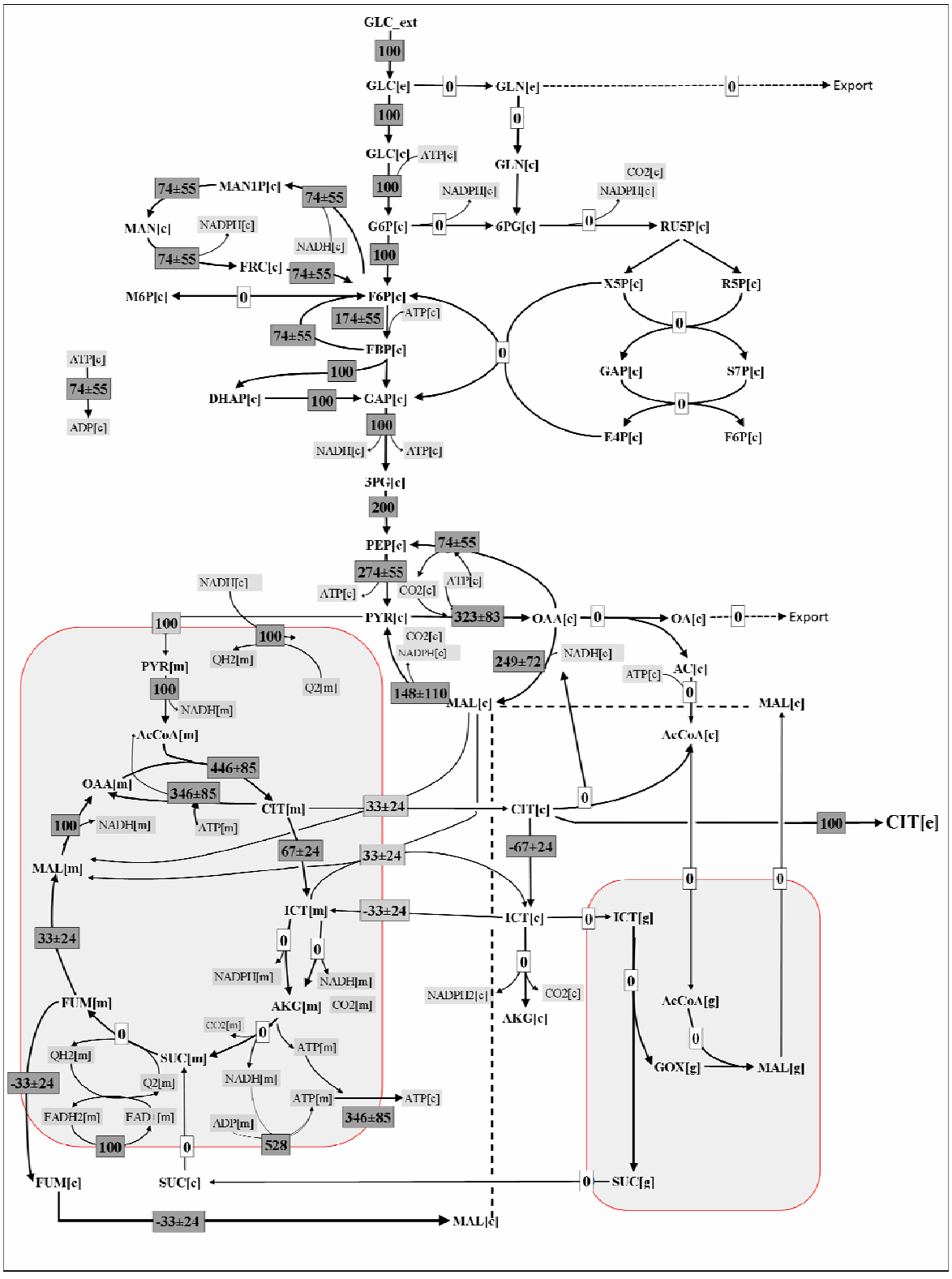

Figure 44: Optimal flux distribution for citrate production by *A. niger* using glucose and ammonium. The relative flux coefficients are averaged from 36 elementary flux modes for maximal production obtained for each target product. All fluxes are given as relative molar fluxes normalized to 1 mol of glucose unit [mol·(mol glucose)$^{-1}$·100].

10.6 Optimal Pathways for Epoxide Hydrolase Production

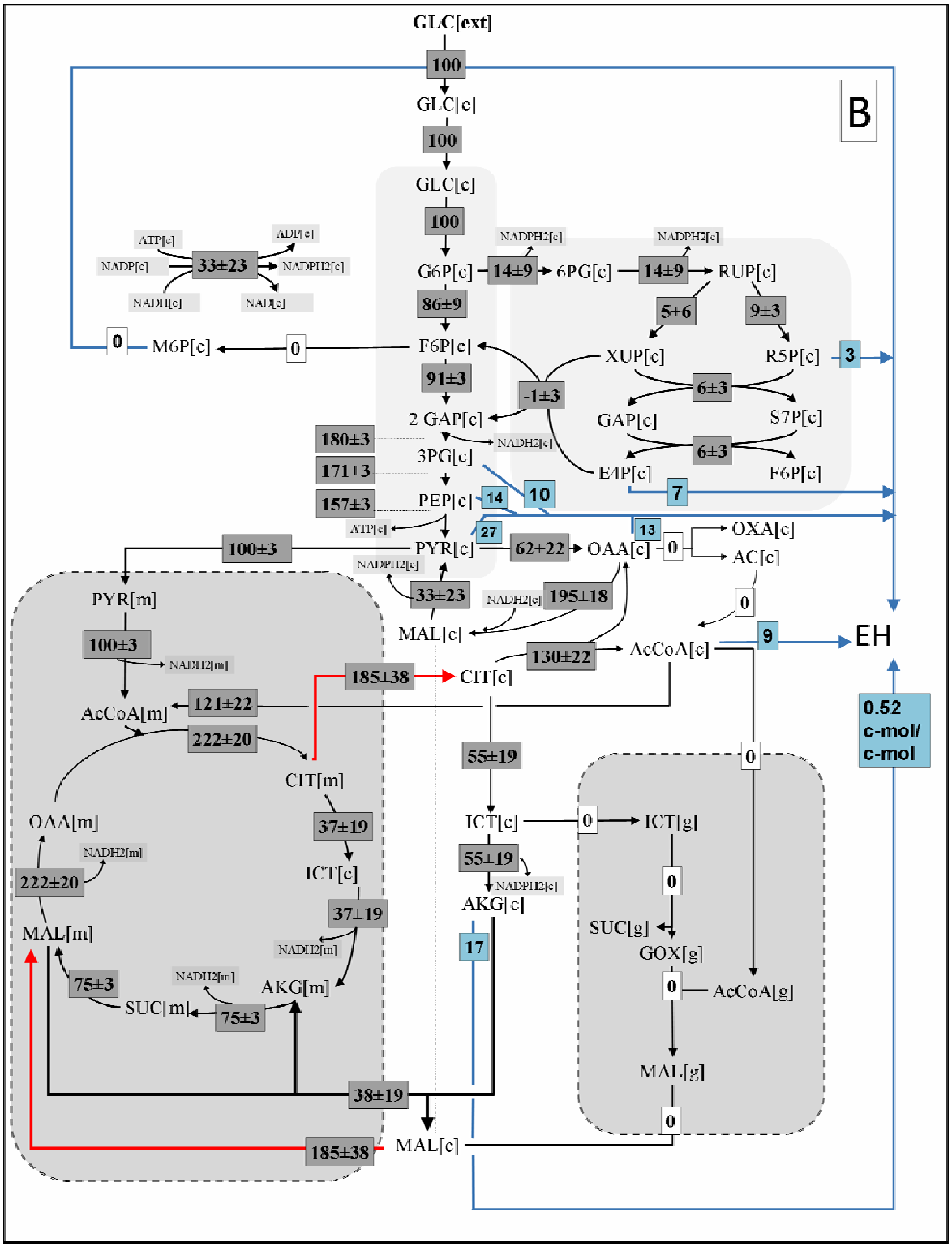

Figure 45: Optimal flux distribution for epoxide hydrolase production using glucose in *S. cerevisiae*. The relative flux coefficients are averaged from 28 elementary flux modes for maximal epoxide hydrolase production. All fluxes are given as relative molar flux normalized to 1 mol of glucose unit [mol. (mol glucose)-1.100].

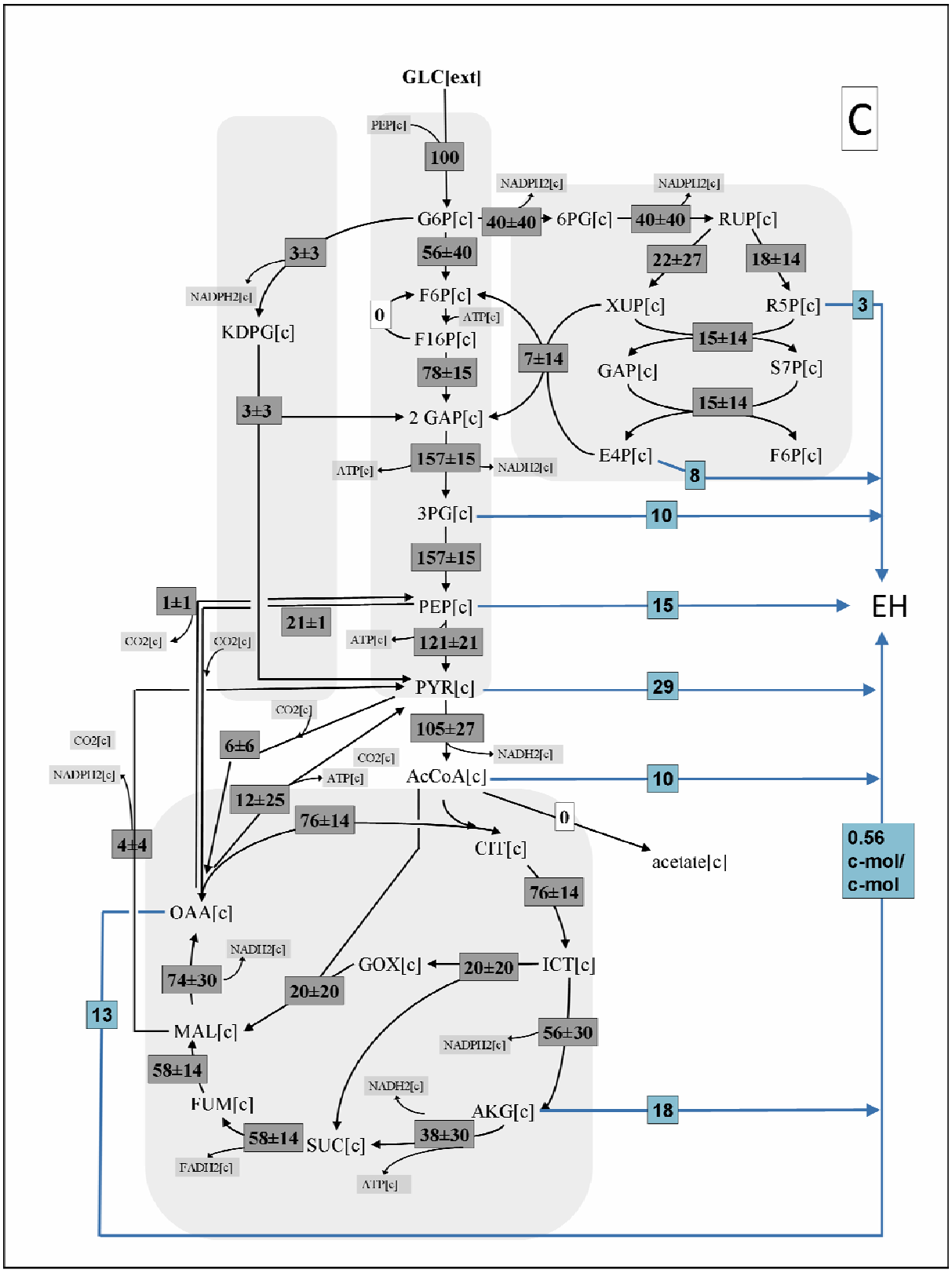

Figure 46: Optimal flux distribution for epoxide hydrolase production using glucose in *E. coli*. The relative flux coefficients are averaged from 49 elementary flux modes for maximal epoxide hydrolase production. All fluxes are given as relative molar flux normalized to 1 mol of glucose unit [mol. (mol glucose)-1.100].

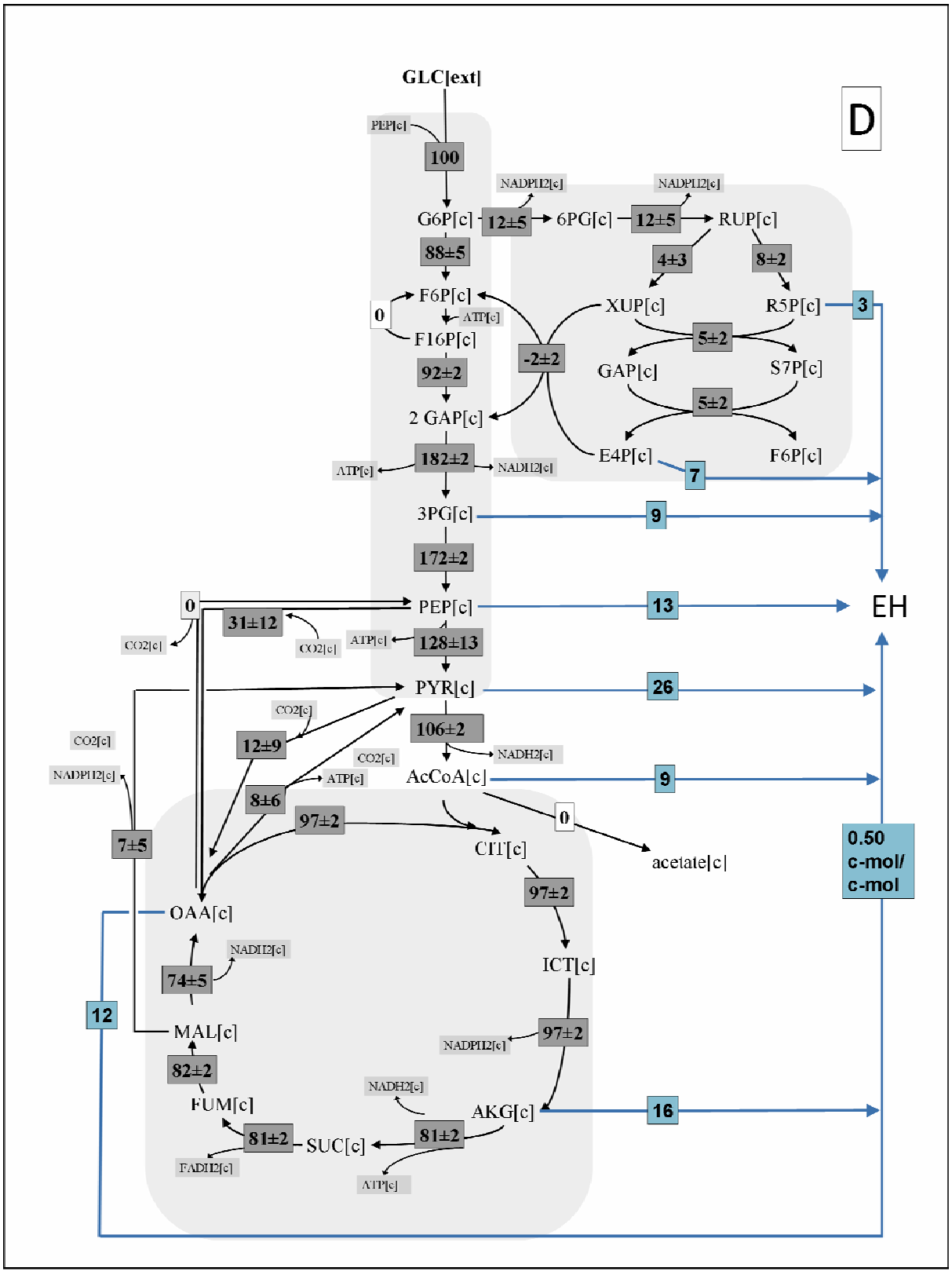

Figure 47: Optimal flux distribution for epoxide hydrolase production using glucose in *B. subtilis*. The relative flux coefficients are averaged from 18 elementary flux modes for maximal epoxide hydrolase production. All fluxes are given as relative molar flux normalized to 1 mol of glucose unit [mol. (mol glucose)-1.100].

10.7 Metabolic Flux Analysis – Example

10.7.1 Description of the metabolic network

In the simple reaction network, the substrate S is changed into A (this may consider as the intake of substrate from outside of the cell), through reaction r_S. A is also converted to B by reaction r_1, C by reaction r_2 and B is converted to C through r_3. Finally, P_1 is being formed from C through reaction r_4 and P_2 from B through reaction r_5.

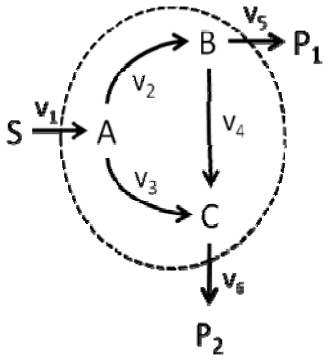

10.7.2 Metabolite balances and matrix notation

Additional, material balances on the seven species S, A, B, C, P_1 and P_2 can be notated to:

$$\text{Substrate}: \quad \frac{dS}{dt} = -v_1$$

$$\text{Metabolites}: \quad \frac{dA}{dt} = v_1 - v_2 - v_3 \;;\; \frac{dB}{dt} = v_2 - v_4 - v_5 \;;\; \frac{dC}{dt} = v_3 + v_4 - v_6$$

$$\text{Products}: \quad \frac{dP_1}{dt} = v_5 \;;\; \frac{dP_2}{dt} = v_6$$

The term used is the compact form as a matrix notation:

$$\frac{d}{dt}\begin{pmatrix} S \\ A \\ B \\ C \\ P_1 \\ P_2 \end{pmatrix} = \begin{pmatrix} -1 & 0 & 0 & 0 & 0 & 0 \\ 1 & -1 & -1 & 0 & 0 & 0 \\ 0 & 1 & 0 & -1 & 0 & -1 \\ 0 & 0 & 1 & 1 & -1 & 0 \\ 0 & 0 & 0 & 0 & 1 & 0 \\ 0 & 0 & 0 & 0 & 0 & 1 \end{pmatrix}\begin{pmatrix} v_1 \\ v_2 \\ v_3 \\ v_4 \\ v_5 \\ v_6 \end{pmatrix}$$

which can simply written as:

$$\frac{d}{dt}\underline{x} = \underline{\underline{G}}^T \underline{v}$$

where

$$\underline{x} = \begin{pmatrix} S \\ A \\ B \\ C \\ P_1 \\ P_2 \end{pmatrix}; \underline{\underline{S}}^T = \begin{pmatrix} -1 & 0 & 0 & 0 & 0 & 0 \\ 1 & -1 & -1 & 0 & 0 & 0 \\ 0 & 1 & 0 & -1 & 0 & -1 \\ 0 & 0 & 1 & 1 & -1 & 0 \\ 0 & 0 & 0 & 0 & 1 & 0 \\ 0 & 0 & 0 & 0 & 0 & 1 \end{pmatrix} \text{ and } \underline{r} = \begin{pmatrix} v_1 \\ v_2 \\ v_3 \\ v_4 \\ v_5 \\ v_6 \end{pmatrix}$$

In general, a vector and a matrix are indicated by a single and a double underline, respectively. In this case, x is commonly known as the state vector containing the state variables (in this case the concentration of each of the species), G^T is the stoichiometric matrix, and v is the reaction rector.

10.7.3 Matrix conversion

For further calculation, it is useful to distinguish between external metabolites and the intracellular metabolites. For this, the matrix can be separated into the part of external substrates and a part considering the intra-cellular metabolites.

$$\frac{d}{dt}\begin{pmatrix} S \\ P_1 \\ P_2 \end{pmatrix} = \begin{pmatrix} -1 & 0 & 0 & 0 & 0 & 0 \\ 0 & 0 & 0 & 0 & 1 & 0 \\ 0 & 0 & 0 & 0 & 0 & 1 \end{pmatrix} \begin{pmatrix} v_1 \\ v_2 \\ v_3 \\ v_4 \\ v_5 \\ v_6 \end{pmatrix} = \begin{pmatrix} -1 & 0 & 0 \\ 0 & 1 & 0 \\ 0 & 0 & 1 \end{pmatrix} \begin{pmatrix} v_1 \\ v_5 \\ v_6 \end{pmatrix}$$

$$\frac{d}{dt}\begin{pmatrix} A \\ B \\ C \end{pmatrix} = \begin{pmatrix} 1 & -1 & -1 & 0 & 0 & 0 \\ 0 & 1 & 0 & -1 & 0 & -1 \\ 0 & 0 & 1 & 1 & -1 & 0 \end{pmatrix} \begin{pmatrix} v_1 \\ v_2 \\ v_3 \\ v_4 \\ v_5 \\ v_6 \end{pmatrix}$$

10.8 Computational Algorithm

10.8.1 Elementary flux modes

A program for computation of elementary flux modes was written for MatLab during a student research project [213], which was used for preparatory examinations in this study. The code for nullspace approach was based on the principles of the nullspace algorithm introduced by Wagner [181].

Finally, all data presented in this work were obtained by the bit pattern tree algorithm, an indexing technique for optimized searching of subsets during elementarity testing and candidate narrowing. This is a new recursive enumeration method which was introduced in [182]. A MATLAB/Java tool to compute elementary flux modes with the extended bit pattern tree algorithm of metabolic networks is available from http://www.csb.ethz.ch/tools/index.

10.9 Algorithm of Post-processing

Matrix of elementary flux modes $\underline{\underline{mnet.efms}}$ with dimension dim($\underline{\underline{mnet.efms}}$) = q **x** n, with q = number of reactions and n = number of elementary modes. For further calculation, transpose $\underline{\underline{mnet.efms}}$ into matrix $\underline{\underline{M}}$ with dim($\underline{\underline{M}}$) = n **x** q.

10.9.1 Calculation of theoretical flux yields

Flux coefficients in each column q are normalized to substrate uptake (coefficients in first column, B=1).

```
function x=postpro1(M,B)
% M=M(:,[3 1 2 4])
M;
N=M;
M(:,1)=N(:,B);
M(:,B)=N(:,1);
M;
[nr nc]=size(M)
A=[];
for i=2:1:nc
    for j=1:1:nr
        A(j,i-1)=M(j,i)/M(j,1);
    end
end
A;
csvwrite('POSTPRO1.txt',A)
```

Entries of the matrix were accounted to search for non-zero entries.

```
function reactioncount(A)
[norow nocol]=size(A)
numreaction=[];
for i=1:1:norow

    zaehler=0;
    for j=1:1:nocol
        if A(i,j)~=0
            zaehler=zaehler+1;
        end
    end
    %zaehler
    numreaction=[numreaction; zaehler];

end
 numreaction;
 csvwrite('numreaction_gesamt_reaction.text',numreaction)
end
```

10.10 Statistical Evaluation

Table 29: Statistical analysis of simulation data. Growth associated fructofuranosidase production using glucose. R^2: regression coefficient, alpha: slope-correlation coefficient, NOSTAT: no statistical evaluation. The values correspond to Figure 7 Glu(+). The entries of '#DIV/0' regarded to constant values (or complete zeros) of stoichiometric coefficients for the corresponding enzyme.

Enzyme name / Gene name	ANgxx number	R^2	alpha	evaluation correlation
biomass export		0.352311652	-0.109221022	NOSTAT
FFase export		1	1.230773813	1.230773813
oxalate export	non carrier mediated	#DIV/0!	0	#DIV/0!
gluconate export	non carrier mediated	#DIV/0!	0	#DIV/0!
ammonium uptake	non carrier mediated	0.022946574	0.161134208	NOSTAT
sulphate uptake	non carrier mediated	0.174959655	-0.010229275	NOSTAT
oxygen uptake	non carrier mediated	0.022530627	-1.04906417	NOSTAT
carbon dioxide export	non carrier mediated	0.034122498	-1.270776356	NOSTAT
oxygen uptake	non carrier mediated	0.070491976	-1.889291636	NOSTAT
oxygen diffusion	non carrier mediated	0.067125596	-1.853359474	NOSTAT
carbon dioxide diffusion	non carrier mediated	0.155527522	2.818842808	NOSTAT
ADP/ATP translocator	An18g04220	0.018245566	-2.461399495	NOSTAT
pyruvate shuttle		0.247738662	-1.426147784	NOSTAT
citrate/malate shuttle	An11g11230	0.021545061	-0.445832433	NOSTAT
isocitrate/malate shuttle		0.01241524	-0.348055432	NOSTAT
isocitrate shuttle		0.000347135	-0.064069871	NOSTAT
succinate shuttle		0.015223633	-0.204469595	NOSTAT
fumarate shuttle		0.008097846	-0.268533506	NOSTAT
nad5 nuo51 nd4L / NADH-ubiquinone oxidoreductase	An02g05470	0.163672612	1.439296996	NOSTAT
glucose uptake		0.752575699	-1.680611209	-1.680611209
hxk / hexokinase	An02g14380	0.07732267	-2.402548047	NOSTAT
glucose-6-phosphate isomerase	An16g05420	0.789917944	-1.603528871	-1.603528871
pfkA / phosphofructokinase	An18g01670	0.030156325	-1.463891431	NOSTAT
fructose 1,6-bis-phosphate aldolase	An02g07470	0.724938027	-0.741932599	-0.741932599
triose-phosphate isomerase	An14g04920	0.711773734	-0.733206822	-0.733206822
gpdA / phosphoglycerate kinase	An16g01830 / An08g02260	0.517971387	-0.913616331	NOSTAT
phosphoglycerate mutase / enolase	An16g02990 / An18g06250	0.481803021	-0.971561428	NOSTAT
pkiA / pyruvate kinase	An07g08990	0.21701276	-1.301432214	NOSTAT
mannitol 1-phosphate DH (NADH2)	An02g05830	0.054614243	-1.128503552	NOSTAT
mannitol 1-phosphatase		0.054614243	-1.128503552	NOSTAT
mannitol 1-phosphate DH (NADPH2)	An02g05830	0.052710404	-1.10525737	NOSTAT
hxk / hexokinase	An02g14380	0.052710404	-1.10525737	NOSTAT
glucose 6- phosphatase		0.007575139	-0.721938267	NOSTAT
fructose 1,6-bis-phosphate phosphatase	An04g05300	0.007575139	-0.721938267	NOSTAT
mannose 6-phosphate isomerase	An08g06350	0.997647678	0.365968546	0.365968546
phosphoenolpyruvate carboxykinase	An11g02550	0.01227409	-0.25937989	NOSTAT
pyc / pyruvate carboxylase (mitochondrial)	An04g02090	0.038901428	-1.134935221	NOSTAT
goxC / glucose oxidase	An12g0430	0.752575888	1.680613139	1.680613139
gluconate transport		0.752575888	1.680613139	1.680613139
catR / catalsae R	An01g01820	0.75257413	0.840301661	0.840301661
gluconokinase	An01g07300	0.752575888	1.680613139	1.680613139
gsdA / glucose-6-phosphate DH	An02g12140	0.067940975	0.075515743	NOSTAT
phosphogluconate DH	An11g02040	0.818656444	1.756128882	1.756128882
ribulose-5-phosphate epimerase	An09g03450	0.811244808	1.163618148	1.163618148
ribulose-5-phosphate isomerase	An02g02930	0.824709545	0.592507555	0.592507555
transketolase I	An08g06430	0.826820992	0.602152396	0.602152396
transaldolase	An07g03850	0.826820992	0.602152396	0.602152396
transketolase II	An08g06430	0.791592651	0.561466484	0.561466484
malate DH (decarboxylating)	An05g00930	0.022929292	-0.575354951	NOSTAT
malate DH (cytosolic)	An07g02160	0.089439284	-1.471585238	NOSTAT
ATP citrate lyase	An11g00510	0.094941337	-0.543610688	NOSTAT
oahA / oxalacetase	An10g00820	#DIV/0!	0	#DIV/0!
acetyl-CoA synthetase	An04g05620	#DIV/0!	0	#DIV/0!
aconitase	An02g11040	0.001126931	0.097777001	NOSTAT
icdA / isocitrate DH (NADPH2, cytosolic)	An08g05580	0.011556961	0.018254744	NOSTAT
succinate dehydrogenase	An16g07150	0.008097846	-0.268533506	NOSTAT
ATP excess /maintenance		0.007575139	-0.721938267	NOSTAT
ATP excess /maintenance		0.007575139	-0.721938267	NOSTAT
isocitrate shuttle (glyoxysomal)		0.015223633	-0.204469595	NOSTAT
isocitrate lyase	An01g09270	0.015223633	-0.204469595	NOSTAT
succinate shuttle (glyoxysomal)		0.015223633	-0.204469595	NOSTAT
malate synthase (glyoxysomal)	An15g01860	0.015223633	-0.204469595	NOSTAT
malate shuttle (glyoxysomal)		0.015223633	-0.204469595	NOSTAT
L-carnitine shuttle	An08g04990	0.015223633	-0.204469595	NOSTAT
pyruvate DH	An01g00100	0.247738662	-1.426147784	NOSTAT
citA / citrate synthase	An09g06680	0.039916329	-9.984822946	NOSTAT
aconitase	An02g11040	0.074638363	-0.980318545	NOSTAT
icdA / isocitrate DH (mitochondrial)	An02g12430	0.023264029	-0.348169299	NOSTAT
icdA / isocitrate DH (mitochondrial)	An02g12430	0.023264029	-0.348169299	NOSTAT
ATP citrate lyase	An11g00510	0.031521839	-8.558682089	NOSTAT
	An04g04750 + An11g11280 + An07g06840	0.059197613	-0.696338597	NOSTAT
succinate dehydrogenase	An16g07150	0.121155468	-0.900792017	NOSTAT
fumarate hydratase	An12g07850	0.036920871	-0.632264205	NOSTAT
malate DH (mitochondrial)	An07g02160	0.247738662	-1.426147784	NOSTAT
NADH2 transhydrogenase (mitochondrial)	An02g09810	0.016455367	-0.348362239	NOSTAT
NADH2 transhydrogenase	An02g09810	0.023264029	-0.348169299	NOSTAT
sulpate reduction	An08g08910	0.174959655	-0.010229275	NOSTAT
ATP synthase	An01g05670	0.209935265	-2.12245947	NOSTAT
succinate dehydrogenase	An01g13930	0.009058189	0.269228043	NOSTAT
sucrase synthesis		1	1.230773813	1.230773813
sucrase secretion		1	1.230773813	1.230773813
biomass synthesis		0.352311652	-0.109221022	NOSTAT

Table 30: Statistical analysis of simulation data. Non-growth associated fructofuranosidase production using glucose. R^2: regression coefficient, alpha: slope-correlation coefficient, NOSTAT: no statistical evaluation. The values correspond to Figure 7 Glu(-). The entries of '#DIV/0' regarded to constant values (or complete zeros) of stoichiometric coefficients for the corresponding enzyme.

Enzyme name / Gene name	ANgxx number	R^2	alpha	evaluation correlation
biomass export		#DIV/0!	0	#DIV/0!
FFase export		1	1.230771013	1.230771013
oxalate export	non carrier mediated	#DIV/0!	0	#DIV/0!
gluconate export	non carrier mediated	#DIV/0!	0	#DIV/0!
ammonium uptake	non carrier mediated	1	0.936612389	0.936612389
sulphate uptake	non carrier mediated	1	0.006153856	0
oxygen uptake	non carrier mediated	1	-6.145237924	-6.145237924
carbon dioxide export	non carrier mediated	1	-6.257238673	-6.257238673
oxygen uptake	non carrier mediated	0.9862851	-6.181857287	-6.181857287
oxygen diffusion	non carrier mediated	0.9862851	-6.181857287	-6.181857287
carbon dioxide diffusion	non carrier mediated	0.823534949	6.265824919	6.265824919
ADP/ATP translocator	An18g04220	0.592113701	12.10559225	NOSTAT
pyruvate shuttle		0.482440177	-1.587963285	NOSTAT
citrate/malate shuttle	An11g11230	0.000375196	0.033347425	NOSTAT
isocitrate/malate shuttle		0.020083248	-0.278640915	NOSTAT
isocitrate shuttle		0.160800731	-0.996273193	NOSTAT
succinate shuttle		0.060973199	0.26287613	NOSTAT
fumarate shuttle		0.116106671	-0.733394613	NOSTAT
nad5 nuo51 nd4L / NADH-ubiquinone oxidoreductase	An02g05470	0.233428993	-2.433889024	NOSTAT
glucose uptake		0.002516492	-0.073233123	NOSTAT
hxk / hexokinase	An02g14380	0.002177844	0.290170153	NOSTAT
glucose-6-phosphate isomerase	An16g05420	0.001470745	0.116431523	NOSTAT
pfkA / phosphofructokinase	An18g01670	5.84395E-05	-0.046195152	NOSTAT
fructose 1,6-bis-phosphate aldolase	An02g07470	0.140937294	-0.409599348	NOSTAT
triose-phosphate isomerase	An14g04920	0.140937294	-0.409599348	NOSTAT
gpdA / phosphoglycerate kinase	An16g01830 / An08g02260	0.457679376	-0.928975269	NOSTAT
phosphoglycerate mutase / enolase	An16g02990 / An18g06250	0.534704782	-1.084028785	NOSTAT
pkiA / pyruvate kinase	An07g08990	0.532871351	-1.194307351	NOSTAT
mannitol 1-phosphate DH (NADH2)	An02g05830	0.039958064	0.451235927	NOSTAT
mannitol 1-phosphatase		0.039958064	0.451235927	NOSTAT
mannitol 1-phosphate DH (NADPH2)	An02g05830	0.039958064	0.451235927	NOSTAT
hxk / hexokinase	An02g14380	0.039958064	0.451235927	NOSTAT
glucose 6- phosphatase		0.003732756	0.363403663	NOSTAT
fructose 1,6-bis-phosphate phosphatase	An04g05300	0.003732756	0.363403663	NOSTAT
mannose 6-phosphate isomerase	An08g06350	1	0.379075423	0.379075423
phosphoenolpyruvate carboxykinase	An11g02550	0.002496876	0.0312956	NOSTAT
pyc / pyruvate carboxylase (mitochondrial)	An04g02090	0.084824241	0.471317846	NOSTAT
goxC / glucose oxidase	An12g0430	0.002516478	0.073232885	NOSTAT
gluconate transport		0.002516478	0.073232885	NOSTAT
catR / catalsae R	An01g01820	0.002516429	0.036616151	NOSTAT
gluconokinase	An01g07300	0.002516478	0.073232885	NOSTAT
gsdA / glucose-6-phosphate DH	An02g12140	0.006975683	-0.211815869	NOSTAT
phosphogluconate DH	An11g02040	0.002082345	-0.138583162	NOSTAT
ribulose-5-phosphate epimerase	An09g03450	0.004739357	-0.139564889	NOSTAT
ribulose-5-phosphate isomerase	An02g02930	9.40168E-07	0.000980533	NOSTAT
transketolase I	An08g06430	0.000866887	-0.02978707	NOSTAT
transaldolase	An07g03850	0.000866887	-0.02978707	NOSTAT
transketolase II	An08g06430	0.011649556	-0.109788915	NOSTAT
malate DH (decarboxylating)	An05g00930	0.029925859	0.19760327	NOSTAT
malate DH (cytosolic)	An07g02160	0.162578939	0.620440811	NOSTAT
ATP citrate lyase	An11g00510	0.100766805	0.345337223	NOSTAT
oahA / oxalacetase	An10g00820	#DIV/0!	0	#DIV/0!
acetyl-CoA synthetase	An04g05620	#DIV/0!	0	#DIV/0!
aconitase	An02g11040	0.0358854	-0.311988341	NOSTAT
icdA / isocitrate DH (NADPH2, cytosolic)	An08g05580	0.999999999	0.142769083	0.142769083
succinate dehydrogenase	An16g07150	0.116106671	-0.733394613	NOSTAT
ATP excess /maintenance		0.003732756	0.363403663	NOSTAT
ATP excess /maintenance		0.003732756	0.363403663	NOSTAT
isocitrate shuttle (glyoxysomal)		0.060973199	0.26287613	NOSTAT
isocitrate lyase	An01g09270	0.060973199	0.26287613	NOSTAT
succinate shuttle (glyoxysomal)		0.060973199	0.26287613	NOSTAT
malate synthase (glyoxysomal)	An15g01860	0.060973199	0.26287613	NOSTAT
malate shuttle (glyoxysomal)		0.060973199	0.26287613	NOSTAT
L-carnitine shuttle	An08g04990	0.060973199	0.26287613	NOSTAT
pyruvate DH	An01g00100	0.482440177	-1.587963285	NOSTAT
citA / citrate synthase	An09g06680	0.923518976	-4.416295628	-4.416295628
aconitase	An02g11040	0.420529956	-1.621303324	NOSTAT
icdA / isocitrate DH (mitochondrial)	An02g12430	0.283450054	-1.169467181	NOSTAT
icdA / isocitrate DH (mitochondrial)	An02g12430	0.283450054	-1.169467181	NOSTAT
ATP citrate lyase	An11g00510	0.920330688	-4.257481268	-4.257481268
	An04g04750 + An11g11280 + An07g06840	0.788376925	-2.338934362	-2.338934362
succinate dehydrogenase	An16g07150	0.80823363	-2.076048732	-2.076048732
fumarate hydratase	An12g07850	0.288211205	-1.342660051	NOSTAT
malate DH (mitochondrial)	An07g02160	0.482440177	-1.587963285	NOSTAT
NADH2 transhydrogenase (mitochondrial)	An02g09810	0.018525154	-0.80860062	NOSTAT
NADH2 transhydrogenase	An02g09810	0.283450054	-1.169467181	NOSTAT
sulpate reduction	An08g08910	1	0.006153856	0
ATP synthase	An01g05670	0.790347315	-3.926896155	-3.926896155
succinate dehydrogenase	An01g13930	0.630926833	-2.254974042	NOSTAT
sucrase synthesis		1	1.230771013	1.230771013
sucrase secretion		1	1.230771013	1.230771013
biomass synthesis		#DIV/0!	0	#DIV/0!

Table 31: Statistical analysis of simulation data. Growth associated fructofuranosidase production using xylose. R^2: regression coefficient, alpha: slope-correlation coefficient, NOSTAT: no statistical evaluation. The values correspond to Figure 7 Xyl(+). The entries of '#DIV/0' regarded to constant values (or complete zeros) of stoichiometric coefficients for the corresponding enzyme.

Enzyme name / Gene name	ANgxx number	R^2	alpha	evaluation correlation
biomass export		0.966601947	-0.123610388	-0.123610388
FFase export		1	1.025640816	1.025640816
oxalate export	non carrier mediated	#DIV/0!	0	#DIV/0!
gluconate export	non carrier mediated	#DIV/0!	0	#DIV/0!
ammonium uptake	non carrier mediated	0.261726931	-0.09713083	NOSTAT
sulphate uptake	non carrier mediated	0.93806359	-0.013413199	0
oxygen uptake	non carrier mediated	0.266700935	0.646583095	NOSTAT
carbon dioxide export	non carrier mediated	0.1433055	0.429057339	NOSTAT
oxygen uptake	non carrier mediated	0.266700935	0.646583095	NOSTAT
oxygen diffusion	non carrier mediated	0.689417794	0.163796909	NOSTAT
carbon dioxide diffusion	non carrier mediated	0.733482946	1.855994286	1.855994286
ADP/ATP translocator	An18g04220	0.793295511	-2.857100986	-2.857100986
pyruvate shuttle		0.78555794	-1.221343113	-1.221343113
citrate/malate shuttle	An11g11230	0.102931247	-0.492490578	NOSTAT
isocitrate/malate shuttle		0.050276616	-0.339736439	NOSTAT
isocitrate shuttle		0.002436161	0.07178902	NOSTAT
succinate shuttle		0.124701124	-0.236826036	NOSTAT
fumarate shuttle		0.016480082	-0.165039115	NOSTAT
nad5 nuo51 nd4L / NADH-ubiquinone oxidoreductase	An02g05470	0.877266874	3.959111085	3.959111085
substrate uptake (glc, xyl, gly, oelic)		#DIV/0!	0	#DIV/0!
hxk / hexokinase	An02g14380	#DIV/0!	0	#DIV/0!
glucose-6-phosphate isomerase	An16g05420	0.749613183	-2.312060364	-2.312060364
pfkA / phosphofructokinase	An18g01670	0.850115678	-0.82132042	-0.82132042
fructose 1,6-bis-phosphate aldolase	An02g07470	0.820583005	-0.871626666	-0.871626666
triose-phosphate isomerase	An14g04920	0.81815873	-0.861738156	-0.861738156
gpdA / phosphoglycerate kinase	An16g01830 / An08g02260	0.865792594	-0.91097365	-0.91097365
phosphoglycerate mutase / enolase	An16g02990 / An18g06250	0.878153732	-0.930222065	-0.930222065
pkiA / pyruvate kinase	An07g08990	0.891241792	-0.967788144	-0.967788144
mannitol 1-phosphate DH (NADH2)	An02g05830	0.257572961	-2.450767484	NOSTAT
mannitol 1-phosphatase		0.257572961	-2.450767484	NOSTAT
mannitol 1-phosphate DH (NADPH2)	An02g05830	0.253518753	-2.424426349	NOSTAT
hxk / hexokinase	An02g14380	0.253518753	-2.424426349	NOSTAT
glucose 6- phosphatase		0.203099854	1.047077494	NOSTAT
fructose 1,6-bis-phosphate phosphatase	An04g05300	0.203099854	0.050306245	NOSTAT
mannose 6-phosphate isomerase	An08g06350	0.999916018	0.301067552	0.301067552
phosphoenolpyruvate carboxykinase	An11g02550	#DIV/0!	0	#DIV/0!
pyc / pyruvate carboxylase (mitochondrial)	An04g02090	0.045466375	-0.946390383	NOSTAT
goxC / glucose oxidase	An12g0430	0.203099854	1.047077494	NOSTAT
gluconate transport				
catR / catalsae R	An03g05660	0.203099854	0.523551529	NOSTAT
gluconokinase	An01g01820	0.203099854	1.047077494	NOSTAT
gsdA / glucose-6-phosphate DH	An01g07300	0.534199704	1.444258268	NOSTAT
phosphogluconate DH	An02g12140	0.769185702	2.491335762	2.491335762
ribulose-5-phosphate epimerase	An11g02040	0.767887466	1.66691124	1.66691124
ribulose-5-phosphate isomerase	An09g03450	0.771743311	0.824436733	0.824436733
transketolase I	An02g02930	0.775045041	0.844548315	0.844548315
transaldolase	An08g06430	0.775045041	0.844548315	0.844548315
transketolase II	An07g03850	0.760510957	0.822369162	0.822369162
malate DH (decarboxylating)	An08g06430	0.071312855	-1.171433116	NOSTAT
malate DH (cytosolic)	An05g00930	0.124997557	-1.601767172	NOSTAT
ATP citrate lyase	An07g02160	0.532043066	-0.645244244	NOSTAT
oahA / oxalacetase	An11g00510	#DIV/0!	0	#DIV/0!
acetyl-CoA synthetase	An10g00820	#DIV/0!	0	#DIV/0!
aconitase	An04g05620	0.011392034	0.152754139	NOSTAT
icdA / isocitrate DH (NADPH2, cytosolic)	An02g11040	0.412371582	-0.021942856	NOSTAT
succinate dehydrogenase	An08g05580	0.016480082	-0.165039115	NOSTAT
ATP excess /maintenance	An16g07150	#DIV/0!	0	#DIV/0!
ATP excess /maintenance		#DIV/0!	0	#DIV/0!
isocitrate shuttle (glyoxysomal)		0.124701124	-0.236826036	NOSTAT
isocitrate lyase	An01g09270	0.124701124	-0.236826036	NOSTAT
succinate shuttle (glyoxysomal)		0.124701124	-0.236826036	NOSTAT
malate synthase (glyoxysomal)	An15g01860	0.124701124	-0.236826036	NOSTAT
malate shuttle (glyoxysomal)		0.124701124	-0.236826036	NOSTAT
L-carnitine shuttle	An08g04990	0.124701124	-0.236826036	NOSTAT
pyruvate DH	An01g00100	0.78555794	-1.221343113	-1.221343113
citA / citrate synthase	An09g06680	0.78555794	-1.221343113	-1.221343113
aconitase	An02g11040	0.204432566	-0.728847914	NOSTAT
icdA / isocitrate DH (mitochondrial)	An02g12430	0.05410099	-0.158660022	NOSTAT
icdA / isocitrate DH (mitochondrial)	An02g12430	0.05410099	-0.158660022	NOSTAT
ATP citrate lyase	An11g00510	#DIV/0!	0	#DIV/0!
2-oxoglutarate dehydrogenase complex	An04g04750 + An11g11280 + An07g06840	0.166570219	-0.317320044	NOSTAT
succinate dehydrogenase	An16g07150	0.791511865	-0.55414608	-0.55414608
fumarate hydratase	An12g07850	0.084935813	-0.38910922	NOSTAT
malate DH (mitochondrial)	An07g02160	0.78555794	-1.221343113	-1.221343113
NADH2 transhydrogenase (mitochondrial)	An02g09810	0.700649902	0.81501731	0.81501731
NADH2 transhydrogenase	An02g09810	0.05410099	-0.158660022	NOSTAT
sulpate reduction	An08g08910	0.93806359	-0.013413199	0
ATP synthase	An01g05670	0.879089661	-1.538669394	-1.538669394
succinate dehydrogenase	An01g13930	0.888175592	1.702515029	1.702515029
sucrase synthesis		1	1.025640816	1.025640816
sucrase secretion		1	1.025640816	1.025640816
biomass synthesis		0.966601947	-0.123610388	-0.123610388
xyrA / xylulose-reductase	An01g03740	#DIV/0!	0	#DIV/0!
xylulose reductase	An05g02260	#DIV/0!	0	#DIV/0!
xylulose kinase	An07g03140	#DIV/0!	0	#DIV/0!

Table 32: Statistical analysis of simulation data. Non-growth associated fructofuranosidase production using xylose. R^2: regression coefficient, alpha: slope-correlation coefficient, NOSTAT: no statistical evaluation. The values correspond to Figure 7 Xyl(-). The entries of '#DIV/0' regarded to constant values (or complete zeros) of stoichiometric coefficients for the corresponding enzyme.

Enzyme name / Gene name	ANgxx number	R^2	alpha	evaluation correlation
biomass export		#DIV/0!	0	#DIV/0!
FFase export		1	1.025638821	1.025638821
oxalate export	non carrier mediated	#DIV/0!	0	#DIV/0!
gluconate export	non carrier mediated	#DIV/0!	0	#DIV/0!
ammonium uptake	non carrier mediated	1	0.78051198	0.78051198
sulphate uptake	non carrier mediated	1	0.005128213	0
oxygen uptake	non carrier mediated	0.999999999	-5.121025279	-5.121025279
carbon dioxide export	non carrier mediated	0.999999999	-5.21433386	-5.21433386
oxygen uptake	non carrier mediated	0.999999999	-5.121025279	-5.121025279
oxygen diffusion	non carrier mediated	0.934054325	-5.24329042	-5.24329042
carbon dioxide diffusion	non carrier mediated	0.84169385	5.332658957	5.332658957
ADP/ATP translocator	An18g04220	0.266497962	8.088716461	NOSTAT
pyruvate shuttle		0.565682728	-1.872209189	NOSTAT
citrate/malate shuttle	An11g11230	0.022793122	-0.245103502	NOSTAT
isocitrate/malate shuttle		0.051413091	-0.394081094	NOSTAT
isocitrate shuttle		0.055632213	-0.49717098	NOSTAT
succinate shuttle		0.018625584	-0.164857018	NOSTAT
fumarate shuttle		0.13395006	-0.662025446	NOSTAT
nad5 nuo51 nd4L / NADH-ubiquinone oxidoreductase	An02g05470	0.210145603	-1.386540155	NOSTAT
substrate uptake (glc, xyl, gly, oelic)		#DIV/0!	0	#DIV/0!
hxk / hexokinase	An02g14380	0.00231479	-0.374674205	NOSTAT
glucose-6-phosphate isomerase	An16g05420	0.026723074	-0.398044194	NOSTAT
pfkA / phosphofructokinase	An18g01670	0.01243244	-0.87841491	NOSTAT
fructose 1,6-bis-phosphate aldolase	An02g07470	0.285652067	-0.506357658	NOSTAT
triose-phosphate isomerase	An14g04920	0.285652067	-0.506357658	NOSTAT
gpdA / phosphoglycerate kinase	An16g01830 / An08g02260	0.579053043	-0.939159459	NOSTAT
phosphoglycerate mutase / enolase	An16g02990 / An18g06250	0.640329811	-1.06842925	NOSTAT
pkiA / pyruvate kinase	An07g08990	0.187349473	-1.163604954	NOSTAT
mannitol 1-phosphate DH (NADH2)	An02g05830	0.049316559	0.475886945	NOSTAT
mannitol 1-phosphatase		0.049316559	0.475886945	NOSTAT
mannitol 1-phosphate DH (NADPH2)	An02g05830	0.049316559	0.475886945	NOSTAT
hxk / hexokinase	An02g14380	0.049316559	0.475886945	NOSTAT
glucose 6- phosphatase		0.000244923	-0.130226677	NOSTAT
fructose 1,6-bis-phosphate phosphatase	An04g05300	0.002285126	-0.372040984	NOSTAT
mannose 6-phosphate isomerase	An08g06350	0.999999999	0.315895491	0.315895491
phosphoenolpyruvate carboxykinase	An11g02550	8.91384E-05	0.022734036	NOSTAT
pyc / pyruvate carboxylase (mitochondrial)	An04g02090	0.011886465	0.29808409	NOSTAT
goxC / glucose oxidase	An12g0430	0.007637499	0.244444949	NOSTAT
gluconate transport				
catR / catalsae R	An03g05660	0.007637912	0.122224121	NOSTAT
gluconokinase	An01g01820	0.007637499	0.244444949	NOSTAT
gsdA / glucose-6-phosphate DH	An01g07300	0.005056311	0.135146274	NOSTAT
phosphogluconate DH	An02g12140	0.024360406	0.379591523	NOSTAT
ribulose-5-phosphate epimerase	An11g02040	0.017500823	0.213740643	NOSTAT
ribulose-5-phosphate isomerase	An09g03450	0.041132581	0.165847147	NOSTAT
transketolase I	An02g02930	0.029744172	0.140201415	NOSTAT
transaldolase	An08g06430	0.029744172	0.140201415	NOSTAT
transketolase II	An07g03850	0.008364101	0.073540683	NOSTAT
malate DH (decarboxylating)	An08g06430	0.00732144	-0.145912503	NOSTAT
malate DH (cytosolic)	An05g00930	0.000604033	0.041769532	NOSTAT
ATP citrate lyase	An07g02160	0.006411681	-0.096126477	NOSTAT
oahA / oxalacetase	An11g00510	#DIV/0!	0	#DIV/0!
acetyl-CoA synthetase	An10g00820	#DIV/0!	0	#DIV/0!
aconitase	An04g05620	0.010582436	-0.148977593	NOSTAT
icdA / isocitrate DH (NADPH2, cytosolic)	An02g11040	1	0.11897437	0.11897437
succinate dehydrogenase	An08g05580	0.13395006	-0.662025446	NOSTAT
ATP excess /maintenance	An16g07150	0.00231479	-0.374674205	NOSTAT
ATP excess /maintenance		0.00231479	-0.374674205	NOSTAT
isocitrate shuttle (glyoxysomal)		0.018625584	-0.164857018	NOSTAT
isocitrate lyase	An01g09270	0.018625584	-0.164857018	NOSTAT
succinate shuttle (glyoxysomal)		0.018625584	-0.164857018	NOSTAT
malate synthase (glyoxysomal)	An15g01860	0.018625584	-0.164857018	NOSTAT
malate shuttle (glyoxysomal)		0.018625584	-0.164857018	NOSTAT
L-carnitine shuttle	An08g04990	0.018625584	-0.164857018	NOSTAT
pyruvate DH	An01g00100	0.565682728	-1.872209189	NOSTAT
citA / citrate synthase	An09g06680	0.815348306	-3.609450682	-3.609450682
aconitase	An02g11040	0.487476964	-1.627118238	NOSTAT
icdA / isocitrate DH (mitochondrial)	An02g12430	0.257937061	-0.865102141	NOSTAT
icdA / isocitrate DH (mitochondrial)	An02g12430	0.257937061	-0.865102141	NOSTAT
ATP citrate lyase	An11g00510	0.79827248	-3.422172406	-3.422172406
2-oxoglutarate dehydrogenase complex	An04g04750 + An11g11280 + An07g06840	0.67292119	-1.730204283	NOSTAT
succinate dehydrogenase	An16g07150	0.848505899	-1.895054297	-1.895054297
fumarate hydratase	An12g07850	0.332029146	-1.233033972	NOSTAT
malate DH (mitochondrial)	An07g02160	0.565682728	-1.872209189	NOSTAT
NADH2 transhydrogenase (mitochondrial)	An02g09810	0.010080222	-0.242508079	NOSTAT
NADH2 transhydrogenase	An02g09810	0.257937061	-0.865102141	NOSTAT
sulpate reduction	An08g08910	1	0.005128213	0
ATP synthase	An01g05670	0.834983441	-3.60243746	-3.60243746
succinate dehydrogenase	An01g13930	0.693092127	-1.640837301	NOSTAT
sucrase synthesis		1	1.025638821	1.025638821
sucrase secretion		1	1.025638821	1.025638821
biomass synthesis		#DIV/0!	0	#DIV/0!
xyrA / xylulose-reductase	An01g03740	#DIV/0!	0	#DIV/0!
xylulose reductase	An05g02260	#DIV/0!	0	#DIV/0!
xylulose kinase	An07g03140	#DIV/0!	0	#DIV/0!

Table 33: Statistical analysis of simulation data. Growth associated fructofuranosidase production using glycerol. R^2: regression coefficient, alpha: slope-correlation coefficient, NOSTAT: no statistical evaluation. The values correspond to Figure 7 Gly(+). The entries of '#DIV/0' regarded to constant values (or complete zeros) of stoichiometric coefficients for the corresponding enzyme.

Enzyme name / Gene name	ANgxx number	R^2	alpha	evaluation correlation
biomass export		0.136659652	-0.407334548	NOSTAT
FFase export		1	1	#DIV/0!
oxalate export	non carrier mediated	#DIV/0!	0	#DIV/0!
gluconate export	non carrier mediated	#DIV/0!	0	#DIV/0!
ammonium uptake	non carrier mediated	0.17752297	0.252269007	NOSTAT
sulphate uptake	non carrier mediated	0.016528817	-0.001487209	NOSTAT
oxygen uptake	non carrier mediated	0.176649845	-1.652918747	NOSTAT
carbon dioxide export	non carrier mediated	0.198826373	-1.73942511	NOSTAT
oxygen uptake	non carrier mediated	0.176649845	-1.652918747	NOSTAT
oxygen diffusion	non carrier mediated	0.176233621	-1.663594425	NOSTAT
carbon dioxide diffusion	non carrier mediated	0.188180256	1.671223515	NOSTAT
ADP/ATP translocator	An18g04220	0.000398964	-0.231745421	NOSTAT
pyruvate shuttle		0.274471334	-0.716689705	NOSTAT
citrate/malate shuttle	An11g11230	0.017163477	-0.169878195	NOSTAT
isocitrate/malate shuttle		0.014475001	-0.163585636	NOSTAT
isocitrate shuttle		0.003792924	-0.094040439	NOSTAT
succinate shuttle		0.021075302	-0.099956616	NOSTAT
fumarate shuttle		0.020397993	-0.193994118	NOSTAT
nad5 nuo51 nd4L / NADH-ubiquinone oxidoreductase	An02g05470	0.074810602	-0.865826859	NOSTAT
substrate uptake (glc, xyl, gly, oelic)		#DIV/0!	0	#DIV/0!
hxk / hexokinase	An02g14380	0.022944225	-0.841695735	NOSTAT
glucose-6-phosphate isomerase	An16g05420	0.006364028	-0.020746831	NOSTAT
pfkA / phosphofructokinase	An18g01670	0.022944225	-0.841695735	NOSTAT
fructose 1,6-bis-phosphate aldolase	An02g07470	0.334562913	-0.163988263	NOSTAT
triose-phosphate isomerase	An14g04920	0.317020518	-0.161552936	NOSTAT
gpdA / phosphoglycerate kinase	An16g01830 / An08g02260	0.326633123	-0.326838409	NOSTAT
phosphoglycerate mutase / enolase	An16g02990 / An18g06250	0.330744845	-0.377293895	NOSTAT
pkiA / pyruvate kinase	An07g08990	0.078526826	-0.762455158	NOSTAT
mannitol 1-phosphate DH (NADH2)	An02g05830	0.000657449	-0.089940086	NOSTAT
mannitol 1-phosphatase		0.000657449	-0.089940086	NOSTAT
mannitol 1-phosphate DH (NADPH2)	An02g05830	0.00056778	-0.083464401	NOSTAT
hxk / hexokinase	An02g14380	0.00056778	-0.083464401	NOSTAT
glucose 6- phosphatase		0.020795338	-0.800166836	NOSTAT
fructose 1,6-bis-phosphate phosphatase	An04g05300	0.014992081	-0.677705776	NOSTAT
mannose 6-phosphate isomerase	An08g06350	0.997568551	0.185887781	0.185887781
phosphoenolpyruvate carboxykinase	An11g02550	0.016330543	-0.334185023	NOSTAT
pyc / pyruvate carboxylase (mitochondrial)	An04g02090	0.008942256	-0.370551368	NOSTAT
goxC / glucose oxidase	An12g0430	0.152702109	0.041528747	NOSTAT
gluconate transport				
catR / catalsae R	An03g05660	0.15270262	0.020764256	NOSTAT
gluconokinase	An01g01820	0.152702109	0.041528747	NOSTAT
gsdA / glucose-6-phosphate DH	An01g07300	0.007028407	0.016826226	NOSTAT
phosphogluconate DH	An02g12140	0.071834859	0.058354973	NOSTAT
ribulose-5-phosphate epimerase	An11g02040	0.035413658	0.026470165	NOSTAT
ribulose-5-phosphate isomerase	An09g03450	0.13887801	0.031884729	NOSTAT
transketolase I	An02g02930	0.136286476	0.027757887	NOSTAT
transaldolase	An08g06430	0.136286476	0.027757887	NOSTAT
transketolase II	An07g03850	0.000329138	-0.001287908	NOSTAT
malate DH (decarboxylating)	An08g06430	0.006870809	-0.224135033	NOSTAT
malate DH (cytosolic)	An05g00930	0.009038718	-0.263661037	NOSTAT
ATP citrate lyase	An07g02160	0.055834174	-0.176171618	NOSTAT
oahA / oxalacetase	An11g00510	#DIV/0!	0	#DIV/0!
acetyl-CoA synthetase	An10g00820	#DIV/0!	0	#DIV/0!
aconitase	An04g05620	2.51721E-05	0.006292558	NOSTAT
icdA / isocitrate DH (NADPH2, cytosolic)	An02g11040	0.150502367	0.036697398	NOSTAT
succinate dehydrogenase	An08g05580	0.020397993	-0.193994118	NOSTAT
ATP excess /maintenance	An16g07150	0.022944225	-0.841695735	NOSTAT
ATP excess /maintenance		0.022944225	-0.841695735	NOSTAT
isocitrate shuttle (glyoxysomal)		0.021075302	-0.099956616	NOSTAT
isocitrate lyase	An01g09270	0.021075302	-0.099956616	NOSTAT
succinate shuttle (glyoxysomal)		0.021075302	-0.099956616	NOSTAT
malate synthase (glyoxysomal)	An15g01860	0.021075302	-0.099956616	NOSTAT
malate shuttle (glyoxysomal)		0.021075302	-0.099956616	NOSTAT
L-carnitine shuttle	An08g04990	0.021075302	-0.099956616	NOSTAT
pyruvate DH	An01g00100	0.274471334	-0.716689705	NOSTAT
citA / citrate synthase	An09g06680	0.093480466	-8.806829484	NOSTAT
aconitase	An02g11040	0.107198231	-0.546816744	NOSTAT
icdA / isocitrate DH (mitochondrial)	An02g12430	0.043337862	-0.238636857	NOSTAT
icdA / isocitrate DH (mitochondrial)	An02g12430	0.043337862	-0.238636857	NOSTAT
ATP citrate lyase	An11g00510	0.084301363	-8.090041099	NOSTAT
2-oxoglutarate dehydrogenase complex	An04g04750 + An11g11280 + An07g06840	0.103456824	-0.477273714	NOSTAT
succinate dehydrogenase	An16g07150	0.169384738	-0.577231079	NOSTAT
fumarate hydratase	An12g07850	0.061717922	-0.383233851	NOSTAT
malate DH (mitochondrial)	An07g02160	0.274471334	-0.716689705	NOSTAT
NADH2 transhydrogenase (mitochondrial)	An02g09810	0.023717301	-0.500129033	NOSTAT
NADH2 transhydrogenase	An02g09810	0.043337862	-0.238636857	NOSTAT
sulpate reduction	An08g08910	0.016528817	-0.001487209	NOSTAT
ATP synthase	An01g05670	0.231603556	-1.193957817	NOSTAT
succinate dehydrogenase	An01g13930	0.097098597	-0.469650131	NOSTAT
sucrase synthesis		1	0.615384327	0.615384327
sucrase secretion		1	0.615384327	0.615384327
biomass synthesis		0.136663229	-0.03042826	NOSTAT
glycerol kinase	An04g04890	#DIV/0!	0	#DIV/0!
glycerol 3-P dehydrogenase / FAD dep)	An08g00210	0.049884466	0.503786401	NOSTAT
glycerol dehydrogenase	An01g06970	0.049884466	-0.503786401	NOSTAT
glycerone kinase	An14g06500	0.049884466	-0.503786401	NOSTAT

Table 34: Statistical analysis of simulation data. Non-growth associated fructofuranosidase production using glycerol. R^2: regression coefficient, alpha: slope-correlation coefficient, NOSTAT: no statistical evaluation. The values correspond to Figure 7 Gly(-). The entries of '#DIV/0' regarded to constant values (or complete zeros) of stoichiometric coefficients for the corresponding enzyme.

Enzyme name / Gene name	ANgxx number	R^2	alpha	evaluation correlation
biomass export		#DIV/0!	0	#DIV/0!
FFase export		1	1	#DIV/0!
oxalate export	non carrier mediated	#DIV/0!	0	#DIV/0!
gluconate export	non carrier mediated	#DIV/0!	0	#DIV/0!
ammonium uptake	non carrier mediated	1	0.468311719	0.468311719
sulphate uptake	non carrier mediated	0.999999999	0.003076936	0
oxygen uptake	non carrier mediated	0.999999999	-3.072616823	-3.072616823
carbon dioxide export	non carrier mediated	0.999999999	-3.128620058	-3.128620058
oxygen uptake	non carrier mediated	0.999999999	-3.072616823	-3.072616823
oxygen diffusion	non carrier mediated	0.995298733	-3.101511312	-3.101511312
carbon dioxide diffusion	non carrier mediated	0.971192121	3.259543458	3.259543458
ADP/ATP translocator	An18g04220	0.571379462	6.281598674	NOSTAT
pyruvate shuttle		0.784494039	-0.913430304	-0.913430304
citrate/malate shuttle	An11g11230	0.001434701	-0.028332182	NOSTAT
isocitrate/malate shuttle		0.038372282	-0.171404943	NOSTAT
isocitrate shuttle		0.169629417	-0.459370299	NOSTAT
succinate shuttle		0.028063515	0.073509168	NOSTAT
fumarate shuttle		0.154481084	-0.385861013	NOSTAT
nad5 nuo51 nd4L / NADH-ubiquinone oxidoreductase	An02g05470	0.22115855	-0.930486474	NOSTAT
substrate uptake (glc, xyl, gly, oelic)		#DIV/0!	0	#DIV/0!
hxk / hexokinase	An02g14380	0.001106842	0.109250991	NOSTAT
glucose-6-phosphate isomerase	An16g05420	0.077261629	-0.12634515	NOSTAT
pfkA / phosphofructokinase	An18g01670	0.001106842	0.109250991	NOSTAT
fructose 1,6-bis-phosphate aldolase	An02g07470	0.770030858	-0.266321021	-0.266321021
triose-phosphate isomerase	An14g04920	0.770029711	-0.266320335	-0.266320335
gpdA / phosphoglycerate kinase	An16g01830 / An08g02260	0.92888486	-0.526014638	-0.526014638
phosphoglycerate mutase / enolase	An16g02990 / An18g06250	0.945045532	-0.603554149	-0.603554149
pkiA / pyruvate kinase	An07g08990	0.95545447	-0.674266507	-0.674266507
mannitol 1-phosphate DH (NADH2)	An02g05830	0.283164912	0.384470375	NOSTAT
mannitol 1-phosphatase		0.283164912	0.384470375	NOSTAT
mannitol 1-phosphate DH (NADPH2)	An02g05830	0.283164912	0.384470375	NOSTAT
hxk / hexokinase	An02g14380	0.283164912	0.384470375	NOSTAT
glucose 6- phosphatase		0.00256058	0.167027283	NOSTAT
fructose 1,6-bis-phosphate phosphatase	An04g05300	0.012944088	0.375571588	NOSTAT
mannose 6-phosphate isomerase	An08g06350	0.999999998	0.189538475	0.189538475
phosphoenolpyruvate carboxykinase	An11g02550	0.006945106	5.75834E-05	NOSTAT
pyc / pyruvate carboxylase (mitochondrial)	An04g02090	0.116641855	0.195273652	NOSTAT
goxC / glucose oxidase	An12g0430	0.018036267	0.057776403	NOSTAT
gluconate transport				
catR / catalsae R	An03g05660	0.018036599	0.028888468	NOSTAT
gluconokinase	An01g01820	0.018036267	0.057776403	NOSTAT
gsdA / glucose-6-phosphate DH	An01g07300	0.072952656	0.057491453	NOSTAT
phosphogluconate DH	An02g12140	0.06515204	0.115267856	NOSTAT
ribulose-5-phosphate epimerase	An11g02040	0.032388478	0.053255296	NOSTAT
ribulose-5-phosphate isomerase	An09g03450	0.153648731	0.062012851	NOSTAT
transketolase I	An02g02930	0.09308444	0.046627822	NOSTAT
transaldolase	An08g06430	0.09308444	0.046627822	NOSTAT
transketolase II	An07g03850	0.002069285	0.006627448	NOSTAT
malate DH (decarboxylating)	An08g06430	0.04274772	0.114877847	NOSTAT
malate DH (cytosolic)	An05g00930	0.149027843	0.227493653	NOSTAT
ATP citrate lyase	An07g02160	0.065725079	0.11474074	NOSTAT
oahA / oxalacetase	An11g00510	#DIV/0!	0	#DIV/0!
acetyl-CoA synthetase	An10g00820	#DIV/0!	0	#DIV/0!
aconitase	An04g05620	0.038835108	-0.143072761	NOSTAT
icdA / isocitrate DH (NADPH2, cytosolic)	An02g11040	1	0.071384938	0.071384938
succinate dehydrogenase	An08g05580	0.154481084	-0.385861013	NOSTAT
ATP excess /maintenance	An16g07150	0.001106842	0.109250991	NOSTAT
ATP excess /maintenance		0.001106842	0.109250991	NOSTAT
isocitrate shuttle (glyoxysomal)		0.028063515	0.073509168	NOSTAT
isocitrate lyase	An01g09270	0.028063515	0.073509168	NOSTAT
succinate shuttle (glyoxysomal)		0.028063515	0.073509168	NOSTAT
malate synthase (glyoxysomal)	An15g01860	0.028063515	0.073509168	NOSTAT
malate shuttle (glyoxysomal)		0.028063515	0.073509168	NOSTAT
L-carnitine shuttle	An08g04990	0.028063515	0.073509168	NOSTAT
pyruvate DH	An01g00100	0.784494039	-0.913430304	-0.913430304
citA / citrate synthase	An09g06680	0.94158744	-2.271423257	-2.271423257
aconitase	An02g11040	0.596357009	-0.885097389	NOSTAT
icdA / isocitrate DH (mitochondrial)	An02g12430	0.321659029	-0.586531252	NOSTAT
icdA / isocitrate DH (mitochondrial)	An02g12430	0.321659029	-0.586531252	NOSTAT
ATP citrate lyase	An11g00510	0.930879888	-2.180054973	-2.180054973
2-oxoglutarate dehydrogenase complex	An04g04750 + An11g11280 + An07g06840	0.880110445	-1.173062503	-1.173062503
succinate dehydrogenase	An16g07150	0.982780668	-1.099551425	-1.099551425
fumarate hydratase	An12g07850	0.382435489	-0.713691762	NOSTAT
malate DH (mitochondrial)	An07g02160	0.784494039	-0.913430304	-0.913430304
NADH2 transhydrogenase (mitochondrial)	An02g09810	0.006851298	0.019795486	NOSTAT
NADH2 transhydrogenase	An02g09810	0.321659029	-0.586531252	NOSTAT
sulpate reduction	An08g08910	0.999999999	0.003076936	0
ATP synthase	An01g05670	0.980909116	-2.086498518	-2.086498518
succinate dehydrogenase	An01g13930	0.980921596	-1.015023321	-1.015023321
sucrase synthesis		1	0.615386217	0.615386217
sucrase secretion		1	0.615386217	0.615386217
biomass synthesis		#DIV/0!	0	#DIV/0!
glycerol kinase	An04g04890	#DIV/0!	0	#DIV/0!
glycerol 3-P dehydrogenase / FAD dep)	An08g00210	4.06354E-37	-1.08339E-18	NOSTAT
glycerol dehydrogenase	An01g06970	4.06354E-37	1.08339E-18	NOSTAT
glycerone kinase	An14g06500	4.06354E-37	1.08339E-18	NOSTAT

Table 35: Statistical analysis of simulation data. Growth associated fructofuranosidase production using oleic acid. R^2: regression coefficient, alpha: slope-correlation coefficient, NOSTAT: no statistical evaluation. The values correspond to Figure 7 Oel(+). The entries of '#DIV/0' regarded to constant values (or complete zeros) of stoichiometric coefficients for the corresponding enzyme.

Enzyme name / Gene name	ANgxx number	R^2	alpha	evaluation correlation
biomass export		0.829628764	-0.386206067	-0.386206067
FFase export		0.999999999	3.692296335	3.692296335
oxalate export	non carrier mediated	#DIV/0!	0	#DIV/0!
gluconate export	non carrier mediated	#DIV/0!	0	#DIV/0!
ammonium uptake	non carrier mediated	0.002962662	0.067741269	NOSTAT
sulphate uptake	non carrier mediated	0.693292258	-0.039468773	NOSTAT
oxygen uptake	non carrier mediated	0.002583452	-0.415528729	NOSTAT
carbon dioxide export	non carrier mediated	0.019926858	-1.139370732	NOSTAT
oxygen uptake	non carrier mediated	0.002583452	-0.415528729	NOSTAT
oxygen diffusion	non carrier mediated	0.002252133	-0.39887339	NOSTAT
carbon dioxide diffusion	non carrier mediated	0.090941061	1.554163708	NOSTAT
ADP/ATP translocator	An18g04220	0.003888641	-3.132186099	NOSTAT
pyruvate shuttle		0.090941061	-1.554163708	NOSTAT
citrate/malate shuttle	An11g11230	0.007470342	-0.986583519	NOSTAT
isocitrate/malate shuttle		0.000576556	-0.312775989	NOSTAT
isocitrate shuttle		0.000280736	0.231125013	NOSTAT
succinate shuttle		0.002675139	-0.14948746	NOSTAT
fumarate shuttle		3.56445E-05	0.081650977	NOSTAT
nad5 nuo51 nd4L / NADH-ubiquinone oxidoreductase	An02g05470	0.06096373	2.396546494	NOSTAT
substrate uptake (glc, xyl, gly, oelic)		#DIV/0!	0	#DIV/0!
hxk / hexokinase	An02g14380	0.000729281	-1.239726422	NOSTAT
glucose-6-phosphate isomerase	An16g05420	0.000584164	0.036873035	NOSTAT
pfkA / phosphofructokinase	An18g01670	0.000729281	-1.239726422	NOSTAT
fructose 1,6-bis-phosphate aldolase	An02g07470	0.345378014	-0.480847628	NOSTAT
triose-phosphate isomerase	An14g04920	0.310114236	-0.449896287	NOSTAT
gpdA / phosphoglycerate kinase	An16g01830 / An08g02260	0.348997524	-0.809662126	NOSTAT
phosphoglycerate mutase / enolase	An16g02990 / An18g06250	0.358206602	-0.931154209	NOSTAT
pkiA / pyruvate kinase	An07g08990	0.016785207	3.211543184	NOSTAT
mannitol 1-phosphate DH (NADH2)	An02g05830	0.091794388	-6.746299995	NOSTAT
mannitol 1-phosphatase		0.091794388	-6.746299995	NOSTAT
mannitol 1-phosphate DH (NADPH2)	An02g05830	0.089850771	-6.66399165	NOSTAT
hxk / hexokinase	An02g14380	0.089850771	-6.66399165	NOSTAT
glucose 6- phosphatase		0.000474244	-0.999384317	NOSTAT
fructose 1,6-bis-phosphate phosphatase	An04g05300	0.000274733	-0.758881491	NOSTAT
mannose 6-phosphate isomerase	An08g06350	0.999629398	1.09088671	1.09088671
phosphoenolpyruvate carboxykinase	An11g02550	0.029718056	4.316326589	NOSTAT
pyc / pyruvate carboxylase (mitochondrial)	An04g02090	0.048040374	6.247839516	NOSTAT
goxC / glucose oxidase	An12g0430	0.163208693	0.240328539	NOSTAT
gluconate transport				
catR / catalsae R	An03g05660	0.163211096	0.120165944	NOSTAT
gluconokinase	An01g01820	0.163208693	0.240328539	NOSTAT
gsdA / glucose-6-phosphate DH	An01g07300	0.031016351	0.27425879	NOSTAT
phosphogluconate DH	An02g12140	0.101740012	0.514587329	NOSTAT
ribulose-5-phosphate epimerase	An11g02040	0.100216526	0.343120391	NOSTAT
ribulose-5-phosphate isomerase	An09g03450	0.102656994	0.171470792	NOSTAT
transketolase I	An02g02930	0.159484278	0.222047692	NOSTAT
transaldolase	An08g06430	0.159484278	0.222047692	NOSTAT
transketolase II	An07g03850	0.051380635	0.121076813	NOSTAT
malate DH (decarboxylating)	An08g06430	0.01934456	1.696971412	NOSTAT
malate DH (cytosolic)	An05g00930	0.001512746	0.465377068	NOSTAT
ATP citrate lyase	An07g02160	0.066818358	-1.369074187	NOSTAT
oahA / oxalacetase	An11g00510	#DIV/0!	0	#DIV/0!
acetyl-CoA synthetase	An10g00820	#DIV/0!	0	#DIV/0!
aconitase	An04g05620	0.001134572	0.382478829	NOSTAT
icdA / isocitrate DH (NADPH2, cytosolic)	An02g11040	0.003589017	-0.011975449	NOSTAT
succinate dehydrogenase	An08g05580	3.56445E-05	0.081650977	NOSTAT
ATP excess /maintenance	An16g07150	0.000729281	-1.239726422	NOSTAT
ATP excess /maintenance		0.000729281	-1.239726422	NOSTAT
isocitrate shuttle (glyoxysomal)		0.002675139	-0.14948746	NOSTAT
isocitrate lyase	An01g09270	0.002675139	-0.14948746	NOSTAT
succinate shuttle (glyoxysomal)		0.002675139	-0.14948746	NOSTAT
malate synthase (glyoxysomal)	An15g01860	0.002675139	-0.14948746	NOSTAT
malate shuttle (glyoxysomal)		0.002675139	-0.14948746	NOSTAT
L-carnitine shuttle	An08g04990	0.000538482	-0.1256957	NOSTAT
pyruvate DH	An01g00100	0.090941061	-1.554163708	NOSTAT
citA / citrate synthase	An09g06680	0.003319692	-2.770146234	NOSTAT
aconitase	An02g11040	0.002135907	-0.543887579	NOSTAT
icdA / isocitrate DH (mitochondrial)	An02g12430	#DIV/0!	0	#DIV/0!
icdA / isocitrate DH (mitochondrial)	An02g12430	#DIV/0!	0	#DIV/0!
ATP citrate lyase	An11g00510	0.000729281	-1.239726422	NOSTAT
2-oxoglutarate dehydrogenase complex	An04g04750 + An11g11280 + An07g06840	#DIV/0!	0	#DIV/0!
succinate dehydrogenase	An16g07150	0.002675139	-0.14948746	NOSTAT
fumarate hydratase	An12g07850	0.000280736	-0.231125013	NOSTAT
malate DH (mitochondrial)	An07g02160	0.052625955	-1.53043782	NOSTAT
NADH2 transhydrogenase (mitochondrial)	An02g09810	0.028333414	-3.210386053	NOSTAT
NADH2 transhydrogenase	An02g09810	#DIV/0!	0	#DIV/0!
sulpate reduction	An08g08910	0.693292258	-0.039468773	NOSTAT
ATP synthase	An01g05670	0.055553009	-1.531796595	NOSTAT
succinate dehydrogenase	An01g13930	0.066149419	1.132781858	NOSTAT
sucrase synthesis		0.999999999	3.692296335	3.692296335
sucrase secretion		0.999999999	3.692296335	3.692296335
biomass synthesis		0.829628764	-0.386206067	-0.386206067

Table 36: Statistical analysis of simulation data. Growth associated fructofuranosidase production using oleic acid. R^2: regression coefficient, alpha: slope-correlation coefficient, NOSTAT: no statistical evaluation. The values correspond to Figure 7 Oel(-). The entries of '#DIV/0' regarded to constant values (or complete zeros) of stoichiometric coefficients for the corresponding enzyme.

Enzyme name / Gene name	ANgxx number	R^2	alpha	evaluation correlation
biomass export		#DIV/0!	0	#DIV/0!
FFase export		0.999999982	3.692377724	3.692377724
oxalate export	non carrier mediated	#DIV/0!	0	#DIV/0!
gluconate export	non carrier mediated	#DIV/0!	0	#DIV/0!
ammonium uptake	non carrier mediated	0.999999971	2.809710893	2.809710893
sulphate uptake	non carrier mediated	0.999999971	0.018462819	0
oxygen uptake	non carrier mediated	0.999999916	-1.84348811	-1.84348811
carbon dioxide export	non carrier mediated	0.999999999	-1.877192796	-1.877192796
oxygen uptake	non carrier mediated	0.999999916	-1.84348811	-1.84348811
oxygen diffusion	non carrier mediated	0.78786043	-1.74169845	-1.74169845
carbon dioxide diffusion	non carrier mediated	0.310092956	4.912129498	NOSTAT
ADP/ATP translocator	An18g04220	0.121372148	-5.957564465	NOSTAT
pyruvate shuttle		0.310092956	-4.912129498	NOSTAT
citrate/malate shuttle	An11g11230	0.04601781	-7.637117999	NOSTAT
isocitrate/malate shuttle		0.009390082	-3.734050625	NOSTAT
isocitrate shuttle		0.006840631	3.263922447	NOSTAT
succinate shuttle		0.367729446	-2.793737111	NOSTAT
fumarate shuttle		0.000142835	0.470128178	NOSTAT
nad5 nuo51 nd4L / NADH-ubiquinone oxidoreductase	An02g05470	0.011420019	3.711362122	NOSTAT
substrate uptake (glc, xyl, gly, oelic)		#DIV/0!	0	#DIV/0!
hxk / hexokinase	An02g14380	0.028110785	-25.74355376	NOSTAT
glucose-6-phosphate isomerase	An16g05420	0.484391633	10.6523734	NOSTAT
pfkA / phosphofructokinase	An18g01670	0.028110785	-25.74355376	NOSTAT
fructose 1,6-bis-phosphate aldolase	An02g07470	0.26605136	2.205637546	NOSTAT
triose-phosphate isomerase	An14g04920	0.26605136	2.205637546	NOSTAT
gpdA / phosphoglycerate kinase	An16g01830 / An08g02260	0.030281163	0.64736194	NOSTAT
phosphoglycerate mutase / enolase	An16g02990 / An18g06250	0.002466051	0.182147334	NOSTAT
pkiA / pyruvate kinase	An07g08990	0.002294806	4.724382484	NOSTAT
mannitol 1-phosphate DH (NADH2)	An02g05830	0.000917254	3.259340486	NOSTAT
mannitol 1-phosphatase		0.000917254	3.259340486	NOSTAT
mannitol 1-phosphate DH (NADPH2)	An02g05830	0.000917254	3.259340486	NOSTAT
hxk / hexokinase	An02g14380	0.000917254	3.259340486	NOSTAT
glucose 6- phosphatase		0.052176429	-35.34277589	NOSTAT
fructose 1,6-bis-phosphate phosphatase	An04g05300	0.033097377	-27.94901227	NOSTAT
mannose 6-phosphate isomerase	An08g06350	0.999999999	1.137236058	1.137236058
phosphoenolpyruvate carboxykinase	An11g02550	0.002501259	4.966888956	NOSTAT
pyc / pyruvate carboxylase (mitochondrial)	An04g02090	0.012496136	12.66198824	NOSTAT
goxC / glucose oxidase	An12g0430	0.411628724	-9.599190144	NOSTAT
gluconate transport				
catR / catalsae R	An03g05660	0.411629984	-4.799639438	NOSTAT
gluconokinase	An01g01820	0.411628724	-9.599190144	NOSTAT
gsdA / glucose-6-phosphate DH	An01g07300	0.021331118	-1.119573159	NOSTAT
phosphogluconate DH	An02g12140	0.48749856	-10.7187633	NOSTAT
ribulose-5-phosphate epimerase	An11g02040	0.497302597	-7.287346715	NOSTAT
ribulose-5-phosphate isomerase	An09g03450	0.467333	-3.431391638	NOSTAT
transketolase I	An02g02930	0.480571156	-3.523755106	NOSTAT
transaldolase	An08g06430	0.480571156	-3.523755106	NOSTAT
transketolase II	An07g03850	0.513500057	-3.763734226	NOSTAT
malate DH (decarboxylating)	An08g06430	0.004433535	3.978291587	NOSTAT
malate DH (cytosolic)	An05g00930	0.006526324	-5.069182505	NOSTAT
ATP citrate lyase	An07g02160	0.292245095	-12.26957818	NOSTAT
oahA / oxalacetase	An11g00510	#DIV/0!	0	#DIV/0!
acetyl-CoA synthetase	An10g00820	#DIV/0!	0	#DIV/0!
aconitase	An04g05620	0.018081641	4.632417787	NOSTAT
icdA / isocitrate DH (NADPH2, cytosolic)	An02g11040	0.99999999	0.428297178	0.428297178
succinate dehydrogenase	An08g05580	0.000142835	0.470128178	NOSTAT
ATP excess /maintenance	An16g07150	0.028110785	-25.74355376	NOSTAT
ATP excess /maintenance		0.028110785	-25.74355376	NOSTAT
isocitrate shuttle (glyoxysomal)		0.367729446	-2.793737111	NOSTAT
isocitrate lyase	An01g09270	0.367729446	-2.793737111	NOSTAT
succinate shuttle (glyoxysomal)		0.367729446	-2.793737111	NOSTAT
malate synthase (glyoxysomal)	An15g01860	0.367729446	-2.793737111	NOSTAT
malate shuttle (glyoxysomal)		0.367729446	-2.793737111	NOSTAT
L-carnitine shuttle	An08g04990	0.300573	-12.5169872	NOSTAT
pyruvate DH	An01g00100	0.310092956	-4.912129498	NOSTAT
citA / citrate synthase	An09g06680	0.064750262	-40.37868106	NOSTAT
aconitase	An02g11040	0.040375625	-6.99803023	NOSTAT
icdA / isocitrate DH (mitochondrial)	An02g12430	#DIV/0!	0	#DIV/0!
icdA / isocitrate DH (mitochondrial)	An02g12430	#DIV/0!	0	#DIV/0!
ATP citrate lyase	An11g00510	0.028110785	-25.74355376	NOSTAT
2-oxoglutarate dehydrogenase complex	An04g04750 + An11g11280 + An07g06840	#DIV/0!	0	#DIV/0!
succinate dehydrogenase	An16g07150	0.367729446	-2.793737111	NOSTAT
fumarate hydratase	An12g07850	0.006840631	-3.263922447	NOSTAT
malate DH (mitochondrial)	An07g02160	0.380144162	-14.63509349	NOSTAT
NADH2 transhydrogenase (mitochondrial)	An02g09810	0.005167647	-8.514705583	NOSTAT
NADH2 transhydrogenase	An02g09810	#DIV/0!	0	#DIV/0!
sulpate reduction	An08g08910	0.999999971	0.018462819	0
ATP synthase	An01g05670	0.389436879	-14.0949231	NOSTAT
succinate dehydrogenase	An01g13930	0.096289943	-3.322544948	NOSTAT
sucrase synthesis		0.999999982	3.692377724	3.692377724
sucrase secretion		0.999999982	3.692377724	3.692377724
biomass synthesis		#DIV/0!	0	#DIV/0!

Band 1 **Sunder, Matthias**: Oxidation grundwasserrelevanter Spurenverunreinigungen mit Ozon und Wasserstoffperoxid im Rohrreaktor. 1996. FIT-Verlag · Paderborn, ISBN 3-932252-00-4

Band 2 **Pack, Hubertus**: Schwermetalle in Abwasserströmen: Biosorption und Auswirkung auf eine schadstoffabbauende Bakterienkultur. 1996. FIT-Verlag · Paderborn, ISBN 3-932252-01-2

Band 3 **Brüggenthies, Antje**: Biologische Reinigung EDTA-haltiger Abwässer. 1996. FIT-Verlag · Paderborn, ISBN 3-932252-02-0

Band 4 **Liebelt, Uwe**: Anaerobe Teilstrombehandlung von Restflotten der Reaktivfärberei. 1997. FIT-Verlag · Paderborn, ISBN 3-932252-03-9

Band 5 **Mann, Volker G.**: Optimierung und Scale up eines Suspensionsreaktorverfahrens zur biologischen Reinigung feinkörniger, kontaminierter Böden. 1997. FIT-Verlag · Paderborn, ISBN 3-932252-04-7

Band 6 **Boll Marco**: Einsatz von Fuzzy-Control zur Regelung verfahrenstechnischer Prozesse. 1997. FIT-Verlag · Paderborn, ISBN 3-932252-06-3

Band 7 **Büscher, Klaus**: Bestimmung von mechanischen Beanspruchungen in Zweiphasenreaktoren. 1997. FIT-Verlag · Paderborn, ISBN 3-932252-07-1

Band 8 **Burghardt, Rudolf**: Alkalische Hydrolyse – Charakterisierung und Anwendung einer Aufschlußmethode für industrielle Belebtschlämme. 1998. FIT-Verlag · Paderborn, ISBN 3-932252-13-6

Band 9 **Hemmi, Martin**: Biologisch-chemische Behandlung von Färbereiabwässern in einem Sequencing Batch Process. 1999. FIT-Verlag · Paderborn, ISBN 3-932252-14-4

Band 10 **Dziallas, Holger**: Lokale Phasengehalte in zwei- und dreiphasig betriebenen Blasensäulenreaktoren. 2000. FIT-Verlag · Paderborn, ISBN 3-932252-15-2

Band 11 **Scheminski, Anke**: Teiloxidation von Faulschlämmen mit Ozon. 2001. FIT-Verlag · Paderborn, ISBN 3-932252-16-0

Band 12 **Mahnke, Eike Ulf**: Fluiddynamisch induzierte Partikelbeanspruchung in pneumatisch gerührten Mehrphasenreaktoren. 2002. FIT-Verlag · Paderborn, ISBN 3-932252-17-9

Band 13 **Michele, Volker**: CDF modeling and measurement of liquid flow structure and phase holdup in two- and three-phase bubble columns. 2002. FIT-Verlag · Paderborn, ISBN 3-932252-18-7

Band 14 **Wäsche, Stefan**: Einfluss der Wachstumsbedingungen auf Stoffübergang und Struktur von Biofilmsystemen. 2003. FIT-Verlag · Paderborn, ISBN 3-932252-19-5

Band 15 **Krull Rainer**: Produktionsintegrierte Behandlung industrieller Abwässer zur Schließung von Stoffkreisläuren. 2003. FIT-Verlag · Paderborn, ISBN 3-932252-20-9

Band 16 **Otto, Peter**: Entwicklung eines chemisch-biologischen Verfahrens zur Reinigung EDTA enthaltender Abwässer. 2003. FIT-Verlag · Paderborn, ISBN 3-932252-21-7

Band 17 **Horn, Harald**: Modellierung von Stoffumsatz und Stofftransport in Biofilmsystemen. 2003. FIT-Verlag · Paderborn, ISBN 3-932252-22-5

Band 18 **Mora Naranjo, Nelson**: Analyse und Modellierung anaerober Abbauprozesse in Deponien. 2004. FIT-Verlag · Paderborn, ISBN 3-932252-23-3

Band 19 **Döpkens, Eckart**: Abwasserbehandlung und Prozesswasserrecycling in der Textilindustrie. 2004. FIT-Verlag · Paderborn, ISBN 3-932252-24-1

Band 20 **Haarstrick, Andreas**: Modellierung millieugesteuerter biologischer Abbauprozesse in heterogenen problembelasteten Systemen. 2005. FIT-Verlag · Paderborn, ISBN 3-932252-27-6

Band 21 **Baaß, Anne-Christina**: Mikrobieller Abbau der Polyaminopolycarbonsäuren Propylendiamintetraacetat (PDTA) und Diethylentriaminpentaacetat (DTPA). 2004. FIT-Verlag · Paderborn, ISBN 3-932252-26-8

Band 22 **Staudt, Christian**: Entwicklung der Struktur von Biofilmen. 2006. FIT-Verlag · Paderborn, ISBN 3-932252-28-4

Band 23 **Pilz, Roman Daniel**: Partikelbeanspruchung in mehrphasig betriebenen Airlift-Reaktoren. 2006. FIT-Verlag · Paderborn, ISBN 3-932252-29-2

Band 24 **Schallenberg, Jörg**: Modellierung von zwei- und dreiphasigen Strömungen in Blasensäulenreaktoren. 2006. FIT-Verlag · Paderborn, ISBN 3-932252-30-6

Band 25 **Enß, Jan Hendrik**: Einfluss der Viskosität auf Blasensäulenströmungen. 2006. FIT-Verlag · Paderborn, ISBN 3-932252-31-4

Band 26 **Kelly, Sven**: Fluiddynamischer Einfluss auf die Morphogenese von Biopellets filamentöser Pilze. 2006. FIT-Verlag · Paderborn, ISBN 3-932252-32-2

Band 27 **Grimm, Luis Hermann**: Sporenaggregationsmodell für die submerse Kultivierung koagulativer Myzelbildner. 2006. FIT-Verlag · Paderborn, ISBN 3-932252-33-0

Band 28 **León Ohl, Andrés**: Wechselwirkungen von Stofftransport und Wachstum in Biofilsystemen. 2007. FIT-Verlag · Paderborn, ISBN 3-932252-34-9

Band 29 **Emmler, Markus**: Freisetzung von Glucoamylase in Kultivierungen mit *Aspergillus niger*. 2007. FIT-Verlag · Paderborn, ISBN 3-932252-35-7

Band 30 **Leonhäuser, Johannes**: Biotechnologische Verfahren zur Reinigung von quecksilberhaltigem Abwasser. 2007. FIT-Verlag · Paderborn, ISBN 3-932252-36-5

Band 31 **Jungebloud, Anke**: Untersuchung der Genexpression in *Aspergillus niger* mittels Echtzeit-PCR. 1996. FIT-Verlag · Paderborn, ISBN 978-3-932252-37-2

Band 32 **Hille, Andrea**: Stofftransport und Stoffumsatz in filamentösen Pilzpellets. 2008. FIT-Verlag · Paderborn, ISBN 978-3-932252-38-9

Band 33 **Fürch, Tobias**: Metabolic characterization of recombinant protein production in *Bacillus megaterium*. 2008. FIT-Verlag · Paderborn, ISBN 978-3-932252-39-6

Band 34 **Grote, Andreas Georg**: Datenbanksysteme und bioinformatische Werkzeuge zur Optimierung biotechnologischer Prozesse mit Pilzen. 2008. FIT-Verlag · Paderborn, ISBN 978-3-932252-40-120

Band 35 **Möhle, Roland Bernhard**: An Analytic-Synthetic Approach Combining Mathematical Modeling and Experiments – Towards an Understanding of Biofilm Systems. 2008. FIT-Verlag · Paderborn, ISBN 978-3-932252-41-9

Band 36 **Reichel, Thomas**: Modelle für die Beschreibung das Emissionsverhaltens von Siedlungsabfällen. 2008. FIT-Verlag · Paderborn, ISBN 978-3-932252-42-6

Band 37 **Schultheiss, Ellen**: Charakterisierung des Exopolysaccharids PS-EDIV von *Sphingomonas pituitosa*. 2008. FIT-Verlag · Paderborn, ISBN 978-3-932252-43-3

Band 38 **Dreger, Michael Andreas**: Produktion und Aufarbeitung des Exopolysaccharids PS-EDIV aus *Sphingomonas pituitosa*. 1996. FIT-Verlag · Paderborn, ISBN 978-3-932252-44-0

Band 39 **Wiebels, Cornelia**: A Novel Bubble Size Measuring Technique for High Bubble Density Flows. 2009. FIT-Verlag · Paderborn, ISBN 978-3-932252-45-7

Band 40 **Bohle, Kathrin**: Morphologie- und produktionsrelevante Gen- und Proteinexpression in submersen Kultivierungen von *Aspergillus niger*. 2009. FIT-Verlag · Paderborn, ISBN 978-3-932252-46-2

Band 41 **Fallet, Claas**: Reaktionstechnische Untersuchungen der mikrobiellen Stressantwort und ihrer biotechnologischen Anwendungen. 2009. FIT-Verlag · Paderborn, ISBN 978-3-932252-47-1

Band 42 **Vetter, Andreas**: Sequential Co-simulation as Method to Couple CFD and Biological Growth in a Yeast. 2009. FIT-Verlag · Paderborn, ISBN 978-3-932252-48-8

Band 43 **Jung, Thomas**: Einsatz chemischer Oxidationsverfahren zur Behandlung industrieller Abwässer. 2010. FIT-Verlag· Paderborn, ISBN 978-3-932252-49-5

Band 45 **Herrmann, Tim**: Transport von Proteinen in Partikeln der Hydrophoben Interaktions Chromatographie. 2010. FIT-Verlag · Paderborn, ISBN 978-3-932252-51-8

Band 46 **Becker, Judith**: Systems Metabolic Engineering of *Corynebacterium glutamicum* towards improved Lysine Production. 2010. Cuvillier-Verlag · Göttingen, ISBN 978-3-86955-426-6